Česká zemědělská univerzita v Praze

Fakulta lesnická a dřevařská

Katedra hospodářské úpravy lesů

Využití moderních technik laserového skenování pro sběr dat o lesních ekosystémech

Disertační práce

Autor: Ing. Martin Slavík

Školitel: doc. Priv. – Doz. Ing. Peter Surový, Ph.D.

Konzultant: Ing. Karel Kuželka, Ph.D.

2020

Prohlášení

Prohlašuji, že jsem rešerší pro disertační práci na téma: Využití moderních technik laserového skenování pro sběr dat o lesních ekosystémech vypracoval samostatně pod vedením doc. Priv. – Doz., Ing. Petera Surového, Ph.D. a použil jen prameny, které uvádím v seznamu použitých zdrojů. Jsem si vědom, že zveřejněním disertační práce souhlasím s jejím zveřejněním dle zákona č. 111/1998 Sb. o vysokých školách v platném znění, a to bez ohledu na výsledek její obhajoby.

V Přelíci dne 15. 12. 2020 Ing. Martin Slavík

Poděkování

Na prvním místě bych velmi rád poděkoval mému školiteli, váženému doc. Priv. – Doz. Ing. Peteru Surovému, Ph.D. za jeho příkladné vedení v průběhu celého mého dosavadního studia. Dále bych velmi rád poděkoval Ing. Karlu Kuželkovi, Ph.D. za jeho odborné rady a přátelský přístup. Mé poděkování také patří i všem kolegům, se kterými jsem měl tu čest pracovat. V neposlední řadě bych také rád poděkoval mojí rodině a blízkým za vytvoření podmínek v osobním životě, díky nimž jsem mohl toto studium uskutečnit.

Zadání

Česká zemědělská univerzita v Praze

Fakulta lesnická a dřevařská

ZADÁNÍ DISERTAČNÍ PRÁCE

Autor práce:	Ing. Martin Slavík
Studijní program:	Lesní inženýrství
Obor:	Hospodářská úprava lesa
Vedoucí práce:	Ing. Peter Surový, PhD.
Garantující pracoviště:	Katedra hospodářské úpravy lesů
Jazyk práce:	Čeština
Název práce:	**Využívání moderních technik laserového skenování pro sběr dat v lesních ekosystémech**
Název anglicky:	**Using modern laser scanning techniques for data acquisition in forest ecosystems**
Cíle práce:	Cíl 1 – odvodit bodová mračna o vysoké přesnosti a hustotě k získání reprezentativních bodových mračen individuálních stromů na úrovni nadzemních stromových komponent. Cíl 2 – analyzovat a zhodnotit možnosti vysokého časového i prostorového rozlišení metody ULS. Cíl 3 – analyzovat a zhodnotit několik vybraných metod pro detekci a delineace individuálních stromů. Cíl 4 – analyzovat a zhodnotit vybrané metody odvozování tloušťky ve výčetní výšce (DBH) a výšky individuálních stromů z bodových mračen.
Metodika:	Získaní zručnosti a schopnosti k ovládání přístrojů sloužících ke sběru laserových dat. Výběr zkusných ploch s využitím probíhajících projektů s cílem minimalizovat časovou zátěž pro pozemní sběr kalibračních a verifikačních dat. V případě potřeby doměření chybějících dat k analýze přesnosti a správnosti laserových dat. Laserový data budou sesbírany pomocí různých prostředků, podle možnosti prověřit i možnost kombinace senzorů. Budou otestovány dostupná softwarová řešení pro analýzu, spracování a tvorbu mračen. Budou ověřeny metody a praktiky spracování mračen a odvozování dendrometrických veličin, zejména výška a tloušťka stromu.
Doporučený rozsah práce:	80-100 stran
Klíčová slova:	UAV, laserové skenování

Doporučené zdroje informací:

1. JAAKKOLA, Anttoni, Juha HYYPPÄ, Antero KUKKO, Xiaowei YU, Harri KAARTINEN, Matti LEHTOMÄKI a Yi LIN, 2010. A low-cost multi-sensoral mobile mapping system and its feasibility for tree measurements. ISPRS Journal of Photogrammetry and Remote Sensing [online]. 65(6), 514–522. ISSN 09242716. Dostupné z: doi:10.1016/j.isprsjprs.2010.08.002
2. LIANG, Xinlian, Ville KANKARE, Juha HYYPPÄ, Yunsheng WANG, Antero KUKKO, Henrik HAGGRÉN, Xiaowei YU, Harri KAARTINEN, Anttoni JAAKKOLA, Fengying GUAN, Markus HOLOPAINEN a Mikko VASTARANTA, 2016. Terrestrial laser scanning in forest inventories. ISPRS Journal of Photogrammetry and Remote Sensing [online]. 115, 63–77. ISSN 09242716. Dostupné z: doi:10.1016/j.isprsjprs.2016.01.006
3. PUTTONEN, Eetu, Christian BRIESE, Gottfried MANDLBURGER, Martin WIESER, Martin PFENNIGBAUER, András ZLINSZKY a Norbert PFEIFER, 2016. Quantification of overnight movement of birch (Betula pendula) branches and foliage with short interval terrestrial laser scanning. Frontiers in Plant Science [online]. 7(FEB2016). ISSN 1664462X. Dostupné z: doi:10.3389/fpls.2016.00222
4. WALLACE, Luke, Arko LUCIEER, Christopher WATSON a Darren TURNER, 2012. Development of a UAV-LiDAR system with application to forest inventory. Remote Sensing [online]. 4(6), 1519–1543. ISSN 20724292. Dostupné z: doi:10.3390/rs4061519

Předběžný termín:	2020/21 ZS - FLD - SDZ
Konzultant:	Ing. Karel Kuzelka, Ph.D.

Obsah

Seznam obrázků:

Seznam použitých zkratek a symbolů:

3D – Tři Dimenze

ABA – Area Based Approach

ALS – Airborne Laser Scanning

ATZ – Letištní provozní zóna

BS – Base Station

CE – Clark–Evans Index

CHM – Canopy Height Model

CTR – Řízený okrsek letiště

CRP – Close Range Photogrammetry

ČSN – Česká Státní Norma

DBH – Diameter at Breast Height

DSM – Digital Surface Model

DTM – Digital Terain Model

DPZ – Dálkový Průzkum Země

GEDI – Global Ecosystem Dynamics Investigation

GLONAS – Globální Navigační Satelitní Systém

GNSS – Global Navigating Space System

GPS – Global Positin System

IMU – Inertial Measurement Unit

ISS – International Space Station

IWS – Inverse Watershed Segmentation

LiDAR – Light Detection And Ranging

MLS – Mobile Laser Scaning

PPK – Post Processing Kinematics

QSM – Quantitative Structural Models

RANSAC – Random Sample Consensus

RF – Random Forest

RGB – Red Grean Blue

RINEX – Receiver Independent Exchange

RLTS – Robust Least Trimmed Squares

RPAS – Remotely Piloted Aerial System

RTK – Real Time Kinematics

SBET – Smoothed Best Estimated Trajectory

SJTS-K – Systém Jednotné Trigonometrické Sítě Katastrální

SLAM – Simultaneous Localization and Mapping

SPI – Stem Presence Indicator

SW – Software

TLS – Terestrila Laser Scanning

UA – Bezpilotní letadlo

UAS – Unmanned Aerial System

UAV – Unamanned Aerial Vehicle

UCL – Úřad pro Civilní Letectví

ULS – Unmannead aerial Laser Scanning

UTM – Universal Transverse Mercator

VRS – Virtual Refference Station

WGS – World Geodetic System

WLS – Wearable Laser Scanning

1. Úvod

Standardní metody sběru dat o lesních ekosystémech jsou při použití standardních lesnických registračních pomůcek velmi časově náročné. Je nutné jednotlivě přistupovat ke každému individuálnímu stromu a přímo, či nepřímo jednotlivé údaje změřit, nebo odvodit. V posledních několika letech se ovšem naskýtají široké možnosti nepřímého sběru dat, které umožňují najednou pracovat s celými porosty.

Díky dosavadnímu rozvoji počítačového zobrazování a technologie dálkového průzkumu země (DPZ) se v současné době naskýtá nová možnost sběru dat o lesních ekosystémech i individuálních stromech pomocí různých metod DPZ. Využití metod DPZ v oblasti lesnictví se momentálně nachází ve stádiu experimentálního použití pro sběr různých typů dat a jejich následné vyhodnocování. Vzhledem k možnostem katedry hospodářské úpravy lesů je cílem disertační práce využít bezpilotních prostředků nesoucích laserový senzor Light Detection And Ranging (LiDAR) a také metod pozemního laserového skenování, které vytváří velmi podrobná, hustá bodová mračna pro 3D (tři dimenze) zobrazování a modelování lesních porostů s vysokou přesností pouhých několika mm. Pro zmíněnou vysokou přesnost dat je tak, na základě výsledků práce, možné identifikovat jednotlivé nadzemní komponenty (větve) individuálních stromů a detekovat tak jejich pohyb, nebo případně popsat jejich strukturu vzhledem ke klasifikaci dřevin. Hustá 3D bodová mračna pořízená pomocí technologie LiDAR umožňují pomocí níže popsaných metod detekci individuálních stromů a odvození tak jejich výšky a tloušťky ve výčetné výšce.

Technologii LiDAR je ovšem velmi vhodné doplnit fotogrammetrickou metodou 3D modelování porostů lesních dřevin pomocí bezpilotních prostředků nesoucích RGB kameru, případně pomocí metody pozemní fotogrammetrie. Na toto téma byla také zpracována diplomová práce.

V současné době používané souřadnicové systémy vnášejí do zpracování 3D dat určité problémy, které je při jejich použití nutné vzít v úvahu. Jedná se zejména o jejich formát

2. Cíle práce

Cílem práce je prezentovat využití moderních technik laserového skenování pro sběr dat o lesních ekosystémech a také metody fotogrammetrie pro odvozování vybraných stromových charakteristik. Práce prezentuje ucelený přehled doposud publikovaných nejvýznamnějších vědeckých prací se zaměřením na využití technologie LiDAR v lesnictví. Jsou zde prezentovány metody mobilního laserového skenování (MLS), pozemního laserového skenování, bezpilotního laserového skenování (ULS) a leteckého laserového skenování (ALS) včetně představení základních principů fungování jednotlivých technologií. Vzhledem k jednotlivým použitým metodám je zde prezentováno základní odvozování 3D bodových mračen s ohledem na potenciální problémy při sběru dat přes samotnou práci s body až po finální zpracování dat.

S přihlédnutím k formě celé práce bylo vyvozeno několik dílčích cílů.

Cíl 1 – odvodit bodová mračna o vysoké přesnosti a hustotě k získání reprezentativních bodových mračen individuálních stromů na úrovni nadzemních stromových komponent.

Cíl 2 – analyzovat a zhodnotit možnosti vysokého časového i prostorového rozlišení metody ULS.

Cíl 3 – analyzovat a zhodnotit několik vybraných metod pro detekci a delineace individuálních stromů.

Cíl 4 – analyzovat a zhodnotit vybrané metody odvozování tloušťky ve výčetní výšce (DBH) a výšky individuálních stromů z bodových mračen.

3. Rozbor problematiky

3.1. Platformy pro sběr dat

Techniky laserového skenování jsou současní vědního oboru Dálkový průzkum Země (DPZ), který již v současnosti zahrnuje velmi rozsáhlé spektrum technik pro nepřímé zjišťování informací o skutečnostech nacházejících se vně, přímo na, nebo pod Zemským povrchem. Zmíněná data lze získávat rozmanitými způsoby na úrovní pozice senzoru pro nepřímý sběr dat. Sběr dat je možné provádět na úrovni pozemní, nebo za pomoci letících platforem. Letící platformy lze definovat následujícím způsobem:

- Vysoko letící platformy – satelity
- Středně vysoko letící platformy – letadla
- Nízko letící platformy – bezpilotní letadla

Vysoko letící platformy

Jejich využití pro sběr dat nalézá uplatnění zejména pro plošně rozsáhlá území. Kvalita dat je zde ovšem velmi zásadně ovlivňována oblačností v daném území a velmi nízkým rozlišením na 1 m^2. V zahraniční literatuře jsou též označovány jako Spaceborne, tedy z vesmíru.

Středně vysoko letící platformy

Letadla, a proto tedy Airborne jsou využívána pro sběr dat území na úrovni jednotlivých států. Data jsou opět samozřejmě ovlivňována povětrnostními podmínkami, tedy především oblačností, která značně ovlivňuje především fotogrammetrická data zakrytím části dané oblasti. Data pořízená tímto způsobem oproti předchozí úrovni dokážou dosáhnout mnohem většího detailu z pohledu fotogrammetrie, a navíc je zde možné použít více senzorů např. laserové skenery, tedy technologii LiDAR, které ovšem dosahují hustoty pouze několik bodů na 1 m^2.

Nízko letící platformy

Bezpilotní letadla, drony, bezpilotní systémy, unmanned aerial vehicles (UAV), unmanned aerial systems (UAS), remotely piloted aerial systems (RPAS) jsou definována legislativou České Republiky konkrétně dle legislativního dokumentu

Předpis L2 Doplněk X zákona č. 49/1997 Sb. z roku 2014 (Czech Republic 2014) následujícím způsobem:

Autonomní letadlo

Bezpilotní letadlo, které neumožňuje zásah pilota do řízení letu.

Bezpilotní letadlo (UA)

Letadlo určené k provozu bez pilota na palubě.

Bezpilotní systém (UAS)

Systém skládající se z bezpilotního letadla, řídicí stanice a jakéhokoliv dalšího prvku nezbytného k umožnění letu, jako například komunikačního spojení a zařízení pro vypuštění a návrat. Bezpilotních letadel, řídicích stanic nebo zařízení pro vypuštění a návrat může být v rámci bezpilotního systému více.

Model letadla

Letadlo, které není schopné nést člověka na palubě, je používané pro soutěžní, sportovní nebo rekreační účely, není vybaveno žádným zařízením umožňujícím automatický let na zvolené místo, a které, v případě volného modelu, není dálkově řízeno jinak, než za účelem ukončení letu nebo které, v případě dálkově řízeného modelu, je po celou dobu letu pomocí vysílače přímo řízené pilotem v jeho vizuálním dohledu.

Dle výše zmíněného vyplývá, že pro praktické experimentální použití v lesnictví jsou využívány bezpilotní systémy, tedy kombinace UAV a neseného senzoru případně jejich kombinace. Výše zmíněný doplněk se zabývá rozdělením bezpilotních letadel podle váhy:

do 0,91 kg

0,91 kg až 7 kg

7 kg až 20 kg

nad 20 kg

Toto váhové dělení vyplývá především z bezpečnosti použití jednotlivých UAV. Jeho následné zdůvodnění je zřejmé v obrázku č. 1.

Tabulka 1 (viz ust. 16)										
ř.	maximální vzletová hmotnost	≤ 0,91 kg		> 0,91 kg a < 7 kg		7 – 25 kg		> 25 kg		bezpilotní letadlo provozované mimo dohled pilota
-	účel použití ---------- požadavek	rekreačně sportovní	výdělečné, experimentální, výzkumné	rekreačně sportovní	výdělečné, experimentální, výzkumné	rekreačně sportovní	výdělečné, experimentální, výzkumné	rekreačně sportovní	výdělečné, experimentální, výzkumné	
1	evidence letadla	ne	ano	ne	ano	ne	ano	ano	ano	ano
2	evidence pilota	ne	ano	ne	ano	ne	ano	ano	ano	ano
3	praktický a teoretický test pilota	ne	ano	ne	ano	ne	ano	ano	ano	ano
4	povolení k létání	ne	ano	ne	ano	ne	ano	ano	ano	ano
5	povolení k provádění LP a LČPVP	nelze	ano	nelze	ano	nelze	ano	nelze	ano	nelze
6	označení UA: ID štítek / ID štítek + pozn. značka	ne / ne	ano / ano	ano / ne	ano / ano	ano / ne	ano / ano	ano / ne	ano / ano	ano / ano
7	min. ve vzdálenosti (m): vzlet, přistání / osoby, stavby / osídlený prostor	bezpečná	bezpečná	bezpečná	bezpečná	bezpečná, ale minimálně 50/100/150	bezpečná, ale minimálně 50/100/150	bezpečná, ale minimálně 50/100/150	bezpečná, ale minimálně 50/100/150	bezpečná, ale minimálně 50/100/150
8	pojištění: běžný provoz / LVV (mil. Kč)	ne / 0,25	dle nař. č. 785/2004[1]	ne / 1	dle nař. č. 785/2004[1]	ne / 3 od 20 kg dle nař. č. 785/2004 [1]	dle nař. č. 785/2004[1]	dle nař. č. 785/2004[1]	dle nař. č. 785/2004[1]	dle nař. č. 785/2004[1]
9	dozor	ne	ne	ne	ne	ne	ne	ano	ano	ne
10	„failsafe“ systém	ne	ano	ano	ano	ano	ano	ano	ano	ano
11	provozní příručka UAS	ne	ano	ne	ano	ne	ano	ne	ano	ne
12	hlášení událostí	ne	ano	ne	ano	ne	ano	ano	ano	ano

Obrázek 1 – Odkaz na ustanovení č. 16 Z (Předpis L2 Doplněk X zákona č. 49/1997 Sb.)

ČSN 31 0001 (HRUŠKA a SVITÁK 2007) definuje bezpilotní letadlo následujícím způsobem: letadlo způsobilé létat bez pilota, které je za letu řízené automatickým zařízením, nebo dálkově ze země.

Nízkoletící platformy UAV je také možné rozdělit dle způsobu letu. Některé UAV využívají pro svůj let pouze vrtule vzhledem k absenci nosných ploch křídel a jsou proto nazývány koptry neboli multirotorová zařízení. Koptr je tedy označení pro vrtulník nebo vrtulové zařízení bez křídla. Dle počtu vrtulí lze potom slovo koptr doplnit příslušnou předponou pro přesné označení multirotorového stroje typu koptr.

Trikoptr – 3 vrtule
Kvadrikoptr – 4 vrtule
Hexakoptr – 6 vrtulí
Oktakoptr – 8vrtulí

Pro názorné uspořádání jednotlivých ramen nesoucích vrtule daného typu koptru slouží obrázek č. 2. U jednotlivých vrtulí je zvýrazněný i směr jejich rotace. Je zde zřetelné, že vrtule se netočí všechny stejným směrem, proto jsou označovány jako vrtule protisměrné.

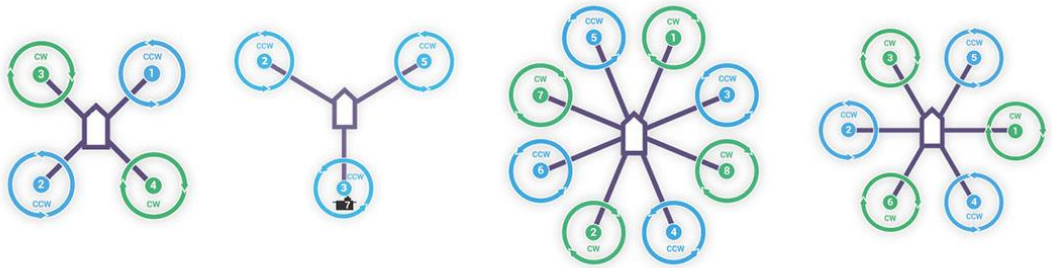

Obrázek 2 – Uspořádání vrtulí, u nichž je specifikovaný směr otáčení dané vrtule CW – clock wise (po směru hodinových ručiček) a CCQ – counter clock wise (proti směru hodinových ručiček), dostupné z: https://www.droni.cz/wp-content/

Obrovskou nevýhodou je okamžitý pád, který nastává při zastavení vrtulí umožňujících koptru let. Ovšem velkou výhodou je možnost zastavení letadla ve vzduchu a také možnost letu při předem definované rychlosti v řádech jednotek m/s. Ty dvě výhody jsou velmi cenné pro sběr leteckých fotografií ve vysokém rozlišení a dalších dat, jakými mohou být nejen snímky z termokamery, ale i multi či hyper spektrální snímky, bodová mračna získaná pomocí technologie LiDAR a další.

Možnost nastavení rychlosti letu koptru je fundamentálním základem pro získání dat s dostatečným překryvem mezi jednotlivými přelety (Dandois a Ellis 2013).

Druhou kategorií jsou tedy bezpilotní letadlo s křídly. Tato letadla jsou také poháněna k letu vrtulí, ale po zastavení vrtule nedojde k okamžitému pádu k zemi z důvodu nosných ploch křídel. Nevýhodou je, že takovýto bezpilotní letadlo není schopen ve vzduchu zastavit a letí vyšší rychlostí, proto jsou křídla využívána ke sběru dat o územích s větší rozlohou, než na kterých jsou běžně nasazovány koptry (Puliti et al. 2015).

Z obrázku č. 1 také vyplývají následující legislativní omezení pro výzkumné činnosti:

- Je nutné provést registraci UAV
- Je nutné provést registraci pilota, který podléhá zkouškám
- Je nutné provést zkoušky UAV, a to musí být opatřeno systémem failsave
- Pro každé UAV musí být zpracována provozní příručka podléhající nařízení UCL (Úřad pro Civilní Letectví)

Systém failsave není přesně definovaný legislativou České republiky, nýbrž je však definováno, co by takový systém měl být schopen provádět za aktivity při letu. Musí kontrolovat kapacitu baterie a při dosáhnutí kritické kapacity být schopen návratu na definovaný domovský bod (Home Point) pomocí GNSS modulu v rámci předletové přípravy. V případě koptru musí být UAV schopno za letu zastavit a provádět úhybné manévry pro případ střetu s dalšími letící objekty. V případě křídla je předpokládána možnost náhlé změny směru letu nejčastěji prudkým klesáním, nebo stoupáním.

Dále je nutné dle (Předpis L2 Doplněk X zákona č. 49/1997 Sb.) dodržovat zejména minimální horizontální bezpečnou vzdálenost 50 m od lidí a 100 m od budov. V provozní příručce každého UAV je zároveň i detailně popsána předletová příprava a také kroky po samotném ukončení letu. Maximální letová hladina je definována maximální výškou nad zemí 300 m mimo prostory ATZ (letištní provozní zóna), případně CTR (řízený okrsek letiště). Zóny letišť jsou zřetelné na obrázcích č 3 a č. 4.

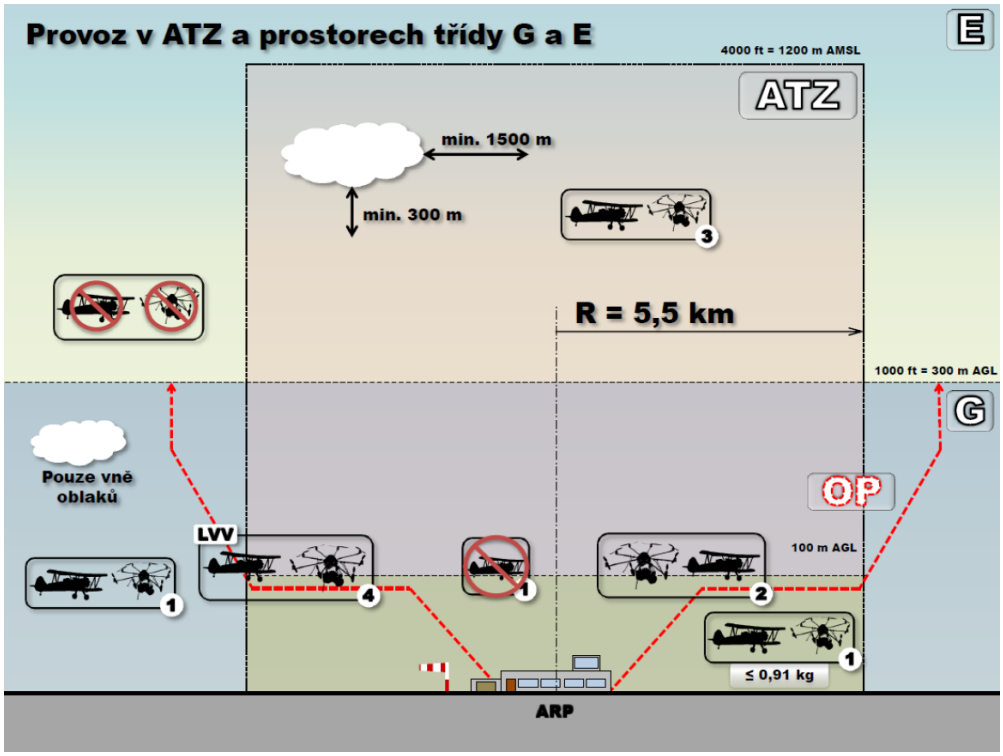

Obrázek 3 – Provoz v letištní provozní zóně – ATZ z (Předpis L2 Doplněk X zákona č. 49/1997 Sb.)

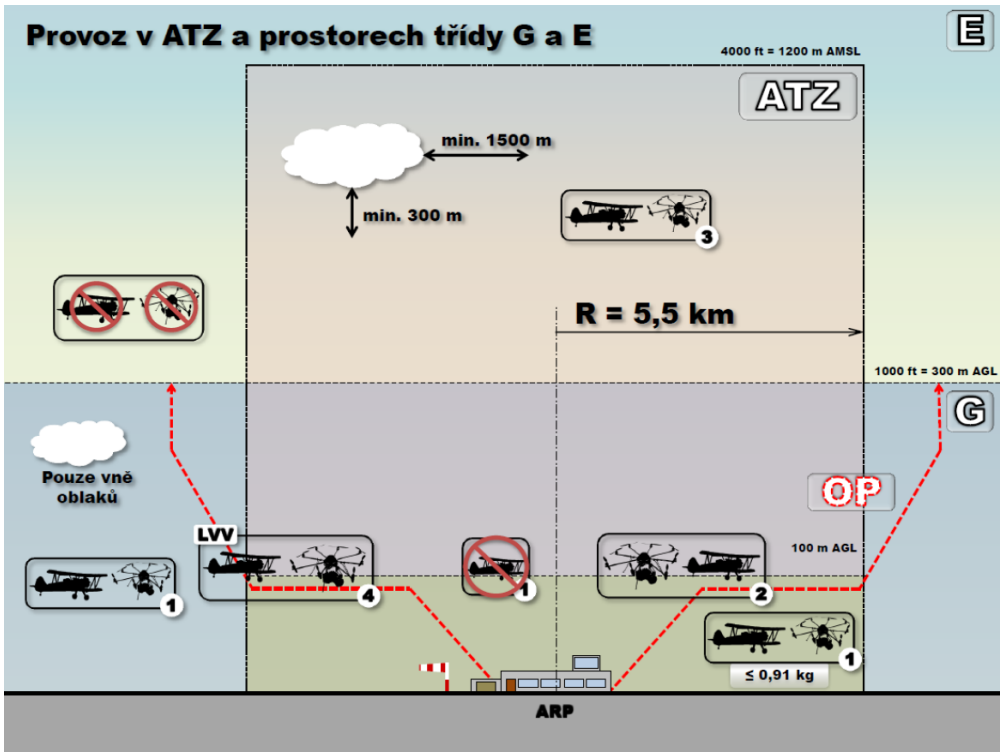

Obrázek 4 – Provoz v řízeném okrsku letiště – CTR z (Předpis L2 Doplněk X zákona č. 49/1997 Sb.)

Terestrické metody

Sběr dat pomocí prostředků DPZ nemusí probíhat nutně jen za pomoci letících platforem, ale lze využít i metod pozemních, kdy je senzor nesen člověkem, nebo upraveným jiným zařízením jako například automobil, stativ atd. Lze tak provádět sběr dat z jednoho či více stanovisek rotací podél svislé osy, nebo procházením / projížděním po cílovém prostoru s účelem sběru dat pro nepřímé měření požadovaných údajů. Jednotlivá konkrétní využití jsou prezentována v podkapitole 3.3.4.

Tyto metody jsou nejvhodnější pro rekonstrukci kmenových partií a zejména pro odhad DBH (Diameter at Breast Height), tedy tloušťky ve výčetní výšce, především pro možnost tvorby hustého bodového mračna a velmi přesné možnosti jejich georeferencování (Liang et al. 2016; 2018).

3.2. Principy fungování technologie LiDAR

Počátky využívání technologie LiDAR sahají do počátku šedesátých let dvacátého století při vojenském využití se zaměřením na detekci ponorek z letadel, jednalo se tedy o počátky ALS (Maltamo et al. 2014).

Princip fungování laserového skenování tkví v principu měření času od vypuštění laserového paprsku jeho zdrojem po návrat na přijímač odraženého světelného paprsku s vlnovou délkou mezi 600 - 1550nm od povrchu skenovaného objektu. Pro výpočet vzdálenosti mezi bodem, od kterého byl odražen laserový paprsek a laserovým skener lze odvodit jednoduchý, obecně známý vzorec (1) (Maltamo et al. 2014):

$$s = \frac{(c \times t)}{2} \tag{1}$$

kdy s je rovno vzdálenosti bodu od laserového skeneru, c je konstanta udávající rychlost světla a t je rovno času od vyslání do přijmutí laserového paprsku.

Tento vzorec je platný za předpokladu známé rychlosti světla, která činí 299 792 458 m s^{-1}, tedy přibližně 0,3 m ns^{-1} a přesně změřené doby letu laserového

paprsku od jeho zdroje, přes odražení od povrchu cíle až po jeho dopad na přijímač s přesností menší než 1 ns (Maltamo et al. 2014).

Zmíněným způsobem je vypočítána pouze vzdálenost bodu od laserového skeneru, ovšem není determinována jeho pozice v prostoru. Pro přesný výpočet pozice bodu v prostoru je nutné také znát úhel směru vyslaného laserového paprsku a přesnou pozici laserového skeneru v prostoru.

Přesnou pozici laserového skeneru v prostoru vypočítá jeho IMU (Inertial Measurement Unit) s pomocí GNSS (Global Navigation Space System) přijímače, přesněji řečeno přepočtem své pozice od pozice antény GNSS přijímače (RIEGL 2019b). Přesnost GNSS modulu lze zvýšit použitím RTK (Real Time Kinematics) GPS (Global Positioning System). Přepočtem pozice z GNSS modulu a informací z přijímače na laserovém skeneru lze získat 3D (troj dimenzionální) digitální mračno bodů – point cloud, které je přesně georeferencováno, tedy každý bod bodového mračna má vypočítanou svou přesnou pozici na zemském povrchu dle definovaného koordinačního systému.

3.3. Využití technologie LiDAR v lesnictví

Laserové skenování v lesnictví představuje v současné době jednu z vrcholných technologií pro sběr dat o lesních ekosystémech na úrovni jednotlivých komponent individuálních, přes úroveň porostní až po úroveň celých lesních komplexů či dokonce celých států. Finanční náročnost, časová náročnost a požadovaná přesnost jsou závislé proměnné, se kterými je nutné počítat při přípravě sběru dat pomocí technologie LiDAR, tedy laserového skenování (Mweresa et al. 2017).

Čím větší detail je požadován, tím hustší bodové mračno na 1 m^2 porostní plochy je třeba odvodit. Metody terestriální v současnosti dosahují největší hustoty bodových mračen v této oblasti.

První pokusy o odvození kmenových profilů a kompletní struktury individuálních stromů na základě bodových mračen pořízených pomocí technologie LiDAR prezentoval ve své práci Solodukhin (Solodukhin et al. 1976). Pro experiment bylo vybráno několik vzorníků smrku ztepilého (*Picea abies L.*), které byly po skácení dále uchyceny do speciálních držáků v horizontální poloze. Dále byly tyto vzorníky oskenovány pomocí laserového skeneru, jenž musel být vzhledem ke své hmotnosti upevněn na hydraulické rameno jeřábu. Bohužel vzhledem k umístění individuálních

stromů v horizontální poloze nebyla získaná bodová mračna dostatečně reprezentativní z důvodu ohybu větví. Ovšem kmenové profily byly odvozeny úspěšně.

3.3.1. Satelitní laserové skenování

Velmi významným počinem je zařazení LiDAR modulu do mezinárodní kosmické stanice ISS (International Space Station) během listopadu roku 2018 na dvouletou misi s názvem GEDI (Global Ecosystem Dynamics Investigation). Cílem GEDI je provádět skenování celého zemského povrchu v zeměpisné délce do 22° od rovníku směrem k oběma pólům Země a každých 500 m provést skenování na ploše o průměru 25 m. Na ploše je měřena výška vegetace, odhad nadzemní biomasy, vertikální struktura a nadmořská výška. To vše se zaměřením pouze na lesní ekosystémy (Lee et al. 2018; Qi a Dubayah 2016). Modul GEDI tak reprezentuje vysoko letící platformy v rámci laserového skenování.

3.3.2. Letecké laserové skenování – Airborne Laser Scanning (ALS)

Laserové skenování pomocí technologie LiDAR nesené na letadlech je využíváno pro rozsáhlá území. V současnosti však dosahuje hustoty jen několika desítek bodů na 1 m^2 v závislosti na prostředí, letové hladině a konfiguraci skeneru. Toto použití vyžaduje rozsáhlé finanční a technologické zázemí podpořené kvalitní infrastrukturou, tedy letišti vhodnými ke startu letadel nesoucích laserový skener (Morsdorf et al. 2009).

Přímým využitím je odvozování modelů DTM (Digital Terain Model) a DSM (Digital Surface Model) pro odvozování CHM (Canopy Height Medel) zjištěním rozdílu mezi nimi (Morsdorf et al. 2009) dle rovnice (2), kterou popisuje například (Panagiotidis et al. 2017) ve své práci:

$$DSM - DTM = CHM \tag{2}$$

Nicméně velmi nízká hustota bodových mračen vede pouze k omezené možnosti jejich zhodnocení na úrovni individuálních stromů. Pro tuto možnost je třeba využít metody ULS, TLS či MLS (Brede et al. 2017).

Mezi nejvýznamnější autory v oblasti ASL patří Næsset (Næsset 2002; Næsset a Gobakken 2005; Næsset et al. 2011) se svým přínosem area based approach (ABA),

založeným na principu odvozování porostních charakteristik z ALS dat pomocí pozemních kalibračních ploch na základě CHM. Dalším významným autorem je Socha (Socha et al. 2017; 2020), který se zaměřuje především na kalibraci ABA pomocí alometrických modelů a následné odvozování bonifikace jednotlivých porostů.

3.3.3. Laserové skenování pomocí UAV – UAV Laser Scanning (ULS)

Tato metoda se dle dostupné literatury jeví jako časově nejméně náročná při možnosti nepřímého sběru dat na úrovni porostu či jednotlivých individuálních stromů ba dokonce i jednotlivých stromových komponent – větví. Základem úspěšného odhadu stromových veličin (výška, tloušťka, horizontální průmět koruny, atd.), které je již možné odhadnout pomocí technologie UAV (Díaz-Varela et al. 2015; Panagiotidis et al. 2017; Brede et al. 2017; Wieser et al. 2017), je odvození kvalitního a reprezentativního bodového mračna, z něhož je fundamentálním základem odvodit, vyinterpolovat či klasifikovat digitální model terénu DTM.

DTM získaný z digitálního mračna bodů odvozeného pomocí metod letecké fotogrammetrie pomocí interpolace značně ovlivňuje a lze říci, že vnáší jistou chybu do dalších výpočtů pro nepřímý odhad stromových veličin. Děje se tak především z důvodu zakrývání zemského povrchu korunami stromů a důsledkem jsou chybějící informace o zakrytém prostoru. Výsledný DTM je tak tedy pouze interpolací mezi místy viditelnými z UAV a proto není dostatečně reprezentativní pro odhad především výšek jednotlivých individuálních stromů (Panagiotidis et al. 2017).

Díky multiodrazovým laserovým skenerům lze eliminovat výše popsaný problém letecké fotogrammetrie, kdy jako body terénu jsou brány poslední odrazy zaznamenané laserovým skenerem (Brede et al. 2017; Wieser et al. 2017), nebo lze body ležící na terénu matematicky klasifikovat.

Jako prvního průkopníka využívání UAS lze považovat Jaakkolu (Jaakkola et al. 2010), který sestrojil první UAV Sensei nesoucí laserový skener pro Finský Geodetický Institut. Sensei nesl profilový laserový skener Ibeo Lux and Sick LMS151, jenž vyprodukoval bodová mračna o hustotě 100–1500 bodů na m^2 a mohl tak být využit pro detekci jednotlivých individuálních stromů. Dalším významným autorem je Wallace (Wallace et al. 2012), který využil stejný skener jako (Jaakkola et al. 2010) ovšem na plantážích eukalyptu pro odhad DTM a výšky individuálních stromů při využití automatizovaných hodnoticích technik. (Wallace et al. 2012) popsal vývoj

výše zmíněného skeneru, a dále v roce 2016 (spolu s kolegou z katedry HUL Petrem Vopěnkou) zanalyzovali srovnání s fotogrammetrickými bodovými mračny (Wallace et al. 2016). Neméně zajímavý je počin Kaňuka (Kaňuk et al. 2018), který využil skener VUX-1 na UAV se spalovacím motorem pro tvorbu DTM a kontrolu kolejí i s detekcí drážních elektrických rozvodů, kdy byly detekovány jednotlivé dráty vysokého napětí. Vysokou přesnost a rozlišení zmíněného laserového skeneru potvrzuje například také (Chen et al. 2018) ve své práci při hodnocení stavu elektrické rozvodné sítě vysokého napětí. Tyto dvě poslední zmíněné studie jsou zmíněny zejména z důvodu demonstrace přesnosti daného laserového skeneru pro schopnost zachytit jednotlivé dráty elektrické rozvodné sítě.

Aktuálně jsou však dostupné pouze dvě studie zabývající se využitím UAS VUX-SYS v lesnictví. Obě dvě využívají jako referenční metodu využití pozemního laserového skeneru RIEGL VZ-400 TLS pro odhad tloušťky ve výškách 0.8, 1.3 a 1.8 m od paty kmene a výšky jednotlivých individuálních stromů.

První studií je (Brede et al. 2017) který georeferencoval bodová mračna pomocí pozemních kontrolních bodů, jež daly dále možnost kombinace obou bodových mračen. Metoda TLS byla použita jako metoda referenční. Byla standardně odvozena (dle možností software dodávaného společností Riegl) bodová mračna, ze kterých byly následně odvozeny modely DTM, DSM a CHM pro měření výšek jednotlivých individuálních stromů. Z bodových mračen byly manuálně vybrány dolní kmenové partie pro odhad výše zmíněných tlouštěk. V závislosti na druhu dřeviny dosahovala bodová mračna hustoty od 10^1 až po 10^6 bodů na 1 m^2. Z výsledků studie vyplývá vhodnost kombinování obou metod ULS a TLS. Metoda ULS lépe detekovala vrcholky jednotlivých individuálních stromů a pro odhad DBH se jevila jako dostačující. Oproti tomu metoda TLS lépe zobrazila dolní kmenové partie a při rekonstrukci korunových partií jednotlivých individuálních stromů, především těch nejvyšších, vykazovala jisté nedostatky.

Druhou studií zabývající se použitím UAS VUX-SYS v lesnictví je studie (Wieser et al. 2017) s cílem opět odhadnout DBH na vybraných zkusných plochách lužních porostů při podmínkách leafs of, tedy bez olistění. Ve studii je popsán způsob fitování válců na kmeny jednotlivých individuálních stromů ve výšce 0,8 až 1,8 m od paty kmene. Při porovnávání TLS a ULS byla zjištěna vhodnost využití TLS

pro stromy o tloušťce do 30 cm a také využití pro zobrazení kmenových partií stromů s křivým kmenem, jako na příklad *salix sp.* Využití ULS pro zobrazování jednotlivých individuálních stromů bylo doporučeno v nižších výškách pro možnost získání hustších digitálních bodových mračen a pro stromy o tloušťkách vyšších než 30 cm s přímým kmenem.

Významnou prací využívající ULS data pro sběr dat a porovnávající jednotlivé metody delineace a jejich vzájemným porovnáním je práce (Liu et al. 2018), kde jsou porovnávány metod IWS, convex hull a k-Nearest Neighbors použité při delineace bodových mračen individuálních stromů.

3.3.4. Pozemní laserové skenování

Pozemní laserové skenování lze vzhledem k použité „platformě" rozdělit na dvě základní kategorie, kterými jsou statické laserové skenování a mobilní laserové skenování. Použité platformy v tomto případě jsou stativ (tripod, trojnožka) u metody TLS a vozidlo případně i člověk u metody MLS.

Statické laserové skenování – Terestrial Laser Scanning (TLS)

Metoda pozemního laserového skenování TLS při využití pro sběr dat o lesních ekosystémech je velmi náročná z pohledu časové i finanční náročnosti (Liang et al. 2016; Čerňava et al. 2017). Tuto metodu lze však využít pro velmi kvalitní zobrazování zejména dolních kmenových partií. Je však nutné postavit laserový skener na několik stanovisek pro oskenování celého zájmového prostoru, aby tak bylo zabráněno zastínění, a tak možnému úplnému vynechání individuálních stromů z bodového mračna. Bodové mračno tak dosahuje největší hustotu v blízkosti skeneru (Brede et al. 2017).

Počátky využití TLS ke sběru dat o lesních ekosystémech lze zařadit okolo roku 2000. Tyto studie byly zaměřeny především na popis možností této metody (Pfeifer et al. 2004; Simonse et al. 2003). Dále byla metoda TLS využita pro možnost determinace několika stromových atributů/veličin, které nejsou jednoduše odvoditelné při použití konvenčních lesnických měřičských pomůcek, jako je například zakřivení kmene (Liang et al. 2014). Odhady objemu individuálních stromů, či celých porostů s porovnáním s lokálními alometrickými modely byly později prezentovány

ve studiích (Yu et al. 2013; Kankare et al. 2013; Astrup et al. 2014). Nicméně významné rozdíly v použitém vybavení, struktuře lesních porostů, hodnotících kritérií a celkových postupů ve zmíněných studiích dělají zhodnocení metody TLS pro sběr inventarizačních dat velmi náročné. Velmi významným kritériem v některých studiích označovaným až za fundamentální kritérium (Astrup et al. 2014; Liang et al. 2018), bylo využití tzv. multi-scan data aproach, tedy sběru dat na základě několika stanovišť na úrovni plochy či porostu, což zapříčinilo zvýšení detekce individuálních stromů z 20% na celkových 100% (Yao et al. 2011; Olofsson et al. 2014; Liang et al. 2018)

Metoda TLS je v současné době považována za geometricky nejpřesnější metodu pro sběr dat o lesních ekosystémech na úrovni zkusné plochy (Liang et al. 2016; 2018; Hyyppä et al. 2020b; 2020a), které je využíváno pro inventarizační sběr dat (Liang et al. 2016; 2018), nebo také například pro odvozování kvantitativních strukturálních modelů (QSM) (Lau et al. 2018). Metoda TLS je ale také mnohdy používána jako referenční metoda (Wieser et al. 2017; Brede et al. 2017) při hodnoceních dalších metod DPZ jako například ULS či MLS.

Mobilní laserové skenování – Mobile Laser Scanning (MLS)

Metoda MLS je v současné době nejméně využívaným způsobem pro sběr dat o lesních ekosystémech v porovnání s výše zmíněnými metodami. Doposud existuje jen několik málo studií zabývajících se využitím MLS v lesnictví. Mezi nejvýznamnější studie patří Bauwens zabývající se porovnáním TLS a ručního MLS (Bauwens et al. 2016), Bienert porovnání TLS a MLS (Bienert et al. 2018), Cabo porovnávající TLS a ruční MLS (Cabo et al. 2018), Liang porovnávající TLS, ULS a MLS (Liang et al. 2019) a Hyyppä porovnávající ve svých dvou studiích ruční MLS, MLS systém v batohu a ULS (Hyyppä et al. 2020b).

Pro eliminaci časové náročnosti přenášení pozemního laserového skeneru při metodě TLS lze využít metodu mobilního laserového skenování MLS, kterou například v našich zeměpisných podmínkách popisuje (Čerňava et al. 2017), který osadil laserový skener VMX-250 společnosti Riegl na kolový traktor Zetor Horal 7245. Celá studie se zabývá odhadem DBH z digitálních mračen bodů. Pro konkrétní odhady DBH individuálních stromů byl použit software DendroCloud, vyvinutý Milanem Koreněm a jeho využití je popsáno v publikacích (Koreň et al. 2015; 2017).

Bauwens (Bauwens et al. 2016) porovnává ve své studii ruční MLS se dvěma přístupy ke sběru dat pomocí TLS, tedy pouze jeden sken anebo kombinaci více skenů k odhadu DBH. Pro sběr dat pomocí TLS byl použit skener FARO Focus 3 D 120 (FARO, 250 Technology Park Lake Mary, FL 32746, United States) a pro MLS ZEB1 2D skener fungující na principu Simultaneous Localization and Mapping (SLAM). Oba dva zmíněné skenery dosahovaly stejné vlnové délky 905 nm. Nejlepší výsledků bylo dosaženo u kombinace více skenů z TLS. U MLS bylo dosaženo RMSE 1.11 cm při odhadu DBH při detekci 91 % stromů.

Bienert (Bienert et al. 2018) porovnává data z MLS a TLS s ohledem na automatické odvozování QSM a standardních inventarizačních hodnot (DBH a výška). Výsledky pro odvozování DBH a výšky byly obdobné jako u ostatních autorů, avšak vzhledem k dosavadním přesnostem a rozlišení MLS byla tato metoda, zatím, shledána jako nevhodná pro odvozování QSM.

Cabo (Cabo et al. 2018) se ve své studii zabývá porovnání TLS a tzv. wearable laser scanning (WLS) což je opět ruční MLS. Jedná se tedy pouze o změnu terminologie. Opět bylo porovnání provedeno na úrovni odvozování DBH a výšky individuálních stromů z bodových mračen. Výsledkem bylo porovnání přesnosti obou metod na základě statistických metod. Dále byl řešen vliv rozdílu hustoty bodových mračen pro odvozování DBH, který nebyl prokázán. Nicméně bylo prokázáno, že MLS/WLS metoda podhodnocuje výšky individuálních stromů vzhledem k nízké hustotě bodů v horních partiích bodových mračen.

Liang (Liang et al. 2019) porovnává TLS, ULS MLS a tzv. PLS (laserový skener umístěný na zádech „v batohu“) vzhledem k hustotě porostu rozděleného do tří kategorií pro detekci individuálních stromů a z jejich bodových mračen opětovné odvození DBH a výšky. Metoda MLS byla zhodnocena v porovnání se třemi dalšími metodami jako nejméně úspěšná v detekci individuálních stromů a odvozování jejich parametrů.

Hyyppä ve své studii (Hyyppä et al. 2020b) porovnává vlastní prototyp modifikovaného MLS SLAM s Riegl VUX- 1HA MLS pro odvozování kmenových profilů a výpočtu objemu stojících individuálních stromů. Použitý postup vedl k detekci 100 % individuálních stromů na zkusných plochách. Přesnost odhadu objemů individuálních stromů z dat pořízených pomocí MLS byla srovnatelná s daty

z TLS. Dále byly výsledky úspěšně porovnány s Finským alometrickým modelem používaným k výpočtu objemu individuálních stromů. Výzkum dokázal významnost detekce křivosti podél kmenových profilů pro zpřesnění výpočtu odhadu objemu individuálních stromů.

3.4. Souřadnicové systémy

Pro přesné georeferencování bodových mračen je nutné vzít v úvahu metodu, jakou budou dále získaná data zpracována a podle toho zvolit vhodný souřadnicový systém. Každé bodové mračno je nejprve odvozeno v lokálním souřadnicovém systému a dále je až při exportování dat nutné vybrat vhodný souřadnicový systém. Pro zjednodušení práce s databázemi souřadnicových systémů má každý z nich přiřazeno unikátní číslo převzaté z databáze EPSG. EPSG je zkratka European Petroleum Survey Group, tedy společnosti zabývající se mapováním naftových polí, která v rámci zjednodušení práce se souřadnicovými systémy každému z nich přiřadila unikátní číslo (Megies et al. 2011).

Mapová zobrazení jsou používána k zobrazení zemského 3D povrchu na plochu vzhledem k použitým matematicko-geometrickým metodám. Z tohoto důvodu je nutné zobrazit sférický nebo lépe elipsoidní povrch na odvoditelný povrch, jenž může být protnut řezy a zobrazen tak na plochu pomocí metod kuželového, válcového (transverzálního), nebo azimutálního zobrazení, viz obrázek č. 5 (Janssen 2009).

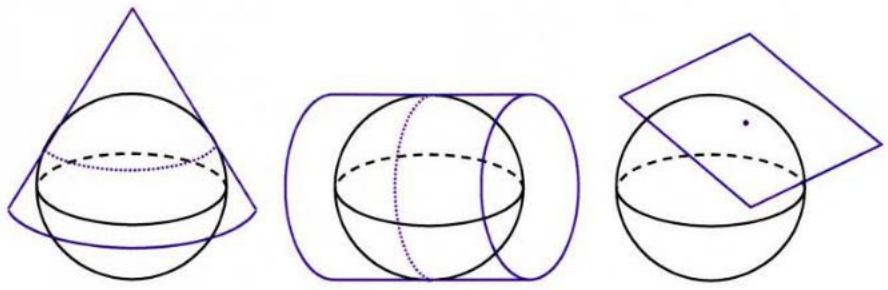

Obrázek 5 – Kuželové, válcové (transversální) a úhlové zobrazení (Janssen 2009)

V této části budou prezentovány tři souřadnicové systémy. Prvním je lokální souřadnicový systém České republiky SJTS-K. Dalšími dvěma jsou mezinárodní souřadnicové systémy WGS 84 a UTM.

Souřadnicový systém Jednotné sítě trigonometrické a katastrální – SJTS-K

SJTS-K je vítězný návrh Ing. Josefa Křováka z roku 1922 (Buchar a Hojovec 2020) používaný v České republice dodnes. Jedná se o konformní kuželové zobrazení s jedinou souřadnicovou soustavou a minimálními deformacemi, jež bylo odvozeno pro tehdejší uspořádání státu. Je však nutné podotknout, že se jedná o souřadnicový systém s lokálním charakterem, který není vhodný pro mapy mezinárodního charakteru (Surový et al. 2019).

Pro zobrazení bylo použito tak zvané dvojité konformní kuželové zobrazení v obecné poloze. U konformního zobrazení dochází ke zkreslení ploch a délek, ovšem nikoli úhlů (Cimbálník a Mervart 1997). Osy v souřadnicovém systému SJTS-K mají atypickou orientaci, tedy osa X je orientovaná na jih a osa Y na západ. Hodnota souřadnice na ose X je vždy vyšší, než na ose Y. Standardně je v aplikacích geografických informačních systémů (GIS) používáno Křovákovo zobrazení s EPSG kódem 5514 případně 5221 s označením Easth North vzhledem k nutnosti korekce souřadnic. Problematika zobrazení a os je demonstrována na obrázku č. 6 z publikace (Surový et al. 2019).

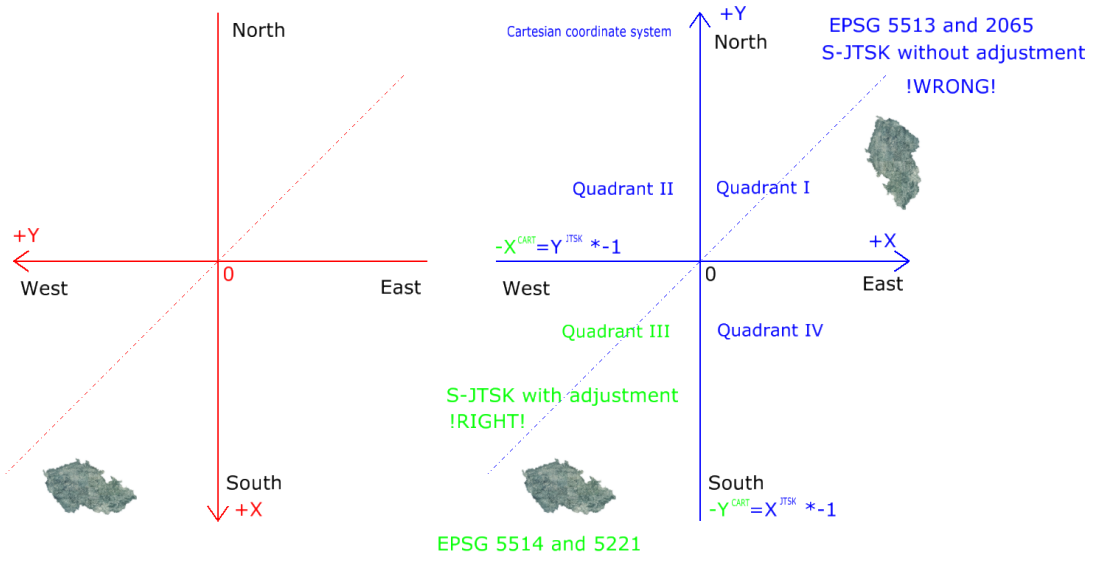

Obrázek 6 – Křovákovo zobrazení (Surový et al. 2019)

World Geodetic System 1984 – WGS 84

Vývoj GNSS položil základy vývoje konceptu globálního souřadnicového systému vzhledem k nutnosti porovnání pozice z GNSS a doposud existujících map (Boucher a Altamimi 2001).

Vzhledem k neustálému pohybu zemských desek se souřadnice bodů na zemském povrchu v tomto souřadnicovém systému neustále mění. V tomto systému jsou používány souřadnice GPS přijímačů, které jsou dále zaznamenávány v podobě zeměpisné délky, šířky a výšky nad referenčním elipsoidem (Surový et al. 2019). Jako referenční plocha je použit elipsoid WGS84 s počátkem souřadnicového systému v těžišti Země (Buchar a Hojovec 2020; Cimbálník a Mervart 1997). Data ve WGS 84 nemají standardní povahu souřadnic pro hodnoty os X, Y a Z, nýbrž dva úhly a výšku nad konstitučním geoidem používaným ve WGS 84 formou Easting Northing a Headding.

Universal Transverse Mercator – UTM

Geocentrický globální souřadnicový systém WGS 84 lze také zobrazit pomocí různých zobrazení. UTM je jeho tak zvanou geografickou transverzální mercator projekcí. Jedná se tedy o konformní (nezkreslující úhly) válcové zobrazení. Jednotlivé poledníkové pásy se zobrazují samostatně, viz obrázek č. 7. Jednotlivé pásy jsou 6° široké. Obecně se mohou vyskytovat záporné souřadnice X a Y. Z tohoto důvodu je k souřadnici X připočítávána konstanta 500 km a k souřadnici Y konstanta 10 000 km. Tímto způsobem vznikla soustava šedesáti poledníkových pásů, viz obrázek č. 7. Dále vzhledem k jednotlivým polokoulím jsou pásy rozděleny na jižní – S (South) a severní – N (North) zóny. Česká republika se nachází primárně v zóně 33N. V zóně 34N se nalézá jen Ostrava a východní část Slezska (Buchar a Hojovec 2020; Cimbálník a Mervart 1997; Surový et al. 2019).

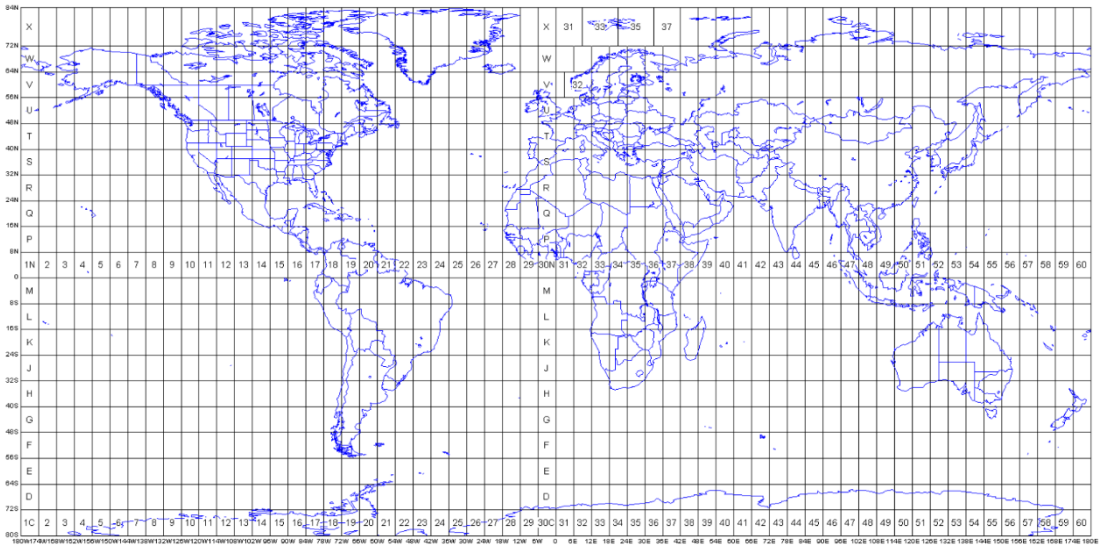

Obrázek 7 – UTM zóny (http://www.dmap.co.uk/utmworld.htm)

Z výše zmíněného vyplývá, že nejvhodnějším souřadnicovým systémem pro georeferencování bodových mračen je souřadnicový systém UTM 33N (EPSG 32633) případně UTM 34N (EPSG 32634) pro potřeby zpracování dat v rámci České republiky. V souřadnicovém systému SJTS – K lze pracovat také, ovšem je potřeba provést dodatečnou souřadnicovou transformaci souřadnic jednotlivých bodů z důvodu jeho pouze lokálního významu, a tak jej nepodporuje velká část komerčně dostupných SW. Standardní WGS 84 není vhodný především z důvodu absence kartézských souřadnic jednotlivých bodů bodového mračna (jsou udávány dva úhly a výška, jak bylo zmíněno výše).

4. Metodika

V této kapitolu jsou představeny jednotlivé použité senzory včetně popsání postupů jejich použití pro sběr dat o lesních ekosystémech. Dále zde jsou popsány metody odvozování bodových mračen, jejich georeferencování a následné zpracování dat pro odvozování konkrétních informací.

4.1. Sběr dat a jejich pre-processing

V této podkapitole jsou popsány způsoby sběru dat včetně příslušných senzorů a zásad jejich užívání. Dále je zde popsán použitý SW k odvozování bodových mračen tedy data pre-processing.

4.1.1. VUX-SYS

Pro zpracování této práce byl ke sběru dat použit UAS VUX-SYS od Rakouské společnosti Riegl sídlící ve městě Horn. Celý UAS se skládá z (RIEGL 2019b):

- RIEGL VUX-1UAV senzoru LiDAR + IMU/GNSS systému
- AP20 kontrolní jednotka
- GPS/GLONASS přijímače
- UAV RiCOPTER

VUX-SYS je speciálně vyvinut a designován, aby byl jednoduše instalován a přizpůsobován uživatelem. Je tím myšlena integrace na různé typy nosičů, ale i možnost kalibrace a úprava přepočtových matic pozice skeneru.

VUX-1UAV skener se záběrem 330º váží sám o sobě 4.2 kg a kontrolní jednotka váží dalších 0,9 kg, celkem je tedy UAV zatíženo 5.1 kg. Mezi klíčové vlastnosti patří maximální vzdálenost od skenovaného objektu 920 m a minimální vzdálenost 3 m při zachování přesnosti 10 mm a správnosti 5 mm. Frekvence skenovacích paprsků dosahuje 550 kHz s rychlostí 200 skenů s^{-1}. Skener je schopen zpracovat až 11 odrazů.

Kontrolní jednotka AP20 slouží ke komunikaci UAV RiCOPTER s GNSS. Při skenování pomocí UAV je kontrolní jednotka AP20 integrována přímo v těle UAV RiCOPTER.

GPS/GLONASS přijímače – GNSS přijímače jsou přímo spojeny s kontrolní jednotkou AP20, která dále přerozděluje GNSS informace do UAV a skeneru. Přesnost přijímače dosahuje v horizontálním směru přesnost méně než 0.05m a ve vertikálním směru méně než 0.1 m. Od antény GNSS přijímače je vždy nutné znát vzdálenost ve všech třech rovinách tedy změnu souřadnic Δx, Δy a Δz, protože veškeré údaje o pozici jsou přepočítávány vzhledem k pozici antény v korekční matici přímo v nastavení skeneru. Tuto vlastnost lze považovat za velmi zásadní pro univerzálnost použití skeneru VUX-1UAV.

RiCOPTER je multirotorové zařízení osazené 8 rotory na čtyřech ramenech s celkovou maximální vzletovou hmotností 24.99 kg. Rotory jsou osazeny vrtulemi z uhlíkových vláken o rozměrech 27“ × 8,8“ nebo 28“ × 9.2“ v závislosti na teplotě okolí a tlaku vzduchu. Pro zvýšení bezpečnosti a zamezení ztráty kontroly je UAV RiCOPTER osazeno zdvojenou kontrolní jednotkou GR-32 Dual HOTT. Pro napájení jsou použity čtyři LiPo (Lithium Polymer) baterie o napětí 29.6 V, kapacitě 12500 mAh a hmotnosti 2 kg. Dále je opatřeno také optickým gyroskopem. Gyroskopy obecně jsou senzory používané k měření úhlové rotace kolem zadaného směru vzhledem k IMU. Hlavním rysem optického gyroskopu je, že světlo je rozděleno na dva svazky a vedeno protiběžně po uzavřené dráze optického vlákna navinutého na kruhovou cívku (HORÁK 2012). Díky této technologii je UAV RiCOPTER schopno stabilizovat senzor, detekovat změny polohy a pohybu, měřit náklon a rozpoznat převrácení. Dále pak gyroskop slouží ke korekci a zpřesnění polohy získané pomocí GNSS modulu.

Obrázek 8 – VUX-SYS připravený ke vzletu a sběru dat (foto autor)

Obrázek č. 8 zobrazuje UAV RiCOPTER osazené skenerem VUX-1UAV, tedy celý systém VUX-SYS připravený ke vzletu na misi za účelem sběru dat. Na obrázku je zřetelný laserový skener VUX-1UAV osazený na spodní části UAV RiCOPTER, které stojí na plachtě zabraňující kontaktu odletujících nečistot a větších fragmentů s UAV při vzletu a přistání.

4.1.2. Terénní sběr dat pomocí ULS

V současné době je využití metody ULS pro sběr dat náročné jak uživatelsky vzhledem k technologickým znalostem a požadovaným schopnostem pilota či operátora, tak také z finančního hlediska. Pořizovací cena UAV nesoucího laserový skener není otázkou několika desítek tisíc korun, jako jsou například ready to fly solutins pro leteckou fotogrammetrii, nýbrž milionů Kč počáteční investice do dané technologie (Surový et al. 2019).

Cílem sběru dat pomocí metody ULS je získat přesné, husté a reprezentativní bodové mračno. Aby bylo tohoto cíle dosaženo a bylo zamezeno možným

nepřesnostem či problémům při odvozování výsledných bodových mračen, je zcela bezpodmínečně nutné postupovat podle v praxi odvozených následně popsaných postupů při využití daného UAS.

Před samotným sběrem dat pomocí ULS je nutná kancelářská příprava. S přihlédnutím k legislativním omezením (Předpis L2 Doplněk X zákona č. 49/1997 Sb.) je vhodné například pomocí internetové aplikace AisView (https://dronview.rlp.cz/) zkontrolovat vzdušný prostor nad místem sběru dat. Tato aplikace umožňuje kontrolu vzdušného prostoru v okně internetového prohlížeče, nebo také jako mobilní aplikace. Velkou výhodou je aktuálnost situace s případným přesným časovým i prostorovým vymezením uzavření dané části vzdušného prostoru. Obrázek č. 9 zobrazuje informace o vzdušném prostoru České republiky vztažené k letu UAV. Například jsou zde červenou barvou vyznačeny všechny bezletové zóny letišť a národních parků, hnědou barvou jsou potom označeny řízené okrsky letišť.

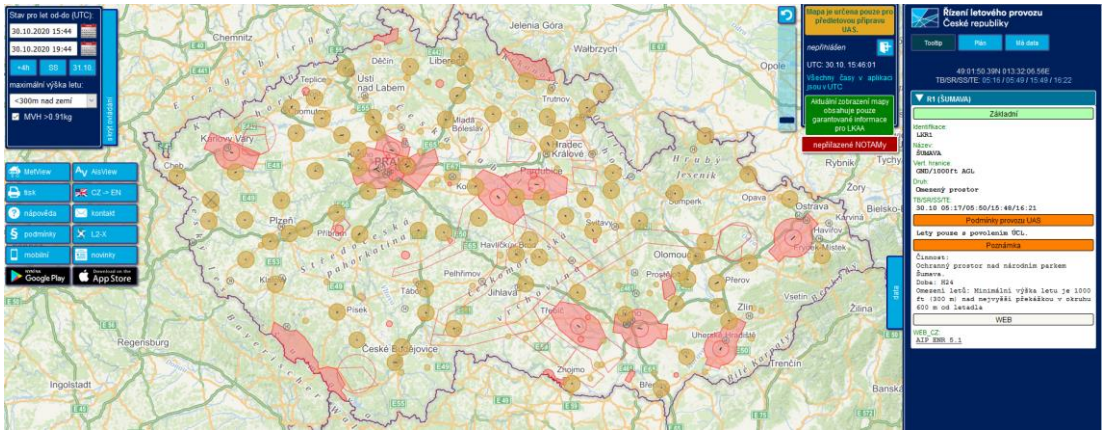

Obrázek 9 – Ukázka aplikace AisView pro kontrolu vzdušného prostoru (dostupné z https://dronview.rlp.cz/)

Po ověření dostupnosti letového prostoru následuje příprava veškerého potřebného vybavení. Tato příprava je shrnuta v následujícím CHECK list:

Notebook/tablet

- Nabitý notebook pro UGCS
- Stažená kompletní off-line mapa v UGCS pro případ absence mobilního signálu na ploše

RiCOPTER

- Upevněný skener (všechny šrouby upevnění k UAV utaženy)
- Kamery přišroubovány ke skeneru
- Skener, kamery a anténa vzájemně propojeny přes IMU
- V krabici je letový CHECK list
- Naformátované a prázdné karty kamer umístěny v kamerách
- Dostatek místa na HDD skeneru
- Nabyté baterie (vždy celá sada) 4x/8x v kufru na baterie

GPS

- Nabité baterie (přijímač i kontroler)
- Kontroler
- Přijímač
- Nivelační trojnožka
- Stativ
- Nabíječka na kontroler (při vícedenním výjezdu)
- Nabíječka na přijímač (při vícedenním výjezdu)

Rádio – remote controller

- Nabito
- Šrouby k ramenům 4x (jsou uloženy zde pro zamezení jejich ztráty)
- Imbusový klíč na šrouby k ramenům
- Vycpávka
- Nabíječka

Kufr s vybavením

- Sada imbusových klíčů
- Battery controler
- Popruhy k rádiu
- Datalink
- Kabely k datalinku (napájecí + USB propojovací)
- Kolíky k plachtě
- Imbusový klíč s hvězdicovou hlavou (pro kontrolu upevnění skeneru k UAV)

- Sada náhradních šroubů
- Sada náhradních krytek
- Převodník proudu z 12 V na 220 V
- Baterie pro datalink (plochá 8000 mAh/powerbanka)
- Range finder
- Chladič (při vícedenním výjezdu)
- LAN kabel (při vícedenním výjezdu)
- Napájecí kabel řídicí jednotky (při vícedenním výjezdu)

Vybavení zvlášť

- Plachta
- Skládací stůl

Nabíječka velkých baterií (při vícedenním výjezdu)

- 1x/2x
- Napájecí kabel 1x každá
- Kontrolní kabel LiPOL baterie 2x
- Držáky baterií 2x/4x

Neustálá kontrola a opakování ověřených postupů je tím nejlepším způsobem k zamezení problémů při sběru dat chybějícími součástmi počínaje a havárií UAV konče.

Transport UAV, velikosti jako je RiCOPTER, se vším potřebným příslušenstvím je z pohledu sběru dat o lesních ekosystémech nezanedbatelným problémem. Proto je nutné využít zpravidla terénní automobil s dostatečným úložným prostorem.

Po příjezdu na vybrané místo je nutné zajistit bezpečnost letu v souladu s Předpis L2 Doplněk X zákona č. 49/1997 Sb. S přihlédnutím k zvolené metodě referenční stanice (vysvětleno v části 4.2.1. PosPAC MMS) je nutné zahájit statické měření diferenciální GPS na předem známém bodě (zaměřeném pomocí RTK GPS/na geodeticky zaměřeném bodě) s intervalem měřením 1 s a menším. Pro tyto účely je využívána pozemní stanice sestávající z Trimble TSC3 kontroleru a Trimble R2 GNSS přijímače (Trimble, Sunnyvale, California, USA).

Pro komplexnost celého VUX-SYS je pro sběr dat dodáván samostatný CHECK list pro dvoučlenný tým operující při sběru dat sestávající z pilota a operátora, viz obrázek č. 10. Celý CHECK list je rozdělen do jednotlivých kroků s označením, který člen týmu jej má vykonávat.

Obrázek 10 – Dvoučlenný tým VUX-SYS provádějící předletovou kontrolu pomocí CHECK list; vlevo pilot vpravo operátor (foto archiv KHUL).

Při sběru dat je využíváno automatického letu pod neustálou kontrolou pilota. Pilot ze země je jen velmi obtížně schopen dodržet konstantní rychlost a výšku letu. Pro dodržení dostatečné hustoty a také reprezentativnosti bodového mračna, tedy aby byly všechny stromy v daném porostu oskenovány ze všech stran, je využíváno tzv. perpendicular zig-zag pattern, tedy letu dvou na sebe navzájem kolmých segmentů sestávajících z rovnoběžných linií trajektorií letu. Pro plánování letu je využíván SW UGCS (Universal Ground Control Station), ve kterém je pomocí kontrolních bodů nastavena trajektorie letu. Nastavovány u jednotlivých bodů jsou následující parametry: výška nad DTM z daného SW, rychlost letu a způsob otočení. Způsob otočení je významný zejména proto, protože v případě VUX-SYS je samotný laserový skener ovládán přímo pilotem UAV. Z tohoto důvodu byl jako nejvhodnější způsob

otáčky vybrán stop and turn, tedy zastavení a následné otočení. Příklad plánování letu je na obrázku č. 11. Je zde zobrazeno více letových trajektorií nad zájmovým územím.

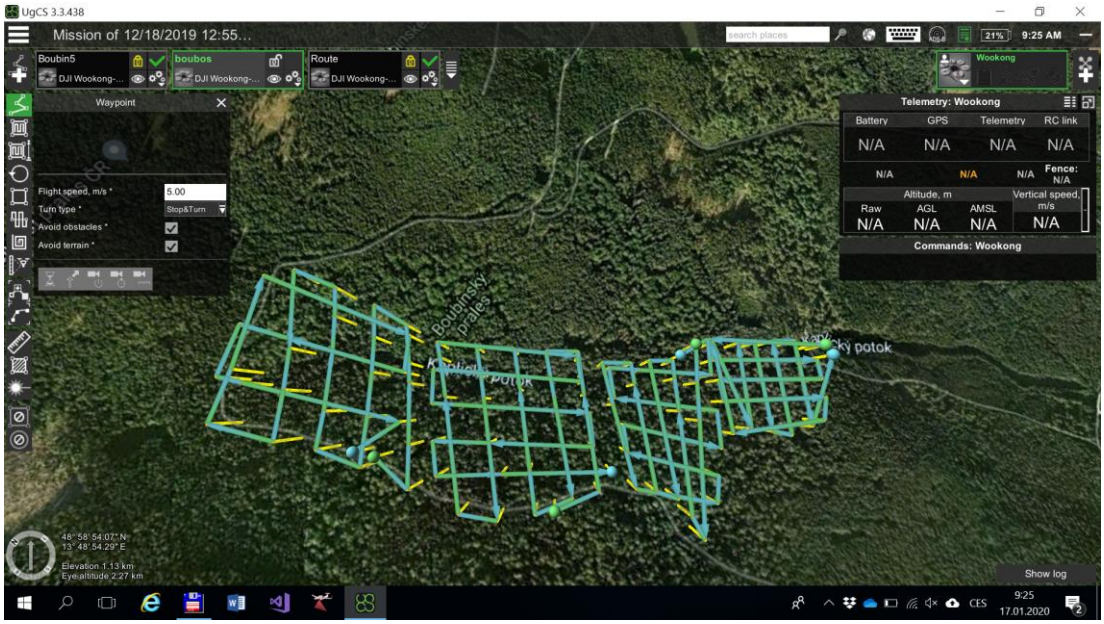

Obrázek 11 – Využití plánovacího SW UGCS

Po ukončení sběru dat je vhodné zálohovat data, která jsou uložena na SSD laserového skeneru. Komunikace se skenerem probíhá pomocí LAN portu za využití protokolu IPv 4.

4.1.3. Trimble TX 8

Trimble TX8 (Trimble, Sunnyvale, California, USA) je 11 kg vážící statický/pozemní laserový skener skenující v blízkém infračerveném spektru o frekvenci 1 500 nm vyvinutý pro velmi přesný sběr dat v nejrůznějších oborech. Díky RGB kameře je schopen sbírat také obrazová data, která dále slouží k obarvení hustých bodových mračen. Vzhledem k otočené hlavě je možné provádět skenování v rozsahu 360° podél svislé osy a FOV rotačního sklíčka činí 317° vzhledem k upevnění skeneru na trojnožku. Skenovací rychlost činí 1 milion bodů s^{-1}. Celkový dosah skeneru činí při limitování hustoty na 312 milionů bodů při vzdálenosti dvou bodů 75.4 mm ve vzdálenosti 300 m od skeneru skenovaná až 320 m oproti parametrům nejvyšší hustoty 555 milionů bodů při dosažení vzdálenosti dvou bodů 5.7 mm v 30 m od skeneru. Data jsou ukládána na USB 3.0 disk (Trimble 2016).

Obrázek 12 – Trimble TX8 na stanovisku při probíhajícím skenování daného porostu. V pozadí jsou vidět koregistrační sférické cíle. (Foto autor)

Vzhledem k absenci GNSS modulu je pro georeferencování bodových mračen (které není vždy nutné) provádět skenování pomocí Trimble TX8 ze stanoviska s předem známými souřadnicemi. Toho lze docílit pomocí totální stanice nebo v případě dostupnosti GNSS RTK signálu také pomocí RTK GPS, jakým je například již výše zmíněný Trimble TSC3 kontroler a Trimble R2 GNSS přijímač. Jak je vidět na obrázku č. 12, skener je umístěn na trojnožce nad stanoviskem označeným geodetickým kolíkem. Pro správnou koregistraci dat, je nutné znát výšku skenovacího centra, označeného značkou na boku skeneru, nad stanoviskem, o kterou jsou dále upraveny zaměřené souřadnice stanoviště. Skener samotný je vybavený kompenzátorem, kterým je schopen kompenzovat drobné nepřesnosti při horizontaci stroje. Centrace je prováděna standardně pomocí periskopu.

Pro koregistraci jednotlivých bodových mračen z jednotlivých stanovisek lze na základě prostředí použít několik typů koregistračních cílů, či koregistrační cíle zcela nepoužít (mračna lze koregistrovat i na základě detekce ploch např. v urbanizovaném prostředí, to je ovšem relativně nepřesné, a proto se vždy doporučuje používat

koregistrační cíle). Prvním a do lesního prostředí nejvhodnějším způsobem v pro jeho 3 D povahu je použít sférických cílů o předem známém rozměru, viz obrázek č. 13. Je však nutné dodržet zásadu, kdy pro úspěšnou koregistraci dvou se překrývajících bodových mračen musí mít tato dvě mračna společné alespoň tři cíle, které neleží na jedné přímce. Na jedné přímce proto, aby bylo eliminováno úhlové zkreslení. Proto je vhodné použít více sférických cílů. Cíle se během skenování nesmí hýbat. Dále je možné použít čtvercové reflexní štítky rozdělené na čtyři stejné čtverce a jejich střed zaměřit. Tato metoda se ovšem v lesním prostředí neosvědčila.

Obrázek 13 – Detail sférického cíle o rozměru 145 mm ukotveného v borce stromu. (Foto autor)

4.2. Odvozování bodových mračen

Před samotnou analýzou dat je kruciální částí celého procesu odvozování geometricky správných a přesně georeferencovaných bodových mračen z ULS či TLS. Zásadní kroky jsou popsány níže i s ohledem na výše popsané postupy při sběru dat.

4.2.1. PosPAC MMS

Velmi důležité vzhledem k ULS je v této části zmínit použití SW PosPAC MMS (Applanix: a Trimble company, Ontario, Canada), v tomto konkrétním řešení byla použita verze 8.1. PosPAC MMS je software sloužící k aplikaci PPK na trajektorie roveru (UAV) vzhledem k rekalkulaci, tedy zpřesnění jeho pozice. Výsledkem je aktualizovaná trajektorie pohybu zvoleného roveru, která dále vstupuje jako kruciální základ při polohovém a geometrickém odvození bodových mračen z VUX-1UAV.

Nejprve je nutné v celkové struktuře projektu z VUX-1SYS najít surová data trajektorie, která se nacházejí v uspořádané struktuře složek „02_INS-GPS_RAW\02_FULL\INS-GPS_1“ pod označením datum_GPSčas_INS-GPS_1. Dále do výpočtu vstupují, vzhledem k používané metodě Base Station, data z pozemní referenční stanice, nebo z virtuální referenční stanice ve formátu RINEX (Receiver Independent Exchange) 2.11. Pozemní referenční stanice (BS) je diferenciální GPS založená na systému dvou přijímačů a je schopna dopočítat odchylku měření (Konecký 2009). Koregistrace měření probíhá na základě GPS času.

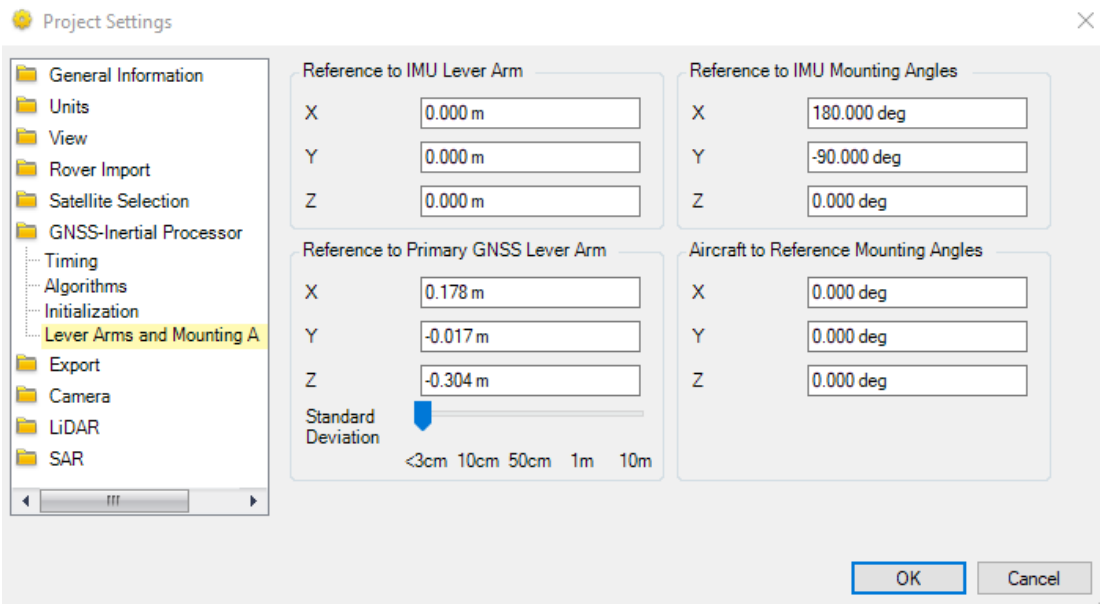

Obrázek 14 – Nastavení pozice senzoru v PosPAC MMS 8.1

Pozice UAV/roveru je zaznamenávána vzhledem k poloze antény přijímající GNSS signál. Ovšem pro potřeby přesného výpočtu pozice jednotlivých bodů bodového mračna je nezbytné provést korekci o rozdíl mezi pozicí IMU laserového

skeneru a GNSS anténou. Tento rozdíl se nazývá lever arms. Na obrázku č. 14 je patrná úhlová i polohová změna podle os X, Y a Z vzhledem k pozici skeneru. Kdyby tyto korekce nebyly brány v úvahu, tak by při použití tohoto konkrétního trajectory based solution nedošlo k přesné koregistraci jednotlivých skenů z UAV a byl by tak mezi nimi zřetelný posun. Trajektorii lze přepočítávat s určitou požadovanou mírou přesnosti, kterou zde reprezentuje maximální přípustná hodnota směrodatné odchylky (Standard Deviation). Ta, když bude přesáhnuta, tak nebude trajektorie zaznamenána a bude nutné počítat s vyšší chybou. V prostředí PosPAC MMS lze také použít výpočet trajektorie jednosměrný (vpřed) nebo přesnější obousměrný (vpřed i vzad), kdy jsou potom obě dvě trajektorie porovnány a při nepřesáhnutí maximální přípustné chyby je trajektorie dále akceptována. V případě potřeby je také možné nastavit preferovaný GNSS systém (GPS, GALILEO, BeiDou, GLONASS).

Výsledná trajektorie je zřetelná na obrázku č. 15 jako zelená čára, která je svou polohou odlišná od původní trajektorie, která je zde jako fialová čára, před jejím zpřesněním. Dále je zde zobrazena i použitá referenční stanice pod označením V007, kdy se v tomto konkrétním případě jedná o virtuální BS s měřením polohy každou sekundu. Virtuální referenční stanice byla použita z Trimble VRS NOW (Virtual Reference Station) serveru.

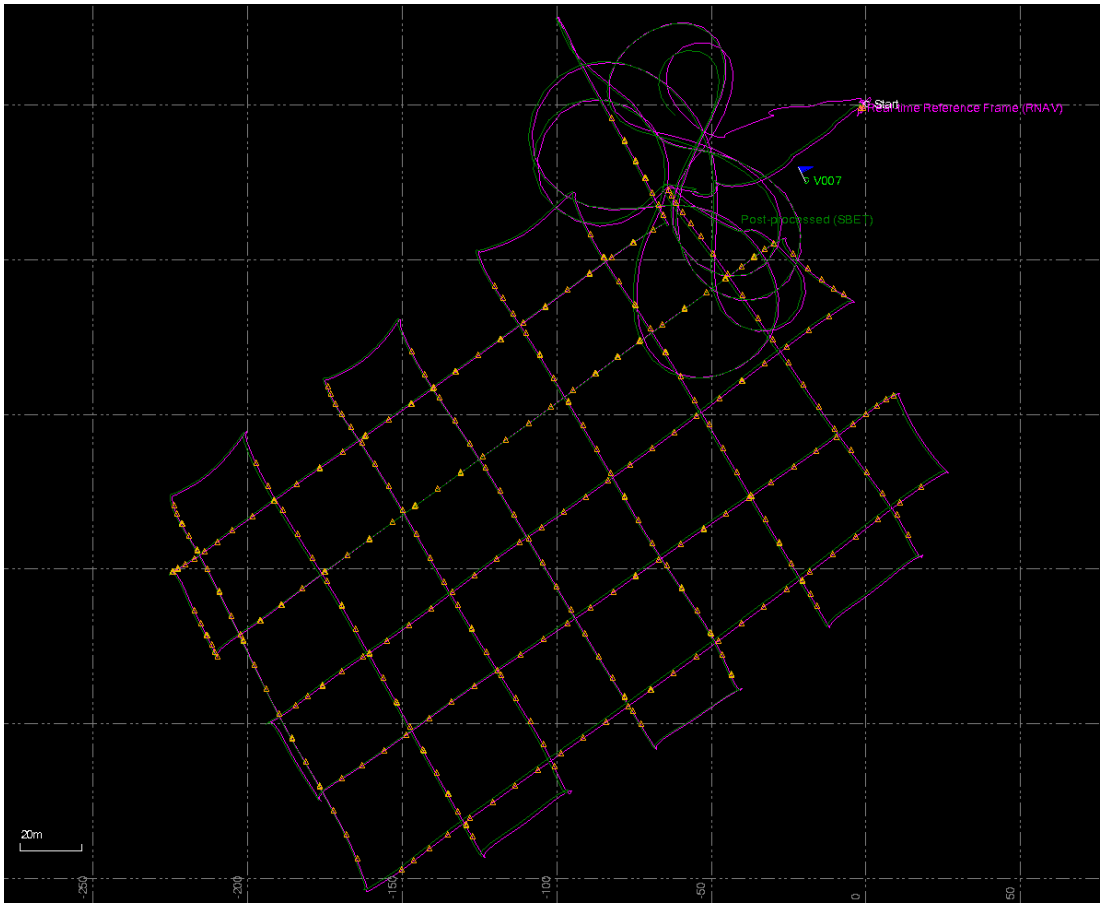

Obrázek 15 – Výsledná plocha trajektorie kdy: fialová je surová trajektorie, zelená přepočtená trajektorie, V007 je pozice virtuální referenční stanice

Do dalšího kroku odvozování již konkrétního bodového mračna tedy vstupuje nová trajektorie jako smoothed best estimated of trajectory (SBET).

4.2.2. RiPROCESS

V prostředí RiPROCESS probíhá samotné odvozování bodových mračen, jejich základní klasifikace a čištění od šumu, tedy bodů, kterým byly nesprávně vypočteny souřadnice na základě náhodného odrazu, při odražení paprsku od drobné částice ve vzduchu, či od částice vzdušné vlhkosti, nebo od jiných reflexních povrchů. Výstupem je potom čisté mračno, složené z vzájemně přesně koregistrovaných jednotlivých skenů se základní klasifikací bodů (RIEGL 2020).

Obrázek č. 16 zobrazuje korekční matici k jednotlivým osám, které jsou odvozeny pro letící UAV. UAV letí při sběru dat pod náklonem několika desetin stupňe, které potom dále do celého procesu odvození bodových mračen vkládají

chybu. Aby se této chybě předešlo, tak je na začátku celého procesu odvozena zmíněná korekční matice, která potom dále upravuje POP Matrix – obrázek č. 17 determinující vzájemné vztahy jednotlivých os a rotací podél nich v rámci daného bodového mračna.

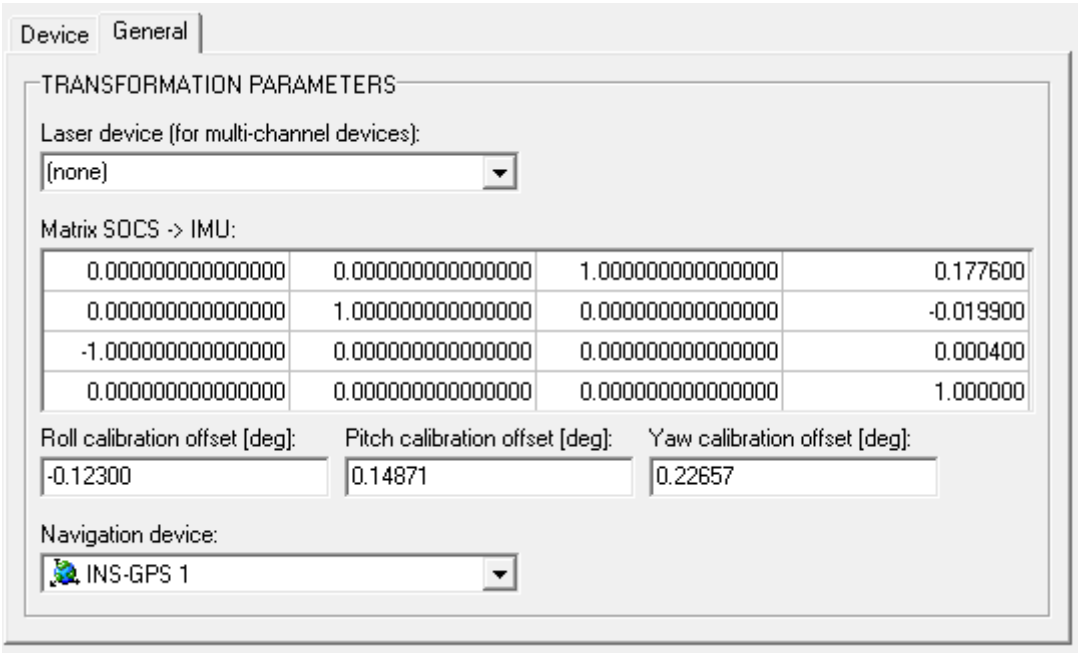

Obrázek 16 – Transformační parametry skeneru vzhledem ke kalibraci offset úhlů dle jednotlivých os

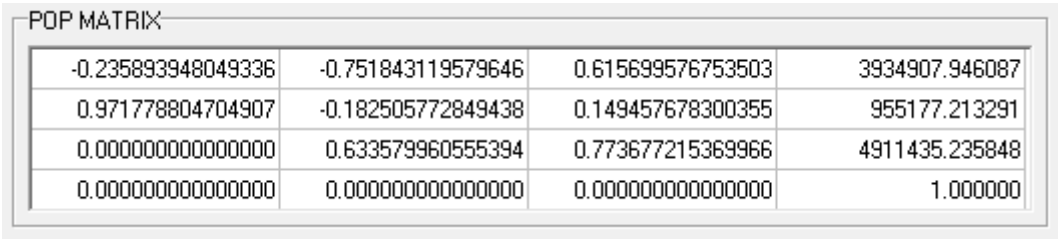

Obrázek 17 – POP Matrix

V iniciální fázi odvozování bodového mračna je nutné provést koregistraci surových dat ze skeneru s daty zpřesněné trajektorie. K tomu slouží poziční soubor. Příklad hlavičky pozičního souboru reprezentuje obrázek č. 18. V této hlavičce jsou determinovány základní údaje o celém bodovém mračnu maximální a minimální zeměpisná délka, šířka a nadmořská výška (Longitude, Latitude a Altitude), dále je zde determinován celý časový úsek na základě GPS času. Délka času je důležitým faktorem při nákupu VRS. Posledním řádkem je navigační rámec, který určuje pořadí

zaznamenávaných zeměpisných souřadnic, což je významné především při exportování dat vzhledem k správné orientaci bodového mračna.

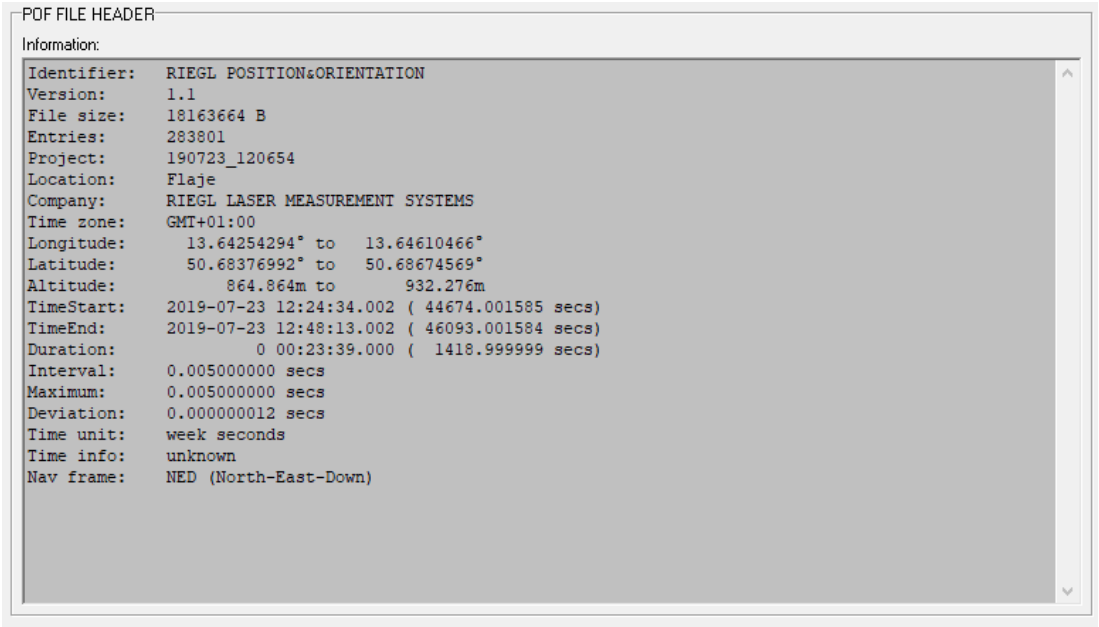

Obrázek 18 – Hlavička pozičního souboru

Protože laserový skener VUX-1UAV je schopen dosahovat frekvence až 550 KHz (RIEGL 2019a), tak při zaznamenávání odrazů jednotlivých paprsků je schopen otočit rotačním sklem před jejich zaznamenáním. Dále také probíhá zaznamenání paprsků odražených od spodní části UAV. Vzhledem k těmto okolnostem a jiným dalším je nutné při tvorbě iniciálního bodového mračna determinovat extrakční parametry jednotlivých bodů. Obrázek č. 19 představuje nastavení jednotlivých extrakčních parametrů. Multiple Time Around (MTA) řeší automatické detekování odrazů jednotlivých paprsků při otočení rotačního skla. Region of interest reprezentuje možnosti manuálního nastavení extrakce pouze určitých odrazů, které splňují předem definované podmínky. Podmínkami mohou být: výskyt v určité úhlové výseči vzhledem ke svislé rovině procházející osou skeneru, vzdálenost od skeneru, určitý časový úsek, definovaný interval odrazivosti, definovaný interval síly signálu nebo definovaná hodnota odchylky.

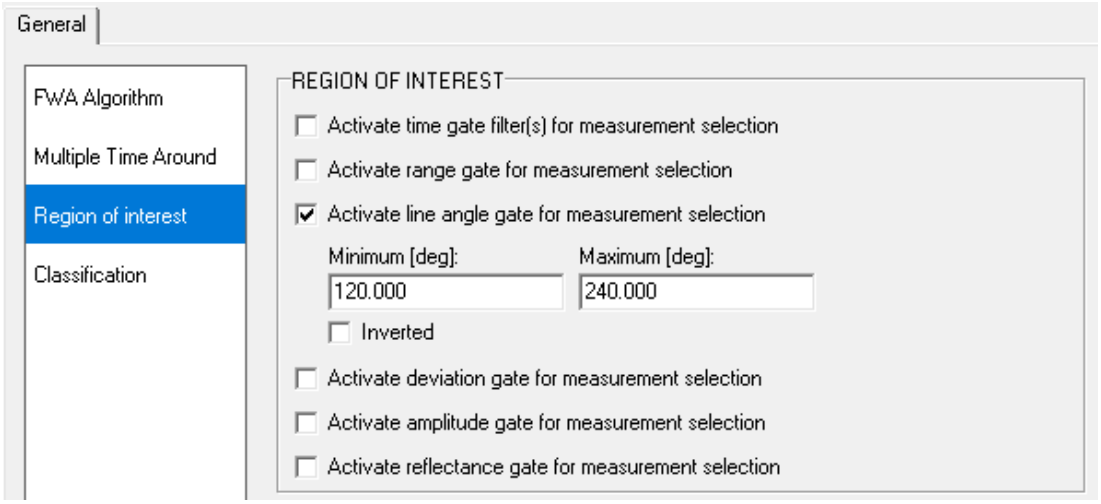

Obrázek 19 – Extrakční parametry

Pro přesnou koregistraci jednotlivých skenů obsahuje prostředí RiPROCESS modul RiPRECISSION UAV. Označení UAV znamená, že modul je navržen pro práci s daty z bezpilotních letadel i s jejich danými specifikacemi (především hustota bodů vzhledem k vyskytujícím se objektům) (RIEGL 2019b). RiPROCESS provede zpřesnění koregistraci jednotlivých skenů zejména podél osy Z.

Přesně odvozené a koregistrované bodové mračno je dále možné také klasifikovat. Z lesnického pohledu jsou prováděny dva typy klasifikací. Prvním je klasifikovat body ležící na zemském povrchu, přidat jim atribut ground (v las formátu calss 2) a definovat body které náleží vegetaci (v las formátu calss 4). Klasifikace probíhá na základě geometrických charakteristik, viz obrázek č. 20. Na obrázku č. 20 je ukázka nastavení zmíněných geometrických parametrů, jakými jsou maximální výšky a šířky předpokládaného stromu a maximální skon terénu.

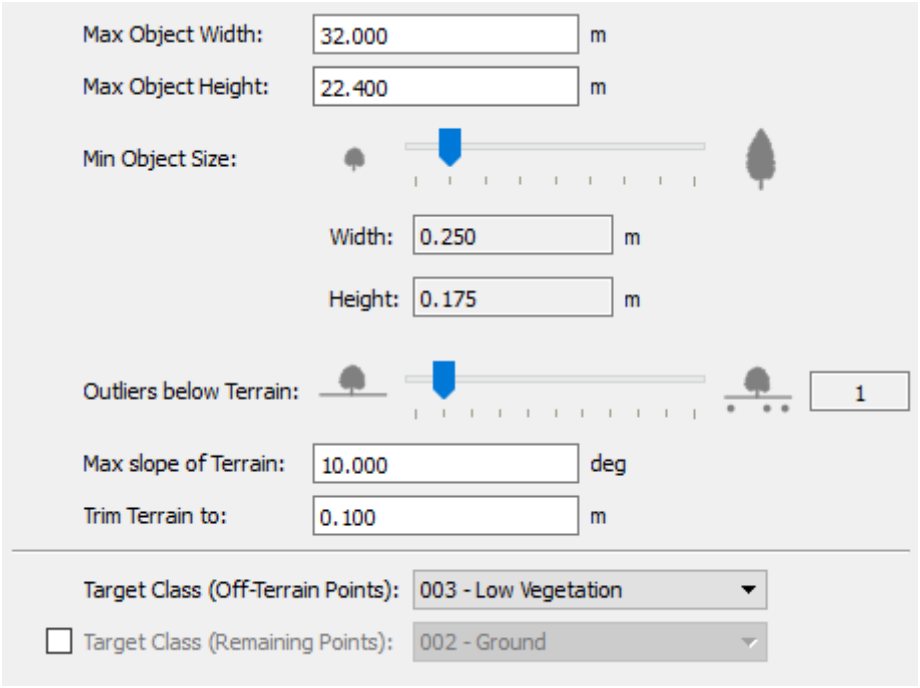

Obrázek 20 – Off terain classifier (nastavení parametrů klasifikace bodů)

Na obrázku č. 21 je zřejmý výsledek klasifikace bodového mračna vzhledem k vegetaci a zemskému povrchu – ground. Je zde zcela zřejmé, že ne všechny body, které přímo leží na zemském povrchu, jsou klasifikovány jako ground. Ovšem tato klasifikace je pro další zpracování dat zcela dostačující. Na obrázku č. 21 je možné vidět dvouetážový porost vzniklý podsadbou rozpadajícího se porostu.

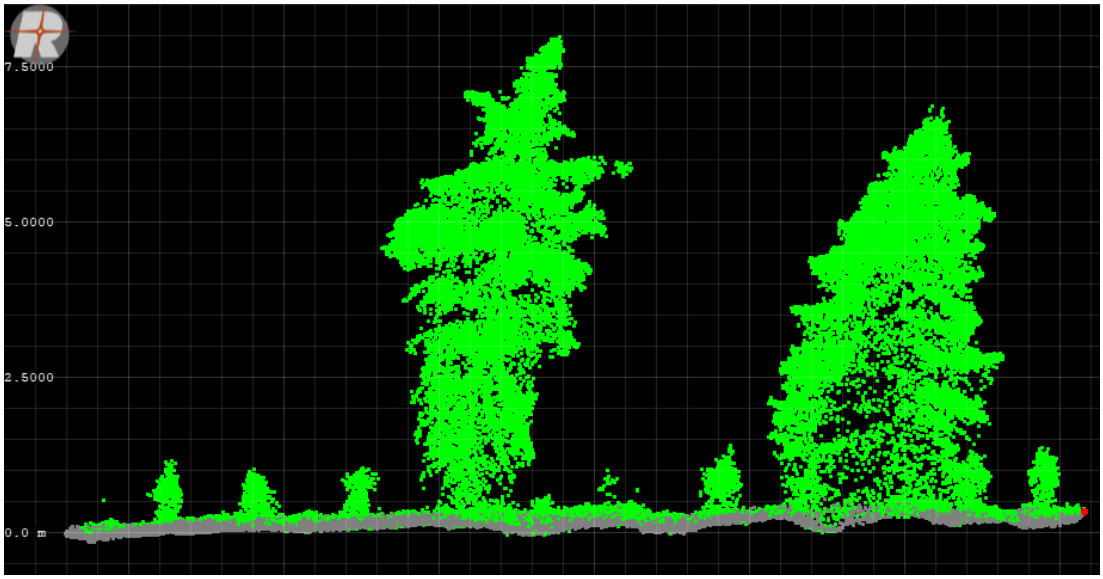

Obrázek 21 – Ukázka klasifikovaného bodového mračna; šedá body náležící povrchu terénu (ground); zelená klasifikovaná vegetace. Zkusná plocha Fláje

Druhá klasifikace bodů prováděná v prostředí RiPROCESS je klasifikace šumu – noise. Jako šum je označen každý bod, který nesplní předem definované podmínky. Okolo každého bodu je vytyčena virtuální koule a předem definovaném průměru a v ní je vypočítán počet sousedních bodů. Jako limitující podmínky jsou tedy nastaveny pouze dva parametry: průměr koule a minimální počet bodů.

Obrázek č. 22 představuje pohled shora na bodové mračno ze zkusné plochy Fláje skládající se celkem ze dvanácti jednotlivých skenů. Každý sken je obarven vlastní barvou. V tomto konkrétním bodovém mračně byla dosažena průměrná hustota 2 500 bodů m^{-2}.

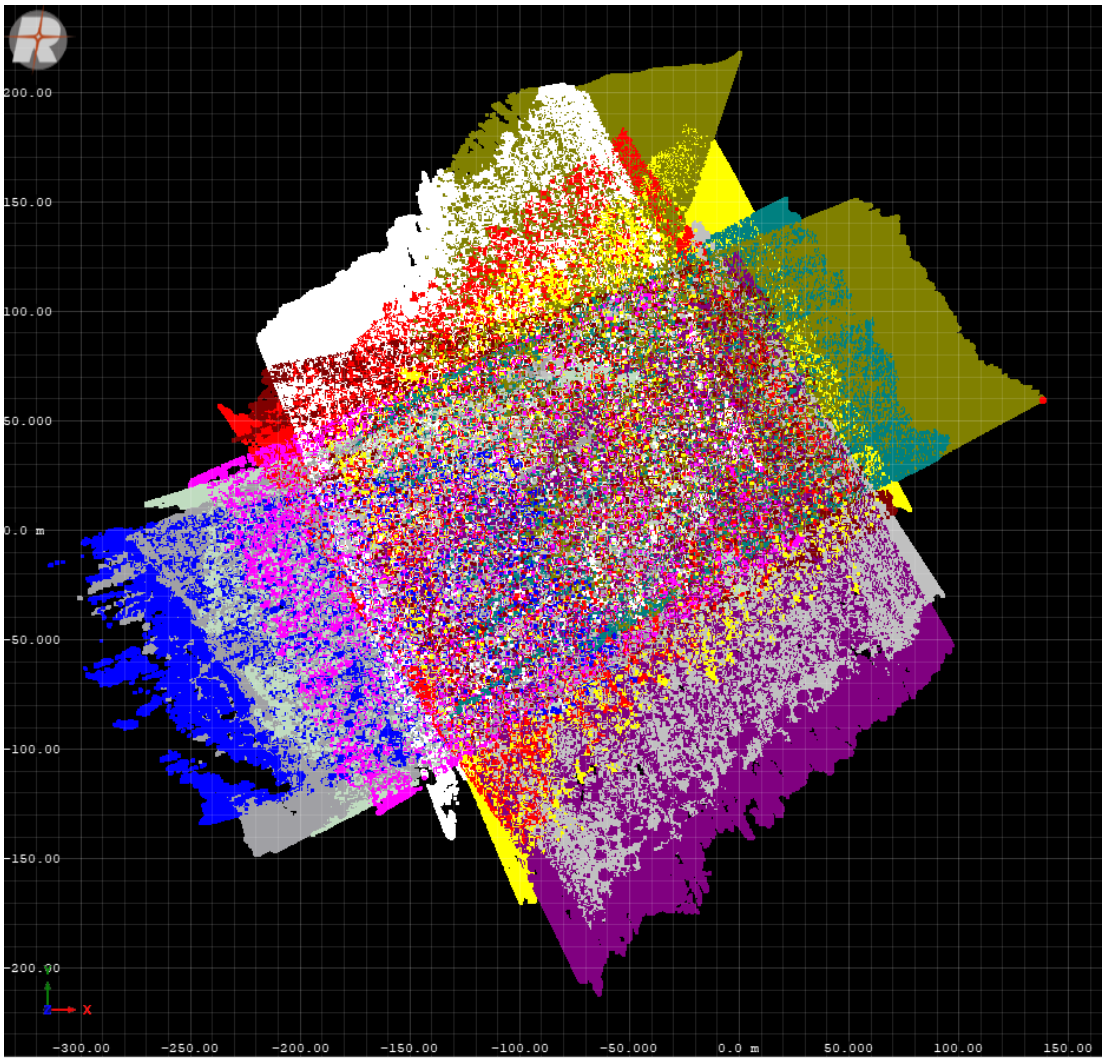

Obrázek 22 – Ukázka překryvu jednotlivých 12 skenů (zkusná plocha Fláje)

4.2.3. Trimble RealWorks

Trimble RealWorks (Trimble Inc. 2016) je obdobné prostředí pro koregistraci a základní práci s bodovými mračny, jakým je výše zmíněný SW RiPROCESS. Ovšem zde je možné, oproti RiPROCESS, importovat i data třetích stran a nikoli pouze projekty vytvořené zařízeními dané společnosti.

Primární funkcí je však zpracování dat z TLS. Vzhledem k tomu, že je vždy nutné, vybrat jedno výchozí mračno/stanovisko, se kterým se budou další mračna z jednotlivých stanovisek koregistrovat, je nutné s tímto krokem počítat již při samotném sběru dat a navrhnout si tak jeho celý design. V případě linie (obrázek č. 24) je vhodné začít od prostředního stanoviska a v případě plošného skenování (obrázek č. 23), je vhodné začít od stanoviska ležícího ve středu celé plochy.

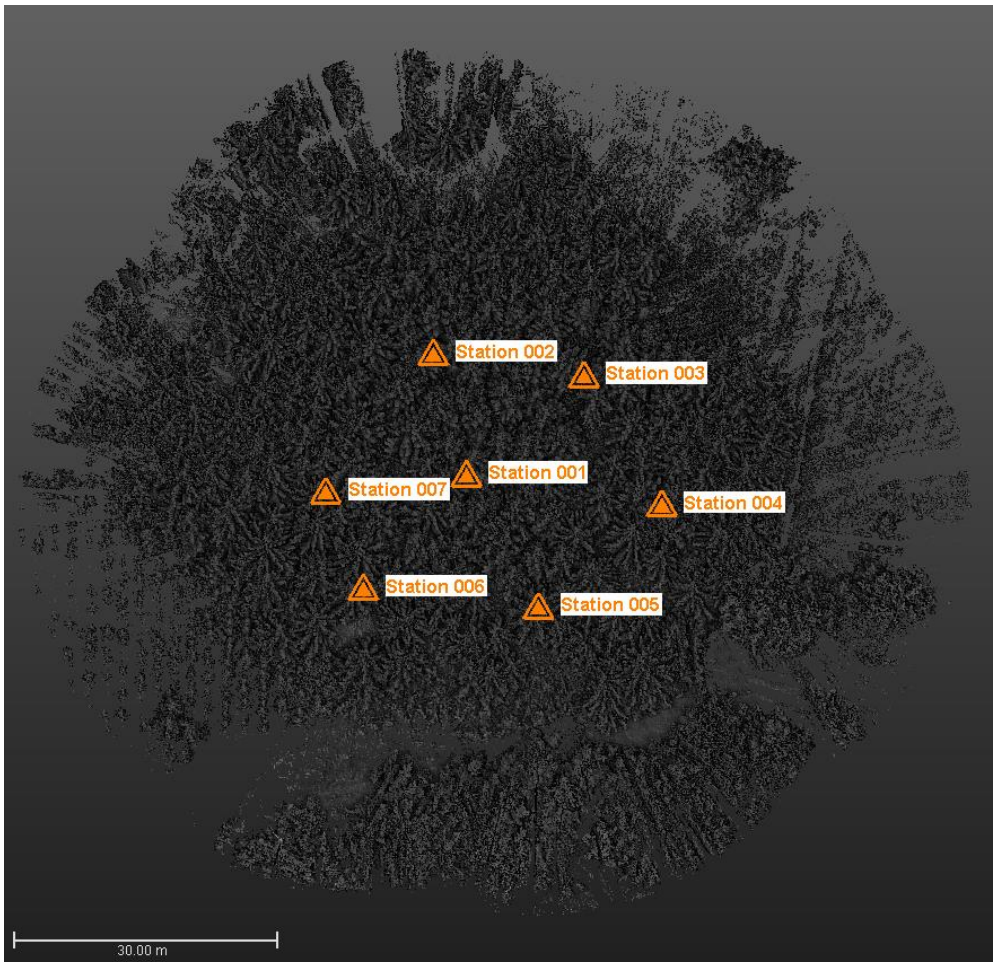

Obrázek 23 – Sběr dat pomocí TLS na ploše (plocha ŠLP Kostelec n. Č. L.).

Již zmíněná samotná koregistraci může proběhnout několika způsoby, kterými jsou automatická detekce a extrakce cílů, manuální detekce cílů, koregistraci pomocí detekovaných ploch anebo manuálně tzv. mračno na mračno.

Významným faktorem je přímé georeferencování bodových mračen pomocí známých souřadnic jednotlivých stanovisek, nebo konkrétních bodů v bodovém mračnu přepočtených o výšku stroje nad nimi (pouze v případě stanoviska). Dále je důležitá možnost ředění bodových mračen, nebo jejich částí a jejich exportu dle požadovaných hustot v různých souřadnicových systémech.

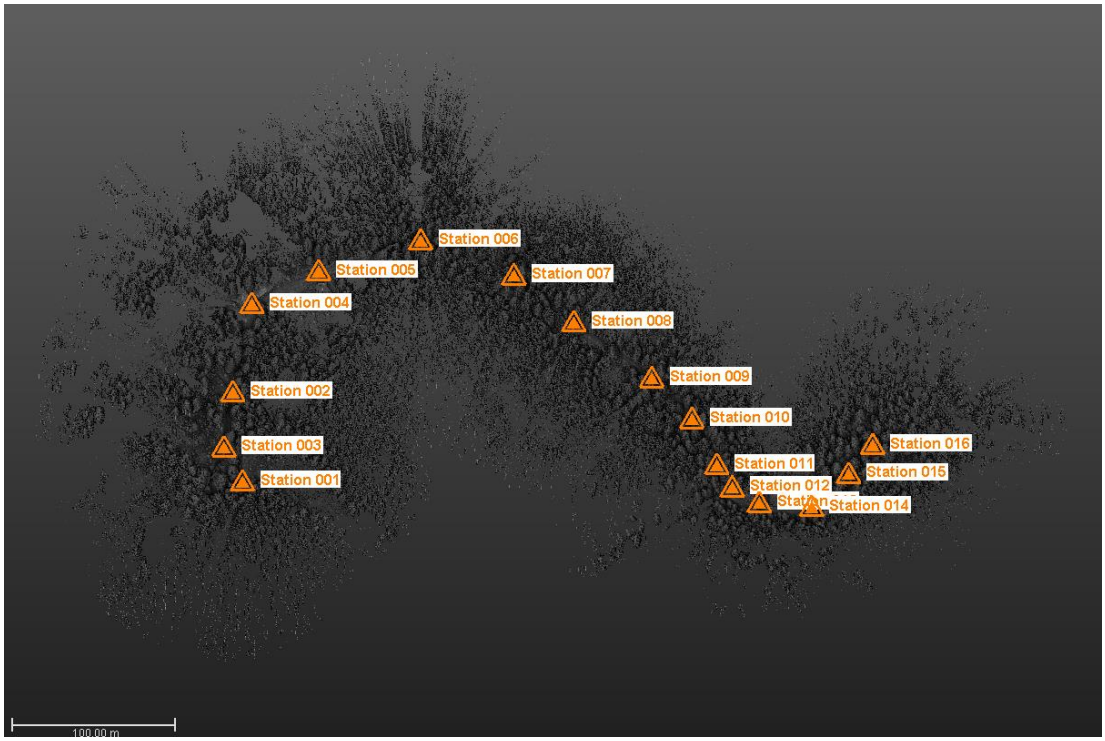

Obrázek 24 – Sběr dat pomocí TLS v linii (plocha NPČŠ).

4.3. Detekování individuálních stromů

Pro účely této práce a zmíněných publikací byly použity tři metody detekce individuálních stromů. První metodou byla detekce pomocí inverse watershed segmentation (IWS) na základě detekce lokálních maxim, jakož to vrcholů a dále delineace na základě odvozených horizontálních průmětů korun individuálních stromů. Tato zmíněná metoda byla již detailně krok po kroku popsána v diplomové práci autora (Slavík 2017), která vycházela z publikace (Panagiotidis et al. 2017).

Na základě metod detailně popsaných ve výše zmíněné diplomové práci byl dále publikován výstup (Grznárová et al. 2019).

IWS byla vždy primárně používána na data z letecké fotogrammetrie na základě DSM a interpolovaného DTM, což vždy vnášelo značnou míru nepřesnosti do ostatních výpočtů, ze kterých byl odvozen CHM, kde proběhla samotná detekce individuálních stromů.

Pro účely této práce byla detekce provedena na základě klasifikovaného bodového mračna z ULS, kdy byly jasně detekovány body DTM i v prostoru pod korunami a v rámci zpracování rastrových dat pomocí IWS tak bylo možné dosáhnout detekce výškového přírůstu na úrovni individuálních stromů (popsané v bakalářské práci (Divíšek 2020)), nebo na úrovni stromových komponent (větví) (Slavík et al. 2020a).

K zjednodušení procesu IWS byl použit toolbox 3D Sample Tools v prostředí Arc GIS 10.6. (ESRI, Redlands, CA, USA), primárně vytvořený ke zpracování dat z ALS.

Další metoda detekce individuálních stromů byla popsána v publikaci Kuželky (Kuželka et al. 2020), která vycházela z voxelizace bodového mračna a na základě analýzy hustoty bodových mračen byly detekovány kmeny individuálních stromů. Velikost jednotlivých voxelů byla stanovena na 0.5 m na horizontální úrovni a 1 m na vertikální úrovni s ohledem na ULS data. Dále byl nastaven limit 0.5 m nad terénem (vycházející z klasifikovaného mračna) a maximum zpracovávaného prostoru bylo nastaveno na 9.5 m. Tyto parametry byly nastaveny na základě typické hustoty bodových mračen z ULS. Tak jak byly odvozeny počty bodů v jednotlivých voxelech, bylo nutné dále determinovat i počty bodů v sousedních voxelech ke každému populovanému voxelu minimálním počtem bodů. Vzhledem ke 3D struktuře voxelizovaného prostoru byl použit indikátor přítomnosti kmenů stem presence indicator (SPI) (3) jako:

$$\mathrm{SPI}_{i,j} = \sum_{k=1}^{m-1} \sum_{l=k+1}^{m} n_{i,j,k} \cdot n_{i,j,l} \tag{3}$$

kde $SPI_{i,j}$ je hodnotou *i,j* té buňky v daném rastru (vrstvy v 3 D prostoru); *m* je počet voxelů ve vertikálním směru; $n_{i,,j,k}$ je počet bodů v *i,j,k* tých voxelech, kde *i,j* a *k* jsou indexy voxelů podél os X, Y a Z. Tento indikátor preferuje kontinuitu a uniformitu počtů bodů a zdůrazňuje vyšší bodové hodnoty. Obecně vzato vysoké hodnoty SPI od terénu po korunovou část detekují kmeny stromů, a proto tak mohou být odděleny od objektů procházejících podkorunovým prostorem jenž nejsou kontinuální, jako jsou například větve (Kuželka et al. 2020).

Jako poslední metodu použitou pro potřeby této práce, lze označit metodu použitou v práci (Panagiotidis et al. 2020), která se zakládala ve vytvoření řezu (kros sekce) v předem definované výšce nad terénem (1.25 – 1.35 m) a zde byly pomocí metody detekce lokálních maxim s aplikací buffer zóny extrahovány cílové části individuálních stromů pro odvození DBH (obrázek č. 25). Celý proces probíhal ve Visual Studio Enterprise 2015 V.14.0.24720.00 (Microsoft, Redmond, 99 Washington United States, 1975).

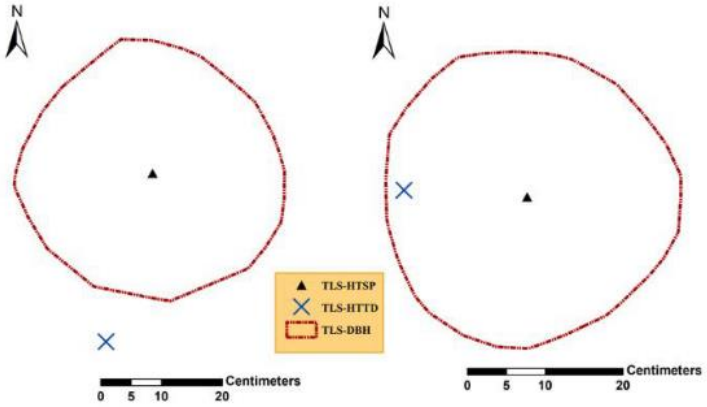

Obrázek 25 – Rozdíl mezi detekovaným vrcholem individuálního stromu (modré x) a středu stromu pro odvození tloušťky (černý trojúhelník). Zdroj: (Panagiotidis et al. 2020)

4.4. Metriky individuálních stromů

Metriky individuálních stromů pro potřeby jednotlivých výstupů byly odvozovány z bodových mračen individuálních stromů v prostředí R (R Core Team, Statistic Department of The University of Auckland, 1997) jakož to hodnoty

deskriptivních statistiky a další hodnoty (Pekár a Brabec 2016). Jednotlivé metriky a práce s nimi je dále popsána v této podkapitole.

Před samotným odvozováním metrik bodových mračen individuálních stromů byly individuální stromy delineovány na základě metody IWS popsané v předchozí podkapitole. Dále byla v případě studie (Slavík et al. 2020b) vypočtena normalizovaná výška pro možnost validního porovnání jednotlivých bodových mračen individuálních stromů.

Jako metriky bodových mračen individuálních stromů byly dle prací (Næsset a Gobakken 2005; Kamińska et al. 2018) použity následující deskriptivní statistiky: interquartil range (IQR), rozptyl/variance (VAR), směrodatná odchylka/standard deviation (SD), moment (MOM), koeficient šikmosti/skewness (SKEW), aritmetický průměr (MEAN), kvadratický průměr (KVAD), kubický průměr (CUB), mean absolute deviatian (MAD), kvantil/quantile (Q*n*; kdy *n* bylo stupňováno po pěti či deseti procentech).

Dále byl použit Clark–Evans agregační index (CE) (Clark a Evans 1954), který byl vyvinut pro popis vzoru uspořádání jednotlivých bodů v souboru. CE zjednodušeně řečeno numericky kvantifikuje stupeň klastrování bodového mračna na základě srovnání s Poissonovým prostorovým rozdělením, kde hodnoty blízko 1 jsou shledávány pro kompletně náhodnou distribucí bodů, zatím co hodnoty nižší než 1 indikují pravidelné uspořádání a hodnoty vyšší než 1 indikují klastrování. Pro výpočet CE byl použit vzorec (4) z (Fabrika a Pretsch 2011) jako:

$$CE = \frac{\frac{1}{n} \times \sum_{i=1}^{n} r}{\frac{1}{2} \times \sqrt{\frac{A}{n}}} \tag{4}$$

kde hodnota *CE* je vypočtena na základě *n* jako počtu bodů; *r*; *A*. Hodnota CE byla odvozena pro každý řez 5% normalizované výšky.

5. Výsledky

V této kapitole jsou stručně prezentovány jednotlivé vědecké práce týkající se zpracování bodových mračen a obrazových informací pomocí metod DPZ, tak jako byly popsány v kapitole řešení. První tři práce v podkapitolách 5.1. až 5.3. se zabývají zpracováním dat z ULS, konkrétně z popsaného VUX-SYS. Práce v podkapitole 5.4. popisuje využití metody TLS pro odhad nadzemní biomasy individuálních stromů. Podkapitola 5.5. se zabývá zpracováním fotogrammetrických bodových mračen o vysoké hustotě pro odvozování DBH. Využití IWS je popsáno v podkapitole 5.6. s ohledem na rozdíly mezi jehličnatými a listnatými dřevinami při zpracování dat.

5.1. Slavík, M.; Kuželka, K.; Modlinger, R.; Tomášková, I.; Surový, P. UAV Laser Scans Allow Detection of Morphological Changes in Tree Canopy. 2020.

Práce prezentuje dvě velmi zásadní výhody ULS a těmi jsou vysoké prostorové a časové rozlišení. Vysoké prostorové rozlišení proto, protože vychází z teoretického předpokladu možnosti detekce struktury bodových mračen na úrovni jednotlivých stromových komponent, tedy větví. Vysoké časové rozlišení proto, protože lze zmíněné změny detekovat v čase, díky nízké časové náročnosti pro sběr dat, tedy vysoké operativnosti metody ULS. Na obrázku č. 26 jsou zřetelná bodová mračna dvou vedle sebe stojících stromů na zkusné ploše Fláje (stromy č. 265 a č. 273), kdy strom vlevo (č. 265) nevykazuje známky změny ve struktuře koruny oproti stromu vpravo (č. 273) vykazujícímu změny ve struktuře koruny. Tyto změny jsou potom patrné na výškovém rastru na obrázku č. 27.

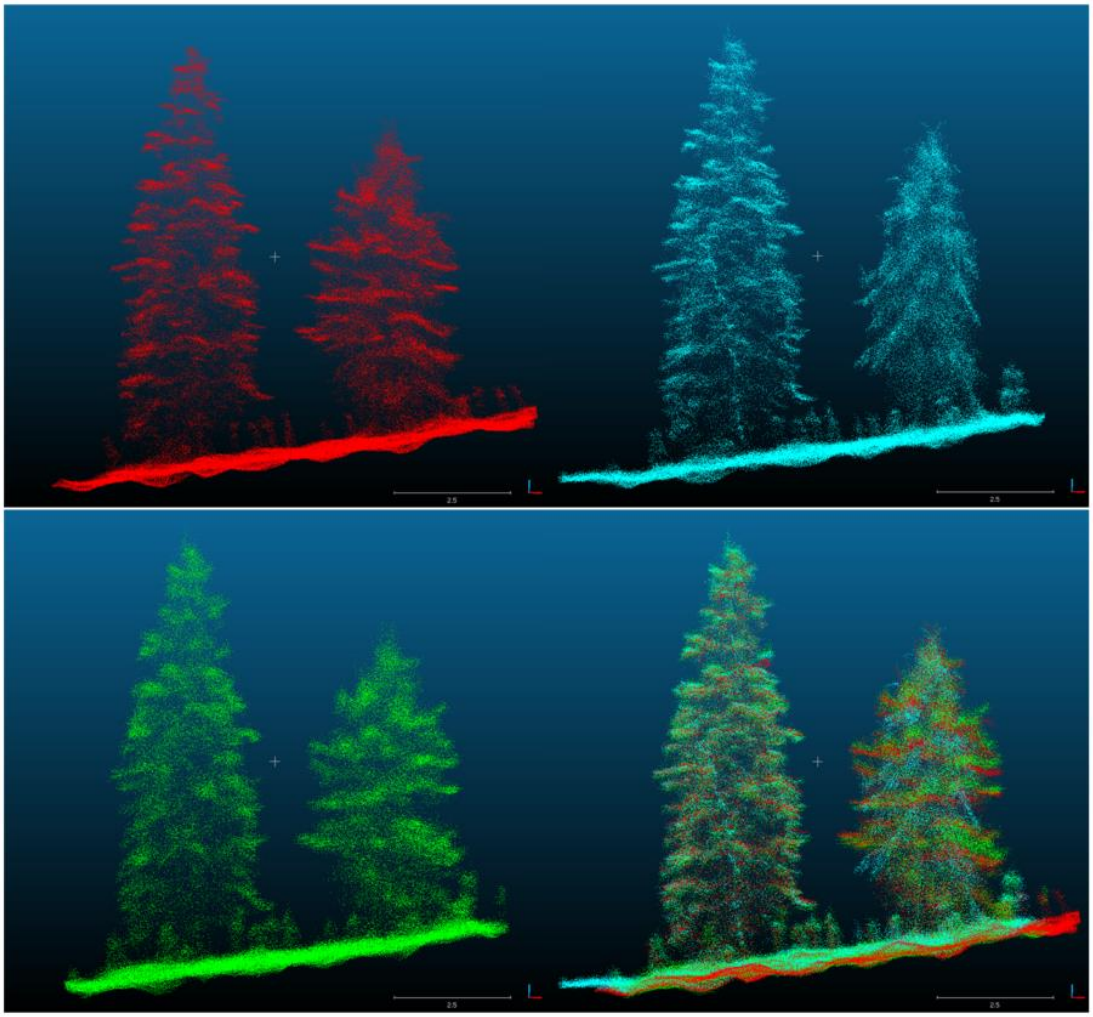

Obrázek 26 – Ukázky bodových mračen dvou vybraných stromů v měsících květnu (červená), červenci (modrá) a listopadu (zelená).

Na zkusné ploše smrku pichlavého (*Picea pungens* Englem.) o rozloze 2,2 ha bylo pomocí IWS detekováno a delineováno 460 jedinců, jejichž zdravotní stav byl při jarním a podzimním sběru dat zhodnocen vzhledem k defoliaci pomocí metodiky (Bosshard a Müller 1986). Každý strom byl očíslován a je tak zajištěna možnost kontinuálního výzkumu na dané ploše. Celkem byly pomocí ULS provedeny tři lety pro sběr dat (květen, červenec a listopad 2019). Na základě delineace individuálních stromů byly pro každé bodové mračno náležící danému stromu odvozeny popisné metriky. Celý dataset byl rozdělen na dva dílčí datasety tedy tréninkový a validační, kde byl odvozen a následně ověřen odvozením GLM pro detekci stromů ohýbajících větve během daného časového období.

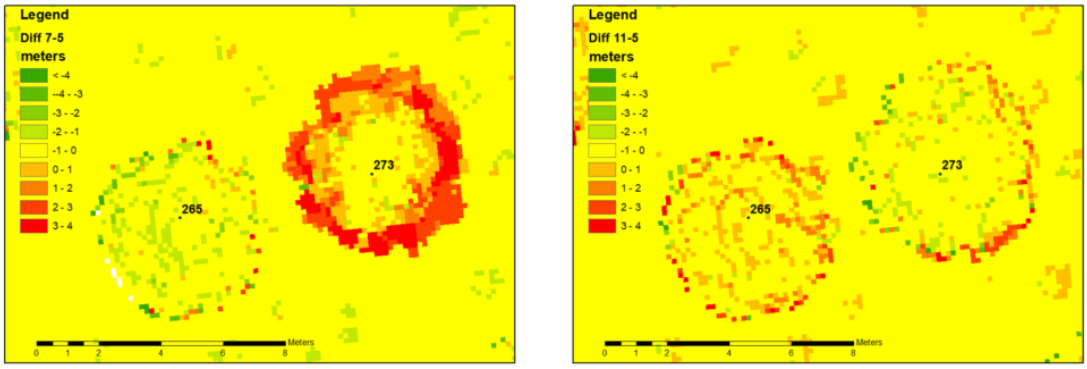

Obrázek 27 – Rastr (10 cm pixel) zobrazující rozdíl mezi strom s ohybem větví (273) a bez ohybu větví (269) při rozdílu dat za měsíce měsíců červenec - květen a listopad - květen.

Prostorová změna na úrovni horizontálních průmětů korun v čase je významným faktorem ovlivňujícím mnoho DPZ metod, vycházejících ze základních poznatků o jednotlivých stromových a porostních veličinách.

5.2. Slavík, M.; Kuželka, K.; Hroššo, B.; Surový, P. Spatial analysis of dense LiDAR point clouds for tree species classification.

Cílem této práce bylo popsat rozdíly mezi jehličnatými a listnatými dřevinami na základě metrik odvozených z bodových mračen individuálních stromů z ULS s důrazem na automatický průběh celého procesu. Jako metriky byly použity různé deskriptivní statistiky odvozené z výškově normalizovaných bodových mračen individuálních stromů a dále byla také hodnocena struktura bodových mračen v jednotlivých percentilech s použitím Clark – Evans Indexu (Clark a Evans 1954) vycházejícího z Poissonova rozdělení. Pro klasifikaci byly zvoleny dvě metody – GLM a Random Forest (Breiman 1999).

Vzhledem k velkému množství proměnných bylo nutné před odvozením GLM provést jejich redukci pomocí metody nejmenších čtverců. Odvození GLM i RF proběhlo vždy dvakrát se zahrnutím a bez CE. CE se v obou případech projevil jako významný faktor pro klasifikaci bodových mračen na úrovni individuálních stromů vzhledem k rozdílnému habitu listnatých a jehličnatých dřevin. Obrázek č. 28 zobrazuje rozdíly v řezech mezi listnatými a jehličnatými dřevinami na základě odvozených významných prediktorů z GLM v jednotlivých řezech bodovými mračny.

Obrázek 28 – Řezy v jednotlivých percentilech normalizovaných výšek zobrazující rozdíl mezi listnatými a jehličnatými dřevinami na základě prediktorů vybraných pomocí GLM.

5.3. Kuželka, K.; Slavík, M.; Surovỳ, P. Very High Density Point Clouds from UAV Laser Scanning for Automatic Tree Stem Detection and Direct Diameter Measurement. *Remote Sens.* 2020.

Studie prezentuje metody detekce individuálních stromů v bodových mračnech pořízených pomocí ULS. Celkem byly provedeny přelety nad šesti zkusnými plochami, kdy tři zkusné plochy se nacházely v monokulturních porostech se zastoupením borovice lesní (*Pinus sylvestris L.*) a tři se zastoupením smrku ztepilého (*Picea abies L.*), jakož to dvou nejvýznamnějších jehličnatých dřevin v České republice. Všechny stromy na zkusných plochách o rozměrech 25×25 m byly v rámci verifikačního datasetu zaměřeny pozičně pomocí totální stanice a bylo také změřeno jejich DBH. Jednotlivé zkusné plochy jsou prezentovány na obrázku č. 29.

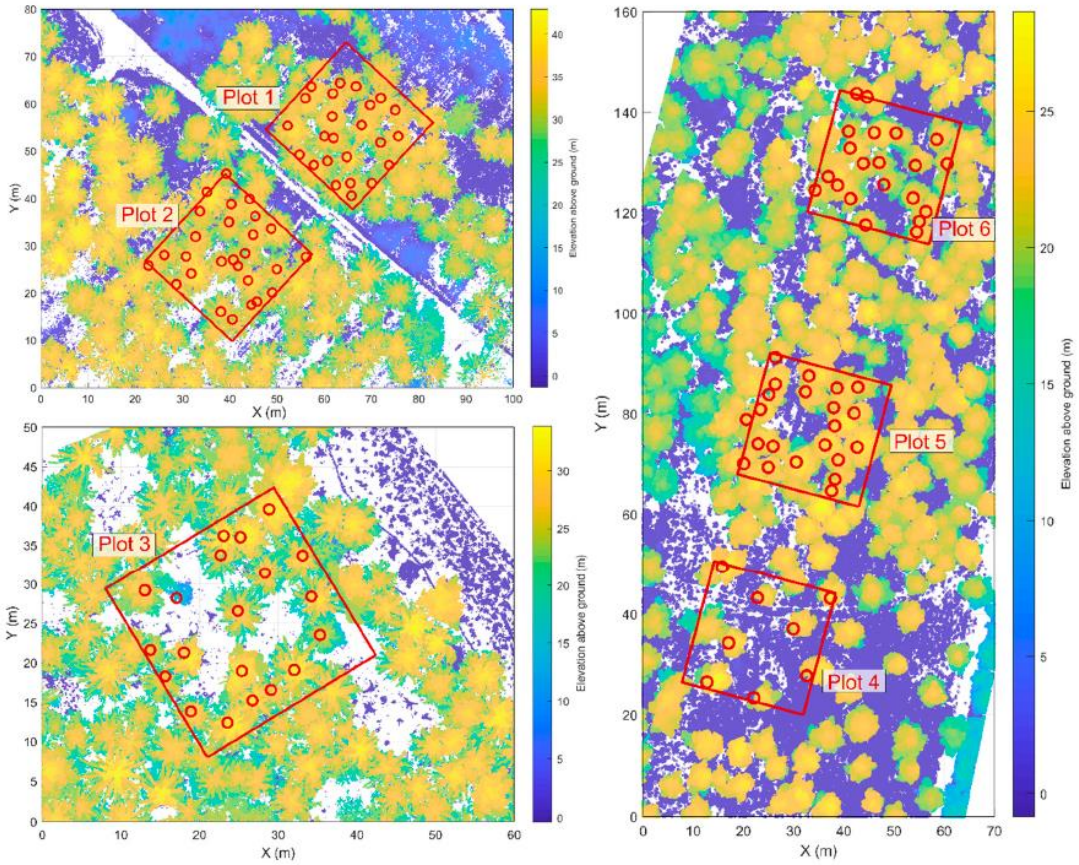

Obrázek 29 – Pozice stromů v bodových mračnech v rámci jednotlivých zkusných ploch.

Kmeny individuálních stromů byly segmentovány na základě voxelizace podkorunového prostoru s přihlédnutím k hustotě bodů v daných voxelech s použitím SPI. Dále byly aplikovány tři metody Hough transform, robust least trimmed squares (RLTS) a random sample consesnsus (RANSAC) pro fitování kruhu ve zvolených příčných profilech podél kmenových profilů viz obrázek č. 30 (ten s kruhy podél kmene).

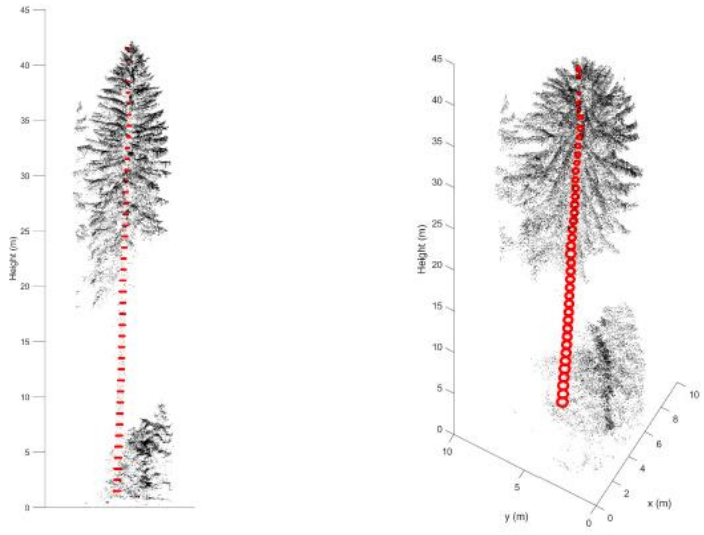

Obrázek 30 – Fitování kruhu podél celého kmenového profilu rozděleného do metrových sekcí.

Jako nejúspěšnější metoda byla zvolena RLTS s detekcí 99 až 100 % stromů v rámci zkusných ploch viz obrázek č. 31. Metoda Hough transofrm byla zhodnocena neúspěšně v rámci fitování kruhu v neúplných datech (nekompletních kmenových profilech), zatím co RLTS a RANSAC byly v tomto ohledu úspěšné. RLTS metoda dosáhla při odhadování obvodu 6.0 cm RMSE s dosažením - 0.1 cm průměrné odchylky.

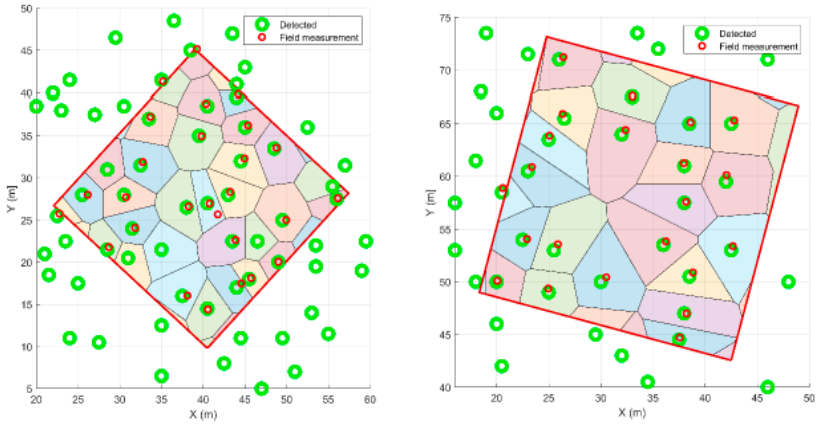

Obrázek 31 – Porovnání úspěšnosti automaticky detekovaných stromů s validačními daty.

5.4. Panagiotidis, D.; Abdollahnejad, A.; Slavík, M. Accuracy assessment of stem attributes for estimation of total stem volume using high-cost survey-grade terrestrial laser scanner : An application of precision forestry.

V této práci byla použita data z TLS na dvou zkusných plochách. První plocha se zastoupení dubu (*Quearcu sp.*) a druhá plocha se zastoupením smrku ztepilého (*Picea abies L.*). Z TLS dat byly odvozeny výška a DBH jednotlivých stromů pro odhad objemu jejich kmene. Byly zde použity dvě různé metody pro odhad výšky. První metoda byla založena na modifikaci metody local maxima popsaná v (Panagiotidis et al. 2017) a druhá byla založena na pozici kmene. Odhad DBH byl založen na základě metody hierarchical cluster analysis (HCA)

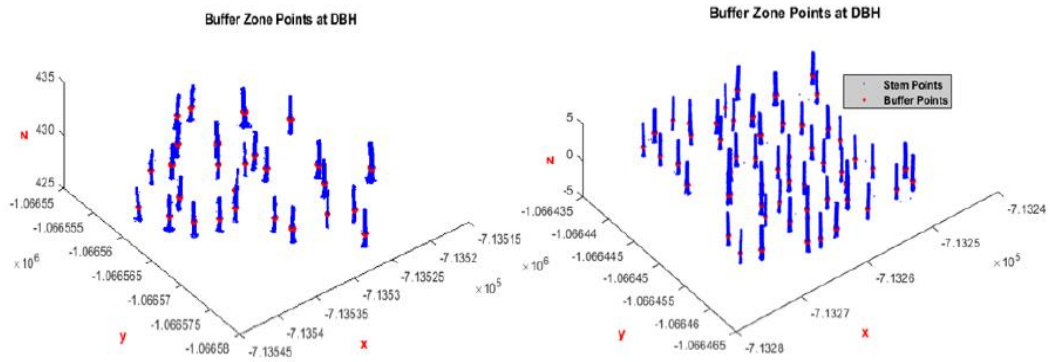

Obrázek 32 – Segmentace bodových mračen a fitování kruhů pro dovození DBH na obou plochách.

Na základě koeficientu determinace byl zjištěn silný vztah mezi naměřenými a odhadovanými metodami pro obě použité metody pro odhad výšky. Tato práce demonstruje použitelnost dat s vysokým rozlišením v kombinaci s robustními metodami pro automatické modelování objemů kmenů individuálních stromů pro maloplošné studie s ohledem na moderní trend precizního lesnictví.

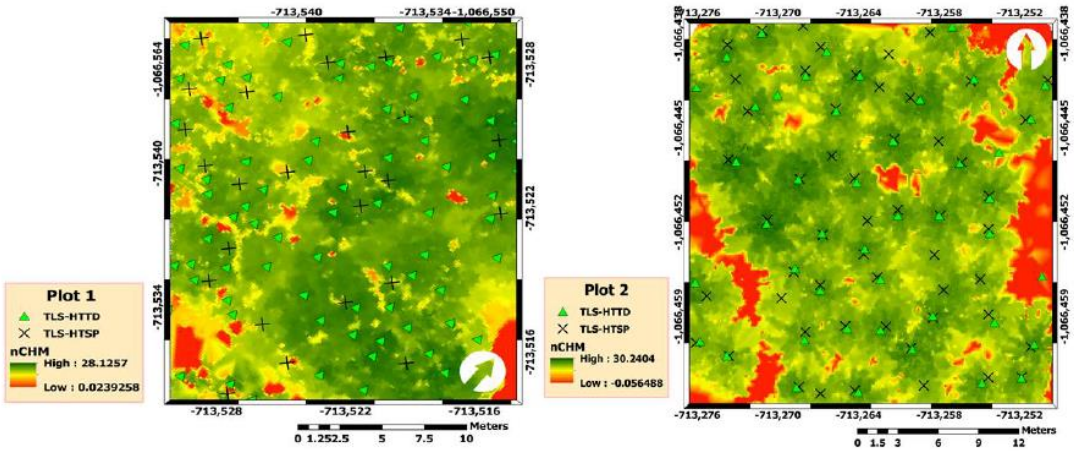

Obrázek 33 – Porovnání dvou použitých metod pro detekci individuálních stromů.

5.5. Mokroš, M.; Výbošťok, J.; Tomaštík, J.; Grznárová, A.; Valent, P.; Slavík, M.; Merganič, J. High precision individual tree diameter and perimeter estimation from close-range photogrammetry. *Forests* 2018, *9*.

Tato studie prezentuje možnosti přesného měření tloušťky z bodových mračen získaných pomocí metod CRP v prostředí DendroCloud (Koreň et al. 2017; 2015). Rekonstrukce kmenových profilů jednotlivých stromů byla provedena pro každý individuální strom separátně. Na každém stromě byla označena čtyři místa ve třech výškách (0.8 m, 1.3 m a 1.8 m) pro měření tloušťky a také zde byl změřen obvod.

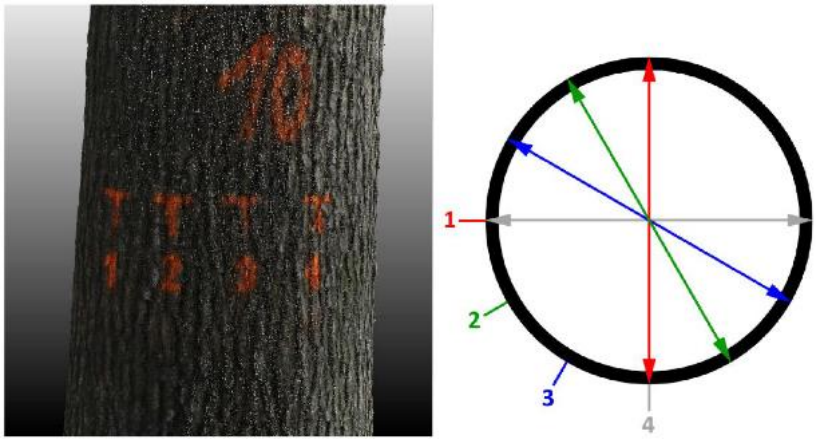

Obrázek 34 – Příklad vzoru měření tloušťky vzhledem ke značkám na kůře.

Byl odhalen vliv použitého objektivu na výsledné odvození tloušťky a obvodu kmene z bodových mračen, jakož to i vliv jednotlivých dřevin. Nejlepších výsledků pro 3D rekonstrukci kmenových profilů z CPR byl na základě dosažené dosáhl fish-eye objektiv.

Obrázek 35 – Bodové mračno individuálního stromu s referenčními body pro měření tloušťky. Okolo jsou rozmístěny 16bitové tabulky pro referencování bodového mračna.

5.6. Grznárová, A.; Mokroš, M.; Surový, P.; Slavík, M.; Pondelík, M.; Merganič, J. THE CROWN DIAMETER ESTIMATION FROM FIXED WING TYPE OF UAV. 2019*, XLII*, 10–14.

Článek prezentuje úspěšnost delineace jednotlivých stromů na základě použití metody IWS z letící platformy typu fixed-wing eBee Plus RTK/PPK s ohledem na příslušnost k listnatým či jehličnatým dřevinám. Z fotografií byly odvozeny DSM a DTM z nichž byl následně odvozen nCHM (normalizovaný). Významnou součástí práce bylo zautomatizování celého procesu a eliminace volný prostorů mezi korunami jednotlivých stromů.

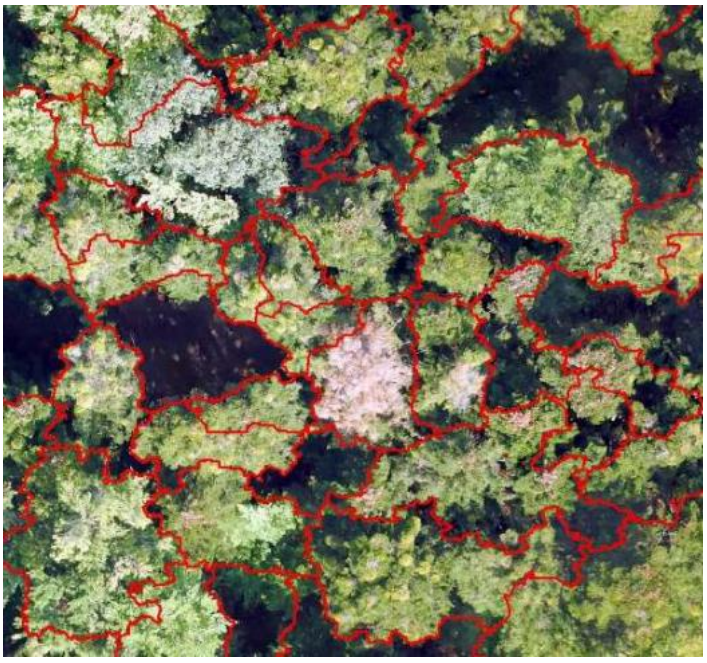

Obrázek 36 – Příklad delineace korun jednotlivých stromů na základě jejich horizontálních průměrů pomocí IWS.

Rozdíl v úspěšnosti delineace jednotlivých stromů v zapojených porostech prokázán vzhledem k zařazení mezi jehličnaté či listnaté dřeviny. Celý postup při zpracování a vyhodnocení dat byl zopakován dle diplomové práce (Slavík 2017).

6. Diskuse

V porovnání s metodou TLS je metoda ULS pro sběr dat o lesních ekosystémech časově mnohem méně náročná. Během jednoho 21 minut trvajícího letu lze pořídit bodová mračna o vysoké hustotě, z nichž lze dosáhnout obdobných výsledků při odvozování DBH a výšky individuálních stromů jako u metody TLS, jejíž použití vyžaduje v takové ploše řádově dny pro sběr dat (Brede et al. 2017; Wieser et al. 2017).

Za jeden let UAV je možné získat LiDAR data o 10 až 20 hektarech. S přihlédnutím k celkové časové náročnosti sběru dat (příprava UAV, plánování letu, přesun mezi lokalitami) lze denně zmapovat až 100 ha (Kuželka et al. 2020).

6.1. Pohyb stromových komponent

Vysoká úspěšnost detekce individuálních stromů pomocí IWS na zkusné ploše Fláje byla zapříčiněna velmi nízkým zakmeněním celého porostu, což obecně vzato bylo způsobilo zejména omezený dotyk korun (Means et al. 2000). Dále se zde také nevyskytoval žádný podrost.

Odvozené metriky významné v odvozeném GLM reprezentují významná místa změny počtu bodů v bodových mračnech individuálních stromů, tedy přesun bodů podél kmenových profilů, který lze chápat jako pohyb/ohyb větví. V nejnižších kmenových partiích byl tak detekován přírůst bodů, které byly odraženy od větví, jež se do příslušných míst ohnuly. Oproti tomu v nejvyšších partiích tedy nastal úbytek bodů taktéž zapříčiněný pravděpodobně ohybem větví. Pro zajištění uniformity sběru dat byla vždy pro let použita totožná trajektorie.

Doposud publikované studie prokázaly detekci cirkadiálního pohybu pouze na živých rostlinách (Barak et al. 2000) nebo na živých stromech (Ibañez et al. 2008; Solomon et al. 2010). Tato studie detekoval pohyb větví u mrtvých stromů, který také detekoval Putman (Putman et al. 2018) při použití TLS a však pouze ze dvou měření a nedetekoval tak návrat větví do původní pozice.

Významnou vědeckou otázkou je, jak mohou ohyby větví ovlivnit výsledky analýz zakládajících se na hodnocení struktury bodových mračen jako ABA (Næsset a Gobakken 2005), nebo může v závislosti na ohybu větví dojít také k nepřesnosti studií založených na IWS (Panagiotidis et al. 2017), nebo třeba také (Grznárová et al.

2019). Dále je také nutné zmínit vztah mezi velikostí koruny a DBH (Verma et al. 2014; Shimano 1997), který je změnami ve velikosti koruny významně ovlivněn. Změny v korunové části porostu, tak jak je popisuje Pokorný (Pokorny et al. 2011), mohou také ovlivnit, jak bylo zjištěno pomocí odvozeného GLM, výsledky ABA. S ohledem na aktuální kůrovcovou kalamitu ve střední Evropě, může dojít také k významnému ovlivnění výsledků mise GEDI, jehož analýzy jsou založeny na základě hodnocení hustoty bodových mračen vzhledem k jejich distribuci podél kmenových profilů (Lee et al. 2018; Qi a Dubayah 2016).

6.2. Klasifikace bodových mračen

Rozdíle mezi listnatými a jehličnatými dřevinami byl již dříve popsán na základě CHM s ohledem na sezónní změny v korunové části porostu Reitbergerem (Reitberger et al. 2008), nicméně tento přístup je senzitivní zejména pro opadavé jehličnaté dřeviny, které jsou na základě detekce změny klasifikovány jako listnaté dřeviny. Klasifikace na základě časové řady je vysoce časově náročná pro nutnost časového rozdílu několika měsíců pro sběr dat. Výsledky úspěšnosti klasifikace mohly být také negativně ovlivněny pro sběr dat během olistění, jak zmiňují (Reitberger et al. 2008; Liang a Matikainen 2007; Kim et al. 2009), ovšem v takovém případě by použitá metoda ztratila na svojí robustnosti.

Pro klasifikaci zejména pomocí GLM byl brán v úvahu především tvar koruny z hlediska dvou základních předpokladů. První předpoklady byl zaměřen na spodní část tedy na začátek koruny podél kmenového profilu. Druhý předpoklad vycházel z odlišného tvaru vrcholových částí koruny, kdy byl přepokládán odlišný tvar (Ørka et al. 2009). Pozitivní vliv normalizace výšky pro porovnání tvaru individuálních stromů byl potvrzen na základě studie Brandtberga (Brandtberg 2007).

Dále byly odvozeny dvě RF klasifikace. Jednou se zahrnutím CE a podruhé s jeho vyloučením z použitých prediktorů. Zahrnutí CE potvrdilo výše zmíněné předpoklady vzhledem k rozdílu v agregovanosti bodů ve zmíněných partiích, ovšem při odvození RF klasifikace bez CE byly předpoklady potvrzeny na základě zhodnocení signifikantních prediktorů ležících v obdobných percentilech, v jakých byl zhodnocen pozitivní vliv CE. Zejména se může jednat o popisu shlukování bodů

vzhledem k radiálnímu větvení jehličnatých dřevin oproti jednomu či více kmenům u listnatých dřevin použitých v dané studii.

Přesnost použité RF klasifikace byla jistě ovlivněna faktem, že zkusné plochy se nacházely na různých místech České republiky (Vetrivel et al. 2015). Ovšem v porovnání přesnosti klasifikace (okolo 88%) bylo dosaženo obdobných výsledků jako u studie (Pal 2005), kde bylo použito kombinace různých metod (hyperspektrální data a ALS). Nicméně použitá metoda klasifikace pomocí RF byla zvolena vzhledem k její nízké senzitivitě na tréninková data (Belgiu a Drăgu 2016). RF klasifikace na základě 3D tvaru byla také použita s daty z ALS v kombinaci s multispektrálními daty v podmínkách České republiky pro detekci individuálních stromů a také pro detekci mrtvých stojících stromů s úspěšností 90% ve studii (Krzystek et al. 2020).

6.3. Odhad DBH a výšky

RLTS byl primárně určen k fitování válců, ovšem lze jej také využít i k fitování kruhů jejichž průměr lze použít jako odhad DBH i pro nekompletní data, stejně tak i pro data obsahující značné množství šumu (Nurunnabi et al. 2017). V takto komplikovaných podmínkách dosahoval RLTS lepších výsledků než RANSAC, který ovšem zejména v bodových mračnech s nižší hustou dosahoval lepších výsledků. Tento fenomén může být důsledkem faktu, že RANSAC odstraní danou část bodů s největšími rezidui. Metoda Hough transform byla prezentována zejména pro odhad DBH z TLS dat (Simonse et al. 2003). Vzhledem k principu Hough transform, byla nutná struktura bodů formujících téměř dokonalý kruh, nebo jeho část, pro správné výsledky.

V případě metody TLS bylo s největší pravděpodobností dosaženo vysoké shody mezi testovaným a validačním datasetem z několika důvodů: a) relativně malá rozloha zkusné plochy b) vysoká bodová hustota TLS bodových mračen s vysokým detailem vzhledem k jejich struktuře v kombinaci s c) použitím více skenů pokrývajících kmeny stromů pod různými úhly a d) malá úhlová odchylka skenovacího zařízení. Dosažené výsledky odchylek při odvozování DBH z TLS dat byly konzistentní s předchozími studiemi jako například (Giannetti et al. 2018; Wang et al. 2019).

Odhadování DBH pomocí technik pozemní fotogrammetrie je ve srovnání s ULS, MLS a TLS nesporně finančně levnější metodou. Ovšem sběr dat o individuálních stromech vyžaduje mnohem větší časovou náročnost při dosažení přibližně stejné přesnosti dat, která však reprezentují pouze velmi omezenou část stromu, zejména tedy pouze dolní kmenové partie. Sub centimetrová přesnost při odvozování DBH byla již zmíněna v práci (Surový et al. 2016). Zatím co zvolení vhodného objektivu bylo potvrzeno na základě (Berveglieri et al. 2017), kde byla i potvrzena srovnatelnost výsledků s pozemním šetřením při využití standardních lesnických registračních pomůcek, jako je například průměrka. Velmi významným faktorem při odvozování dat na základě fotografií je jejich rozlišení (Mokroš et al. 2017; Puliti et al. 2015; Wallace et al. 2016). Dále je zpracování fotogrammetrických dat velmi náročné na výpočetní sílu (Mokroš et al. 2018) zejména v oblasti odvozování bodových mračen.

Jako nejjednodušší metodu pro odhad výšky z bodových mračen použitou pro účely této lze označit metodu rozdílu Z souřadnice nejvýše položeného bodu v polygonu horizontálního průmětu koruny s Z souřadnicí nejníže položeného bodu. Je však nutné podotknout, že tato metoda nenabízí odhad přesné výšky zejména z důvodu zahrnutí bodů ležících na terénu pod určitým sklonem, a tak zpravidla dochází k celkovému nadhodnocování výšky. Ovšem tato metoda je vhodná pro detekci výškového přírůstu individuálních stromů, což bylo také ověřeno v rámci vedené Bakalářské práce (Divíšek 2020).

Při porovnávání odhadu výšky pomocí TLS s pozemním šetřením pomocí standardních lesnických registračních pomůcek (laserový výškoměr) bylo zjištěno nadhodnocování z dat z TLS. Toto lze odůvodnit přesností laserového výškoměru a zejména možnostmi měřiče při sběru dat. Při pozemním šetření je zejména správná interpretace vrcholu individuálního stromu ovlivněna možnostmi měřiče. Často bývá jako vrchol individuálního stromu interpretována jin část stromu (Šmelko 2000).

7. Závěr

Laserové skenování na všech zmíněných úrovních je nesporným krokem vpřed v rámci sběru dat o lesních ekosystémech. Díky využití technologie LiDAR se otevírá možnost detailně zkoumat strukturu stromů a jejich vývoj/změny na úrovni jejich jednotlivých nadzemních komponent. Takovou možnost v rámci 3D struktury doposud žádná jiná technologie s daným vysokým rozlišením neumožňuje. Dále je nutné vyzdvihnout vysokou operační variabilitu zejména metody ULS pro sběr dat, kdy je teoreticky možné detekovat pozice individuálních stromů při vzniku porostu a sledovat tak jejich vývoj v rámci celého jejich života při provádění periodických sběrů dat. Nelze však opomíjet vysoké pořizovací náklady, které jsou aktuálně na úrovni jednotek milionů Korun českých, nebo na úrovni desítek až stovek tisíc Eur. Dále je nutné k samotné technologii zajistit vysoce specializovaný a disciplinovaný personál, který bude schopen dodržet přesné postupy při práci s LiDAR senzory a jejich nosiči.

S přihlédnutím k výše zmíněným skutečnostem je praktické využití technologie LiDAR v lesnictví, zatím, pouze na experimentální úrovni, oproti dnes již běžnému praktickému využití například ve stavebním či důlním průmyslu, nebo také při odvozování DTM na úrovni států. Ovšem její využití na experimentální úrovni je řazeno mezi nejmodernější trendy.

Z praktického hlediska, je v současné době v moderním lesnictví nejdostupnější metoda ALS na úrovni jednotlivých lesních hospodářských celků. Ta však vyžaduje značné množství kalibračních měření, k dosažení vysoké přesnosti a správnosti získaných dat. Metoda ULS je vhodná ke sběru dat o lesních ekosystémech na úrovni jednotlivých dílců, v rámci prostorových jednotek rozdělení lesa, kdy dosavadní experimentální algoritmy umožní s vysokou přesností detekovat pozice jednotlivých stromů a odvodit/odhadnout jejich DBH a výšku. Metodu ULS lze taktéž použít jako kalibrační metodu pro odvozování porostních charakteristik na úrovni celých LHC z dat získaných metodou ALS.

Tato práce prezentuje jednotlivé metody pro sběr dat přes jejich zpracování až po jejich vyhodnocení formou odborných vědeckých publikací s vysokým důrazem na minimalizaci časové náročnosti při zpracování dat, tedy s důrazem na automatizaci veškerých možných procesů a minimalizováním tak lidské intervenci v rámci nich.

8. Seznam použitých zdrojů:

ASTRUP, Rasmus, Mark J DUCEY, Aksel GRANHUS, Tim RITTER a Nikolas VON LÜPKE, 2014. Approaches for estimating stand-level volume using terrestrial laser scanning in a single-scan mode. *Canadian Journal of Forest Research* [online]. **44**(6), 666–676. Dostupné z: doi:10.1139/cjfr-2013-0535

BARAK, Simon, Elaine M. TOBIN, Rachel M. GREEN, Christos ANDRONIS a Shoji SUGANO, 2000. All in good time: The Arabidopsis circadian clock. *Trends in Plant Science* [online]. **5**(12), 517–522. ISSN 13601385. Dostupné z: doi:10.1016/S1360-1385(00)01785-4

BAUWENS, Sébastien, Harm BARTHOLOMEUS, Kim CALDERS a Philippe LEJEUNE, 2016. Forest inventory with terrestrial LiDAR: A comparison of static and hand-held mobile laser scanning. *Forests* [online]. **7**(6). ISSN 19994907. Dostupné z: doi:10.3390/f7060127

BELGIU, Mariana a Lucian DRĂGU, 2016. Random forest in remote sensing: A review of applications and future directions. *ISPRS Journal of Photogrammetry and Remote Sensing* [online]. **114**, 24–31. ISSN 09242716. Dostupné z: doi:10.1016/j.isprsjprs.2016.01.011

BERVEGLIERI, Adilson, Antonio TOMMASELLI, Xinlian LIANG a Eija HONKAVAARA, 2017. Photogrammetric measurement of tree stems from vertical fisheye images. *Scandinavian Journal of Forest Research* [online]. **32**(8). ISSN 16511891. Dostupné z: doi:10.1080/02827581.2016.1273381

BIENERT, Anne, Louis GEORGI, Matthias KUNZ, Hans Gerd MAAS a Goddert VON OHEIMB, 2018. Comparison and combination of mobile and terrestrial laser scanning for natural forest inventories. *Forests* [online]. **8**(2), 1–25. ISSN 19994907. Dostupné z: doi:10.3390/f9070395

BOSSHARD, Walter a Erich MÜLLER, 1986. *Kronenbilder: mit Nadel-und Blattverlustprozenten*. B.m.: Eidgen. Anstalt für das forstliche Versuchswesen.

BOUCHER, C. a Z. ALTAMIMI, 2001. ITRS, PZ-90 and WGS 84: Current realizations and the related transformation parameters. *Journal of Geodesy* [online]. **75**(11), 613–619. ISSN 09497714. Dostupné z: doi:10.1007/s001900100208

BRANDTBERG, Tomas, 2007. Classifying individual tree species under leaf-off and leaf-on conditions using airborne lidar. *ISPRS Journal of Photogrammetry and Remote Sensing* [online]. **61**(5), 325–340. ISSN 09242716. Dostupné z: doi:10.1016/j.isprsjprs.2006.10.006

BREDE, Benjamin, Alvaro LAU, Harm M. BARTHOLOMEUS a Lammert KOOISTRA, 2017. Comparing RIEGL RiCOPTER UAV LiDAR derived canopy height and DBH with terrestrial LiDAR. *Sensors (Switzerland)* [online]. **17**(10), 1–16. ISSN 14248220. Dostupné z: doi:10.3390/s17102371

BREIMAN, Leo, 1999. Random Forests - Random Features, Tecnical Report 567, Statistic Department, University of California, Berkeley, (https://www.stat.berkeley.edu/~breiman/random-forests.pdf, 08.10.2018'de erişildi). 1–29.

BUCHAR, Petr a Vladislav HOJOVEC, 2020. Matematická kartografie 10. *Sensors (Switzerland)*. 19.

CABO, Carlos, Susana DEL POZO, Pablo RODRÍGUEZ-GONZÁLVEZ, Celestino ORDÓÑEZ a Diego GONZÁLEZ-AGUILERA, 2018. Comparing terrestrial laser scanning (TLS) and wearable laser scanning (WLS) for individual tree modeling at plot level. *Remote Sensing* [online]. **10**(4). ISSN 20724292. Dostupné z: doi:10.3390/rs10040540

ČERŇAVA, Juraj, Ján TUČEK, Milan KOREŇ a Martin MOKROŠ, 2017. Estimation of diameter at breast height from mobile laser scanning data collected under a heavy forest canopy. *Journal of Forest Science* [online]. **63**(9), 433–441. ISSN 1805935X. Dostupné z: doi:10.17221/28/2017-JFS

CHEN, Chi, Bisheng YANG, Shuang SONG, Xiangyang PENG a Ronggang HUANG, 2018. Automatic clearance anomaly detection for transmission line corridors utilizing UAV-Borne LIDAR data. *Remote Sensing* [online]. **10**(4). ISSN 20724292. Dostupné z: doi:10.3390/rs10040613

CIMBÁLNÍK, Miloš a Leoš MERVART, 1997. *Vyšší geodézie 1*. B.m.: ČVUT, Stavební fakulta. ISBN 8001015971.

CLARK, Philip J a Francis C EVANS, 1954. Distance to Nearest Neighbor as a Measure of Spatial Relationships in Populations Stable URL : http://www.jstor.org/stable/1931034 REFERENCES Linked references are

available on JSTOR for this article : You may need to log in to JSTOR to access the linked. *Ecology*. **35**(4), 445–453.

CZECH REPUBLIC, 2014. *LETECKÝ PŘEDPIS L 2 PRAVIDLA LÉTÁNÍ*. 2014.

DANDOIS, Jonathan P. a Erle C. ELLIS, 2013. High spatial resolution three-dimensional mapping of vegetation spectral dynamics using computer vision. *Remote Sensing of Environment* [online]. **136**, 259–276. ISSN 00344257. Dostupné z: doi:10.1016/j.rse.2013.04.005

DÍAZ-VARELA, Ramón A., Raúl DE LA ROSA, Lorenzo LEÓN a Pablo J. ZARCO-TEJADA, 2015. High-resolution airborne UAV imagery to assess olive tree crown parameters using 3D photo reconstruction: Application in breeding trials. *Remote Sensing* [online]. **7**(4), 4213–4232. ISSN 20724292. Dostupné z: doi:10.3390/rs70404213

DIVÍŠEK, Martin, 2020. *Využití laserového skenování z bezpilotních letadel pro sběr dat v lesních ekosystémech*. 2020.

EDSON, Curtis a Michael G. WING, 2011. *Airborne light detection and ranging (LiDAR) for individual tree stem location, height, and biomass measurements* [online]. ISBN 1541737431. Dostupné z: doi:10.3390/rs3112494

FABRIKA, M a H PRETSCH, 2011. Analysis and modelling of forest ecosystems. *Technical University, Zvolen*. 1–599.

GIANNETTI, Francesca, Nicola PULETTI, Valerio QUATRINI, Davide TRAVAGLINI, Francesca BOTTALICO, Piermaria CORONA a Gherardo CHIRICI, 2018. Integrating terrestrial and airborne laser scanning for the assessment of single-tree attributes in Mediterranean forest stands. *European Journal of Remote Sensing* [online]. **51**(1), 795–807. ISSN 22797254. Dostupné z: doi:10.1080/22797254.2018.1482733

GRZNÁROVÁ, A., M. MOKROŠ, P. SUROVÝ, M. SLAVÍK, M. PONDELÍK a J. MERGANI, 2019. The crown diameter estimation from fixed wing type of uav imagery. In: *International Archives of the Photogrammetry, Remote Sensing and Spatial Information Sciences - ISPRS Archives* [online]. ISSN 16821750. Dostupné z: doi:10.5194/isprs-archives-XLII-2-W13-337-2019

HORÁK, Richard, 2012. *Fyzikální základy laserových dálkoměrů a gyroskopů*. 2012. B.m.: Olomouc: Chlup. net.

HRUŠKA, Zbyněk a Pavel SVITÁK, 2007. ČSN 31 0001 aneb o leteckém názvosloví. *Letectví+ kosmonautika*. **83**(1), 98.

HYYPPÄ, Eric, Juha HYYPPÄ, Teemu HAKALA, Antero KUKKO, Michael A. WULDER, Joanne C. WHITE, Jiri PYÖRÄLÄ, Xiaowei YU, Yunsheng WANG, Juho Pekka VIRTANEN, Onni POHJAVIRTA, Xinlian LIANG, Markus HOLOPAINEN a Harri KAARTINEN, 2020a. Under-canopy UAV laser scanning for accurate forest field measurements. *ISPRS Journal of Photogrammetry and Remote Sensing* [online]. **164**(December 2019), 41–60. ISSN 09242716. Dostupné z: doi:10.1016/j.isprsjprs.2020.03.021

HYYPPÄ, Eric, Antero KUKKO, Risto KAIJALUOTO, Joanne C. WHITE, Michael A. WULDER, Jiri PYÖRÄLÄ, Xinlian LIANG, Xiaowei YU, Yunsheng WANG, Harri KAARTINEN, Juho Pekka VIRTANEN a Juha HYYPPÄ, 2020b. Accurate derivation of stem curve and volume using backpack mobile laser scanning. *ISPRS Journal of Photogrammetry and Remote Sensing* [online]. **161**(November 2019), 246–262. ISSN 09242716. Dostupné z: doi:10.1016/j.isprsjprs.2020.01.018

IBAÑEZ, Cristian, Alberto RAMOS, Paloma ACEBO, Angela CONTRERAS, Rosa CASADO, Isabel ALLONA a Cipriano ARAGONCILLO, 2008. Overall Alteration of Circadian Clock Gene Expression in the Chestnut Cold Response. *PLOS ONE* [online]. **3**(10), e3567. Dostupné z: https://doi.org/10.1371/journal.pone.0003567

JAAKKOLA, Anttoni, Juha HYYPPÄ, Antero KUKKO, Xiaowei YU, Harri KAARTINEN, Matti LEHTOMÄKI a Yi LIN, 2010. A low-cost multi-sensoral mobile mapping system and its feasibility for tree measurements. *ISPRS Journal of Photogrammetry and Remote Sensing* [online]. **65**(6), 514–522. ISSN 09242716. Dostupné z: doi:10.1016/j.isprsjprs.2010.08.002

JANSSEN, Volker, 2009. UNDERSTANDING COORDINATE SYSTEMS, DATUMS AND TRANSFORMATIONS IN AUSTRALIA. *Proceedings of the Surveying & Spatial Sciences Institute Biennial International Conference*. (January 2009), 697–715.

KAMIŃSKA, Agnieszka, Maciej LISIEWICZ, Krzysztof STEREŃCZAK, Bartłomiej KRASZEWSKI a Rafał SADKOWSKI, 2018. Species-related single dead tree

detection using multi-temporal ALS data and CIR imagery. *Remote Sensing of Environment* [online]. **219**(October), 31–43. ISSN 00344257. Dostupné z: doi:10.1016/j.rse.2018.10.005

KANKARE, Ville, Markus HOLOPAINEN, Mikko VASTARANTA, Eetu PUTTONEN, Xiaowei YU, Juha HYYPPÄ, Matti VAAJA, Hannu HYYPPÄ a Petteri ALHO, 2013. Individual tree biomass estimation using terrestrial laser scanning. *ISPRS Journal of Photogrammetry and Remote Sensing* [online]. **75**, 64–75. ISSN 09242716. Dostupné z: doi:10.1016/j.isprsjprs.2012.10.003

KAŇUK, Ján, Michal GALLAY, Christoph ECK, Carlo ZGRAGGEN a Eduard DVORNÝ, 2018. Technical Report: Unmanned Helicopter Solution for Survey-Grade Lidar and Hyperspectral Mapping. *Pure and Applied Geophysics* [online]. **175**(9), 3357–3373. ISSN 14209136. Dostupné z: doi:10.1007/s00024-018-1873-2

KIM, Sooyoung, Robert J. MCGAUGHEY, Hans Erik ANDERSEN a Gerard SCHREUDER, 2009. Tree species differentiation using intensity data derived from leaf-on and leaf-off airborne laser scanner data. *Remote Sensing of Environment* [online]. **113**(8), 1575–1586. ISSN 00344257. Dostupné z: doi:10.1016/j.rse.2009.03.017

KONECKÝ, JAKUB, 2009. *MĚŘENÍ VZDÁLENOSTÍ A PLOCHY POMOCÍ GPS*. B.m. VYSOKÉ UČENÍ TECHNICKÉ V BRNĚ.

KOREŇ, Milan, Martin MOKROŠ a Tomáš BUCHA, 2017. Accuracy of tree diameter estimation from terrestrial laser scanning by circle-fitting methods. *International Journal of Applied Earth Observation and Geoinformation* [online]. **63**(July), 122–128. ISSN 1872826X. Dostupné z: doi:10.1016/j.jag.2017.07.015

KOREŇ, Milan, Martin SLANČÍK, Jozef SUCHOMEL a Juraj DUBINA, 2015. Use of terrestrial laser scanning to evaluate the spatial distribution of soil disturbance by skidding operations. *IForest* [online]. **8**, 386–393. ISSN 19717458. Dostupné z: doi:10.3832/ifor1165-007

KRZYSTEK, Peter, Alla SEREBRYANYK, Claudius SCHNÖRR, Jaroslav ČERVENKA a Marco HEURICH, 2020. Large-scale mapping of tree species and dead trees in Sumava National Park and Bavarian Forest National Park

using lidar and multispectral imagery. *Remote Sensing* [online]. **12**(4), 1–22. ISSN 20724292. Dostupné z: doi:10.3390/rs12040661

KUŽELKA, Karel, Martin SLAVÍK a Peter SUROVỲ, 2020. Very High Density Point Clouds from UAV Laser Scanning for Automatic Tree Stem Detection and Direct Diameter Measurement. *Remote Sensing* [online]. Dostupné z: https://www.mdpi.com/2072-4292/12/8/1236

LAU, Alvaro, Lisa Patrick BENTLEY, Christopher MARTIUS, Alexander SHENKIN, Harm BARTHOLOMEUS, Pasi RAUMONEN, Yadvinder MALHI, Tobias JACKSON a Martin HEROLD, 2018. Quantifying branch architecture of tropical trees using terrestrial LiDAR and 3D modelling. *Trees - Structure and Function* [online]. **32**(5), 1219–1231. ISSN 09311890. Dostupné z: doi:10.1007/s00468-018-1704-1

LEE, Seung Kuk, Temilola FATOYINBO, Wenlu QI, Steven HANCOCK, John ARMSTON a Ralph DUBAYAH, 2018. GEDI and TanDEM-X fusion for 3D forest structure parameter retrieval. *International Geoscience and Remote Sensing Symposium (IGARSS)* [online]. **2018-July**, 380–382. Dostupné z: doi:10.1109/IGARSS.2018.8517718

LIANG, X. a L. MATIKAINEN, 2007. Deciduous-Coniferous Tree Classification Using Difference Between First and Last Pulse Laser Signatures. *Iaprs*. **XXXVI**(Part 3 / W52), 253–257.

LIANG, X, V KANKARE, X YU, J HYYPPÄ a M HOLOPAINEN, 2014. Automated Stem Curve Measurement Using Terrestrial Laser Scanning. *IEEE Transactions on Geoscience and Remote Sensing* [online]. **52**(3), 1739–1748. ISSN 1558-0644 VO - 52. Dostupné z: doi:10.1109/TGRS.2013.2253783

LIANG, Xinlian, Juha HYYPPÄ, Harri KAARTINEN, Matti LEHTOMÄKI, Jiri PYÖRÄLÄ, Norbert PFEIFER, Markus HOLOPAINEN, Gábor BROLLY, Pirotti FRANCESCO, Jan HACKENBERG, Huabing HUANG, Hyun Woo JO, Masato KATOH, Luxia LIU, Martin MOKROŠ, Jules MOREL, Kenneth OLOFSSON, Jose POVEDA-LOPEZ, Jan TROCHTA, Di WANG, Jinhu WANG, Zhouxi XI, Bisheng YANG, Guang ZHENG, Ville KANKARE, Ville LUOMA, Xiaowei YU, Liang CHEN, Mikko VASTARANTA, Ninni SAARINEN a Yunsheng WANG, 2018. International benchmarking of

terrestrial laser scanning approaches for forest inventories. *ISPRS Journal of Photogrammetry and Remote Sensing* [online]. **144**(December 2017), 137–179. ISSN 09242716. Dostupné z: doi:10.1016/j.isprsjprs.2018.06.021

LIANG, Xinlian, Ville KANKARE, Juha HYYPPÄ, Yunsheng WANG, Antero KUKKO, Henrik HAGGRÉN, Xiaowei YU, Harri KAARTINEN, Anttoni JAAKKOLA, Fengying GUAN, Markus HOLOPAINEN a Mikko VASTARANTA, 2016. Terrestrial laser scanning in forest inventories. *ISPRS Journal of Photogrammetry and Remote Sensing* [online]. **115**, 63–77. ISSN 09242716. Dostupné z: doi:10.1016/j.isprsjprs.2016.01.006

LIANG, Xinlian, Yunsheng WANG, Jiri PYÖRÄLÄ, Matti LEHTOMÄKI, Xiaowei YU, Harri KAARTINEN, Antero KUKKO, Eija HONKAVAARA, Aimad E.I. ISSAOUI, Olli NEVALAINEN, Matti VAAJA, Juho Pekka VIRTANEN, Masato KATOH a Songqiu DENG, 2019. Forest in situ observations using unmanned aerial vehicle as an alternative of terrestrial measurements. *Forest Ecosystems* [online]. **6**(1). ISSN 21975620. Dostupné z: doi:10.1186/s40663-019-0173-3

LISEIN, Jonathan, Marc PIERROT-DESEILLIGNY, Sťephanie BONNET a Philippe LEJEUNE, 2013. A photogrammetric workflow for the creation of a forest canopy height model from small unmanned aerial system imagery. *Forests* [online]. **4**(4), 922–944. ISSN 19994907. Dostupné z: doi:10.3390/f4040922

LIU, Kun, Xin SHEN, Lin CAO, Guibin WANG a Fuliang CAO, 2018. Estimating forest structural attributes using UAV-LiDAR data in Ginkgo plantations. *ISPRS Journal of Photogrammetry and Remote Sensing* [online]. **146**(November), 465–482. ISSN 09242716. Dostupné z: doi:10.1016/j.isprsjprs.2018.11.001

MALTAMO, Matti, Erik NÆSSET a Jari VAUHKONEN, 2014. Forestry applications of airborne laser scanning. *Concepts and case studies. Manag For Ecosys*. **27**, 460.

MEANS, J E, S A ACKER, B J FITT, M RENSLOW, L EMERSON a C J HENDRIX, 2000. Predicting forest stand characteristics with airborne scanning lidar. *Photogrammetric Engineering & Remote Sensing*. **66**(11), 1367–1371. ISSN ISSN 0099-1112.

MEGIES, Tobias, Moritz BEYREUTHER, Robert BARSCH, Lion KRISCHER a Joachim WASSERMANN, 2011. ObsPy - what can it do for data centers and observatories? *Annals of Geophysics* [online]. **54**(1), 47–58. ISSN 15935213. Dostupné z: doi:10.4401/ag-4838

MOKROŠ, M., J. VÝBOŠT'OK, J. TOMAŠTÍK, A. GRZNÁROVÁ, P. VALENT, M. SLAVÍK a J. MERGANIČ, 2018. High precision individual tree diameter and perimeter estimation from close-range photogrammetry. *Forests* [online]. **9**(11). ISSN 19994907. Dostupné z: doi:10.3390/f9110696

MOKROŠ, Martin, Jozef VÝBOŠT'OK, Ján MERGANIČ, Markus HOLLAUS, Iván BARTON, Milan KOREŇ, Julián TOMAŠTÍK a Juraj ČERŇAVA, 2017. Early stage forest windthrow estimation based on unmanned aircraft system imagery. *Forests* [online]. **8**(9), 1–17. ISSN 19994907. Dostupné z: doi:10.3390/f8090306

MORSDORF, Felix, Caroline NICHOL, Timothy MALTHUS a Iain H. WOODHOUSE, 2009. Assessing forest structural and physiological information content of multi-spectral LiDAR waveforms by radiative transfer modelling. *Remote Sensing of Environment* [online]. **113**(10), 2152–2163. ISSN 00344257. Dostupné z: doi:10.1016/j.rse.2009.05.019

MWERESA, I A, P A ODERA, D N KURIA a Benson Kipkemboi KENDUIYWO, 2017. Estimation of Tree Distribution and Canopy Heights in Ifakara, Tanzania Using Unmanned Aerial System (UAS) Stereo Imagery. *American Journal of Geographic Information System* [online]. **6**(5), 187–200. Dostupné z: doi:10.5923/j.ajgis.20170605.03

NÆSSET, Erik, 2002. Predicting forest stand characteristics with airborne scanning laser using a practical two-stage procedure and field data. *Remote Sensing of Environment* [online]. **80**(1), 88–99. ISSN 00344257. Dostupné z: doi:10.1016/S0034-4257(01)00290-5

NÆSSET, Erik a Terje GOBAKKEN, 2005. Estimating forest growth using canopy metrics derived from airborne laser scanner data. *Remote Sensing of Environment* [online]. **96**(3–4), 453–465. ISSN 00344257. Dostupné z: doi:10.1016/j.rse.2005.04.001

NÆSSET, Erik, Terje GOBAKKEN, Svein SOLBERG, Timothy G. GREGOIRE,

Ross NELSON, Göran STÅHL a Dan WEYDAHL, 2011. Model-assisted regional forest biomass estimation using LiDAR and InSAR as auxiliary data: A case study from a boreal forest area. *Remote Sensing of Environment* [online]. **115**(12), 3599–3614. ISSN 00344257. Dostupné z: doi:10.1016/j.rse.2011.08.021

NUHLÍČEK, Ondřej, Martin SLAVÍK a Jiří DVOŘÁK, 2020. 2D photogrammetry as a forwarder load measurement technique. *Forests* [online]. **11**(9), 6–9. ISSN 19994907. Dostupné z: doi:10.3390/f11090962

NURUNNABI, Abdul, Yukio SADAHIRO a Roderik LINDENBERGH, 2017. Robust cylinder fitting in three-dimensional point cloud data. *International Archives of the Photogrammetry, Remote Sensing and Spatial Information Sciences - ISPRS Archives* [online]. **42**(1W1), 63–70. ISSN 16821750. Dostupné z: doi:10.5194/isprs-archives-XLII-1-W1-63-2017

OLOFSSON, Kenneth, Johan HOLMGREN a Håkan OLSSON, 2014. Tree stem and height measurements using terrestrial laser scanning and the RANSAC algorithm. *Remote Sensing* [online]. **6**(5), 4323–4344. ISSN 20724292. Dostupné z: doi:10.3390/rs6054323

ØRKA, Hans Ole, Erik NÆSSET a Ole Martin BOLLANDSÅS, 2009. Classifying species of individual trees by intensity and structure features derived from airborne laser scanner data. *Remote Sensing of Environment* [online]. **113**(6), 1163–1174. ISSN 00344257. Dostupné z: doi:10.1016/j.rse.2009.02.002

PAL, M., 2005. Random forest classifier for remote sensing classification. *International Journal of Remote Sensing* [online]. **26**(1), 217–222. ISSN 01431161. Dostupné z: doi:10.1080/01431160412331269698

PANAGIOTIDIS, Dimitrios, Azadeh ABDOLLAHNEJAD a Martin SLAVÍK, 2020. Accuracy assessment of stem attributes for estimation of total stem volume using high-cost survey-grade terrestrial laser scanner : An application of precision forestry.

PANAGIOTIDIS, Dimitrios, Azadeh ABDOLLAHNEJAD, Peter SUROVÝ a Vasco CHITECULO, 2017. Determining tree height and crown diameter from high-resolution UAV imagery. *International Journal of Remote Sensing* [online]. **38**(8–10), 2392–2410. ISSN 13665901. Dostupné

z: doi:10.1080/01431161.2016.1264028

PEKÁR, Stanislav a Marek BRABEC, 2016. *Modern analysis of biological data: generalized linear models in R*. B.m.: Masarykova univerzita. ISBN 8021081066.

PFEIFER, Norbert, Ben GORTE, Daniel WINTERHALDER, Remote SENSING a Close RANGE, 2004. Automatic Reconstruction Of Single Trees From TLS Data. *Current* [online]. 1–6. Dostupné z: http://www.natscan.uni-freiburg.de/suite/pdf/040819_1810_1.pdf

POKORNY, R., I. TOMASKOVA a M. V. MAREK, 2011. The effects of elevated atmospheric [CO2] on Norway spruce needle parameters. *Acta Physiologiae Plantarum* [online]. **33**(6), 2269–2277. ISSN 01375881. Dostupné z: doi:10.1007/s11738-011-0766-0

PULITI, Stefano, HansPu OLERKA, Terje GOBAKKEN a Erik NÆSSET, 2015. Inventory of Small Forest Areas Using an Unmanned Aerial System. *Remote Sensing* [online]. **7**(8), 9632–9654. ISSN 2072-4292. Dostupné z: doi:10.3390/rs70809632

PUTMAN, Eric B., Sorin C. POPESCU, Marian ERIKSSON, Tan ZHOU, Paul KLOCKOW, Jason VOGEL a Georgianne W. MOORE, 2018. Detecting and quantifying standing dead tree structural loss with reconstructed tree models using voxelized terrestrial lidar data. *Remote Sensing of Environment* [online]. **209**(February), 52–65. ISSN 00344257. Dostupné z: doi:10.1016/j.rse.2018.02.028

QI, Wenlu a Ralph O. DUBAYAH, 2016. Combining Tandem-X InSAR and simulated GEDI lidar observations for forest structure mapping. *Remote Sensing of Environment* [online]. **187**(2016), 253–266. ISSN 00344257. Dostupné z: doi:10.1016/j.rse.2016.10.018

REITBERGER, J, P KRZYSTEK a U STILLA, 2008. Analysis of full waveform LIDAR data for the classification of deciduous and coniferous trees. *International Journal of Remote Sensing* [online]. **29**(5), 1407–1431. ISSN 0143-1161. Dostupné z: doi:10.1080/01431160701736448

RIEGL, 2019a. *Data Sheet, RIEGL VUX-1UAV*.

RIEGL, 2019b. RIEGL VUX-SYS [online]. 4. Dostupné

z: http://www.riegl.com/uploads/tx_pxpriegldownloads/RIEGL_VUX-SYS_Datasheet_2019-09-02.pdf

RIEGL, 2020. *RiPROCESS - Data Processing SOftware*. 2020.

SAČKOV, Ivan, Róbert SMREČEK a Ján TUČEK, 2014. Forest transportation survey based on airborne laser scanning data and GIS analyses. *GIScience and Remote Sensing* [online]. **51**(1), 83–98. ISSN 15481603. Dostupné z: doi:10.1080/15481603.2014.883213

SHIMANO, Koji, 1997. Analysis of the relationship between DBH and crown projection area using a new model. *Journal of Forest Research* [online]. **2**(4), 237–242. ISSN 13416979. Dostupné z: doi:10.1007/BF02348322

SIMONSE, M, T ASCHOFF, H SPIECKER a M THIES, 2003. AUTOMATIC DETERMINATION OF FOREST INVENTORY PARAMETERS USING TERRESTRIAL LASER SCANNING. In: .

SLAVÍK, Martin, 2017. *Využití dronů pro získání doplňujících inventarizačních dat na úrovni porostu Diplomová Práce*. B.m. ČZU v Praze, Fakulta Lesnická a Dřevařská.

SLAVÍK, Martin, Karel KUŽELKA, Branislav HROŠŠO a Peter SUROVÝ, 2020a. Spatial analysis of dense LiDAR point clouds for tree species classification. *Remote Sensing*. 1–15.

SLAVÍK, Martin, Karel KUŽELKA, Roman MODLINGER, Ivana TOMÁŠKOVÁ a Peter SUROVÝ, 2020b. UAV Laser Scans Allow Detection of Morphological Changes in Tree Canopy. *Remote Sensing* [online]. Dostupné z: doi:10.3390/rs12223829

ŠMELKO, Š, 2000. *Dendrometria*.

SOCHA, Jarosław, Paweł HAWRYŁO, Krzysztof STEREŃCZAK, Stanisław MIŚCICKI, Luiza TYMIŃSKA-CZABAŃSKA, Wojciech MŁOCEK a Piotr GRUBA, 2020. Assessing the sensitivity of site index models developed using bi-temporal airborne laser scanning data to different top height estimates and grid cell sizes. *International Journal of Applied Earth Observation and Geoinformation* [online]. **91**(January), 102129. ISSN 03032434. Dostupné z: doi:10.1016/j.jag.2020.102129

SOCHA, Jarosław, Marcin PIERZCHALSKI, Radomir BAŁAZY a Mariusz

CIESIELSKI, 2017. Modelling top height growth and site index using repeated laser scanning data. *Forest Ecology and Management* [online]. **406**(October), 307–317. ISSN 03781127. Dostupné z: doi:10.1016/j.foreco.2017.09.039

SOLODUKHIN, V I, A Y ZHUKOV, I N MAZHUGIN a V I NARKEVICH, 1976. Metody Izuchenija Vertikal'nyh Sechenij Drevostoev (Method of study of vertical sections of forest stands). *Leningrad Scientific Research Institute of Forestry, Leningrad*. **55**.

SOLOMON, O. L., D. K. BERGER a A. A. MYBURG, 2010. Diurnal and circadian patterns of gene expression in the developing xylem of Eucalyptus trees. *South African Journal of Botany* [online]. **76**(3), 425–439. ISSN 02546299. Dostupné z: doi:10.1016/j.sajb.2010.02.087

SUROVÝ, Peter, Karel KUŽELKA, Azadeh ABDOLAHNEJAD, Kateřina SIROTKOVÁ, Zlatica MELICHOVÁ a Martin SLAVÍK, 2019. *Aplikace dálkového průzkumu Země v lesnictví*. B.m.: ČZU v Praze, Fakulta Lesnická a Dřevařská. ISBN 8001015971.

SUROVÝ, Peter, Atsushi YOSHIMOTO a Dimitrios PANAGIOTIDIS, 2016. Accuracy of reconstruction of the tree stem surface using terrestrial close-range photogrammetry. *Remote Sensing* [online]. **8**(2), 1–13. ISSN 20724292. Dostupné z: doi:10.3390/rs8020123

TRIMBLE, 2016. Trimble TX8. *Trimble TX8 Datasheet* [online]. 2. Dostupné z: https://www.trimble.com/3d-laser-scanning/tx8

TRIMBLE INC., 2016. *Trimble RealWorks User Guide*® [online]. Dostupné z: https://trl.trimble.com/docushare/dsweb/Get/Document-931765/TrimbleRealWorks 11.2 User Guide.pdf

VERMA, Niva Kiran, David W. LAMB, Nick REID a Brian WILSON, 2014. An allometric model for estimating DBH of isolated and clustered Eucalyptus trees from measurements of crown projection area. *Forest Ecology and Management* [online]. **326**, 125–132. ISSN 03781127. Dostupné z: doi:10.1016/j.foreco.2014.04.003

VETRIVEL, Anand, Markus GERKE, Norman KERLE a George VOSSELMAN, 2015. Identification of damage in buildings based on gaps in 3D point clouds from very high resolution oblique airborne images. *ISPRS Journal of*

Photogrammetry and Remote Sensing [online]. **105**, 61–78. ISSN 09242716. Dostupné z: doi:10.1016/j.isprsjprs.2015.03.016

WALLACE, Luke, Arko LUCIEER, Zbyněk MALENOVSKỲ, Darren TURNER a Petr VOPĚNKA, 2016. Assessment of forest structure using two UAV techniques: A comparison of airborne laser scanning and structure from motion (SfM) point clouds. *Forests* [online]. **7**(3), 1–16. ISSN 19994907. Dostupné z: doi:10.3390/f7030062

WALLACE, Luke, Arko LUCIEER, Christopher WATSON a Darren TURNER, 2012. Development of a UAV-LiDAR system with application to forest inventory. *Remote Sensing* [online]. **4**(6), 1519–1543. ISSN 20724292. Dostupné z: doi:10.3390/rs4061519

WANG, Pei, Ronghao LI, Guochao BU a Rui ZHAO, 2019. Automated low-cost terrestrial laser scanner for measuring diameters at breast height and heights of plantation trees. *PLoS ONE* [online]. **14**(1), 1–26. ISSN 19326203. Dostupné z: doi:10.1371/journal.pone.0209888

WIESER, Martin, Gottfried MANDLBURGER, Markus HOLLAUS, Johannes OTEPKA, Philipp GLIRA a Norbert PFEIFER, 2017. A case study of UAS borne laser scanning for measurement of tree stem diameter. *Remote Sensing* [online]. **9**(11). ISSN 20724292. Dostupné z: doi:10.3390/rs9111154

YAO, Tian, Xiaoyuan YANG, Feng ZHAO, Zhuosen WANG, Qingling ZHANG, David JUPP, Jenny LOVELL, Darius CULVENOR, Glenn NEWNHAM, Wenge NI-MEISTER, Crystal SCHAAF, Curtis WOODCOCK, Jindi WANG, Xiaowen LI a Alan STRAHLER, 2011. Measuring forest structure and biomass in New England forest stands using Echidna ground-based lidar. *Remote Sensing of Environment* [online]. **115**(11), 2965–2974. ISSN 00344257. Dostupné z: doi:10.1016/j.rse.2010.03.019

YU, Xiaowei, Xinlian LIANG, Juha HYYPPÄ, Ville KANKARE, Mikko VASTARANTA a Markus HOLOPAINEN, 2013. Stem biomass estimation based on stem reconstruction from terrestrial laser scanning point clouds. *Remote Sensing Letters* [online]. **4**(4), 344–353. ISSN 2150704X. Dostupné z: doi:10.1080/2150704X.2012.734931

9. Přílohy

Příloha č. 1 - Slavík, M., Kuželka, K., Modlinger, R., Tomášková, I., & Surový, P. (2020). UAV Laser Scans Allow Detection of Morphological Changes in Tree Canopy. *Remote Sensing*

remote sensing

MDPI

Technical Note

UAV Laser Scans Allow Detection of Morphological Changes in Tree Canopy

Martin Slavík *, Karel Kuželka, Roman Modlinger, Ivana Tomášková and Peter Surový

Faculty of Forestry and Wood Sciences, Czech University of Life Sciences, Prague, Kamýcká 129, 165 00 Praha, Czech Republic; kuzelka@fld.czu.cz (K.K.); modlinger@fld.czu.cz (R.M.); tomaskova@fld.czu.cz (I.T.); surovy@fld.czu.cz (P.S.)

* Correspondence: mslavik@fld.czu.cz; Tel.: +42-0731-315-937

Received: 14 October 2020; Accepted: 19 November 2020; Published: 21 November 2020

Abstract: High-resolution laser scans from unmanned aerial vehicles (UAV) provide a highly detailed description of tree structure at the level of fine branches. Apart from ultrahigh spatial resolution, unmanned aerial laser scanning (ULS) can also provide high temporal resolution due to its operability and flexibility during data acquisition. We examined the phenomenon of bending branches of dead trees during one year from ULS multi-temporal data. In a multi-temporal series of three ULS datasets, we detected a synchronized reversible change in the inclination angles of the branches of 43 dead trees in a stand of blue spruce (*Picea pungens* Engelm.). The observed phenomenon has important consequences for both tree physiology and forest remote sensing (RS). First, the inclination angle of branches plays a crucial role in solar radiation interception and thus influences the total photosynthetic gain. The ability of a tree to change the branch position has important ecophysiological consequences, including better competitiveness across the site. Branch shifting in dead trees could be regarded as evidence of functional mycorrhizal interconnections via roots between live and dead trees. Second, we show that the detected movement results in a significant change in several point cloud metrics often utilized for deriving forest inventory parameters, both in the area-based approach (ABA) and individual tree detection approaches, which can affect the prediction of forest variables. To help quantify its impact, we used point cloud metrics of automatically segmented individual trees to build a generalized linear model to classify trees with and without the observed morphological changes. The model was applied to a validation set and correctly identified 86% of trees that displayed branch movement, as recorded by a human observer. The ULS allows for the study of this phenomenon across large areas, not only at individual tree levels.

Keywords: ULS; LiDAR; forestry; canopy changes; branch bending; change detection

1. Introduction

Long-term planning, as well as operative decisions in managing forest properties, rely on accurate and up-to-date information. Remote sensing has proven to be a viable method for the fast and accurate acquisition of data describing different aspects of forest conditions for decision-making [1]. Recent remote sensing approaches to evaluating forest inventory parameters are mostly based on three-dimensional (3D) structural information derived from digital aerial photogrammetry (DAP) or aerial laser scanning (ALS). To quantify many important forest inventory parameters, such as heights, basal areas, and volumes, an ABA is often applied to three-dimensional point clouds produced using DAP or ALS [2–4]. Using ABA, entire homogenous areal units, such as forest stands or grid cells, are characterized by a single representative value of a given parameter, which is based on various metrics describing the 3D structure of point clouds, with an emphasis on the vertical component of the

structure. However, intraseasonal changes in tree structure, such as periodic movement of plant organs, can significantly change values of selected point cloud metrics, which would in turn notably affect the estimated inventory parameters based on the relation of tree crown size and diameter at breast height (DBH) [5].

Plant movement has been detected and described by several authors since the nineteenth century [6]. Biological oscillations are driven by more than 20 genes, including TOC1, LHY, and CCA1. The LHY and CCA1 genes stimulate the construction of light harvesting antennas of the photosynthetic apparatus, and concentrations of TOC1 gene products do not begin to increase until the night [7]. The main driving factor is the light captured by photoreceptors. They are responsible for nyctinastic movements, start of flowering, and photomorphogenesis. Differences in osmotic potentials and photoperiodism are the cause of circadian movements, and they are typical for leaves, flowers, and branches. Of all stem and branching properties, branch angle has the highest heritability and is under strong genetic control [8]. Nevertheless, it does change under different environmental conditions [9]. Morphological changes in silver birch (*Betula pendula* Roth) tree crowns during circadian cycles were detected in terrestrial laser scanning (TLS) data in Finland and Austria, with the biggest changes occurring at sunrise and sunset [10]. A second study [11] was aimed at the detection of circadian movements of 18 selected tree species individuals. In both highly-cited studies [10,11], the TLS method was used for data acquisition, and both author collectives concluded that the method was time-demanding. In contrast to TLS, the ULS data acquisition provides lower point cloud density matched with high time efficiency [12–15]. A yearlong investigation of the branch inclination angles using TLS was not performed on forest trees. Similarly, all investigations of crown morphology changes with respect to environmental factors were done exclusively on living trees.

LiDAR (light detection and ranging) technology is based on the active sensing of laser beams and it provides a practical option to measure tree heights and other important tree parameters [16,17]. Relative to other modern remote sensing technologies, LiDAR provides the opportunity to assess detailed characteristics of a single individual tree and its components [18,19]. The first research focused on LiDAR observations of trees was described by [20]. The authors tried to delineate tree stem profiles using harvested trees mounted in a vertical position observed by a LiDAR system mounted on a crane arm; the data were then compared with traditional tape measurements.

The LiDAR laser scanning method for forestry data acquisition can be used at several levels depending on the level of detail (point density) and time consumption per square unit with respect to possible accuracy and precision. The first LiDAR method commonly used in forestry research practice was the ALS, which allowed for observing large areas at regional scales. Individual tree detection based on forest structure canopy profiles in ALS data using returned echoes emitted from a pulse laser scanning device has been described by [21]. Terrestrial laser scanning (TLS) was later used to provide ultra-high-density point clouds at the tree level; it can very precisely represent tree architecture, thus allowing for the definition of specific morphological trends [22]. Two studies have demonstrated the effectiveness of TLS for estimating aboveground biomass (AGB) and quantitative structural models (QSMs) at the individual tree level with regard to high possibility of tree morphology reconstruction at the peripheral tree branch level [23,24].

The ULS method combines the relatively high point density and accuracy of TLS with the time efficiency and possibility of recording several returns in canopy from ALS; however, the ULS method cannot achieve such high accuracy and point density as TLS. Thanks to multi-angle scanning, the ULS data can, with high detail, represent individual trees and their components with accuracy approaching 10 mm at the forest, stand, or sub-compartment scales. The first study aimed at UAV LiDAR data acquisition and evaluation was presented by [25], where the authors used a combination of instruments, Ibeo Lux and a Sick LMS151. The mentioned study presented the pole method for tree detection. The author collective of [26] presents the early development of a low-cost UAV LiDAR TerraLuma, where they reached a point density of 62 points m^2. The same unmanned aerial system (UAS) used for this study is suitable for forestry application. Based on reference data from TLS measurements from several stands in sampled plots, studies have demonstrated the high potential of the ULS VUX-SYS (RIEGL Laser Measurement System GmbH, Horn, Austria) setup for forestry

data acquisition [12,13]. The point densities in the lower stem portions were not as high as those produced using TLS methods, but they would be quite sufficient for the derivation of forest inventory values, such as diameter at breast height (DBH), or for estimating AGB using ULS data. Moreover, both studies suggested the possibility of using ULS data to produce high-resolution digital terrain models (DTM) and canopy height models (CHM).

The utilization of a CHM calculated from a DTM and a digital surface model (DSM) derived from photogrammetry data for forest inventory purposes focused on tree delineation—in particular, individual tree height and crown projection derivations—in the ArcGIS environment using the inverse watershed segmentation (IWS) method has been described with the overall workflow [27]. The photogrammetry RS methods are based on a developed scale-invariant feature transform algorithm [28]. One study [15] described and evaluated several methods for tree detection, including IWS, individual tree segmentation (ITS), and point cloud segmentation (PCS), and ULS has also been used for individual tree detection [25]. The advantage of low cost and feasible multi-temporal data acquisition for the derivation of DTM and individual tree change detection based on CHM will also be used for estimation of carbon stock, describing the carbon dynamics [29], and for describing the forest vertical structure [30] from the International Space Station (ISS) module, NASA's Global Ecosystem Dynamics Investigation (GEDI) data. The forest ecosystems are a carbon source, yet forests have great potential to capture carbon dioxide from the atmosphere [31]. The carbon changes—that is, the carbon losses—were mapped at large scales using LiDAR technology across tropical forests by [32] from time series data based on cell analysis by random forest classification [33].

This study describes the detected movements of dead tree branches and their detection in forest stands using individual tree metrics for the derivation of a generalized linear model (GLM) on two datasets, one for GLM derivation and the second for data validation.

2. Materials and Methods

2.1. Research Area

The forest stand is located in the northern region of the Czech Republic, near the village Moldava (50°41′5.619″N, 13°38′38.500″E) in the Ore Mountains (Figure 1), with orientation to the south and 35 m elevation gain (from 832 m AMSL to 867 m AMSL). The research plot was situated in an approximately 2.2 ha area of an even-aged stand of 460 blue spruce (*Picea pungens* Englem.) trees with mean height 9.12 m (range of height from 3.13 to 12.61 m) and 1.61 height standard deviation. This species was introduced to the mountainous regions as a substitute for the dying forest stands during the 1970s [34], mainly because of the pollution emissions from the coal-powered power plants surrounding the Ore Mountains on both the Czech and German sides of the range. The stand has since been infested by bud blight *Gemmamyces piceae* (Brothw.) Casagr., which has caused the death of 43 individuals on the plot. The impacts of these pathogens across the Ore Mountains have been described by [35].

Figure 1. Location of the research plot in the northern region of the Czech Republic. The plot is marked with green point.

2.2. Data Acquisition

We used the UAS VUX-SYS (RIEGL Laser Measurement System GmbH, Horn, Austria) setup for UAV-borne data acquisition consisting of the UAV RiCOPTER, the VUX-1UAV laser scanner, and the AP-20 inertial measurement unit (IMU). RiCOPTER is an eight-propeller UAV with a carbon body [36], with detailed information given in Table 1. VUX-1UAV is a high-speed infrared laser scanner using online waveform processing with a maximum frequency of 550 MHz and 330° FOV (field of view); this configuration provides a beam range up to 300 m. The AP-20, made by APPLANIX (Applanix, Richmond Hill, ON, Canada), is a multipurpose IMU focused on reaching high accuracy and precision of acquired data in the form of 3D digital point clouds. This component is important in trajectory post-processing with regard to trajectory-based solutions of data derivation and co-registration of single scans acquired during the flight.

Table 1. Detailed information about VUX-SYS provided by [36].

RiCOPTER	Characteristics
Total weight	25 kg
Sensors (VUX-1UAV + cameras)	3.5 kg
Batteries (Li-Pol 29.4V 12,500 mAh)	7.5 kg
Maximum flight time	28 min
Maximum horizontal speed	14 m·s^{-1}
Maximum ascending speed	5 m·s^{-1}
Maximum descending speed	2 m·s^{-1}

UAS data acquisition (Figure 2) was performed during three independent campaigns (7 May, 23 July, and 10 November, 2019) with the use of the UAS VUX-SYS setup. All three flights were flown automatically, following an identical predefined trajectory. The trajectory was planned and the flights

performed using the UgCS (Universal Ground Control Station) mission planning software (SPH Engineering, Riga, Latvia). The trajectory followed a perpendicular zigzag pattern consisting of parallel lines with 50-m spacing. The zigzag pattern with overlaps between individual scan lines was used for reaching high point density, mainly for highly detailed individual tree point clouds. The data were acquired only during the uniform straight-line motion of the UAV; for stops and turns in the trajectory vertices, data acquisition was discontinued. The UgCS software contains DTM, which allowed us to fly the vehicle at a constant aboveground height, which enabled the acquisition of uniform point densities throughout the study site.

The VUX-1UAV laser scanner was set to its maximum pulse frequency of 550 kHz with a registration of 200 scanning lines per second. The flight was performed at a constant altitude of 90 m aboveground, with a constant ground speed of 6 $m \cdot s^{-1}$. This setup reached an average point density of 200 points m^2 for each scanning line. Due to the overlap of individual scanning lines, the final point density was around 2000 points m^2.

During mission planning, we accounted for UAV weather limitations with a maximum wind speed of 10 m/s and a temperature interval from −10 to +40 °C [36]. We also observed all the national law restrictions, summarized in [37], of which the most important are a maximum flight altitude 300 m aboveground, visual line of site between pilot and UAV, availability of the air space (controlled on web portal of Air Navigation Services of the Czech Republic), and minimum distance from people and buildings.

Red-green-blue (RGB) imagery of the research area was acquired with a DJI Phantom 4 Pro (DJI, Shenzhen, China) during a planned automatic flight using the PrecisionFlight mobile phone application. The aboveground flight altitude was 100 m, the maximum speed was set to 6 $m \cdot s^{-1}$, and front and side overlap was 85%.

Figure 2. The UAS VUX-SYS setup and pilot before takeoff during the spring data acquisition (7 May 2019).

2.3. Data Processing

Prior to the initial point cloud creation, we needed to create trajectory calculations. Raw trajectory is not accurate and it does not provide sufficient accuracy for the individual tree level analyses. To develop the appropriate trajectories, we used reference station (RS) post-processing kinematics (PPK) with the virtual BS from Trimble VRS Now, which entered the calculation process as data in RINEX format. With regard to forward and backward calculations not exceeding the difference of 3 cm standard deviation, the RS PPK correction was applied in the environment of software POSPac MMS 8.1 (Applanix: a Trimble company, Richmond Hill, ON, Canada). The result of PPK trajectory calculations was smoothed best estimate of trajectory (SBET). Based on the

recalculated SBET trajectory, the initial point cloud was derived from the raw data of VUX-1UAV in the environment of RiPROCESS (RIEGL Laser Measurement System Gmbh, Horn, Austria). The accuracy of the whole point cloud was improved by module RiPRECISSION included in the RiPROCES software. The RiPRECISSION module improved the co-registration of single scans according to the straight parts of the trajectory, mainly along the Z axis. RiPROCESS also enables basic point cloud classification, which was sufficient for this study. Points were assigned to one of three classes; the first class contained isolated points represented mainly by noise based on the minimum number of neighbors within a defined distance, and all other points were classified as vegetation or ground points. Not all points lying on the ground were classified as ground points, but this basic approximation of ground in the point cloud helped to improve individual tree detection.

RGB geotagged imagery was processed in Agisoft MetaShape 1.6 (Agisoft LLS, St. Petersburg, Russia) following the standard workflow of SfM (structure from motion) scene reconstruction (e.g., as described in [38,39]). Subsequently, we derived an orthomosaic of the whole research area. Segmentation of individual trees in CHM derived from ULS point cloud was performed in ArcGIS 10.6.1 (ESRI, Redlands, CA, USA) with the use of 3D Sample Tools toolbox. Individual tree tops were detected as local maxima of CHM, and crowns of individual trees were segmented using the IWS algorithm described by [27]. The tree positions were assigned a unique ID for individual trees, which were verified on the ground to avoid missing trees. For each individual tree, IWS was used to identify the points associated with the tree, and we could then produce crown segmentation for the tree.

2.4. Field Data Collection

All detected trees were marked in the forest stand by their assigned IDs, which allowed for easy field recognition of each individual tree for human observer-based canopy change detection. The true orthophoto was overlaid with the point layer with IDs of all individual trees, which facilitated orientation and highly limited the possibility of misidentification of the trees in the stand. The health status of each individual tree was evaluated based on the defoliation rate, as described by [40]. Defoliation rate was determined as an indicator of health status according to the grading system used for ICP (International Co-operate Program)-forest monitoring, based on the individual evaluating the defoliation on a scale from 0 to 100%, with 5% increments. Each tree was evaluated from four main cardinal directions by two evaluators, who were trained for such types of evaluation. These data were later used for evaluation of health status of bending branch trees.

2.5. Evaluation

The next step was to verify whether bending tree branch changes could be quantified by a set of canopy metrics and automatically identified. Simultaneously, this step allowed identification of canopy metrics that were significantly affected by the tree habitus (outer look) change. For this purpose, the research area was divided into two parts of equal size. Half of the total 408 trees in the research plot, i.e., 204 trees, served as training data for the model; the other 204 trees were kept retained for validation. The training set and validation sets contained 14 and 29 trees, respectively, with detected habitus changes.

The IWS polygons representing horizontal crown projections of individual trees identified in the spring point clouds were used as clip masks to clip points belonging to individual trees from spring and summer LiDAR point clouds. As a result, a time series of two point cloud representations (spring and summer) with identical spatial extents were available for each of the 408 segmented trees. Vertical (Z) coordinates were normalized so that the normalized height of points in each tree was between 0 and 1. Each tree was sliced into 10 uniform vertical layers, so that layer 1 contained points with normalized heights between 0 and 0.1, and so forth. For each layer, a convex hull of vertical projection of corresponding points was defined and the area of the convex hull was calculated.

For each tree, we quantified eighteen point cloud metrics for both spring and summer point clouds: A1 consecutive through A9 denote areas of convex hulls in layers 1 through 9, respectively; Q1 consecutive through Q9 denote 0.1 through 0.9 quantiles of the normalized heights, respectively. The index describing the spring to summer change in each metric was defined as the summer value

divided by the spring value (i.e., $A1_{change} = A1_{summer}/A1_{spring}$). Index values higher than 1 expressed an increase in the metric, while values lower than 1 demonstrated a decrease in the metric value.

The temporal changes in crown metrics were used as predictors in a generalized linear model to explain the presence or absence of habitus change (the response variable). We used the additive form of the model without interactions, and according to the nature of the response variable, we chose a binomial error distribution model by the stepwise regression method with regard to AIC (Akaike information criterion) value [41].

3. Results

3.1. The Detected Trees

From the three flights were derived three point clouds with an average of 2082 points m² for the first flight, 1525 points per m² for the second flight, and 1582 points per m² for the third flight. A total of 460 individual trees were automatically identified, which correlated with the 460 trees in the forest stand—a detection rate of 100% with 0 omitted trees. Figure 3 shows the derived orthophoto from 179 geotagged images with ground sampled distance 2.81 cm·pixel. Not all trees were properly delineated, as represented by inaccurate automatic creations of horizontal crown projections represented by their polygons in ArcGIS 10.6.1 (ESRI, Redlands, CA, USA). The final dataset was comprised of 408 trees with completely delineated crowns.

Detected individual tree positions are shown in Figure 3; there is an obvious visible space shift caused by different accuracies of the photogrammetry data (geotagged images from DJI Phantom 4 Pro) contrary to the high accuracy of ULS (derived using trajectory of PPK from VRS Now BS).

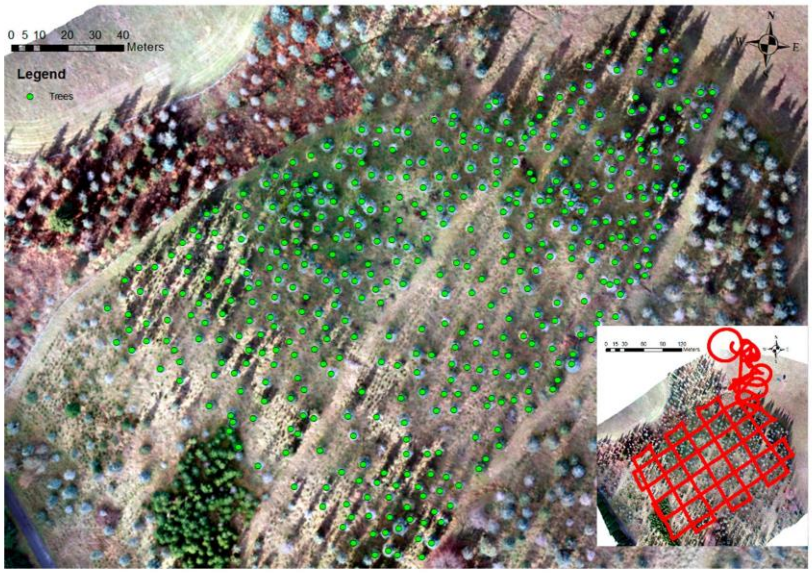

Figure 3. Detected positions of all trees derived from ULS point cloud in the stand overlapping the high-resolution orthophoto. The orthophoto mainly helped with the ground survey for better orientation during field data acquisition and for human observer tree detection verification. The spatial shift is mainly the result of using recalculated trajectory based on PPK from ULS and the aerial imagery from aerial photogrammetry was not corrected. In the bottom right corner is an example of a used trajectory.

Figure 4 highlights an example of height difference rasters and demonstrates the difference between two selected trees. The estimated tree top is marked with an individual Id, detected as a local height maximum and used as a tree position. Tree 273 shows a marked difference in its crown configuration compared to the neighboring tree 265 between spring and summer (Figure 4a), but there is no significant difference between the two trees between spring and autumn (Figure 4b). The red color surrounding tree 273 shows the negative change in height raster values representing the bent branches.

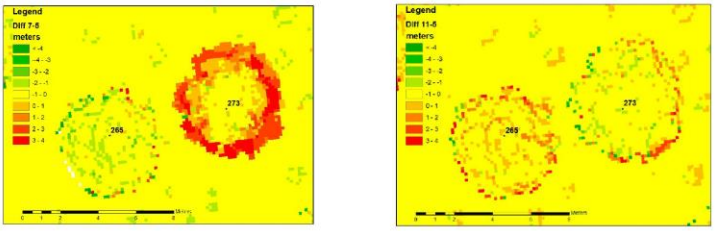

(**a**) (**b**)

Figure 4. Comparison of two selected tree heights (maximum height value in raster cell from 3D point cloud) displaying raster of 10 cm·pixel differences of two flights where tree 265 was not detected to have bending branches and tree 273 was detected to have bending branches: (**a**) Difference between summer and spring flight; raster values around tree 273 are red cells with positive values showing the difference in crown structure (e.g., bent branches); (**b**) Difference between spring and autumn flights; cell values around tree 273 show no difference, as the branches have returned to their spring positions.

Figure 5 depicts two neighboring trees based on the point clouds derived from the three flights; the tree on the right clearly has its branches turned down during the summer (Figure 5b), but the tree on the left displays no significant changes in branch angles over time. In Figure 5d, a noticeable height increment is obvious in the tree on the left (265), compared to the tree on the right (tree 273, a dead tree), where no visible height increment was evident. The reversible bending of the branches of the dead tree followed by the recovery close to the initial position is also evident.

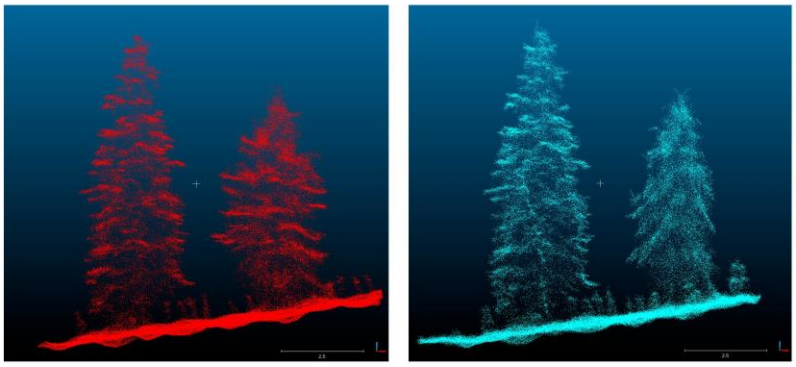

(**a**) (**b**)

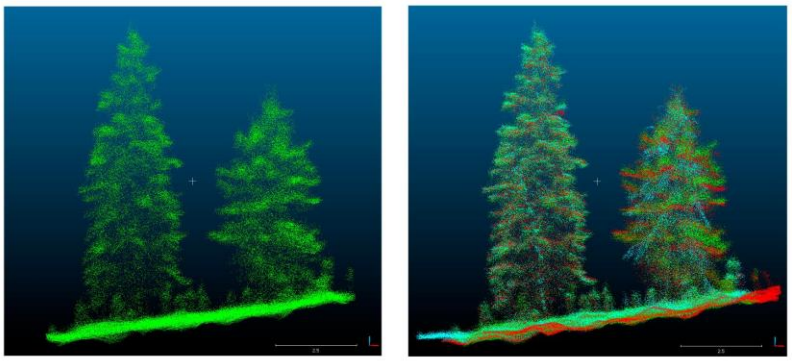

(**c**) (**d**)

Figure 5. Examples of individual tree point clouds for tree 265 (on the left) and tree 273 (on the right). For this example, we used the same two trees as described in Figure 3. The individual plates show the point clouds for the two trees: (**a**) spring flight with tree 273 with branches straight; (**b**) summer flight with tree 273 branches bent; (**c**) autumn flight with tree 273 with branches in the original position; (**d**) all three point clouds overlapped.

Figure 6 displays boxplot distributions of calculated areas (Figure 6a) and quantiles (Figure 6b) for trees with no evidence of bending branches (yellow) and dead trees with bending branches (green). For the derivation of the GLM, we used only the area indices (Figure 6a).

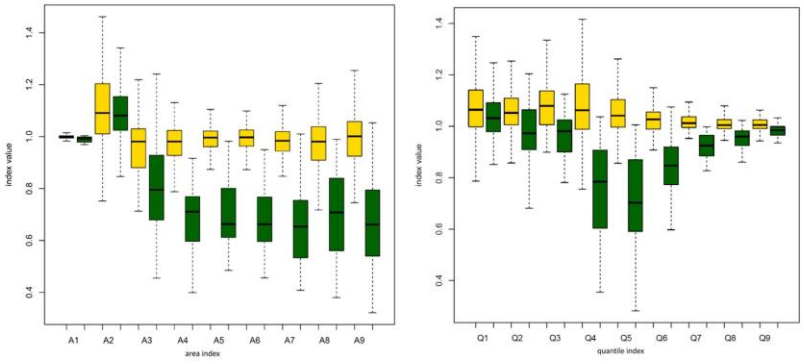

(**a**) (**b**)

Figure 6. Boxplots for calculated areas (**a**) and quantiles (**b**) along tree lengths; yellow bars represent trees with no bending branches, and green bars represent dead trees with evidence of bending branches. On horizontal axis are described the names of used metrics and on the vertical axis are index values.

3.2. Automatic Identification of Trees with Habitus Change

Of the nine predictors representing the temporal changes in canopy metrics, five showed a significant difference, including A1, A2, A5, A6, and A9 (Table 2). The most significant predictor was the area change in the lowest layer (A1), where the increase in layer area was the result of the bending

branches from the upper layer. However, in some trees of the validation set, the area change could not be detected due to the presence of objects, such as stumps or deadwood, in the area of the tree, and the model failed to identify such trees.

The A1 and A2 predictors, representative of the area of the lower crown layers, showed increases interpreted as an increase in lower crown cross-section width due to the bending of branches from upper crown layers. In contrast, the A5, A6, and A9 predictors showed a decrease caused by bending of the grown branches to the lower parts of the tree, decreasing the width of the crown at the respective heights. The initial Akaike Information Criteria (AIC) score was 29.639 and improved to 23.551 with the final GLM.

Table 2. The derived GLM from nine calculated canopy metrics for individual trees.

	Estimate	SE	tStat	*p*-Value
Intercept	32.884	22.659	1.451	0.1467
A1	43.728	30.725	1.423	0.1547
A2	6.350	4.130	1.538	0.1241
A5	−53.701	26.340	−2.039	0.0415
A6	−28.857	15.987	−1.805	0.0711
A9	−15.078	8.609	−1.752	0.0798

AIC 23.551.

In the validation set, morphologic changes were manually detected in 14 trees. The model classified 19 trees into the morphologic change class; 12 (i.e., 86% of the real count) of them were classified correctly, and five represented the commission error (false positive). Datasets comparison is described in Table 3.

Table 3. Explanation of calculated values for training and validation datasets. Trees—total number of trees in dataset; change—number of trees with branch bending detected; false negative—trees with branch bending but not detected; false positive—incorrectly detected as trees with branch bending; correct—correctly detected as trees with branch bending.

Dataset	Trees	Change	False Negative	False Positive	Correct
Training	204	29	1	2	28
Validation	204	14	2	5	12

4. Discussion

The high detection rate was achieved mainly due to the limited stocking of the stand. This greatly limited the possibility of not detecting the actual tree because individual tree canopies were not often connecting, as is mentioned by [27]. The limitations of the IWS segmentation from ULS data in close canopy forest were tested and compared with several other methods by [15]. The study of [26] mentioned reaching high detection potential of individual standing trees. Moreover, there was no substantial undergrowth, except for some Norway spruce (*Picea abies* L.) in the understory that was shorter than the minim tree height threshold of 2 m.

Estimated values of the derived GLM represent the movement of the points along the stem profile in the individual tree point clouds caused by the bending of branches to the lower parts of the tree. Whereas the A1 predictor displayed the highest point increment due to bending of branches from the area above to the space where there were few branches and mainly only the stem (i.e., the points representing the stem); the A2 predictor displayed a lower increment, but still significant for the detection of bending branches in dead trees. The A5 predictor estimated value shows the highest decrease in points to lower parts with also a significant positive increment in points from A6, another significant predictor. Logically, the A9 predictor showed a drop in points from the top part of the tree, where a positive change in cross-section area could not be expected.

In comparison to TLS methods, the ULS is a much less time-demanding method for data acquisition. One 21-min flight can be sufficient for data collection of a forest stand approximately 5 hectares in size; this is in contrast to TLS data acquisition of a comparable area, which may take several days to complete [12,13]. In the case of repeated ULS data acquisition, time required for flight preparation, as flight trajectory optimizing a planning, can be eliminated by using identical predefined trajectory, which was the case in this study. However, the presented methodology for temporal change detection does not require data acquired with flight with identical trajectories. Due to the high pulse frequency of the scanner and multiple returns from beams penetrating the canopy, point clouds of uniform densities of high-precision points are produced. The changes can be detected in the whole scanned area, regardless of the actual trajectory, if the trajectory parameters such as flight height and flight line spacing responsible for point cloud density and accuracy are kept constant. A standard method for the practical evaluation of current status of individual trees or stands is based on human observation while walking in the forest stands. However, this would be an incredibly time-demanding method for the detection of bending branches on individual trees.

Another mapping possibility is the use of the mobile laser scanning (MLS) method in such an open canopy stand. From the MLS point of view, there are GNSS accessibility options under the canopy, which could be limited in such a stand as was used for purposes of this study; however, this is only the case in trajectory-based solutions [42]. Within the simultaneous localization and mapping (SLAM) solutions that were used in the ULS and MLS methods compared for stem detection in the study of Hyppa [43], they may also include a possible trajectory-based solution for use under canopies with insufficient GNSS signal. The MLS method can possibly influence the quality of individual tree point clouds, mainly because of the point cloud density issues due to the necessity of observation of the whole tree profile. The trees in this study had branches very low on the stem, which may have possibly caused laser beam shading obstructions. However, the MLS data collection method for the phenomenon described in this study requires further research.

During the year, the morphological structure of the tree reacts to the circadian rhythm and the changing solar zenith angles. We offer several explanations of the dead branches' movements:

- In cases where portions of the roots are still alive, the existing root connection to neighboring living trees can mediate responses to environmental conditions, even in the case of fatal loss of assimilation apparatus. Fungal interconnections support not only the transfer of water [44] but also carbon and nitrogen compounds [45]. Moreover, mycorrhizal connections act as conduits for signaling between plants [46]. It is highly probable that these conduits can also transport signals associated with solar radiation. Water uptake is driven by the transpiration demands of the assimilation apparatus. In the case of dead trees, water uptake could be due to the transpiration apparatus of the living tree and/or water efflux through the lenticels in the periderm [47,48]. This hypothesis is supported by the close proximity of living blue spruce to all dead trees in the study.
- Water uptake from the soil by any surviving roots of the dead trees without any support from other trees or fungus. This hypothesis supports the highest amount of precipitation during the winter period, e.g., with a surplus of water during the early spring and autumn. The water uptake through root systems which have been killed was described by [49].
- The branch shifting during the year could be related to the branch length [50]. This observation using an RTM approach in a mixed broadleaf forest confirmed the sagging of a branch and on the opposite branch stub rising after losing its terminal part, simply as the total branch weight decreased.

While branch movement has been detected on live plants [51] or live trees [52,53] and has been described by changes in turgor at the molecular level of plant or tree components, in this study, we detected branch movements of dead trees. In contrast, dead branch movement has been observed to be related to the decay process with the loss of branch terminals [50]. Excluding root interconnection between living and dead trees, dead branch movement is not a physiological process but physical one. Our multi-temporal data samples taken throughout one year provide evidence that the branches

of dead trees are capable of returning to their original spring position in the fall after displaying drooping branches during the summer growth period. In contrast to our study, in which we used three scans throughout the year, Barak et al. [51] only used two time-distanced scans per tree; thus, we could determine if the branches returned to their "initial" position. The TLS method is, for this purpose, time-consuming, in contrast to the ULS method, which is adequate for the derivation of representative individual tree point clouds for many common forest inventory values, and its time efficiency compared to TLS methods makes it more practical for surveys across larger areas [12,13,15].

An important scientific question is how these bending branches trees could potentially influence results of the ABA and also the calculation of horizontal crown projections. For example, the relationship between crown size and DBH, an important factor in forestry, was described by [5,54]. In large disturbances, such as recent extensive bark beetle outbreaks in Central Europe, AGB calculations may vary depending on the season of measurement. The points in the individual tree point cloud moved down along the stem profile, as calculated by a GLM, and the bending branches will produce smaller canopy projections. These canopy changes, similarly described by [9], can clearly influence the results of ABA, as highlighted in large disturbance areas with high numbers of dead trees, and the resultant statistical metrics, as presented in [2], may also vary. Carbon stock estimates based on CHM can also be influenced by detected changes in the calculated quantiles. These changes can influence results of some studies, such as [29,30], based on their methods with regard to the current status of dead tree canopy changes in large bark beetle disturbance areas that are currently located throughout Central Europe.

5. Conclusions

The ULS method proved to be adequate to detect an increase or loss at the tree component level based on a flight time series of a blue spruce stand. This study showed high spatial and temporal resolution of ULS with regard to tree branch movements of dead trees throughout the year based on time series of three flights. The detection of trees with bending branches was successful using a derived GLM, which was further tested using a validation dataset. These findings could have important implications for remote sampling of forested areas with large numbers of dead trees.

Author Contributions: Conceptualization, M.S. and P.S.; methodology, M.S., K.K. and P.S.; software, M.S., K.K. and P.S.; validation, M.S., K.K. and P.S.; formal analysis, M.S., K.K. and P.S.; investigation, M.S.; resources, P.S. and R.M.; data curation, M.S., K.K., P.S. and R.M.; writing—original draft preparation, M.S.; writing—review and editing, K.K., P.S. and I.T.; visualization, M.S.; supervision, P.S.; project administration, M.S. and P.S.; funding acquisition, P.S. and R.M. All authors have read and agreed to the published version of the manuscript.

Funding: This research was founded by "OP RDE, grant number CZ.02.1.01/0.0/0.0/15_003/0000433 (Building up an excellent scientific team and its spatiotechnical background focused on mitigation of the impact of climatic changes to forests from the level of a gene to the level of a landscape at the FFWS CZU Prague)" and "Ministry of Agriculture of the Czech Republic grant number QK1920458".

Conflicts of Interest: The authors declare no conflict of interest. The founders had no role in the design of the study; in the collection, analyses, or interpretation of data; in the writing of the manuscript, or on the decision to publish results.

References

1. Surovỳ, P.; Kuželka, K. Acquisition of forest attributes for decision support at the forest enterprise level using remote-sensing techniques—A review. *Forests* **2019**, *10*, 273.
2. Næsset, E.; Gobakken, T. Estimating forest growth using canopy metrics derived from airborne laser scanner data. *Remote Sens. Environ.* **2005**, *96*, 453–465.
3. Means, J.E.; Acker, S.A.; Fitt, B.J.; Renslow, M.; Emerson, L.; Hendrix, C.J. Predicting forest stand characteristics with airborne scanning lidar. *Photogramm. Eng. Remote Sens.* **2000**, *66*, 1367–1371.
4. Packalen, P.; Strunk, J.; Packalen, T.; Maltamo, M.; Mehtätalo, L. Resolution dependence in an area-based approach to forest inventory with airborne laser scanning. *Remote Sens. Environ.* **2019**, *224*, 192–201.
5. Verma, N.K.; Lamb, D.W.; Reid, N.; Wilson, B. An allometric model for estimating DBH of isolated and clustered Eucalyptus trees from measurements of crown projection area. *For. Ecol. Manag.* **2014**, *326*, 125–132.
6. Darwin, C. *The Power of Movement in Plants*; Appleton: 1897.
7. McClung, C.R. The plant circadian oscillator. *Biology* **2019**, *8*, 14.
8. Zobel, B.J.; Jett, J.B. *Genetics of Wood Production*; Springer Science & Business Media: Cham, Switzerland, 2012; ISBN 3642795145.
9. Pokorny, R.; Tomaskova, I.; Marek, M.V. The effects of elevated atmospheric [CO2] on Norway spruce needle parameters. *Acta Physiol. Plant.* **2011**, *33*, 2269–2277.
10. Puttonen, E.; Briese, C.; Mandlburger, G.; Wieser, M.; Pfennigbauer, M.; Zlinszky, A.; Pfeifer, N. Quantification of overnight movement of birch (Betula pendula) branches and foliage with short interval terrestrial laser scanning. *Front. Plant Sci.* **2016**, *7*, 222.
11. Zlinszky, A.; Molnár, B.; Barfod, A.S. Not all trees sleep the same—High temporal resolution terrestrial laser scanning shows differences in nocturnal plant movement. *Front. Plant Sci.* **2017**, *8*, 8.
12. Brede, B.; Lau, A.; Bartholomeus, H.M.; Kooistra, L. Comparing RIEGL RiCOPTER UAV LiDAR derived canopy height and DBH with terrestrial LiDAR. *Sensors* **2017**, *17*, 2371.
13. Wieser, M.; Mandlburger, G.; Hollaus, M.; Otepka, J.; Glira, P.; Pfeifer, N. A case study of UAS borne laser scanning for measurement of tree stem diameter. *Remote Sens.* **2017**, *9*, 1154.
14. Liu, K.; Shen, X.; Cao, L.; Wang, G.; Cao, F. Estimating forest structural attributes using UAV-LiDAR data in Ginkgo plantations. *ISPRS J. Photogramm. Remote Sens.* **2018**, *146*, 465–482.
15. Peng, X.; Li, X.; Wang, C.; Zhu, J.; Liang, L.; Fu, H.; Du, Y.; Yang, Z.; Xie, Q. SPICE-based SAR tomography over forest areas using a small number of P-band airborne F-SAR images characterized by non-uniformly distributed baselines. *Remote Sens.* **2019**, *11*, 975.
16. Wang, Y.; Lehtomäki, M.; Liang, X.; Pyörälä, J.; Kukko, A.; Jaakkola, A.; Liu, J.; Feng, Z.; Chen, R.; Hyyppä, J. Is field-measured tree height as reliable as believed—A comparison study of tree height estimates from field measurement, airborne laser scanning and terrestrial laser scanning in a boreal forest. *ISPRS J. Photogramm. Remote Sens.* **2019**, *147*, 132–145.
17. Jurjević, L.; Liang, X.; Gašparović, M.; Balenović, I. Is field-measured tree height as reliable as believed—Part II, A comparison study of tree height estimates from conventional field measurement and low-cost close-range remote sensing in a deciduous forest. *ISPRS J. Photogramm. Remote Sens.* **2020**, *169*, 227–241.
18. Lefsky, M.; Harding, D.; Blair, J.; Parker, G. Laser altimeter canopy height profiles: methods and validation for closed-canopy, broadleaf forests. *Remote Sens. Environ.* **2001**, *76*, 283–297.
19. Næsset, E.; Gobakken, T. Estimation of above- and below-ground biomass across regions of the boreal forest zone using airborne laser. *Remote Sens. Environ.* **2008**, *112*, 3079–3090.
20. Solodukhin, V.I.; Zhukov, A.Y.; Mazhugin, I.N.; Narkevich, V.I. Metody Izuchenija Vertikal'nyh Sechenij Drevostoev (Method of study of vertical sections of forest stands). *Leningr. Sci. Res. Inst. For. Leningr.* **1976**, *55*.
21. Nelson, R.; Krabill, W.; MacLean, G. Determining forest canopy characteristics using airborne laser data. *Remote Sens. Environ.* **1984**, *15*, 201–212.
22. Rosati, A.; Paoletti, A.; Caporali, S.; Perri, E. The role of tree architecture in super high density olive orchards. *Sci. Hortic. (Amsterdam).* **2013**, *161*, 24–29.
23. Lau, A.; Bentley, L.P.; Martius, C.; Shenkin, A.; Bartholomeus, H.; Raumonen, P.; Malhi, Y.; Jackson, T.; Herold, M. Quantifying branch architecture of tropical trees using terrestrial LiDAR and 3D modelling. *Trees Struct. Funct.* **2018**, *32*, 1219–1231.

24. Gonzalez de Tanago, J.; Lau, A.; Bartholomeus, H.; Herold, M.; Avitabile, V.; Raumonen, P.; Martius, C.; Goodman, R.C.; Disney, M.; Manuri, S.; et al. Estimation of above-ground biomass of large tropical trees with terrestrial LiDAR. *Methods Ecol. Evol.* **2018**, *9*, 223–234.
25. Jaakkola, A.; Hyyppä, J.; Kukko, A.; Yu, X.; Kaartinen, H.; Lehtomäki, M.; Lin, Y. A low-cost multi-sensoral mobile mapping system and its feasibility for tree measurements. *ISPRS J. Photogramm. Remote Sens.* **2010**, *65*, 514–522.
26. Wallace, L.; Lucieer, A.; Watson, C.; Turner, D. Development of a UAV-LiDAR system with application to forest inventory. *Remote Sens.* **2012**, *4*, 1519–1543.
27. Panagiotidis, D.; Abdollahnejad, A.; Surový, P.; Chiteculo, V. Determining tree height and crown diameter from high-resolution UAV imagery. *Int. J. Remote Sens.* **2017**, *38*, 2392–2410.
28. Lowe, D.G. Method and Apparatus for Identifying Scale Invariant Features in an Image. U.S. Patent, US6711293B1, 2004.
29. Lee, S.K.; Fatoyinbo, T.; Qi, W.; Hancock, S.; Armston, J.; Dubayah, R. GEDI and TanDEM-X fusion for 3D forest structure parameter retrieval. *Int. Geosci. Remote Sens. Symp.* **2018**, *2018*, 380–382.
30. Qi, W.; Dubayah, R.O. Combining Tandem-X InSAR and simulated GEDI lidar observations for forest structure mapping. *Remote Sens. Environ.* **2016**, *187*, 253–266.
31. Mitchard, E.T.A. The tropical forest carbon cycle and climate change. *Nature* **2018**, *559*, 527–534.
32. Baccini, A.; Walker, W.; Carvalho, L.; Farina, M.; Houghton, R.A. Response to Comment on "Tropical forests are a net carbon source based on aboveground measurements of gain and loss". *Science* **2019**, *363*, 230–234.
33. Breiman, L. Random forests. *Mach. Learn.* **2001**, *45*, 5–32.
34. Šrámek, V.; Slodičák, M.; Lomský, B.; Balcar, V.; Kulhavý, J.; Hadaš, P.; Pulkráb, K.; Šišák, L.; Pěnička, L.; Sloup, M. The Ore Mountains: Will Successive Recovery of Forests from Lethal Disease Be Successful. *Mt. Res. Dev.* **2008**, *28*, 216–221.
35. Černý, K.; Pešková, V.; Soukup, F.; Havrdová, L.; Strnadová, V.; Zahradník, D.; Hrabětová, M. Gemmamyces bud blight of Picea pungens: A sudden disease outbreak in Central Europe. *Plant Pathol.* **2016**, *65*, 1267–1278.
36. Riegl. *RIEGL VUX-SYS;* 2019; Volume 4. http://www.riegl.com/uploads/tx_pxpriegldownloads/RIEGL_VUX-SYS_Datasheet_2020-10-02_01.pdf (accessed on 20 November 2020)
37. Czech Republic. *Letecký Předpis L 2 Pravidla Létání*; 2014. https://aim.rlp.cz/predpisy/predpisy/dokumenty/L/L-2/data/print/L-2_cely.pdf (accessed on 20 November 2020)
38. Westoby, M.J.; Brasington, J.; Glasser, N.F.; Hambrey, M.J.; Reynolds, J.M. "Structure-from-Motion" photogrammetry: A low-cost, effective tool for geoscience applications. *Geomorphology* **2012**, *179*, 300–314.
39. Lisein, J.; Pierrot-Deseilligny, M.; Bonnet, S.; Lejeune, P. A photogrammetric workflow for the creation of a forest canopy height model from small unmanned aerial system imagery. *Forests* **2013**, *4*, 922–944.
40. Bosshard, W.; Müller, E. *Kronenbilder: Mit Nadel-und Blattverlustprozenten*; Eidgen; Anstalt für das forstliche Versuchswesen: 1986.
41. Pekár, S.; Brabec, M. *Modern Analysis of Biological Data: Generalized Linear Models in R*; Masarykova Univerzita: Brno, Czech Republic, 2016; ISBN 8021081066.
42. Hyyppä, E.; Hyyppä, J.; Hakala, T.; Kukko, A.; Wulder, M.A.; White, J.C.; Pyörälä, J.; Yu, X.; Wang, Y.; Virtanen, J.P.; et al. Under-canopy UAV laser scanning for accurate forest field measurements. *ISPRS J. Photogramm. Remote Sens.* **2020**, *164*, 41–60.
43. Hyyppä, E.; Yu, X.; Kaartinen, H.; Hakala, T.; Kukko, A.; Vastaranta, M.; Hyyppä, J. Comparison of Backpack, Handheld, Under-Canopy UAV, and Above-Canopy UAV Laser Scanning for Field Reference Data Collection in Boreal Forests. *Remote Sens.* **2020**, *12*, 3327.
44. Plamboeck, A.H.; Dawson, T.E.; Egerton-Warburton, L.M.; North, M.; Bruns, T.D.; Querejeta, J.I. Water transfer via ectomycorrhizal fungal hyphae to conifer seedlings. *Mycorrhiza* **2007**, *17*, 439–447.
45. Teste, F.P.; Simard, S.W.; Durall, D.M. Role of mycorrhizal networks and tree proximity in ectomycorrhizal colonization of planted seedlings. *Fungal Ecol.* **2009**, *2*, 21–30.
46. Babikova, Z.; Gilbert, L.; Bruce, T.J.A.; Birkett, M.; Caulfield, J.C.; Woodcock, C.; Pickett, J.A.; Johnson, D. Underground signals carried through common mycelial networks warn neighbouring plants of aphid attack. *Ecol. Lett.* **2013**, *16*, 835–843.

47. Baret, M.; DesRochers, A. Root connections can trigger physiological responses to defoliation in nondefoliated aspen suckers. *Botany* **2011**, *89*, 753–761.
48. Simard, S.W.; Jones, M.D.; Durall, D.M. Carbon and nutrient fluxes within and between mycorrhizal plants. In *Mycorrhizal Ecology*; Springer: Cham, Switzerland, 2003; pp. 33–74.
49. Kramer, P.J. The intake of water through dead root systems and its relation to the problem of absorption by transpiring plants. *Am. J. Bot.* **1933**, *20*, 481–492.
50. Putman, E.B.; Popescu, S.C.; Eriksson, M.; Zhou, T.; Klockow, P.; Vogel, J.; Moore, G.W. Detecting and quantifying standing dead tree structural loss with reconstructed tree models using voxelized terrestrial lidar data. *Remote Sens. Environ.* **2018**, *209*, 52–65.
51. Barak, S.; Tobin, E.M.; Green, R.M.; Andronis, C.; Sugano, S. All in good time: The Arabidopsis circadian clock. *Trends Plant Sci.* **2000**, *5*, 517–522.
52. Ibañez, C.; Ramos, A.; Acebo, P.; Contreras, A.; Casado, R.; Allona, I.; Aragoncillo, C. Overall Alteration of Circadian Clock Gene Expression in the Chestnut Cold Response. *PLoS ONE* **2008**, *3*, e3567.
53. Solomon, O.L.; Berger, D.K.; Myburg, A.A. Diurnal and circadian patterns of gene expression in the developing xylem of Eucalyptus trees. *S. Afr. J. Bot.* **2010**, *76*, 425–439.
54. Shimano, K. Analysis of the relationship between DBH and crown projection area using a new model. *J. For. Res.* **1997**, *2*, 237–242.

Příloha č. 2 - Slavík, M.; Kuželka, K.; Hroššo, B.; Surový, P. Spatial analysis of dense LiDAR point clouds for tree species classification. *Remote Sens.* 2020, 1–15.

remote sensing MDPI

Type of the Paper (Article)

Spatial analysis of dense LiDAR point clouds for tree species classification

Martin Slavík[1*], Karel Kuželka[1], Branislav Hroššo[2,3], Peter Surový[1]

[1] Faculty of Forestry and Wood Sciences, Czech University of Life Sciences, Prague, Kamýcká 129, 165 00 Praha, Czech Republic; mslavik@fld.czu.cz (MS), kuzelka@fld.czu.cz (KK), surovy@fld.czu.cz (PS),
[2] Institute of Forest Ecology, Slovak Academy of Sciences, Zvolen 960 53, Slovakia
[3] Faculty of Ecology and Environmental Sciences, Technical University in Zvolen, Zvolen 960 53, Slovakia
* Correspondence: mslavik@fld.czu.cz; Tel.: +42 0731 315 937

Received: date; Accepted: date; Published: date

Abstract: This study presents individual tree metrics approach (ITMA) for tree species classification in a three-dimensional point cloud from unmanned aerial laser scanning (ULS). We utilize General Linear Model (GLM) and random forest (RF) technique for automatic evaluation of point cloud metrics of individual trees previously extracted by inverse watershed algorithm into two classes: coniferous and broadleaved. We evaluated possible statistical descriptors, among them Clark-Evans spatial aggregation index, which indicates the level of clustering in point clouds and proved to be crucial for correct classification of the individual tree point clouds. In case of RF, the inclusion of Clark-Evans index brought significant improvement in overall accuracy of classification and in case of GLM the index was always selected as significant variable for correct prediction. The statistical descriptor can improve large scale area classification from dense laser point clouds and lead to more accurate estimation of biomass and other tree characteristics.

Keywords: LiDAR, UAV, forestry, species classification, individual tree metrics approach

1. Introduction

LiDAR Light Detection And Ranging (LiDAR) is an active sensing technology, which provides a practical way to measure the tree size and other tree characteristics [1]. Compared with traditional remote sensing technologies, LiDAR can provide detailed characteristics of forest canopy structure in three dimensions [2–4].

The scanning device can be either placed on the ground Terrestrial Laser Scanning (TLS), installed on a mobile platform, on a vehicle or carried by a human Mobile Laser Scanning (MLS), or carried by aircraft Aerial Laser Scanning (ALS), special case of the latter one is UAV equipped with LiDAR sensor.

Details and principles of scanning mechanisms and TLS techniques are presented by [5–7]. Liang [8] is deeply aimed at forest inventory purpose of TLS method starting with data collection to individual tree modeling directly leading to forest stand-level inventory. Large area ALS data acquisition and data processing is detailly commented in [9]. Overview of used instruments, data acquisition techniques and data evaluation to derivation forest inventory variables with its comparison is elaborated by [10]. The study of [11] presents the exact derivation of forest inventory variables with stand total volume estimation with $R^2 = 0.86$. The overall use of MLS and it pros and cons were in general summarized by [12]. Liang [13] brought comparison of TLS and MLS method with aim to its feasibility in forest environment and the MLS advantages were demonstrated on 0.4 ha forest stand where was reached 87.5% stem mapping accuracy. Also [14] compared TLS and MLS methods with regard to segmentation of individual trees where results of TLS data were 92.4% completeness and 95.4%, the corresponding values for MLS data were 94% and 93.7%.

Many scientific publications have dealt with the extraction of individual trees (position and partial point clouds of single trees), dendrometric characteristics of these trees and the creation of forest stand models from ALS data [15–17]. For example [18] evaluate the quality, accuracy, and feasibility of automatic tree extraction methods, mainly based on laser scanner data and [1] deals with comparing the accuracy of tree height estimation obtained by field measurements and using TLS and ALS methods. TLS and ULS methods are compared by [19,20], where is used the same UAS as in this study. The UAV and TLS comparison shoved in study of [19] were described by correlation coefficient of 0.98 and root mean square error 4.24 cm on diameter at breast height (DBH) estimation with TLS used as reference method. The study of [20] was aimed at stem reconstruction and proved the high stem reconstruction potential for trees with DBH higher then 20cm.

In recent years UAS based LiDAR scans has gained more attention despite their high cost when compared to other methods like for example Structure from Motion (SfM) photogrammetry. Works on UAV laser equipment in forestry can be found as early as 2010 in the work [21] where authors presented a novel system based on combination of Ibeo Lux and a Sick LMS151 laser scanner system together with IMU and GPS unit. They were able to achieve accuracy of 30 cm expressed by standard deviation of height measurements of trees. Later [22] presented similar system in addition equipped with high definition (HD) camera for more precise point clouds. They proved that the inclusion of this video information improved the accuracy of final point cloud from 0.61 m to 0.34 m (RMS error assessed against ground control).

Later a comparison study was carried out by [23] comparing laser point clouds with point clouds obtained from Structure from Motion (SfM) techniques. Authors reported lower densities of point cloud on the ground in case of SfM technique sometime being just 1 pixel per square meter. This then resulted in larger error of height estimation for SfM (reported is root mean square error of 0.92 m for ALS and 1.30 m for SfM).

The advantages of UAS systems are the ability to fly at lower speeds and at lower altitudes above ground contrary to disadvantages as possibility of observing only areas up to tens of ha, or weather limitation (wind, temperature). This results in the production of a highly dense point clouds that more faithfully represents the structure of the stand or single trees.

Nonetheless, previous studies based on UAV-LiDAR data mostly focused on the estimation of forest structural attributes such as tree height, DBH, crown area, and showed little interest in the estimation of basal area, volume and aboveground biomass (AGB) [24]. Furthermore, due to the limited payload, short flight time and limited capability of data processing of early UAV-LiDAR, most of the previous studies had been conducted on sample trees in small areas. The distributional metrics extracted from LiDAR data, including height percentile metrics, distribution moment metrics and canopy re-turn density metrics [25,26], have been commonly used to estimate forest structural attributes [11,27,28].

In this study, we analyze the metrics of point clouds of individual trees that were obtained using RiCOPTER system. The first reference to the use of these systems in the scientific literature is the work of [19] where the authors describe in detail the system components and quality of derived Digital Terrain Models (DTMs), Digital Surface Models (DSMs) and Canopy Height Models (CHMs) from the resulting point clouds which compare with models based on point clouds of the same areas obtained with the TLS system RIEGL VZ-400 (RIEGEL Laser Measurement System GmbH, Horn, Austria).

Liu [24] in their study assessed the effectiveness of plot-level metrics (i.e., distributional, canopy volume and Weibull-fitted metrics) and individual-tree-summarized metrics (i.e., maximum, minimum and mean height of trees and the number of trees from the individual tree detection (ITD) results) derived from UAV-LiDAR point clouds, then these metrics were used to fit estimation models of six forest structural attributes by parametric (i.e., partial least squares (PLS)) and non-parametric (i.e., k-Nearest Neighbors (k-NN) and Random Forest (RF)) approaches, within a Ginkgo plantation in east China.

Holmgren at Persson, [29] tested classification of Scots pine versus Norway spruce on an individual tree level using features extracted from airborne laser scanning data.

Now days commonly used deep learning algorithms in forestry studies such as Support Vector Machine (SVM) and RF plays important role in RS data classification. The RF was developed by [30] and there was also presented R package. The overview of RF applications in forestry RS data is presented by [31]. Kamińska [32] tested RF classification of dead trees with regard to their class from ALS and infrared colored imagery with overall accuracy 90%. The SVM was described by [33] and the [34] brings the overview of usage in RS. High accuracy of SVM was highlighted by [35] in terms of vegetation classifications. These two used deep learning algorithms were compared by [36].

In this study, we are looking for point cloud metrics that are significantly different for broad leaf and coniferous trees using descriptive statistics and mentioned deep learning algorithm (RF). We assume that spruce tree has a regular "star" shape of the crown and the distribution of branches has a regular structure. On the other hand, the crown of a broadleaf tree is absolutely asymmetric and the branches are more frequent over the entire trunk.

2. Materials and Methods

2.1 Study Area

For the whole study were used four plots, that differed in tree species and growth conditions. Plots A and B consisted of broadleaf tree species (oak sp.) and plots C and D were coniferous (spruce sp.) The plot A was located in natural reservation Koda in southern central Czech Republic (49°56'00.1"N, 14°06'14.7"E) and the plot B was located near the village Podbořanský Rohozec in western part of the Czech Republic (50°13'9.165"N, 13°13'28.219"E), both was mixed mature only broadleaf stand with dominant species oak (*Quercus petrea* L.). The plot C also as the plot D belonged to the Czech University of Life Sciences forest enterprise located near town Jevany in eastern central Czech Republic (49°57'22.9"N, 14°49'37.8"E) – plot C and plot D were located near town Stribrna Skalice (N 49°54.81395', E 14°52.58753') in both plots was monoculture mature stand of Norway spruce (*Picea abies* L.) monoculture stand. Location of all four plots is indicated in **Figure 1**. The mean height and its standard deviation were calculated from individual tree point clouds for both classes. Mean height for coniferous class was 39.9 m and standard deviation 3.7, for broadleaf it was mean height 21.1 m and standard deviation 3.3.

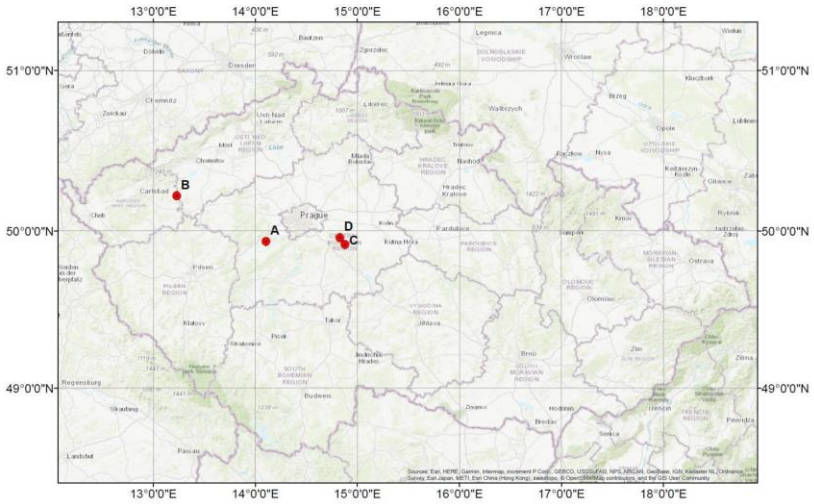

126 **Figure 1**. Location of the plots where plots A and B with broadleaf composition and plots C and D
127 with coniferous tree species composition.

128 *2.2 UAV-borne LiDAR*

129 For data acquisition was used UAS VUX-SYS (RIEGL Laser Measurement System GmbH, Horn,
130 Austria), consisting of UAV RiCOPTER and multi return laser scanner VUX-1UAV.
131 RiCOPTER is a multirotor octocopter UAV with total take of pay load 25 kg, of which 6.5 kg
132 includes mounted sensors. The total flight time with full load for data acquisition is reaching nearly
133 28 minutes. Eight brushless motors on four arms are powered, as the whole UAV, by four Li-Pol
134 batteries for better stability during the flight and for possibility of vibration reduction. The UAV is
135 capable of autonomous flight.
136 VUX-1UAV, as describes [37] is a near infrared multi return laser scanner with 330° FoV (Field
137 of View), because the scanner is mounted on the bottom side of the UAV, therefore is the FoV
138 reduced. Maximum pulse repetition rate is 550 MHz with the maximum effective measurement rate
139 up to 500 000 measurements per second (because of 550kHz and 330° FoV). Electric energy is
140 provided by the RiCOPTER electric system. The laser scanner was remotely controlled by pilot of the
141 UAV. Whole UAS before take-off is presented on **Figure 2**.
142

143 **Figure 2**. The RiCOPTER equipped with VUX-SYS before take-off. Behind the UAV, there is visible
144 Trimble R2 GNSS receiver.

145 *2.3 LiDAR data acquisition*

146 Before the actual flight for data acquisition was set Base Station (BS) consisting of Trimble
147 TSC3 Controller and Trimble R2 GNSS receiver (Trimble, Sunnyvale, California, USA). It was the
148 periodical static measurement that was performed during the whole flight for the later post
149 processing of trajectory. Before the actual static measurement was the position of the GS measured
150 with using of RTK (Real Time Kinematics) measurement. Data were acquired by VUX-SYS with flight

speed 5 $m \cdot s^{-1}$, altitude 80 m above ground level. It was the automatic flight with using of perpendicular zig zag pattern for reaching high density of points in the whole point cloud. The laser scanner was remotely controlled by the pilot of the UAV **Figure 2**. For reaching geometrical accuracy was used the stop and turn method for changing of direction during the flight of UAV. The point cloud density varied from 1 500 to 2 700 points m^{-2}.

2.4 Data processing

The data processing was divided into several steps based on the used software. First part was to calculate dense point clouds with high accuracy, the second part was to prepare dataset of 32 closest trees to the plot center from each plot (in total 128 trees).

Deriving of initial point cloud from each plot was preceded by calculation of trajectory in software PosPAC MMS 8.1 (Applanix: a Trimble company, Ontario, Canada) with using of method Base Station from the Inertial Measurement Unit (IMU) data of the scanner. The precise position of BS was improved by the RTK measurement. After the calculation of the trajectory it was derived the initial dense point cloud in the environment of RiPROCESS (RIEGL Laser Measurement System GmbH, Horn, Austria) software from each single scan. For increasing the accuracy of the initial point cloud was used software tool RiPRECISSION for better co-registration on z axis. Also derived points were classified to several groups (ground, vegetation and noise) for future data evaluation.

The georeferenced classified point cloud was imported to environment of the ArcGIS 10.6.1 (ESRI, Redlands, California, USA) as LAS dataset with using of ALS dataset tool. In this part of data processing were selected thirty-two individual tree point clouds of each tree class (broadleaf and coniferous) from each plot, as polygons based on their horizontal crown projections. The horizontal crown projections were automatically detected by 3D Sample tool from derived CHM (Canopy Height Model). The 3D Sample was tool originally created for ALS data sets for tree detection based on local maxima and Inverse Watershed Segmentation IWS. The IWS was described on mature forest stand plots from aerial photogrammetry points clouds by Panagiotidis [38]. Polygons (crown projections) were afterward transformed to points in the environment of environment of the ArcGIS 10.6.1 to be used in next step as frame for selecting only the points of one single tree from the original point cloud in the environment of MATLAB (The MathWorks, Inc., Natick, Massachusetts, USA). The point cloud of each single tree was in next step manually cleared in Agisoft MetaShape 1.6 (Agisoft LLS, St. Petersburg, Russia)from undergrowth and points belonging to ground for avoiding debasement of next step analyses. The problem during the tree segmentation with other tree artefacts was described for example by [14,39].

The statistical evaluation and GLM derivation was performed in the R environment [40]. For each single point cloud were calculated individual tree metrics (ITM) based on descriptive statistics along the normalized tree height: IQR (Inter Quartile Range), VAR (Variance), SD (Standard Deviation), MOM (Moment), SKEW (Skewness), MEAN, KVAD (Quadratic Mean), CUB (Cubic Mean), MAD (Mean Absolut Deviation), Q*n* (Quantile, where *n* was graded by tens of percent) following the common procedure as described in[32,41]. In total were calculated 42 metrics for each individual tree point cloud.

2.4.1 Clark-Evans spatial aggregation index

Clark and Evans spatial aggregation index (CE) [42] was developed to describe the point pattern aggregation, by simple words to numerically quantify the degree of clustering of the point cloud. Point processes are compared to Poisson spatial distribution where values close to 1 are considered to be completely random and values differing from 1 are indicating either clustering of the point cloud in case of the number being lower than 1 and regular. The **Equation 1** describes the calculation of CE [43]. The CE*n* (where *n* was graded by fives of percent) was also calculated as previously described individual tree metrics.

$$CE = \frac{\frac{1}{n} \times \sum_{i=1}^{n} r}{\frac{1}{2} \times \sqrt{\frac{A}{n}}} \quad (1)$$

For RF was used R free package randomForest [44] and for the training was used the same dataset as for the GLM derivation.

3. Results

3.1. Tree delineation

Individual tree delineation by horizontal crown projection based on detected local maxima with its limitation presented by [38] each polygon presents one individual tree horizontal crown projection. **Figure 3** presents red polygons of delineated ULS point cloud of Plot C. In **Figure 4** are presented examples of individual tree point clouds serving for individual tree metrics derivation.

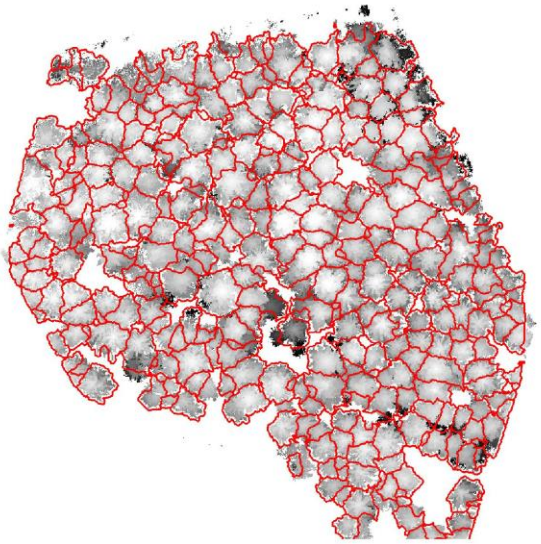

Figure 3. Demonstration of crowns delineated with the use of IWS on the example of monoculture coniferous plot C populated with Norway spruce (*Picea abies* L.).

Individual tree point clouds were afterwards manually inspected for presence of artefacts like branches of neighboring trees etc. For the study were used examples of individual tree point clouds representations as is shown in **Figure 4**. The individual tree point clouds were not modified, only points obviously not belonging to the exact tree were removed for higher individual tree point cloud representability.

(a) (b)

Figure 4 Examples of individual tree point clouds: **(a)** presents an example of coniferous individual tree point cloud; **(b)** presents an example of broadleaf individual tree point cloud. These kind of point clouds served for automatic individual tree metrics derivation.

From the tree habitus (outer look) point of view the **Figure 4** shows two examples of trees used in study, where **Figure 4 (a)** is coniferous tree represented by Norway spruce and **Figure 4 (b)** shows broadleaf tree represented by oak sp. There is clear difference in the habitus of these tree species with regard to branching, crown shape, beginning of the crown, etc. The species might display slightly different habitus from the one shown in the figure when living as solitaire trees as when they are living in denser canopy. Though these differences are not huge and intention of this work is to evaluate automatic classification in closed stands.

3.2. Generalized linear model

As result of this study was derived the GLM from ITM used as predictors. Because of big number of predictors, the most significant predictors were selected by the method of partial least squares. The selected predictors were used to derive the final GLM described in **Table 1**.

Table 1. Derived GLM from all the variables with CE indexes by stepwise regression method showing the most significant predictors.

	Estimate	Std. Error	z value	p. value
Intercept	7.143	3.789	1.885	0.0594
Q60	-0.484	0.111	-4.377	$1.20e^{-5}$
CE100	4.366	2.954	1.478	0.1394
CE45	-4.314	2.284	-1.889	0.0589
KVAD	0.566	0.124	4.572	$4.84e^{-6}$
CE55	-6.321	2.673	-2.365	0.0180
CE95	-8.636	4.261	-2.027	0.0427

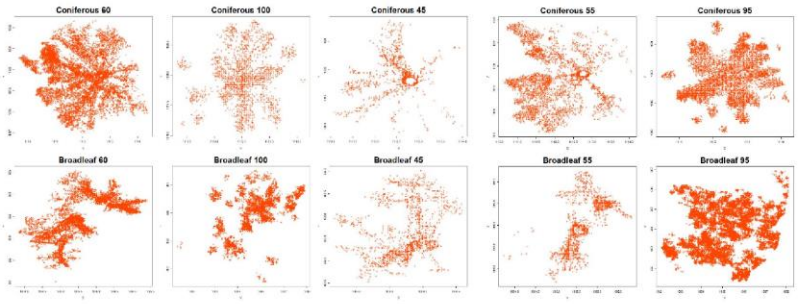

Figure 5 Comparison of horizontal projections of point layers of coniferous (upper row) and broadleaf (bottom row) trees, according to the metrics used in the derived GLM. This figure serves as example of two chosen trees (one for each group) and for each tree, horizontal projections of layers with significantly different values of point metrics between tree classes were plotted. The example trees are presented in **Figure 4**.

The **Figure 5** shows horizontal projections of point cloud layers on an example of one representative from each tree class, demonstrating the difference on derived metrics for both tree groups. For coniferous trees, there is on nearly all metrics visible the trunk part of the chosen point cloud located around the center. There are clearly recognizable lines of branches in radial direction surrounded by smaller branches and needles. This phenomenon is not clearly evident in upper parts of the tree (in metrics from 90 to 95% and 95 to 100%). Contrary to coniferous trees, the broadleaf tree example in **Figure 5** present clustering of points around the branches growing phototropically, not radially as branches of coniferous trees. The CE100 was evaluated with higher p.value then other metrics mainly because it represents the tree top whose shape was not so different according to derived metrics.

Table 2. Derived GLM from all the variables without CE indexes by stepwise regression method showing the most significant predictors.

	Estimate	Std. Error	z value	p. value
Intercept	1.036	3.991	2.597	0.0094
IQR	-0.151	0.051	-2.946	0.0032
MOM	1.450	9.893	1.466	0.1427
MEAN	-5.673	1.437	-3.947	$7.90e^{-5}$
KVAD	3.845	1.242	3.095	0.0020
MAD	-2.284	0.642	-3.558	0.0004
Q10	0.048	0.033	1.418	0.1562
Q40	1.765	0.451	3.916	$8.99e^{-6}$
Q50	-0.964	0.344	-2.801	0.0051
Q90	1.407	0.818	1.721	0.0853
Q95	-1.399	0.954	-1.467	0.1425

Table 3. Confusion matrix of derived GLM from all the variables

	Broadleaf	Coniferous	Class. error
Broadleaf	51	13	20,3%
Coniferous	13	51	20,3%

Table 4. Confusion matrix of derived GLM from all the variables without CE indexes

	Broadleaf	Coniferous	Class. error
Broadleaf	56	8	12,5%
Coniferous	5	59	7,8%

3.3. Random Forest

RF classification showed error estimation rate based on used R toolbox of 10.9% where were classified two classes where for broadleaf was classification error 12.5% and for broad leaf 9.4% For the best results of RF classification, random forest containing 500 decision trees was created. .

Table 2. Confusion matrix of derived RF from all the variables

	Broadleaf	Coniferous	Class. error
Broadleaf	56	8	12.5%
Coniferous	6	58	9.4%

Table 3. Confusion matrix of derived RF from all the variables without CE indexes

	Broadleaf	Coniferous	Class. error
Broadleaf	51	13	20.3%
Coniferous	10	54	15.6%

The significant difference was detected in RF classification without using of CE indexes in higher described layers. The error was negatively influenced for broadleaf estimation increased to 20.3% and for coniferous increased to 15.6%. Both RF classifications are presented in **Table 2**. and **Table 3**.

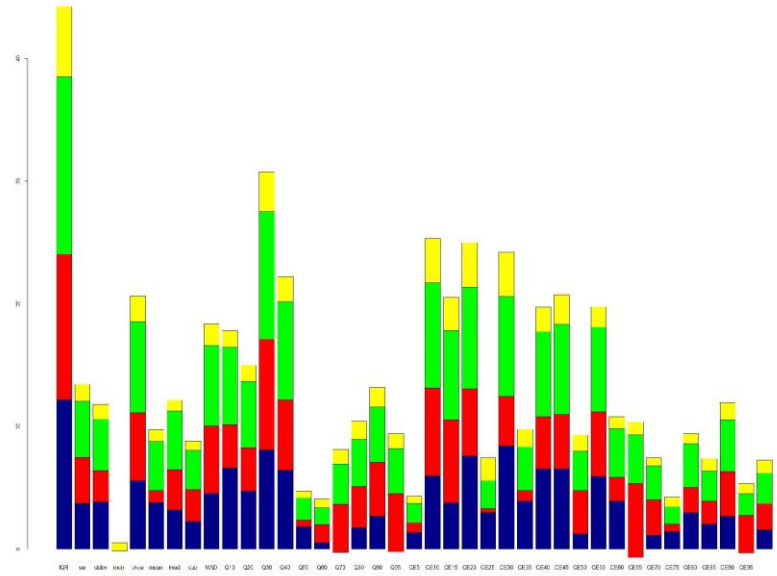

Figure 6. Graph of importance of variables of which was the RF derived from; blue - relative importance for broadleaf, red - relative importance for coniferous, green - mean decrease in accuracy, yellow - mean decrease in gini.

As is presented in **Figure 6,** interesting predictors are Q70, Q95, CE65, and CE95 with no presented relative importance for broad leaf. Each bar in **Figure 6**. **i**s divided into four parts where (starting from bottom): relative importance for broadleaf, relative importance for coniferous, mean decrease in accuracy and mean decrease in gini. In general, relative importance for coniferous of the CE indexes for their determination is lower than the relative importance for broadleaf.

4. Discussion

The benefits of using the VUX-SYS were highlighted by Brede and Wiesser [19,20] with regard to derivation of individual tree representative 3D point clouds along the whole stem profile, where was emphasized the possibility of canopy penetration and data representativeness mainly in top canopy parts. Both author collectives agree with ULS advantage of relative high canopy point density contrary to TLS method. As this study shows the significant predictors for used classification were located mostly in upper part of the stem profile.

The difference between coniferous and broadleaf trees based on difference in CHM with regard to seasonal canopy changes was described by Reitberger [45], however this approach is sensitive on deciduous coniferous trees because these tree species show similar canopy mean height changes from the points belonging to canopy as broadleaf tree species. Nevertheless, time series for canopy changes are time demanding method.

Tree canopy shape was also considered in this study. There were two main assumptions according to the difference in canopy. First was aimed at bottom part e.g. the beginning of the crown part along the stem profile contrary to the second assumption aimed at top of the tree crow, where was expected the difference in shape [46] that could be explained as different number of points in current percentile. The positive impact of height normalization process for tree shape description was mentioned by [47]. Both assumptions were confirmed by derived GLM.

In this study were derived two RF classifications, the first including the CE index showed the importance of quantiles exactly Q70 and Q95 which be described as beginning of the tree crown (Q65) and the difference in shape (coniferous trees included in this study has sharper top then broadleaf trees) represented by Q95). The next two metrics were CE65 and CE95. The impact of CE65 can be considered in grouping of points around single trunk and radially arranged branches in case of coniferous trees contrary to points of broad leaf trees clustered around one or more stems or large branches.

Leaf-on and leaf-off conditions were also compared [45,48,49] and because of leaf-on conditions during the data acquisition for this study the results can be possibly also negatively influenced.

The accuracy of the RF was clearly influenced by the fact of different study areas as is mentioned by [50]. In comparison to accuracy of [36] (around 88%) in this study was observed almost the same accuracy (89%) but with five time more RF decision trees. The study [51] used combination of airborne hyperspectral and LiDAR data for tree species calculations based individual tree metrics with reaching again the similar accuracy, but with combination of two RS methods. As [31] mentions, there have been numerous variable investigations aimed at prediction power, however the nowadays aim is at per-pixel classifications. Nevertheless, RF is less sensitive to the training data [31] then other machine learning algorithms and this was the main reason for its using in this study.

RF classification based on geometric, 3D shape and intensity was also used in conditions of the Czech Republic by [52] on ALS LiDAR data on large scale area for single tree detection and afterwards dead trees detection. In mentioned study were also detected dead trees. The LiDAR data were fused with multispectral data and the overall accuracy was reached over 90%. High accuracy in tree species classification from multi-temporal Sentinel-2 data reached [53] and highlighted the multitemporal data for this data type.

As other classification method should be used SVM [33] with regard to the recent trends in RS [34,35]. However, using of SVM and other deep learning algorithms for this kind of data classification need more development.

5. Conclusions

ULS data provides huge opportunity for spatial analysis on individual tree level mainly thanks to their representativeness through the whole stem profile of individual tree. From the point of view of automatic processes with the limitation of manual work the successful individual tree delineation played important role in the whole data processing process. Both GLM and RF showed promising results in tree species group classification, where was proved the importance of CE index. Derived GLM was mainly build on CE index and testing of RF showed its impact for describing the difference between broadleaf and coniferous trees.

Author Contributions: Conceptualization, M.S. and P.S.; methodology, M.S. and P.S.; software, M.S.; validation, M.S., and K.K.; formal analysis, M.S.; investigation, M.S.; resources, P.S.; data curation, M.S., K.K. and B.H.; writing—original draft preparation, M.S., K.K. and B.H.; writing—review and editing, K.K.; visualization, M.S.; supervision, P.S..; project administration, P.S.; funding acquisition, P.S. All authors have read and agreed to the published version of the manuscript.

Funding: This research was founded by "OP RDE, grant number CZ.02.1.01/0.0/0.0/16_019/0000803 (Advanced Research Supporting the Forestry and Wood-processing Sector´s Adaptation to Global Change and the 4th Industrial Revolution)".

Conflicts of Interest: The authors declare no conflict of interests. The founders have no role in the design of the study; in the collection, analyses, or interpretation of data; in the writing of the manuscript, or on the decision to publish results.

345 **References**

346 1. Wang, Y.; Lehtomäki, M.; Liang, X.; Pyörälä, J.; Kukko, A.; Jaakkola, A.; Liu, J.; Feng, Z.; Chen, R.;
347 Hyyppä, J. Is field-measured tree height as reliable as believed – A comparison study of tree height
348 estimates from field measurement, airborne laser scanning and terrestrial laser scanning in a boreal
349 forest. *ISPRS J. Photogramm. Remote Sens.* **2019**, *147*, 132–145.

350 2. Lefsky, M.; Harding, D.; Blair, J.; Parker, G. Laser altimeter canopy height profiles: methods and
351 validation for closed-canopy, broadleaf forests. *Remote Sens. Environ.* **2001**, *76*, 283–297.

352 3. Lefsky, M.; Cohen, W.; Parker, G.; Harding, D. Lidar Remote Sensing for Ecosystem Studies. *Bioscience*
353 **2006**, *52*, 19.

354 4. Næsset, E.; Gobakken, T. Estimation of above- and below-ground biomass across regions of the boreal
355 forest zone using airborne laser. *Remote Sens. Environ.* **2008**, *112*, 3079–3090.

356 5. Baltsavias, E.P. Airborne laser scanning: Basic relations and formulas. *ISPRS J. Photogramm. Remote Sens.*
357 **1999**, *54*, 199–214.

358 6. Petrie, G.; Toth, C.K. Terrestrial laser scanners. In *Topographic Laser Ranging and Scanning*; CRC Press,
359 2018; pp. 29–88.

360 7. Vosselman, G.; Maas, H.G. Airborne and Terrestrial Laser Scanning, repr. ed. *Whittles, Dunbeath* **2011**.

361 8. Liang, X.; Kankare, V.; Hyyppä, J.; Wang, Y.; Kukko, A.; Haggrén, H.; Yu, X.; Kaartinen, H.; Jaakkola,
362 A.; Guan, F.; et al. Terrestrial laser scanning in forest inventories. *ISPRS J. Photogramm. Remote Sens.* **2016**,
363 *115*, 63–77.

364 9. Gatziolis, D.; Andersen, H.E. A Guide to LIDAR Data Acquisition and Processing for the Forests of the
365 Pacific Northwest. *Gen. Tech. Rep. PNW-GTR-768* **2008**, 1–40.

366 10. Wulder, M.A.; White, J.C.; Nelson, R.F.; Næsset, E.; Ørka, H.O.; Coops, N.C.; Hilker, T.; Bater, C.W.;
367 Gobakken, T. Lidar sampling for large-area forest characterization: A review. *Remote Sens. Environ.* **2012**,
368 *121*, 196–209.

369 11. Lim, K.; Treitz, P.; Baldwin, K.; Morrison, I.; Green, J. Lidar remote sensing of biophysical properties of
370 tolerant northern hardwood forests. *Can. J. Remote Sens.* **2003**, *29*, 658–678.

371 12. Kukko, A.; Kaartinen, H.; Hyyppä, J.; Chen, Y. Multiplatform mobile laser scanning: Usability and
372 performance. *Sensors (Switzerland)* **2012**, *12*, 11712–11733.

373 13. Liang, X.; Hyyppä, J.; Kukko, A.; Kaartinen, H.; Jaakkola, A.; Yu, X. The Use of a Mobile Laser Scanning
374 System for Mapping Large Forest Plots. *IEEE Geosci. Remote Sens. Lett.* **2014**, *11*, 1504–1508.

375 14. Zhong, L.; Cheng, L.; Xu, H.; Wu, Y.; Chen, Y.; Li, M. Segmentation of Individual Trees From TLS and
376 MLS Data. *IEEE J. Sel. Top. Appl. Earth Obs. Remote Sens.* **2017**, *10*, 774–787.

377 15. Maltamo, M.; Packalén, P. Experiences and possibilities of ALS based forest inventory in Finland. *ISPRS*

Work. … **2007**, 270–279.

16. Dalponte, M.; Ørka, H.O.; Ene, L.T.; Gobakken, T.; Næsset, E. Tree crown delineation and tree species classification in boreal forests using hyperspectral and ALS data. *Remote Sens. Environ.* **2014**, *140*, 306–317.

17. Vastaranta, M.; Holopainen, M.; Haapanen, R.; Melkas, T.; Hyyppï¿½, J.; Hyyppï¿½, H. Comparison Between An Area-Based and Individual Tree Detection Method For Low-Pulse Density ALS-Based Forest Inventory. *Int. Arch. Photogramm. Remote Sens. Spat. Inf. Sci.* **2009**, *XXXVIII*, 147–151.

18. Kaartinen, H.; Hyyppä, J.; Yu, X.; Vastaranta, M.; Hyyppä, H.; Kukko, A.; Holopainen, M.; Heipke, C.; Hirschmugl, M.; Morsdorf, F.; et al. An international comparison of individual tree detection and extraction using airborne laser scanning. *Remote Sens.* **2012**, *4*, 950–974.

19. Brede, B.; Lau, A.; Bartholomeus, H.M.; Kooistra, L. Comparing RIEGL RiCOPTER UAV LiDAR derived canopy height and DBH with terrestrial LiDAR. *Sensors (Switzerland)* **2017**, *17*, 1–16.

20. Wieser, M.; Mandlburger, G.; Hollaus, M.; Otepka, J.; Glira, P.; Pfeifer, N. A case study of UAS borne laser scanning for measurement of tree stem diameter. *Remote Sens.* **2017**, *9*, 1–11.

21. Jaakkola, A.; Hyyppä, J.; Kukko, A.; Yu, X.; Kaartinen, H.; Lehtomäki, M.; Lin, Y. A low-cost multi-sensoral mobile mapping system and its feasibility for tree measurements. *ISPRS J. Photogramm. Remote Sens.* **2010**, *65*, 514–522.

22. Wallace, L.; Lucieer, A.; Watson, C.; Turner, D. Development of a UAV-LiDAR system with application to forest inventory. *Remote Sens.* **2012**, *4*, 1519–1543.

23. Wallace, L.; Lucieer, A.; Malenovskỳ, Z.; Turner, D.; Vopěnka, P. Assessment of forest structure using two UAV techniques: A comparison of airborne laser scanning and structure from motion (SfM) point clouds. *Forests* **2016**, *7*, 1–16.

24. Liu, K.; Shen, X.; Cao, L.; Wang, G.; Cao, F. Estimating forest structural attributes using UAV-LiDAR data in Ginkgo plantations. *ISPRS J. Photogramm. Remote Sens.* **2018**, *146*, 465–482.

25. Næsset, E. Effects of different flying altitudes on biophysical stand properties estimated from canopy height and density measured with a small-footprint airborne scanning laser. *Remote Sens. Environ.* **2004**, *91*, 243–255.

26. Véga, C.; Renaud, J.P.; Durrieu, S.; Bouvier, M. On the interest of penetration depth, canopy area and volume metrics to improve Lidar-based models of forest parameters. *Remote Sens. Environ.* **2016**, *175*, 32–42.

27. Means, J.E.; Acker, S.A.; Fitt, B.J.; Renslow, M.; Emerson, L.; Hendrix, C.J. Predicting forest stand characteristics with airborne scanning lidar. *Photogramm. Eng. Remote Sens.* **2000**, *66*, 1367–1371.

28. Zhao, K.; Popescu, S.; Meng, X.; Pang, Y.; Agca, M. Characterizing forest canopy structure with lidar composite metrics and machine learning. *Remote Sens. Environ.* **2011**, *115*, 1978–1996.

29. Holmgren, J.; Persson, Å. Identifying species of individual trees using airborne laser scanner. *Remote Sens. Environ.* **2004**, *90*, 415–423.

30. Breiman, L. Random Forests - Random Features, Tecnical Report 567, Statistic Department, University of California, Berkeley, (https://www.stat.berkeley.edu/~breiman/random-forests.pdf, 08.10.2018'de erişildi). **1999**, 1–29.

31. Belgiu, M.; Drăgu, L. Random forest in remote sensing: A review of applications and future directions. *ISPRS J. Photogramm. Remote Sens.* **2016**, *114*, 24–31.

32. Kamińska, A.; Lisiewicz, M.; Stereńczak, K.; Kraszewski, B.; Sadkowski, R. Species-related single dead tree detection using multi-temporal ALS data and CIR imagery. *Remote Sens. Environ.* **2018**, *219*, 31–43.

33. Vapnik, V. The support vector method of function estimation. In *Nonlinear Modeling*; Springer, 1998; pp. 55–85.

34. Mountrakis, G.; Im, J.; Ogole, C. Support vector machines in remote sensing: A review. *ISPRS J. Photogramm. Remote Sens.* **2011**, *66*, 247–259.

35. Kranjčić, N.; Medak, D.; Župan, R.; Rezo, M. Support Vector Machine accuracy assessment for extracting green urban areas in towns. *Remote Sens.* **2019**, *11*.

36. Pal, M. Random forest classifier for remote sensing classification. *Int. J. Remote Sens.* **2005**, *26*, 217–222.

37. RIEGL *Data Sheet, RIEGL VUX-1UAV*; 2019;

38. Panagiotidis, D.; Abdollahnejad, A.; Surový, P.; Chiteculo, V. Determining tree height and crown diameter from high-resolution UAV imagery. *Int. J. Remote Sens.* **2017**, *38*, 2392–2410.

39. Lau, A.; Bentley, L.P.; Martius, C.; Shenkin, A.; Bartholomeus, H.; Raumonen, P.; Malhi, Y.; Jackson, T.; Herold, M. Quantifying branch architecture of tropical trees using terrestrial LiDAR and 3D modelling. *Trees - Struct. Funct.* **2018**, *32*, 1219–1231.

40. Team, R.C. An introduction to dplR. *Ind. Commer. Train.* **2018**, *0*, 1–16.

41. Næsset, E.; Gobakken, T. Estimating forest growth using canopy metrics derived from airborne laser scanner data. *Remote Sens. Environ.* **2005**, *96*, 453–465.

42. Clark, P.J.; Evans, F.C. Distance to Nearest Neighbor as a Measure of Spatial Relationships in Populations Stable URL : http://www.jstor.org/stable/1931034 REFERENCES Linked references are available on JSTOR for this article : You may need to log in to JSTOR to access the linked. *Ecology* **1954**, *35*, 445–453.

43. Fabrika, M.; Pretsch, H. Analysis and modelling of forest ecosystems. *Tech. Univ. Zvolen* **2011**, 1–599.

44. Breiman, L.; Cutler, A.; Liaw, A.; Wiener, M. Package 'randomForest.' **2018**, 29.

45. Reitberger, J.; Krzystek, P.; Stilla, U. Analysis of full waveform LIDAR data for the classification of

444 deciduous and coniferous trees. *Int. J. Remote Sens.* **2008**, *29*, 1407–1431.

445 46. Ørka, H.O.; Næsset, E.; Bollandsås, O.M. Classifying species of individual trees by intensity and
446 structure features derived from airborne laser scanner data. *Remote Sens. Environ.* **2009**, *113*, 1163–1174.

447 47. Brandtberg, T. Classifying individual tree species under leaf-off and leaf-on conditions using airborne
448 lidar. *ISPRS J. Photogramm. Remote Sens.* **2007**, *61*, 325–340.

449 48. Liang, X.; Matikainen, L. Deciduous-Coniferous Tree Classification Using Difference Between First and
450 Last Pulse Laser Signatures. *Iaprs* **2007**, *XXXVI*, 253–257.

451 49. Kim, S.; McGaughey, R.J.; Andersen, H.E.; Schreuder, G. Tree species differentiation using intensity data
452 derived from leaf-on and leaf-off airborne laser scanner data. *Remote Sens. Environ.* **2009**, *113*, 1575–1586.

453 50. Vetrivel, A.; Gerke, M.; Kerle, N.; Vosselman, G. Identification of damage in buildings based on gaps in
454 3D point clouds from very high resolution oblique airborne images. *ISPRS J. Photogramm. Remote Sens.*
455 **2015**, *105*, 61–78.

456 51. Shen, X.; Cao, L. Tree-species classification in subtropical forests using airborne hyperspectral and
457 LiDAR data. *Remote Sens.* **2017**, *9*.

458 52. Krzystek, P.; Serebryanyk, A.; Schnörr, C.; Červenka, J.; Heurich, M. Large-scale mapping of tree species
459 and dead trees in Sumava National Park and Bavarian Forest National Park using lidar and multispectral
460 imagery. *Remote Sens.* **2020**, *12*, 1–22.

461 53. Immitzer, M.; Neuwirth, M.; Böck, S.; Brenner, H.; Vuolo, F.; Atzberger, C. Optimal input features for
462 tree species classification in Central Europe based on multi-temporal Sentinel-2 data. *Remote Sens.* **2019**,
463 *11*.

464

465

Příloha č. 3 - Kuželka, K.; Slavík, M.; Surovỳ, P. Very High Density Point Clouds from UAV Laser Scanning for Automatic Tree Stem Detection and Direct Diameter Measurement. *Remote Sens.* 2020.

remote sensing

MDPI

Article

Very High Density Point Clouds from UAV Laser Scanning for Automatic Tree Stem Detection and Direct Diameter Measurement

Karel Kuželka *, Martin Slavík and Peter Surový

Faculty of Forestry and Wood Sciences, Czech University of Life Sciences, Prague, Kamýcká 129, 165 00 Praha, Czech Republic; mslavik@fld.czu.cz (M.S.); surovy@fld.czu.cz (P.S.)
* Correspondence: kuzelka@fld.czu.cz; Tel.: +42-022-348-3796

Received: 19 March 2020; Accepted: 12 April 2020; Published: 13 April 2020

check for updates

Abstract: Three-dimensional light detection and ranging (LiDAR) point clouds acquired from unmanned aerial vehicles (UAVs) represent a relatively new type of remotely sensed data. Point cloud density of thousands of points per square meter with survey-grade accuracy makes the UAV laser scanning (ULS) a very suitable tool for detailed mapping of forest environment. We used RIEGL VUX-SYS to scan forest stands of Norway spruce and Scots pine, the two most important economic species of central European forests, and evaluated the suitability of point clouds for individual tree stem detection and stem diameter estimation in a fully automated workflow. We segmented tree stems based on point densities in voxels in subcanopy space and applied three methods of robust circle fitting to fit cross-sections along the stems: (1) Hough transform; (2) random sample consensus (RANSAC); and (3) robust least trimmed squares (RLTS). We detected correctly 99% and 100% of all trees in research plots for spruce and pine, respectively, and were able to estimate diameters for 99% of spruces and 98% of pines with mean bias error of −0.1 cm (−1%) and RMSE of 6.0 cm (19%), using the best performing method, RTLS. Hough transform was not able to fit perimeters in unfiltered and often incomplete point representations of cross-sections. In general, RLTS performed slightly better than RANSAC, having both higher stem detection success rate and lower error in diameter estimation. Better performance of RLTS was more pronounced in complicated situations, such as incomplete and noisy point structures, while for high-quality point representations, RANSAC provided slightly better results.

Keywords: UAV; LiDAR; forestry; tree detection; diameter estimation; DBH; RANSAC; robust fitting

1. Introduction

Recent sustainable forestry standards require careful planning based on highly accurate inventory data of forest stands and properties [1]. Increasing demands on inventory data quality together with increasing costs of human labor in advanced countries force the forest owners to increase the efficiency of data collection and to simplify assessment of required parameters of forest trees and stands in means of automation. In the last decade, special attention has been paid to noncontact data collection methods providing accurate three-dimensional data that allow reconstructing forest stands and effectively estimating their parameters. The novel methods, made possible by advances in technology and computer vision algorithms, are mostly represented by two technologies: laser scanning and multiview photogrammetry.

Laser scanning methods utilize light detection and ranging (LiDAR) technology for precise range measurement of objects in surroundings. The distance calculation is based either on measuring the time needed for a light pulse to travel the distance to the target and back to the sensor, or on measuring

the wave phase of the reflected beam with known wavelength. As result, laser scanners provide 3D positions of up to 1 million points per second with a millimeter level precision.

Multiview photogrammetry is a more recent approach, triggered by recent advances in computer vision and development of algorithms like scale-invariant feature transform (SIFT) [2]. It reconstructs 3D surfaces of objects by calculating 3D positions of identical features identified in subsequent images in image sequences acquired with digital cameras [3].

Although both approaches result in 3D point clouds representing the surface of terrain and other objects, such as trees, due to different nature of data origin, LiDAR and photogrammetric clouds embody different properties. Regarding forest stand reconstruction, photogrammetric data are able to precisely represent the upper canopy envelope, whereas LiDAR data show greater capability to penetrate through canopies [4]. Although canopy height models can be accurately calculated from both types of data [5–7], LiDAR data show markedly superior accuracy for forest structure reconstruction and detailed terrain mapping [8]. During the last decade, LiDAR data were acquired particularly in two ways, aerial laser scanning (ALS) and terrestrial laser scanning (TLS).

ALS usually covers areas on regional scale. High density ALS (10 pulses/m^2 and more) provides sufficient detail to detect individual trees either from ALS-derived canopy height models [9] or the whole depth of ALS data [10], but typically, parameters of forest stands are derived from ALS data using an area-based approach that considers area as the unit of interest and generally includes estimates of forest variables on stand-level, per hectare values or mean tree attributes [11]. Beyond estimating basic forest parameters such as diameters, height, volume [12–14], biomass or biomass change [15,16], ALS data can be related to leaf area index [17], gap fraction, defoliation [18] or site index [19]. Nowadays, approaches for predicting tree diameter distributions from ALS data have emerged [8,20], helping to bridge the gap between area-based and tree-based inventories.

On the contrary, TLS provides ultra-high-density scans for detailed and accurate reconstruction of a forest stand, allowing for deriving virtually any dimension of the forest trees, but produces plot-wise data of low spatial extent and is time- and labor-demanding. As shown by numbers of studies, TLS point clouds allow for automatic detection and mapping of forest trees [21] and estimation of diameters [22] or the complete stem curve and tree architecture [23,24]. Additionally, TLS point clouds allow the determination of accurate nondestructive estimates of aboveground biomass [25] and even temporal development of aboveground biomass [26].

LiDAR data acquired from UAS platforms (ULS) represents a revolutionary type of 3D LiDAR data that joins benefits of both ALS and TLS. Multireturn lightweight laser scanners designated for unmanned aerial vehicle (UAV) carriers can reach a measurement rate of up to hundreds of thousands of measurements per second with the presented distance measurement accuracy/precision of 10 mm/5 mm [27]. Due to the low flying altitude, varying around 100 m above ground level, and arbitrarily low speed of multicopter-type UAV carriers, the density of resulting point clouds can reach the level of thousands of points per square meter. Such point clouds constitute a high-quality representation of 3D structure of forest stands and individual trees. Moreover, a relatively large range of scanning angles ensures a good coverage of ground, forest canopies and even individual tree stems.

The possibility of assessing parameters of individual tree stems in ULS data was recently tested by several authors. Brede et al. [28] showed that it was possible to detect stems and estimate diameters from ULS point clouds acquired with RIEGL VUX-1UAV scanner mounted on RiCOPTER. As they report, about two-thirds of detected stems were suitable to estimate diameter at breast height (DBH), while the DBH extraction workflow comprised a large share of manual work. The possibility of DBH extraction was also investigated by Wieser et al. [29]. They used the same scanning system—RiCOPTER and VUX1-UAV—to acquire ULS data of broadleaf forest in leaf-off condition, thus with very high density of points on stems. Their work was not focused on automatic tree detection; therefore, they manually selected the trunk sections in order to perform the cylindrical fit for DBH estimation.

Automatic workflows for stem recognition and DBH estimation have been published for TLS data. Olofsson et al. [30] successfully utilized random sample consensus (RANSAC) algorithm to

fit the circle on semicircular data representing one side of a stem. A similar problem was solved using Ganders' direct method for data from mobile laser scanning [31]. Other studies [22,32] suggest other algorithms for tree diameter estimation from dense TLS or photogrammetric 3D point clouds. However, the point density on stem surfaces in ULS data is significantly lower than that from terrestrial methods of data collection, and the noise shows markedly higher range. While the tree stem in terrestrial photogrammetric or laser point clouds may be represented by thousands points per meter of the stem length, the ULS data provide only tens of points, and the millimeter-level noise of TLS data grows to centimeter-level in ULS clouds. Moreover, parts of stems may be shaded by canopies, especially in leaf-on conditions or in coniferous stands. As a result, ULS data must be treated differently than TLS data, and the workflows must be modified to respect the ULS data specification.

This study evaluates the possibilities of detection of tree stems and diameter estimation using an automatic workflow in ULS data representing typical mature forest stands of two main economically important coniferous species of Central European forests—Norway spruce and Scots pine.

2. Materials and Methods

2.1. Research Area

For the study, the two most abundant and economically most important tree species of Central European forests were selected: (1) Norway spruce (*Picea abies* (L.) H. Karst.) and (2) Scots pine (*Pinus sylvestris* L.). The research area was located in the Central Bohemia region, Czech Republic, in two locations: (1) spruce-dominated upland (49.956N, 14.828E, 430 m AMSL) for Norway spruce, and (2) pine-dominated sandy area of the Czech basin (50.562N, 14.725E, 330 m AMSL) for Scots pine.

Pure-plantation forest stands were selected for both species: one large forest stand for Scots pine and two smaller stands for Norway spruce. All study stands were homogenous, mature, even-aged stands. The pine forest stand, as well as one of the spruce stands (plot 3) represented the typical structure of mature production forest stands of the given species. The other spruce stand (plots 1 and 2) represented a stand on very high quality site, which is illustrated by tree heights reaching 42 m and presence of dense understory. For validation purposes, six square research plots of the size 25 × 25 m were established, i.e., three for each species. Locations of sample plots and trees are illustrated in the height maps of forest stands in Figure 1. Table 1 describes parameters of forest stands and research plots. The inner structures of forest stands of both species are shown in Figure 2.

Table 1. Parameters of forest stands containing research plots.

Plot ID	Species	Age (Years)	Density (Trees/ha)	Trees in Plot	Diameter (cm)	Mean Height (m)
1	Spruce	130	400	24	29–57	39
2	Spruce	130	450	27	32–67	40
3	Spruce	110	320	20	15–46	31
4	Pine	100	160	8	27–35	24
5	Pine	100	360	22	23–37	26
6	Pine	100	330	21	22–35	25

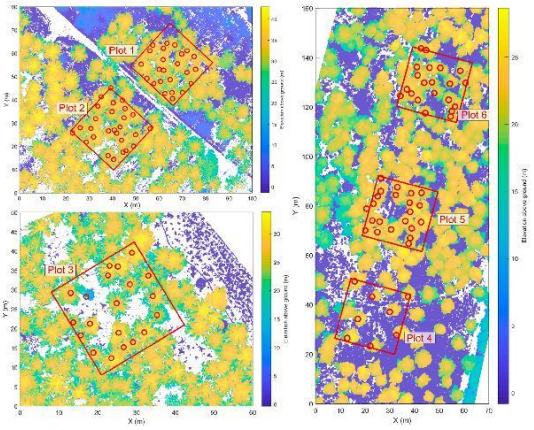

Figure 1. Location of six sample plots (red squares) and positions of measured trees (red circles). Colors in the maps express aboveground height according to the color bars.

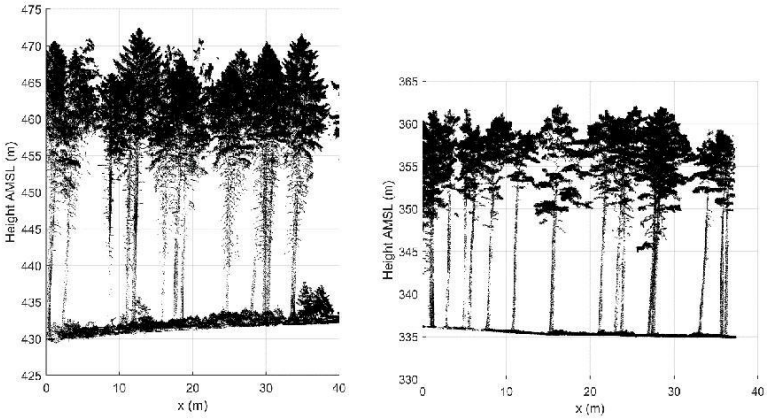

Figure 2. Structure of research forest stands: (**a**) a spruce stand (plot 1); (**b**) a pine stand (plot 5). Images show LiDAR representation of a transect 40 m long and 10 m wide.

2.2. Field Data

The research plots were located in the field using a Trimble C3 (Trimble Inc., Sunnyvale, California USA) total station. Positions of all trees in the square plots were measured and recorded with the total station. A tree position was defined as a center of the cross-section of the stem at 1.3 m above ground. To record the position of the true center of trees, cross-sections the angle offset measuring method was used: the cube corner prism was placed on the side of the tree preserving the distance to the center of the cross-section; subsequently, the angle to the tree center was recorded separately. The total station data were referenced using four RTK GNSS points. The final error of ground truth tree positions should not exceed 5 cm. Two diameters at breast height (DBH), i.e., 1.3 m above ground,

were measured in two perpendicular directions with a digital caliper Digitech Professional DPII (Haglöf Sweden AB, Långsele, Sweden), averaged by the caliper software and recorded as DBH for each tree.

2.3. ULS Data Acquisition

ULS data for the whole forest stands were acquired using a multirotor UAS RiCOPTER (RIEGL Laser Measurement System GmbH, Horn, Austria) equipped with RIEGL VUX-SYS laser scanning system. The VUX-SYS, consisting of VUX-1 UAV laser scanner, a GNSS and IMU system AP20 (Applanix: a Trimble company, Ontario, Canada) and a control unit, represents a complete lightweight solution for aerial laser scanning, primarily designated for the use with UAV platforms. VUX-1 UAV is a lightweight multireturn laser scanner with maximum laser pulse frequency of 550 kHz. For detailed description of the VUX-SYS and RiCOPTER, see [28].

For both locations, identical workflows for data acquisition were applied. Data were collected during an automatically executed flight over a predefined trajectory. The trajectory followed a double grid pattern, consisting of parallel lines with uniform spacing of 50 m, in two perpendicular directions, with stops and turns at vertices of the trajectory. The flight altitude was set to 80 m above ground, and the flight ground speed was set to 6 m s^{-1}. The mentioned flight parameters together with the laser pulse repetition rate of 550 kHz, forming 200 scan lines per second, correspond to average point density of 200 LiDAR points/m^2 for each single flight line. In order to ensure uniform point density and a regular pattern of the points, LiDAR data were collected during straight flight only, and data collection was interrupted while stopping and turning. LiDAR point clouds were generated from raw scan data in postprocessing that consisted of trajectory reconstruction with the use of postprocessing kinematic (PPK) method and Trimble VRS Now reference GNSS data in POSPac software (Applanix: a Trimble company, Ontario, Canada) and subsequent point cloud generation and adjustment with the use of RiPROCESS and RiPRECISION UAV software (RIEGL Laser Measurement System GmbH, Horn, Austria), following the official data processing workflow recommended by RIEGL. The classification of ground vs. nonground points was a part of the standard processing workflow in RiPROCESS. The final products of the processing were classified 3D point clouds stored in ASPRS LAS files.

2.4. Point Cloud Processing

Once the point clouds were produced, the environment of MATLAB R2017b (MathWorks Inc., Natick, Massachusetts, USA) was utilized to carry out analyses and point cloud processing and to generate graphic outputs. Firstly, thinning of the ULS point cloud was carried out to reduce the point cloud size in case of occurrence of areas with superfluous density and to unify the point distances. The minimum distances of the points were set to 0.01 m. To perform the thinning efficiently, the x, y, z coordinates of all points were rounded to the nearest 0.01 m. Subsequently, duplicities in coordinates were detected and removed. As the next step, noise filtering was applied. All points with a distance larger than 0.5 to the nearest group of points were considered as noise and removed. The next data processing comprised tree detection and segmentation and diameter estimation for detected trees.

2.5. Tree Segmentation

Methods for detecting trees in point clouds usually assume that tree stems are continuous solids reaching from ground to the canopy level or tree tops. Therefore the algorithms comprise vertical projections of points to the ground plate either as point counts in horizontal grid [30] or as bounding polygons of point clusters [10] in several horizontal layers, the width of which depends on point density. For ALS data [10], the layer width of 1 m was utilized, while the layer width for TLS data was set to approximately 3 cm [30] or 4 cm [22]. Wieser et al. [29] utilized 1 m layer width to detect the stems and fit cylinders to point structures in ULS data. Similarly, cylinder fitting based on RANSAC was applied to 0.5 m thick layers in detailed UAV-acquired photogrammetric point clouds of tree stems [33].

In this study, detection of individual trees was based solely on evaluating point densities in subcanopy space; the canopy height model (CHM), which serves as input data for several tree-segmentation algorithms, was not included in individual tree segmentation in this study. The whole subcanopy space was divided into voxels. The lower limit for the investigated subcanopy space was set to 0.5 m above ground to avoid low vegetation, and the upper limit was estimated as the average length of stems without branches; simultaneously, the limit was set so that the height of the investigated space was defined by whole number of meters. In our study, the upper limit was set to 9.5 m above ground. The voxel size was set according to the typical point density in ULS point clouds. As the tree stems were represented by 20–50 points per meter of stem length in average, horizontal voxel size was set to 0.5 m and the vertical size to 1 m. Counts of points were assessed in each voxel. Vertical projection of the voxel grid represented a horizontal raster that served for evaluating tree stem presence. A tree stem was more likely present in a raster cell when point counts in the corresponding voxels were high, continuous throughout the voxels and uniform. The raster cells were populated with values of stem presence indicator (SPI) that was formulated as:

$$\mathrm{SPI}_{i,j} = \sum_{k=1}^{m-1} \sum_{l=k+1}^{m} n_{i,j,k} \cdot n_{i,j,l} \quad (1)$$

where $\mathrm{SPI}_{i,j}$ is the value of the i,j-th cell of the raster; m is the number of voxels in vertical direction; and $n_{i,j,k}$ is the point count in the i,j,k-th voxel, where i, j and k are the voxel indices along x, y and z axis, respectively. This indicator prefers continuity and uniformity of point counts and gives provisions for higher point densities. High values of the indicator generally indicate locations where high point densities continue from ground to canopy base; therefore, tree stems can be discriminated from branches and other objects that are not continuous throughout the subcanopy space.

To detect local maxima in SPI raster, a maximum filter was applied and maximum raster $\mathrm{SPI}_{\max}$ was created. The value of i,j-th $\mathrm{SPI}_{\max}$ raster cell was defined as the maximum cell value in SPI raster of cells whose distance to the i,j-th cell was smaller than a defined radius. For a good result, the radius should be set as higher than the half distance between stems, but lower than the distance between stems. In our case, the radius was set to 2 m, according the a priori expected distance between trees. Local maxima in SPI raster are defined as cells where the SPI raster value equals the $\mathrm{SPI}_{\max}$ value, $\mathrm{SPI}_{i,j} = \mathrm{SPI}_{\max(i,j)}$. To remove noise, a threshold for low SPI values was set. The threshold value corresponds to the approximate bottom limit of stem point distribution for subsequent diameter estimation and results from the requirement that the stem points are present and allow diameter estimation in a minimum of three sections. As the approximate minimum point count for efficient diameter estimation was expected to be 15, the appropriate threshold value corresponding to the requirement was 675. Detected local maxima in SPI raster with the value higher than the threshold were considered approximate stem positions.

To segment individual trees according to the detected positions, Delaunay triangulation was applied on the approximate stem positions, and the area of the forest stand was partitioned into polygons according to Voronoi diagram. Points in each polygon were subsequently treated as points belonging to one tree.

2.6. Diameter Estimation

Points representing a tree were partitioned in vertical sections according to their height above ground. With regard to the point densities (20–50 points per meter in average), height sections of 1 m were used for diameter estimation, because smaller sections do not provide enough points for reliable diameter estimation. Projection of points in height section to horizontal plane generated point representation of stem cross-sections. Diameters of the cross-sections were estimated as diameters of circles fitted in the point structures.

Point clouds were not manually cleared, and the cross-section point structures contained laser returns from branches, shrubs and other noise. Moreover, due to dense canopy and stems shading the laser beams, the cross-section representations might be poor or incomplete. Therefore direct least squares fitting techniques proposed in some studies [22,32] could not be utilized. Instead, methods allowing for circle detection in noisy and incomplete data were applied: (1) Hough transform, (2) RANSAC, and (3) robust least trimmed squares (RLTS).

Hough transform is a method originally developed to detect geometric objects in images, however the pixel-based algorithm can be adopted for application on point-based data. The Hough transform circle fitting is based on geometrical definition of a circle: a circle is a set of points with equal distance (i.e., radius) from the center. Therefore, if circles of a given radius are drawn around each point belonging to the circle perimeter, all the new circles will intersect in the center of the original searched circle. In practical application, a raster is established where each cell value represents the count of intersects of newly drawn circles with the given raster cell. A peak in the raster represents the center of the original circle. The weak point of the Hough transform is the need for a priori knowledge of the circle radius. If radius is unknown, the algorithm must be performed repeatedly with a set of different radii. The Hough transform is reported to be insensitive to noise or incompleteness of data [34]. Utilization of Hough transform for stem diameter estimation in TLS data was indicated by [35], together with detailed explanation of the method.

Random sample consensus (RANSAC) is an iterative stochastic method developed to fit a mathematical model in noisy data based on repeated model fitting to random subsamples. For circle fitting, a minimum subsample that defines a circle, i.e., 3 points, is repeatedly randomly selected, and the circle is fitted. The quality of each fit is evaluated by the ratio of points within a defined close distance from the fitted circle, so-called inliers. Finally, inliers of the best fit are used to fit the final circle. The number of iterations was set to 1000. Serviceability of RANSAC in forest mensuration was shown by [36], who utilized RANSAC for delineation of tree crowns in ALS data, and by [30] for diameter fitting in TLS clouds.

Robust least trimmed squares (RLTS) algorithm is a stochastic iterative method based on least squares criterion applied on a defined portion of smallest residues, which makes it more reliable in case of presence of outliers [37]. Analogous to RANSAC, RTLS iteratively fits circles to random subsamples of 3 points. In each iteration, squared residuals—squared distances of all points to the fitted circle—are calculated and sorted. A defined trim portion h ($h > 1/2$) of points with the smallest residuals are selected and least square circle fitting is applied on the selected points. The criterion for evaluating the quality of fit is the sum of squared residuals of the least square circle fit. For detailed description of the method, see [37].

As shown by [30], the general algorithm can be adopted to better match the specific application of tree diameter estimation. Based on the assumption that a tree stem is a continuous solid along the vertical axis and with continuous diameter along the vertical axis, conditions on (1) counts of points inside the circle, (2) position of the circle and (3) radius of the circle can be set in order to eliminate circle fitting error.

The starting point for diameter fitting was determined from the vertical distribution of points as the local minimum in smoothed histogram of above-ground height. This way, the fitting started in a section that is above the shrubs and below the crown base. Optimally, this section contained mostly points belonging to stems and little noise; therefore, fitting should encounter the least problems and errors. After the starting section is fitted, fitting is carried out in the nearest lower section in successive steps. Fitting the subsequent sections can benefit from the known parameters of the previously fitted section.

For the starting section, the lower and upper limits for circle radius were set to 0.05 and 0.4 m as the most common tree radii in production forest; only circles with radii in this interval were searched in projections of section point clouds. If a circle was successfully fitted with radius $\hat{r}_i$ to the points

of section i, the following rules were applied for the radius limit r_{lim} at the nearest lower $(i-1)$th or nearest higher $(i+1)$th section:

$$\begin{aligned} r_{\text{lim}(i-1)} &= \{(0.8,\ 1.5)\cdot\hat{r}_i \\ r_{\text{lim}(i+1)} &= (0.6,\ 1.2)\cdot\hat{r}_i \end{aligned} \tag{2}$$

To limit the position of the circle in the $(i-1)$th section, all points further than $2\cdot\hat{r}_i$ from the center $[\hat{x}_i,\ \hat{y}_i\ ]$ of the fitted circle in the i-th section were disabled. This action also eliminated the risk of false circle fitting in points representing returns from branches or shrubs. For all the circles, the limit count of points inside the circle was set to 25% of the count of perimeter points. Perimeter points were defined as points not further than 0.02 m from the circle perimeter; inside points were points inside the circle with distance to the circle perimeter higher than 0.02 m. For RLTS, the trim portion h was set to two-thirds, i.e., 0.67.

Functions for all three circle fitting methods were written in the MATLAB environment as the general algorithms briefly described in this section and the mentioned adoptions of the algorithms were applied.

2.7. Accuracy Evaluation

Circles were fitted and diameters were estimated for all sections throughout the stem profile. Evaluation of diameter estimation was carried out for diameters at breast height. Diameters of second sections (aboveground height 1–2 m) were compared to field-measured DBH.

Errors of DBH estimations were assessed as a difference of estimated ($\hat{d}_i$) and field-measured (d_i) DBH. Relative error of DBH estimation was defined as DBH estimation error divided by field-measured DBH. At each plot, mean bias error (bias) and root-mean-square error (RMSE) were calculated both from absolute (cm) and relative (%) errors of n trees detected and measured in the plot with each method. Mean bias error expressed the systematic error of diameter estimations in the plot; RMSE illustrated the typical extent of estimation errors.

$$\begin{aligned} \text{bias} &= \frac{1}{n}\cdot\sum_{i=1}^{n}\left(\hat{d}_i - d_i\right) \\ \text{RMSE} &= \sqrt{\frac{1}{n}\cdot\sum_{i=1}^{n}\left(\hat{d}_i - d_i\right)^2} \end{aligned} \tag{3}$$

Position error of tree detection was calculated as a mean distance between detected and field-measured positions of all detected trees in a plot.

Statistical testing was involved in order to reveal factors influencing the accuracy of diameter estimation. Two-way ANOVA was utilized to investigate the influence of circle fitting method and tree species on absolute diameter errors. We also investigated the influence of point counts available for circle fitting on diameter estimation accuracy; to eliminate the effect of the previously mentioned factors, generalized linear model (GLM) was fitted with two categorical (circle fitting method and tree species) predictors and one quantitative (point counts) predictor. Linear regression models were built to quantify the effect of point counts for each fitting method separately.

3. Results

3.1. Point Clouds

The results of laser scanning and laser data processing are 3D point clouds consisting of approximately 2000 points per square meter (Figure 3). In spruce forest, approximately one-quarter of the total count of LiDAR returns was reflected from terrain surface, and the other three-quarters represent returns from vegetation. In pine forest stand, the ratio of ground vs. vegetation returns was

higher due to less dense crowns of pines compared to spruce; ground points represented approximately one-half of the whole amount of returns.

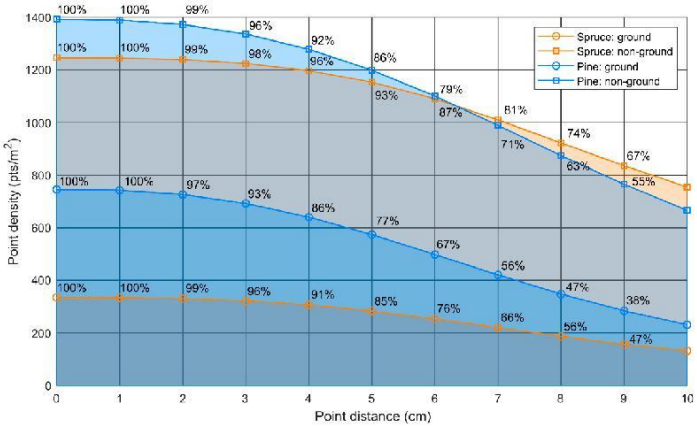

Figure 3. Gradual decline of point densities for voxel-based thinning with increased thinning intensity, i.e., point distances in resulting thinned point clouds. The densities show neglectable drop for thinning in voxels up to 2 cm.

The points were evenly distributed in 3D space, as illustrated by Figure 3, which shows point density and ratio of resulting point cloud size related to original point counts for different levels of thinning. For 1 or 2 cm thinning, the resulting point cloud contained almost 100% of points of original point clouds. For higher levels of thinning, the point counts in resulting clouds decreased. Well-covered surfaces contained points with regular distance of about 2 cm. For further processing, the point clouds were thinned to eliminate points with distances lower than 1 cm. Apparently, almost 100% of the information contained by the original point cloud remained in the thinned point cloud.

Vertical distribution of point densities in forest stands of both species is shown in Figure 4. Only points classified as nonground are displayed here. For both species, highest point densities are in the canopy space, reaching up to 180 points/m^2 in 1 m thick layer for spruce and >200 points/m^2 for pine. The lowest densities are found in the subcanopy space filled only by stems without branches. The average point densities of this space were below 3 points/m^2 both in spruce and pine research plots.

Regarding spruce stands, plot 3 shows a markedly different histogram from plots 1 and 2 due to significantly lower heights of trees in plot 3. Among pine plots, plot 4 shows significantly lower point densities than plots 5 and 6 due to lower canopy closure. Unlike pine, spruce stand (plots 1 and 2) shows increased densities in low above-ground layers (up to 5 m). These points represent returns from understory vegetation.

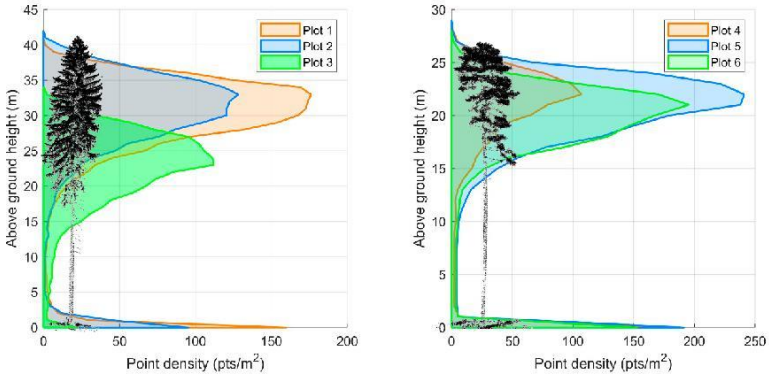

Figure 4. Point densities in spruce (**a**) and pine (**b**) plots. Histograms represent average point counts per square meter in 1 m thick horizontal layers; only points classified as nonground are displayed.

3.2. Tree Segmentation

In pine research plots (plots 4–6), the automatic tree detection was fully successful. Pines are characterized by sparse crowns that allow a large portion of laser beams to penetrate under canopy and to return from stem surface. Moreover, there was no understory in pine plots. As result, the subcanopy part of point cloud consisted of clearly identifiable, well-covered stems. All the stems were correctly identified, and there were no false detections (Table 2).

Table 2. Counts of detected trees and detection errors in research plots. Meaning of columns is as follows: Counts of detected trees in plot (Detected); counts of correctly detected trees within 1 m distance from the real positions (Correct); counts of trees that were not detected (Omission); counts of false detections (Commission); average distance of correctly detected trees to real positions (Distance).

Plot ID	Detected	Correct	Omission	Commission	Distance (m)
1	24 (100%)	24 (100%)	0	0	0.46
2	31 (115%)	26 (96%)	1 (4%)	5 (19%)	0.38
3	20 (100%)	20 (100%)	0	0	0.27
4	8 (100%)	8 (100%)	0	0	0.37
5	22 (100%)	22 (100%)	0	0	0.27
6	21 (100%)	21 (100%)	0	0	0.30

In spruce stands, most laser beams are captured by denser and longer crowns of spruce, and therefore some stem parts or whole stems can obscured and contain too few points to be detected in the subcanopy space. However, in plots 1 and 3, all stems were correctly identified with no false detections (Table 2). Plot 2 was placed in an exceptionally dense forest stand that prevented one of the 27 tree stems, which was located in the densest part of the plot, from being well covered by LiDAR returns. Moreover, dense understory vegetation consisting of young spruces up to 5 m tall resulted in five false detections in plot 2 (Figure 5). However, it should be mentioned that false detections (commission error) do not imply errors in final result. Objects responsible for false stem detections do not have circular cross-sections; therefore, circles cannot be fitted, and the false detections are eliminated in the next step of point cloud processing.

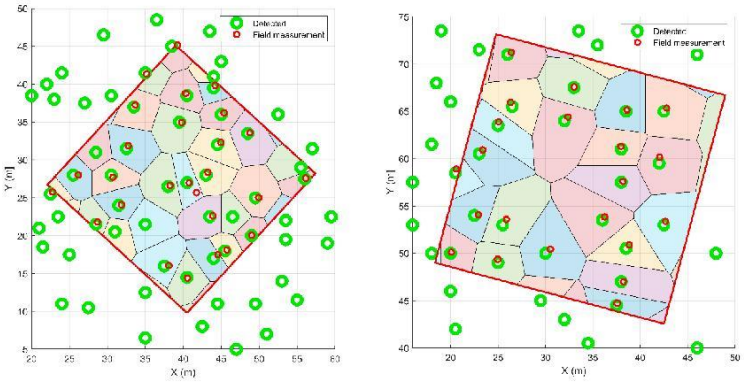

(**a**) (**b**)

Figure 5. Tree positions automatically detected in point clouds and field-measured: (**a**) spruce plot (plot 2); (**b**) pine plot (plot 5). Colored polygons represent Voronoi diagram used to segment the plot area into regions of individual trees.

Tree positions recorded during tree segmentation represent centers of cells of the square grid, and the positions were recorded with 0.5 m resolution. Therefore, positions of detected trees do not correspond to field-measured positions (Figure 5). Distances indicated in Table 2 denote distance between real positions and cell center. The real distance between measured position and detected tree center is specified in the next step.

3.3. Diameter Estimation

Circles were fitted and diameters were estimated for all sections throughout the stem profile (Figure 6). As the figure indicates, circles representing stem cross-sections were well identified in most of the stem profile, even in crown sections containing branches and in bottom sections containing returns from understory vegetation. However, the presented results evaluate only quality of DBH estimation from the second above-ground section. Evaluation of estimated diameters of top sections is not presented here, as field-measured values were available only for DBH.

Not all tree stems automatically detected in the sample plots were represented by sufficient counts of LiDAR returns. Point representation of some trees did not allow for circle fitting in DBH layer due to low point density on the lower stem surface (details in Table 3). This applies especially to spruce trees; DBH of spruces could be quantified for approximately 90% of trees present in the plots, on average, with the RANSAC method. However, RLTS allowed to estimate diameters of 99% of all spruce trees present in the research plots. In pine forests, virtually all trees, with an exception of one tree in plot 5, allowed for DBH estimation.

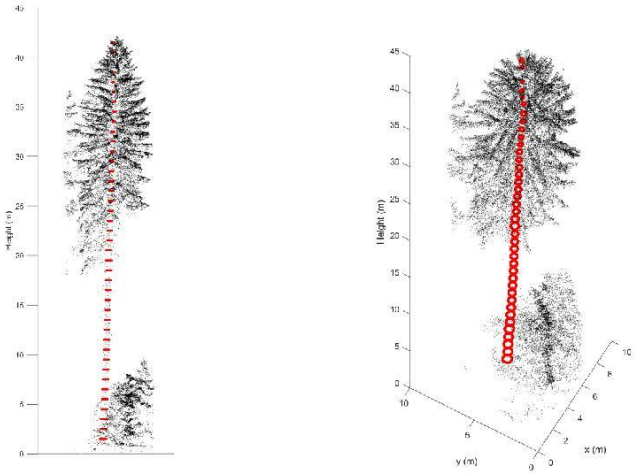

(**a**) (**b**)

Figure 6. Automatically fitted perimeters of stem cross sections (red circles) in a point cloud representing automatically segmented spruce tree: (**a**) side view and (**b**) 3D view. The point cloud was thinned so that the fitted circles are visible in the figure.

The Hough transform method did not show the ability to fit circles to the point structures representing cross-sections of tree stems. In most cases, Hough transform did not find centers and radii of the circles, and the calculated radii were often determined by the radius limits (Figure 7). Therefore, the diameter estimation errors were high, usually with the highest RMSE among the three methods (Table 3).

Table 3. Results of diameter estimation. Table shows counts of trees that allowed for diameter at breast height (DBH) estimation and the respective percentage of present trees (Measured), mean error and RMSE of DBH estimation and mean positional error of detected trees (Position).

Plot ID	Method	Measured	Mean Error (cm)	RMSE (cm)	Position (m)
1	Hough	21 (88%)	5.0 (13%)	8.5 (25%)	0.15
	RANSAC	22 (92%)	0.1 (0%)	9.5 (22%)	0.13
	RLTS	24 (100%)	0.7 (1%)	6.7 (17%)	0.13
2	Hough	19 (70%)	1.0 (5%)	12.2 (28%)	0.29
	RANSAC	24 (89%)	1.4 (4%)	4.2 (10%)	0.15
	RLTS	26 (96%)	−1.1 (−3%)	6.2 (17%)	0.15
3	Hough	19 (95%)	4.9 (14%)	9.0 (31%)	0.25
	RANSAC	20 (100%)	3.2 (10%)	6.2 (22%)	0.12
	RLTS	20 (100%)	1.7 (6%)	5.9 (20%)	0.12

Table 3. *Cont.*

Plot ID	Method	Measured	Mean Error (cm)	RMSE (cm)	Position (m)
Spruce total	Hough	59 (83%)	3.7 (11%)	10.0 (28%)	0.23
	RANSAC	66 (93%)	1.5 (5%)	6.9 (18%)	0.14
	RLTS	70 (99%)	0.3 (1%)	6.3 (18%)	0.13
4	Hough	8 (100%)	−0.7 (−3%)	7.8 (25%)	0.13
	RANSAC	8 (100%)	0.0 (0%)	4.0 (12%)	0.14
	RLTS	8 (100%)	−1.0 (−4%)	4.4 (14%)	0.15
5	Hough	21 (95%)	1.7 (4%)	10 (35%)	0.18
	RANSAC	21 (95%)	1.4 (4%)	4.6 (14%)	0.10
	RLTS	21 (95%)	0.7 (−3%)	4.3 (15%)	0.10
6	Hough	17 (81%)	7.8 (30%)	15.1 (59%)	0.10
	RANSAC	21 (100%)	0.3 (2%)	9.0 (31%)	0.11
	RLTS	21 (100%)	0.7 (−4%)	7.1 (27%)	0.12
Pine total	Hough	46 (90%)	3.6 (12%)	12 (44%)	0.14
	RANSAC	50 (98%)	0.5 (2%)	7.0 (24%)	0.11
	RLTS	50 (98%)	−0.8 (−3%)	5.7 (21%)	0.12
All trees	Hough	105 (86%)	3.6 (11%)	10.9 (36%)	0.19
	RANSAC	116 (95%)	1.2 (4%)	6.8 (20%)	0.13
	RLTS	120 (98%)	−0.1 (−1%)	6.0 (19%)	0.13

The other two algorithms, RANSAC and RLTS, provided much more reasonable results of circle fitting and diameter estimations (Figure 7). In general, RLTS performed slightly better than RANSAC (Table 3), having both higher ratio of measured trees and lower RMSE. In pine research plots, there was almost no difference in mean error (on average 2% and −3% for RANSAC and RLTS, respectively); RMSE of RANSAC (24%) was gently higher than that of RLTS (21%). The difference of the algorithms' performance appeared under the difficult conditions caused by incompleteness of point representations of cross-sections and presence of LiDAR returns from understory vegetation. In the plots with the highest errors (plots 1 and 6), RLTS showed about 2 cm lower RMSE in comparison with RANSAC; in plots with overall lower errors, RMSE of both methods were balanced.

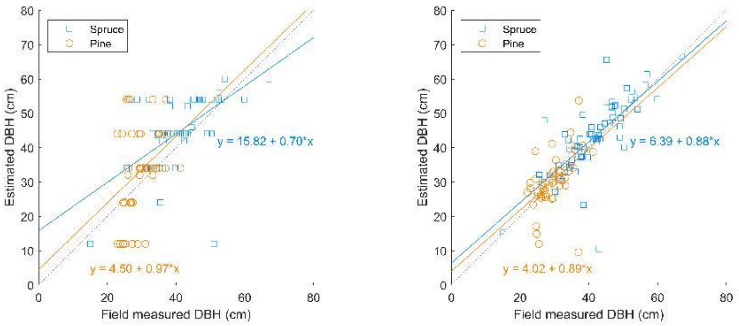

(**a**) (**b**)

Figure 7. *Cont.*

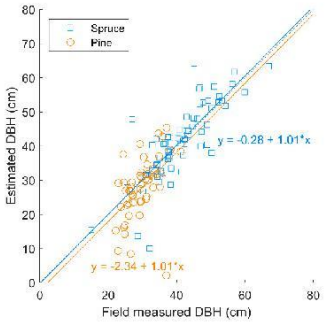

(**c**)

Figure 7. Field-measured vs. estimated diameters: (**a**) Hough transform; (**b**) RANSAC; (**c**) RLTS. Black dashed line expresses the 1:1 trend.

3.4. Factors Affecting the Accuracy of Diameter Estimation

The accuracy of diameter estimation is clearly dependent on the quality of point representation of stem cross-sections (Figure 8). Table 4 shows the dependency of DBH estimation error on point counts that represent the perimeter of stem cross-section. Higher point counts resulted in sections that were better represented, with better fit. As Table 4 indicates, sections with poor point representation were better fitted by RLTS; with increased quality of point representation, the difference between RANSAC and RLTS disappeared. For well-covered sections represented with more than 100 points, RANSAC provided better diameter estimation than RLTS.

Both methods (RANSAC, RLTS) showed significant trend (p-value < 0.05) in DBH estimation error with rising count of points in a section used to fit a circle (95% confidence bounds for slope parameter 0.001, 0.04 for RANSAC and 0.01, 0.05 for RLTS). While the error was negative (diameters were underestimated) for low counts of available points, diameters in sections represented by higher count of points were more likely estimated with positive error (diameters were overestimated).

Regarding the absolute error, a significant decline (p-value < 0.05) of diameter estimation error with rising point counts was observed with the RANSCAC method. More points representing the stem cross-section resulted in more accurate diameter estimation (95% confidence bounds for slope parameter −0.06, −0.002). No such trend was observed with the RLTS method.

Comparison of RANSAC and RLTS methods based on absolute errors showed that RLTS had lower error in comparison with RANSAC in sections where the overall error was high. On the contrary, RANSAC had lower errors in sections with low overall error. In other words, RLTS showed the ability to improve fit in more complicated situations, while RANSAC provided better estimations in sections with better quality of point description.

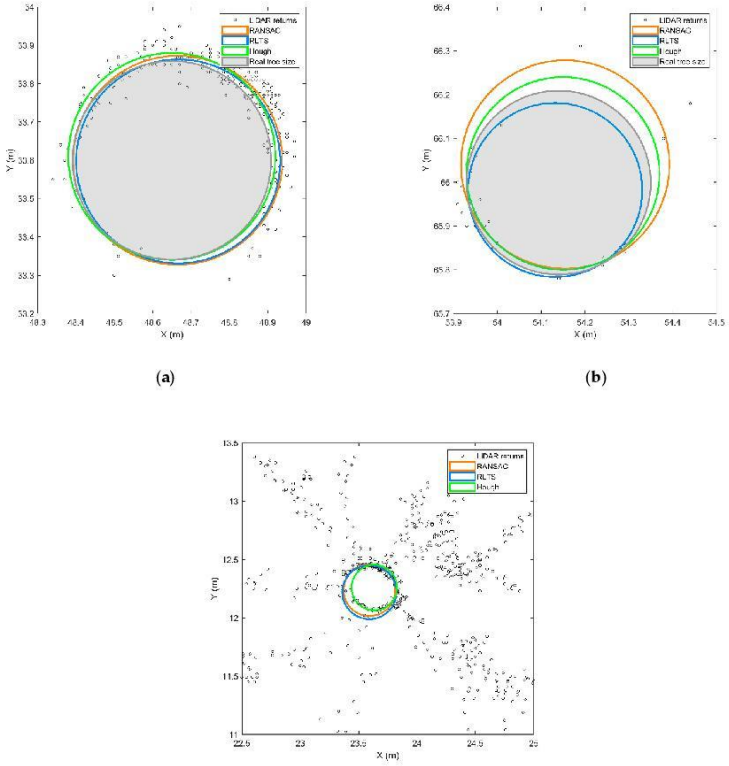

(**a**) (**b**)

(**c**)

Figure 8. Three examples of circle fitting in point representations of stem sections: (**a**) well covered stem section; (**b**) incomplete perimeter of stem section; (**c**) upper stem section with branches. The real diameter was not measured in (**c**).

Table 4. RMSE (cm) of diameter estimation for sections represented with different point counts.

Point Count	Hough	RANSAC	RLTS
>5	11.3	6.8	6.0
>10	10.9	6.1	5.6
>50	10.2	5.5	5.7
>100	10.4	4.7	4.8

Surprisingly, quality of diameter estimation was not influenced by species. Two-way ANOVA (significance level $\alpha = 0.05$) revealed the influence of fitting method (significant differences between Hough transform and the other two methods, $p = 0.02$ for RANSAC, $p = 0.001$ for RLTS; no difference between RANSAC and RLTS, $p = 0.95$) but no influence of species (no significant difference between spruce and pine, $p = 0.24$) on absolute errors of DBH estimate. GLM that tested the influence of (1) fitting method, (2) species and (3) point counts representing the cross-sections showed significant

influence of fitting method ($p = 0.014$) and point counts available ($p = 0.0015$) for circle fitting and again did not reveal any significant influence of species ($p = 0.81$). The point counts available for circle fitting were similar in both species (41 points for spruce and 47 points for pine, on average); the variance in point counts was double in spruce compared to pine.

The average position error of detected trees was 13 cm. This value comprises (1) positional error of acquired point cloud, (2) transformation error of point cloud transformation from WGS-84 coordinate system to the Czech official coordinate system S-JTSK (Krovak East North, EPSG:5514), (3) error of circle fitting methods in segmented point cloud and (4) error of field-measured coordinates of trees with the total station. Unfortunately, we were not able to quantify individual components of the positional errors.

4. Discussion

Three-dimensional LiDAR point clouds acquired from a UAV platform represent a relatively new type of remotely sensed data for forestry and environmental applications. Multireturn lightweight laser scanners designated for UAV carriers can reach a pulse rate more than half a million pulses per second with survey grade accuracy of 10 mm. Due to the low flying altitude, varying around 100 m above ground level, and arbitrarily low speed of multicopter-type UAV carriers, the density of resulting point clouds can reach the level of thousands of points per square meter. Such point clouds constitute a high-quality representation of 3D structure of forest stands and individual trees. In this study, we show that in ULS point clouds individual trees can be segmented and their dimensions measured in a fully automated process.

In our study, point clouds of forests of different species showed slightly different point cloud densities; this may be attributed to topographic effects. While the pine forest was in a flat area, spruce forest stands were located in a hilly area on a slope. As a result, above-ground flight height in a spruce area may vary during the flight, which may cause unequal point densities.

High density of canopy cover, together with understory, as present in plot 2, implicate challenging conditions both for data acquisition and automatic data processing. Moreover, as mentioned by Brede et al. [28], spruce, unlike broadleaved trees as beech and oak, do not allow for higher-order returns due to dense crowns with needles with high content of water. Therefore, we expected much lower success rate of tree detection in plot 2, characterized by tight canopy closure and trees as close as 1.4 m from each other in the densest part. However, with the exception of one single tree shaded by neighboring trees in the densest part, all stems were detected and even measured using RLTS algorithm.

RLTS was presented as an algorithm for robust cylinder fitting [37], but it can be utilized for circle fitting as well. It showed its ability, as declared in [37], to fit incomplete data as well as data containing noise and height percentage of outliers. In difficult conditions of incomplete or noisy data, RLTS performed better than RANSAC. Moreover, the diameters that were not estimated with RANSAC represent more complicated situations for circle fitting and increased the mean errors of RLTS. However, for well-covered tree sections, especially in low-density pine stand, RANSAC provided better estimations. This phenomenon may be caused by the fact that RLTS disables a defined portion of points with highest residuals. Removing noise points in noisy data improves the fit, but utilizing the information present in all points may lead to better estimation in high-quality point representation.

Hough transform was presented as a method for efficient circle fitting for diameter estimation in TLS data [35]. Due to the principle of Hough transform circle detection, point structure forming almost perfect circle or its part is required for the method to return correct results. Therefore, it might be a reasonable method for TLS data, which are characterized by ultra-high point density and low level of noise. ULS provides much lower densities, and LiDAR returns often form incomplete perimeters of cross-sections. Moreover, LiDAR data were not manually segmented or cleared, and the point cloud contained returns from other objects, like branches or understory vegetation. Under such conditions, Hough transform did not perform satisfactorily.

The previously published study of Wieser et al. [29], focusing on diameter estimation from manually delineated tree stems in ULS point cloud, was performed in a deciduous forest during leaf-off season. Thus, their point representation of stem surface was significantly denser. They did not provide RMSE of DBH estimation; however, their errors varied between −18 and 18 cm, with median absolute error of approximately 5 cm. Here, we show that comparable accuracy of DBH estimation can be reached even in coniferous forest with dense canopies and using automated segmentation. Brede et al. [28] report RMSE of diameter estimation 4.24 cm; however, their result is based on fitting 39 trees with the best point representation from the total 58 research trees. Moreover, the suitability for circle fitting was manually inspected for each tree, and outlier points, such as returns from branches, were manually removed. Comparably high RMSE of diameter estimation are reported from RANSAC diameter estimation from TLS data that provide significantly higher point densities and level of detail: Olofsson et al. [30] report RMSE of 33 to 59 mm for data without the removal of outliers. RMSE of 3 to 6 cm for diameter estimation is also reported from detailed photogrammetric reconstruction of forest stands, e.g., [32,38]. The results indicate that for the present we have to accept centimeter-level error for diameter estimation from all kinds of remotely sensed structural data.

The diameter estimation suffers from a relatively large dispersion of points around cross-sections' perimeters. The point dispersion is partially caused by the diameter change along the 1 m sections of tapered trees. However, the point density, which was around 44 points per meter of stem length in average, but sometimes as low as 5 points for the section, did not allow to fit circles in thinner layers. Thinner layers in many cases fail in circle fitting due to insufficient point representation of the circle. Due to the taper, the vertical point projection of a 1 m long section forms a point belt of the thickness of around 1–2 cm instead of a circle. Another component of the point dispersion is caused by LiDAR accuracy (1–2 cm) and bark structure (1–2 cm). These components represent an unavoidable error of the data acquisition. The most important source of point dispersion is the co-registration of scans from individual flight lines. Due to the limited accuracy of the utilized IMU, software-based co-registration of scans must be applied. Accurate co-registration is problematic in environments with complex structure, such as forests [28,29]. The co-registration error may reach several centimeters in forest environments, resulting in inconsistent and dispersed circle representation, visible in Figure 8.

In a single UAV flight, 10 to 20 hectares of forest area can be covered with LiDAR data. Considering time consumption for mission planning, flight preparation and transports between flight locations, the area that can be mapped in a day reaches 100 hectares. As a result, ULS is effective for detailed mapping at the level of forest stands or forest areas up to several hundreds of hectares. We showed that for mature, even-aged production forests, virtually every tree in the mapped area can be localized with an error that usually did not exceed the tree radius. The accuracy of diameter estimates may be sufficient for common stand inventories such as volume assessment before standing timber sale or forest management plan development. An important benefit of USL data is the possibility to measure upper stem diameters to reconstruct the taper curve for wood quality and assortment prediction. The biggest limitation of accurate diameter estimation—centimeter-level noise caused by inaccurate co-registration of scan lines—may limit circle detection in point clouds representing thinner trees. Revision of the methods or setting modifications may be needed in younger forest stands. The applicability of this method for tree detection and measurement in more complex stands, such as two-story stands is a subject for further research.

Most methods of individual tree detection from remotely sensed structural data rely on canopy height models [39,40] or point clouds of tree crowns [41,42]. In this study, we took the challenge of verifying whether tree detection and measurement can benefit from unrivaled density of point clouds acquired with ULS. Tree detection was based solely on points representing tree stems in subcanopy space, and diameters were assessed by direct measurement in acquired point clouds. However, stem points typically represent less than 1% of the total point counts in a vegetation point cloud, not considering the ground returns. Most points describe the structure of tree crowns and canopy. The success rate of tree detection would definitely be improved by involving segmentation

techniques based on structural information of canopy combined with stem detection proposed in this work. This combination would result in a complex method utilizing a higher portion of available information and evaluating the point cloud in its whole depth, in a similar way that was proposed by Ayrey et al. [10] for ALS data. We consider this as a direction of our future effort.

5. Conclusions

We evaluated the suitability of ULS data—laser scanning data acquired from an UAV platform—for individual tree detection and stem diameter estimation in a fully automated workflow. The study was performed in mature pure stands of the most abundant and economically important species, Norway spruce and Scots pine, in their typical growing conditions, which represent the typical situation of need for detailed forest stand inventory in practical management of production forests.

For both species, we were able to detect and localize 98–99% of all trees present in the research plots with an average positional error of 13 cm and estimate their diameters at breast height with bias of 0.1 cm (corresponding to 1% mean relative error) and with RMSE of 6 cm (corresponding to relative RMSE of 19%). We evaluated three algorithms for circle fitting in noisy data structures, Hough transform, random sample consensus (RANSAC) and robust least trimmed squares (RLTS). Hough transform is not a suitable method for diameter fitting in ULS data. RANSAC and RLTS can provide reasonable circle fit, whereas RLTS performs slightly better, especially in lower quality point representations of cross-sections; it shows both higher success rate and lower error.

Author Contributions: Conceptualization, K.K. and P.S.; methodology, K.K.; software, K.K.; validation, K.K. and P.S.; formal analysis, K.K.; investigation, K.K. and M.S.; resources, P.S.; data curation, K.K. and M.S.; writing—original draft preparation, K.K.; writing—review and editing, P.S. and M.S.; visualization, K.K.; supervision, P.S.; project administration, P.S.; funding acquisition, P.S. All authors have read and agreed to the published version of the manuscript.

Funding: This research was funded by OP RDE, grant number CZ.02.1.01/0.0/0.0/15_003/0000433 (Building up an excellent scientific team and its spatiotechnical background focused on mitigation of the impact of climatic changes to forests from the level of a gene to the level of a landscape at the FFWS CULS Prague) and Ministry of Agriculture of the Czech Republic grant number QK1920458

Conflicts of Interest: The authors declare no conflict of interest. The funders had no role in the design of the study; in the collection, analyses, or interpretation of data; in the writing of the manuscript, or in the decision to publish the results.

References

1. *FAO Voluntary Guidelines on National Forest Monitoring*; Food and Agriculture Organization of the United Nations: Rome, Italy, 2017; ISBN 978-92-5-109619-2.
2. Lowe, D.G. Method and Apparatus for Identifying Scale Invariant Features in an Image and Use of Same for Locating an Object in an Image. U.S. Patent No. 6,711,293, 23 March 2004.
3. Baltsavias, E.; Gruen, A.; Eisenbeiss, H.; Zhang, L.; Waser, L.T. High-quality image matching and automated generation of 3D tree models. *Int. J. Remote Sens.* **2008**, *29*, 1243–1259. [CrossRef]
4. Vastaranta, M.; Wulder, M.A.; White, J.C.; Pekkarinen, A.; Tuominen, S.; Ginzler, C.; Kankare, V.; Holopainen, M.; Hyyppä, J.; Hyyppä, H. Airborne laser scanning and digital stereo imagery measures of forest structure: Comparative results and implications to forest mapping and inventory update. *Can. J. Remote Sens.* **2013**, *39*, 382–395. [CrossRef]
5. Gobakken, T.; Bollandsås, O.M.; Næsset, E. Comparing biophysical forest characteristics estimated from photogrammetric matching of aerial images and airborne laser scanning data. *Scand. J. For. Res.* **2015**, *30*, 73–86. [CrossRef]
6. Hernández-Clemente, R.; Navarro-Cerrillo, R.M.; Romero Ramírez, F.J.; Hornero, A.; Zarco-Tejada, P.J. A novel methodology to estimate single-tree biophysical parameters from 3D digital imagery compared to aerial laser scanner data. *Remote Sens.* **2014**, *6*, 11627–11648. [CrossRef]
7. Puliti, S.; Gobakken, T.; Ørka, H.O.; Næsset, E. Assessing 3D point clouds from aerial photographs for species-specific forest inventories. *Scand. J. For. Res.* **2017**, *32*, 68–79. [CrossRef]
8. Penner, M.; Woods, M.; Pitt, D.G. A comparison of airborne laser scanning and image point cloud derived tree size class distribution models in Boreal Ontario. *Forests* **2015**, *6*, 4034–4054. [CrossRef]

9. Hyyppä, J.; Inkinen, M. Detecting and estimating attribute for single trees using laser scanner. *Photogramm. J. Finl.* **1999**, *16*, 27–42.
10. Ayrey, E.; Fraver, S.; Kershaw, J.A.; Kenefic, L.S.; Hayes, D.; Weiskittel, A.R.; Roth, B.E. Layer Stacking: A Novel Algorithm for Individual Forest Tree Segmentation from LiDAR Point Clouds. *Can. J. Remote Sens.* **2017**, *43*, 16–27. [CrossRef]
11. Surový, P.; Kuželka, K. Acquisition of forest attributes for decision support at the forest enterprise level using remote-sensing techniques—A review. *Forests* **2019**, *10*, 273. [CrossRef]
12. Sumnall, M.J.; Hill, R.A.; Hinsley, S.A. Comparison of small-footprint discrete return and full waveform airborne lidar data for estimating multiple forest variables. *Remote Sens. Environ.* **2016**, *173*, 214–223. [CrossRef]
13. Bouvier, M.; Durrieu, S.; Fournier, R.A.; Renaud, J.P. Generalizing predictive models of forest inventory attributes using an area-based approach with airborne LiDAR data. *Remote Sens. Environ.* **2015**, *156*, 322–334. [CrossRef]
14. Næsset, E.; Gobakken, T.; Bollandsås, O.M.; Gregoire, T.G.; Nelson, R.; Ståhl, G. Comparison of precision of biomass estimates in regional field sample surveys and airborne LiDAR-assisted surveys in Hedmark County, Norway. *Remote Sens. Environ.* **2013**, *130*, 108–120. [CrossRef]
15. Skowronski, N.S.; Clark, K.L.; Gallagher, M.; Birdsey, R.A.; Hom, J.L. Airborne laser scanner-assisted estimation of aboveground biomass change in a temperate oak-pine forest. *Remote Sens. Environ.* **2014**, *151*, 166–174. [CrossRef]
16. McRoberts, R.E.; Næsset, E.; Gobakken, T.; Bollandsås, O.M. Indirect and direct estimation of forest biomass change using forest inventory and airborne laser scanning data. *Remote Sens. Environ.* **2015**, *164*, 36–42. [CrossRef]
17. Pearse, G.D.; Morgenroth, J.; Watt, M.S.; Dash, J.P. Optimising prediction of forest leaf area index from discrete airborne lidar. *Remote Sens. Environ.* **2017**, *200*, 220–239. [CrossRef]
18. Solberg, S. Mapping gap fraction, LAI and defoliation using various ALS penetration variables. *Int. J. Remote Sens.* **2010**, *31*, 1227–1244. [CrossRef]
19. Tompalski, P.; Coops, N.C.; White, J.C.; Wulder, M.A. Augmenting site index estimation with airborne laser scanning data. *For. Sci.* **2015**, *61*, 861–873. [CrossRef]
20. Peuhkurinen, J.; Tokola, T.; Plevak, K.; Sirparanta, S.; Kedrov, A.; Pyankov, S. Predicting tree diameter distributions from airborne laser scanning, spot 5 satellite, and field sample data in the Perm Region, Russia. *Forests* **2018**, *9*, 639. [CrossRef]
21. Liang, X.; Litkey, P.; Hyyppä, J.; Kaartinen, H.; Kukko, A.; Holopainen, M. Automatic Plot-Wise Tree Location Mapping Using Single-Scan Terrestrial Laser Scanning. *Photogramm. J. Finl.* **2011**, *22*, 37–48.
22. Koreň, M.; Mokroš, M.; Bucha, T. Accuracy of tree diameter estimation from terrestrial laser scanning by circle-fitting methods. *Int. J. Appl. Earth Obs. Geoinf.* **2017**, *63*, 122–128. [CrossRef]
23. Liang, X.; Kankare, V.; Hyyppä, J.; Wang, Y.; Kukko, A.; Haggrén, H.; Yu, X.; Kaartinen, H.; Jaakkola, A.; Guan, F.; et al. Terrestrial laser scanning in forest inventories. *ISPRS J. Photogramm. Remote Sens.* **2016**, *115*, 63–77. [CrossRef]
24. Dassot, M.; Constant, T.; Fournier, M. The use of terrestrial LiDAR technology in forest science: Application fields, benefits and challenges. *Ann. For. Sci.* **2011**, *68*, 959–974. [CrossRef]
25. Calders, K.; Newnham, G.; Burt, A.; Murphy, S.; Raumonen, P.; Herold, M.; Culvenor, D.; Avitabile, V.; Disney, M.; Armston, J.; et al. Nondestructive estimates of above-ground biomass using terrestrial laser scanning. *Methods Ecol. Evol.* **2015**, *6*, 198–208. [CrossRef]
26. Srinivasan, S.; Popescu, S.C.; Eriksson, M.; Sheridan, R.D.; Ku, N.W. Multi-temporal terrestrial laser scanning for modeling tree biomass change. *For. Ecol. Manag.* **2014**, *318*, 304–317. [CrossRef]
27. *RIEGL RIEGL VUX-1UAV Data Sheet*; RIEGL Laser Measurement Systems GmbH: Horn, Austria, 2019.
28. Brede, B.; Lau, A.; Bartholomeus, H.M.; Kooistra, L. Comparing RIEGL RiCOPTER UAV LiDAR derived canopy height and DBH with terrestrial LiDAR. *Sensors (Switzerland)* **2017**, *17*, 2371. [CrossRef] [PubMed]
29. Wieser, M.; Mandlburger, G.; Hollaus, M.; Otepka, J.; Glira, P.; Pfeifer, N. A Case Study of UAS Borne Laser Scanning for Measurement of Tree Stem Diameter. *Remote Sens.* **2017**, *9*, 1154. [CrossRef]
30. Olofsson, K.; Holmgren, J.; Olsson, H. Tree stem and height measurements using terrestrial laser scanning and the RANSAC algorithm. *Remote Sens.* **2014**, *6*, 4323–4344. [CrossRef]
31. Forsman, M.; Holmgren, J.; Olofsson, K. Tree stem diameter estimation from mobile laser scanning using line-wise intensity-based clustering. *Forests* **2016**, *7*, 206. [CrossRef]

32. Kuželka, K.; Surový, P. Mapping forest structure using UAS inside flight capabilities. *Sensors* **2018**, *18*, 2245. [CrossRef]
33. Fritz, A.; Kattenborn, T.; Koch, B. UAV-based photogrammetric point clouds—Tree stem mapping in open stands in comparison to terrestrial laser scanner point clouds. *Int. Arch. Photogramm. Remote Sens. Spat. Inf. Sci.* **2013**, *40*, 141–146. [CrossRef]
34. Ye, H.; Shang, G.; Wang, L.; Zheng, M. A new method based on hough transform for quick line and circle detection. In Proceedings of the 2015 8th International Conference on Biomedical Engineering and Informatics (BMEI), Shenyang, China, 14–16 October 2015; pp. 52–56.
35. Simonse, M.; Aschoff, T.; Spiecker, H.; Thies, M. Automatic determination of forest inventory parameters using terrestrial laserscanning. In Proceedings of the Scandlaser Scientific Workshop on Airborne Laser Scanning of Forests, Umeå, Sweden, 3–4 September 2003; pp. 1–7.
36. Tittmann, P.; Shafii, S.; Hartsough, B.; Hamman, B. Tree detection, delineation, and measurement from LiDAR point clouds using RANSAC. In Proceedings of the SilviLaser 2011, 11th International Conference on LiDAR Applications for Assessing Forest Ecosystems, University of Tasmania, Australia, 16–20 October 2011; pp. 1–23.
37. Nurunnabi, A.; Sadahiro, Y.; Lindenbergh, R. Robust cylinder fitting in three-dimensional point cloud data. *Int. Arch. Photogramm. Remote Sens. Spat. Inf. Sci. ISPRS Arch.* **2017**, *42*, 63–70. [CrossRef]
38. Mokroš, M.; Liang, X.; Surový, P.; Valent, P.; Čerňava, J.; Chudý, F.; Tunák, D.; Saloň, Š.; Merganič, J. Evaluation of close-range photogrammetry image collection methods for estimating tree diameters. *ISPRS Int. J. GeoInf.* **2018**, *7*, 93. [CrossRef]
39. Barnes, C.; Balzter, H.; Barrett, K.; Eddy, J.; Milner, S.; Suárez, J.C. Individual tree crown delineation from airborne laser scanning for diseased larch forest stands. *Remote Sens.* **2017**, *9*, 231. [CrossRef]
40. Liu, T.; Im, J.; Quackenbush, L.J. A novel transferable individual tree crown delineation model based on Fishing Net Dragging and boundary classification. *ISPRS J. Photogramm. Remote Sens.* **2015**, *110*, 34–47. [CrossRef]
41. Hu, X.; Chen, W.; Xu, W. Adaptive mean shift-based identification of individual trees using airborne LiDAR data. *Remote Sens.* **2017**, *9*, 1–23. [CrossRef]
42. Hamraz, H.; Contreras, M.A.; Zhang, J. A robust approach for tree segmentation in deciduous forests using small-footprint airborne LiDAR data. *Comput. Geosci.* **2017**, *102*, 139–147. [CrossRef]

Příloha č. 4 – PANAGIOTIDIS, Dimitrios, Azadeh ABDOLLAHNEJAD a Martin SLAVÍK, 2020. Accuracy assessment of stem attributes for estimation of total stem volume using high-cost survey-grade terrestrial laser scanner : An application of precision forestry.

sensors

MDPI

Type of the Paper (Article)

Assessment of Stem Volume on Plots using Terrestrial Laser Scanner: A Precision Forestry Application

Dimitrios Panagiotidis [1]*, Azadeh Abdollahnejad [1] and Martin Slavík [1]

[1] Department of Forest Management, Faculty of Forestry and Wood Sciences, Czech University of Life Sciences (CZU Prague), Kamýcká 129, Prague 165 21, Czech Republic; abdolahnejad@fld.czu.cz https://orcid.org/0000-0002-4065-8056, mslavik@fld.czu.cz

* Correspondence: panagiotidis@fld.czu.cz; Tel.: +420-775-099-596; https://orcid.org/0000-0002-5937-3341

Received: date; Accepted: date; Published: date

Abstract: Timber volume is an important asset not only as an ecological component but also as a key source of present and future revenue which requires precise estimates. We utilized the Trimble TX8 survey-grade terrestrial laser scanner (TLS) to create a detailed 3D point cloud for extracting total tree height and diameter at breast height (DBH). Two different height estimation approaches were used to compare the performance of the two methods to accurately estimate total tree height: the first method was based on a modified version of the local maxima algorithm for treetop detection "H_{TTD}", while for the second method we used the centers of stem cross-sections in stump height (30 cm) "H_{TSP}". DBH was estimated by a computationally robust algebraic circle fitting algorithm through agglomerative hierarchical cluster analysis (HCA). This study aimed to assess the accuracy of these descriptors by comparing them with the reference measurements for evaluating total stem volume at tree level. The results revealed that the difference between the estimated total stem volume from H_{TTD} and measured was 2.732 m^3 for European oak and 2.971 m^3 for Norway spruce, whereas between estimated volume from H_{TSP} and measured the difference was 1.228 m^3 for European oak and 2.006 m^3 for Norway spruce respectively. As it appears from the coefficient of determination there was a strong relationship between the measured and estimated total stem volumes from both height methods with an $R^2 = 0.89$ for H_{TTD} and $R^2 = 0.87$ for H_{TSP} for European oak and $R^2 = 0.98$ for both H_{TTD} and H_{TSP} for Norway spruce. Hence, this study has demonstrated the feasibility of finer resolution remote sensing data for semi-automatic stem volumetric modeling of small-scale studies with high accuracy, as a potential advancement in precision forestry.

Keywords: forest biometrics; managed forest; 3D point cloud; stem level assessment; circle fitting; agglomerative hierarchical cluster analysis; modeling stem volume

1. Introduction

Forests are dynamic systems that are constantly in a state of change driven by socio-environmental affection. Tree height and diameter are the most common descriptors in estimating basal area (BA), biomass, stem volume [1]. On the other hand, stem form is another important component for volume estimation [2]. Tree shape varies due to differences in species composition [3] genetic factors [4], climatic factors [5], silvicultural treatments, and forest management practices [6]. Information of stem volume is indispensable for forest managers as the basic input for essential forest

inventory, helps in decision-making, and supports sustainable planning of timber resources [7]. However, significant limitations on stem volume estimation are mainly located in the lack of an accurate, objective, and efficient methodological approach. Timber management is directly related to revenue, intimately tied to the economic evaluation of activities, and requires accurate data on forest resources [8]. Traditionally, field-based methods of data collection have been employed for supporting the construction and update of forest inventories but are time-intensive and laborious.

Stem circumference is usually defined by a circle. Clusters of points from 3D point clouds can be isolated, extracted, and estimated using different types of circle-fitting algorithms. Several methods existing for the estimation of stem diameter and they can be mainly divided into two major categories: algebraic and geometric. In the category of geometric methods, the main representatives are Levenberg-Marquardt and Gauss-Newton. Other geometric approaches are using cylindrical shapes [9] skeletonization [10], polygons [11], and hough transformation [12] to approximate the diameter of stem sections. As for the algebraic methods we can mention the methods of Kasa [13], Pratt [14], and Taubin [15]. In general, the algebraic methods are usually faster and non-iterative compared to the geometric. Pueschel et al. [16] studied several circle fitting methods for showing the significance of outlier removal before the application of any circle fitting approach. In another study, Koreň et al. [17] used several circle fitting methods from TLS, to compare the accuracies of diameter at breast height (DBH). Their results showed that among others optimal circle method (based on the least square algorithm) proved to be the most accurate circle fitting method.

The accuracy of DBH from TLS-based point clouds depending on several factors, among them is the scanning mode, the number of scans, scanner position, scanner settings (e.g. point density), and methods of data processing [18,19]. Also, to ensure high-quality TLS data, suitable environmental and forest conditions are necessary to ensure that stem level characteristics are distinguishable by the TLS. In the case of multiple scans, point clouds are co-registered and combined with the help of matching.

Hierarchical cluster analysis (HCA) hierarchically clusters any dataset using an unsupervised method for nested clustering, as the number of clusters is not established apriori. Unlike factor analysis, HCA makes no distinction between independent and dependent variables. Moreover, HCA is the major statistical method for finding homogenous groups based on the measured characteristics with tremendous capabilities [20].

The determination of ground surface is a semantic parameter that can significantly affect the extraction and estimation accuracy of tree height and stem diameter. For example, Maas et al. [21] used a digital terrain model (DTM), to determine the ground surface points from other points by using the density allocation along the z-axis. In another study, Corte et al. [22] classified ground and off-ground points using the filtering technique available in LAStools for generating a DTM with a resolution of 0.5 for extracting total tree height. Also, the utilization of canopy height models (CHMs) to identify treetops for the extraction of total tree height has been thoroughly studied [23,24,25,26,27].

Many studies have shown the advantages of TLS in practice, using different scaling approaches for estimating several stem parameters, such as height [28,29,30], crown width [28], stem diameter [28,29], and tree species recognition [31]. Other studies have been carried out for deriving plot basal area [32], crown volume [33,34], leaf area index [35], and biomass [36]. However, TLS studies for estimation of stem diameter are of great importance in forestry for assessing volumetric dimensions. Purschel et al. [16] utilized a TLS to estimate the number of structural vegetation parameters, by assessing the effects of scan mode and circle fitting on the extraction of stem diameter and volume. Their results showed that stem volumes exhibit a large variability with deviations from the reference volumes ranging from −34% to 44%. In another study, Astrup et al. [37] explored how volume

estimates of individual trees from a harvester, standard volume functions, and TLS were performed compared with standard inventory estimates. They found that individual-tree volumes from TLS can be estimated with high precision and accuracy; Spearman correlation coefficient was found between 0.77-0.97. In a recent study, Mayamanikandan et al. [38] evaluated tree height and DBH to evaluate tree volume. Their results showed that TLS based variables, such as DBH (R^2 = 0.995), height (R^2 = 0.998), and volume (R^2 = 0.958) are in good accordance with the field measurements.

In this context, the main objectives of this study were (i) to test the performance of TX8 survey-grade TLS in the construction of detailed 3D point clouds for extracting total tree height and DBH, using two different height estimation methods in combination with a computationally robust algebraic circle fitting algorithm through HCA, and (ii) to assess the accuracy of these attributes by comparing them with the reference measurements for evaluating total stem volume, potentially allowing advancements in precision forestry.

2. Materials and Methods

2.1. Characterization of the Study Area

The forest operation site is located in the School Forest Enterprise of the Czech University of Life Sciences (ČZU Prague) in Kostelec nad Černými lesy about 35 km south-east of Prague, nearby the village Oplany (Figure 1). The site in question consists of two experimental plots with a size of 25×25 m each. Plot 1 extends geographically from 49°54'45.15"N; 14°52'11.44"E to 49°54'44.98"N; 14°52'12.75"E and plot 2 from 49°54'50.19"N; 14°52'23.61"E to 49°54'50.12"N; 14°52'24.98"E. In terms of species composition, plot 1 is dominated by European oak (*Quercus robur*), and plot 2 by Norway spruce (*Picea abies* (L.) H. Krast.). The extended area is mainly characterized by even-aged managed forests of cca 50-60 years. The terrain profile in the area is slightly inclined, with an altitude of cca 420 m a.s.l., mean annual temperature 7.5 °C, and mean annual precipitation 600 mm.

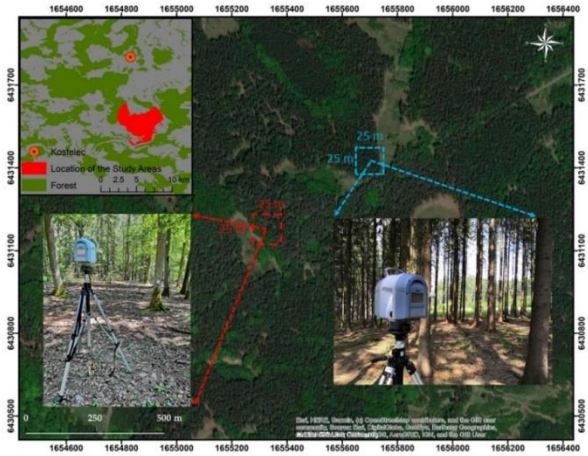

Figure 1. The geographic location of the study plots (plot 1 with red color and plot 2 with blue color). Used coordinate system WGS 1984 Web Mercator (Auxiliary Sphere).

2.2. *Reference Measurements*

Trimble M3 total station (Trimble Inc. Sunnyvale, California USA, 1978) was used to measure the tree positions and helped to verify the exact locations of the trees from TLS (detected trees). At 100 m the error range is ± 23 mm. In total 27 trees were measured in plot 1 and 48 trees in plot 2.

Total tree heights were determined with a Haglöf Laser Geo (distance accuracy 40 mm) while, DBH was determined using a Haglöf DP II (Haglöf Sweden AB, Långsele, Sweden, 2002) computer caliper with millimeter accuracy. Two diameters from perpendicular directions were measured and the DBH was then determined as the average value of these two measurements.

2.3. TLS Data Collection and Pre-processing

In this study, the laser data were obtained using the Trimble TX8 scanning system (Trimble Inc. Sunnyvale, California USA, 1978). The necessary technical specifications of the TLS device are shown in Table 1. The integrated HDR camera offered two different modes for image acquisition a) HDR and b) standard. In our case, the standard mode was used for the colorization of the point clouds. To ensure the optical degree of overlapping between the scanning positions, we used the multi-scan approach with a total of seven scans. The first scan was placed at the center of each plot and the rest in their periphery. Additionally to the scanning parameters, fixed exposure was disabled, while for the scan density level the third level was used. Consequently, the duration for each scan took ~12 min. To calibrate the laser scanner the field instant method was used. Furthermore, to ensure better performance for the scan registration process, the laser scanner reference sphere set was used. In parallel with the scans, marked wooden sticks in each station were placed on the ground. That permitted us to measure the scanning positions using the Trimble M3 total station. The error of the particular total station was 2 mm in the horizontal distance.

Laser scanning in plot 1 was conducted on June 29, 2019, between 11:00-15:00, and in plot 2 on 26 of August 2019 between 12:00-16:00 local time, while the weather conditions were favorable for scanning in both cases (no wind). The registration of the point clouds was conducted in RealWorks software (Trimble Inc. Sunnyvale, California USA, 1978). For optimal accuracy especially in the case of tree height estimation, the point clouds were sampled at 0.01 m (point density), to ensure enough points mainly at the upper portion of the stems closer to the treetops.

Table 1. Main performance indicators of Trimble TX8 terrestrial laser scanning device.

Range Measurement	
Maximum Distance Range	120 m on most surfaces
Range Systematic Error	< 2 mm
Laser Wavelength	1.5 μm, invisible
Laser Beam Diameter	6–10–34 mm @ 10–30–100 m
Scanning	
Scanning Field-of-View	360° x 317°
Scanning Speed	1 million pts/sec
Angular Accuracy	80 μrad

2.4. Normalization Height

After the pre-processing phase, the point clouds were extracted and imported in CloudCompare V.2.10. (Zephyrus, Paris France, 2011) software, where the cloth simulation filter (CSF) algorithm [39] was applied, to separate and extract the ground from non-ground points. In the general parameter

setting tab of the surface base filter, the relief terrain option was chosen due to the slightly inclined plane of the sample plots.

For calibration, cloth resolution was set to 1.1, as for maximum iterations we used the default option. Finally, for classifying the point-clouds into the ground and off-ground layers, the classification threshold was set to 0.1 (the unit was the same as the unit of point clouds). This step was necessary for the classification of all points, by computing the distances between ground (reference points) and non-ground points (compared points) and eliminating the differences in tree height caused by differences in elevation. Ground and off-ground points were then extracted as .las files and imported in ArcGIS desktop V.10.6.1 (ESRI Inc.; Redlands, CA, U.S.A.) to create the digital surface model (DSM) and DTM (Figure 2) with an accuracy of 0.01×0.01 m cell size. The process of normalization height was continued using LAStools (rapidlasso GmbH, Gilching, Germany) toolbox in ArcGIS.

2.5. Tree Height Estimation from H_{TTD} and H_{TSP}

By overlaying the normalized canopy height models (nCHMs) and the extracted tree stump positions from the TLS using the centers of stem cross-sections in stump height (30 cm) [40], we were able to (i) validate tree positions and (ii) extract the total tree heights using the (Feature to Point) tool in ArcGIS. For extracting the total tree heights we considered a hypothetical vertical column along the z-axis passing from the centers of each stem cross-section at stump height up to the treetop, taking into account only the closest to that central point's values. For simplicity, we referred to this height as H_{TSP}.

For the second height estimation method, the local maxima algorithm [41] was applied on the nCHMs as described in [25], for treetop detection and thus the extraction of total tree height, we referred to this height as H_{TTD}. More specifically, the setting parameters for local maxima were determined using the morphological filtering tool of focal statistics. During the processing we have tested several sizes of circular filters, to find out what would be the ideal kernel size for optimal treetop detection in each plot. What we found was that the ideal kernel size was undeniably 1 m for plot 1. That value was selected among others because it resulted in at least one treetop per tree, ensuring (i) the minimum amount of missing trees and (ii) the lowest amount of multi-treetop. On the contrary, a kernel size of 2 m was applied in plot 2. In this case, the decision for optimal kernel size was more straightforward, since the application of local maxima on coniferous trees can successfully detect a single treetop per tree [25]. Thus, in plot 2 only max values were considered in the estimation from H_{TTD}. However, due to the multi-treetop nature of the broadleaves (plot 1), we considered not only the max $H_{TTD}MAX$, but the mean values $H_{TTD}MEAN$ of identified treetops for each tree. We assumed that the mean values of detected treetops will smooth the estimated heights in plot 1 and decrease the modeling error. To match the pixel values from nCHMs and the focal statistic result, we used Equation 1.

$$\mathrm{Con}(\text{'nCHM'} == \text{'focal statistics result'}, 1) \quad (1)$$

This conditional function (Con) performs an if/else evaluation on each input cell of the input raster and it returns the binary value 0 for non-data or 1 for data value. Therefore, the return value was the value when the nCHM value equaled the output of focal statistics. In both cases, (H_{TTD} and

H_{TSP}) total tree height was estimated based on the nCHMs. The entire process for both extraction height methods was conducted in ArcGIS.

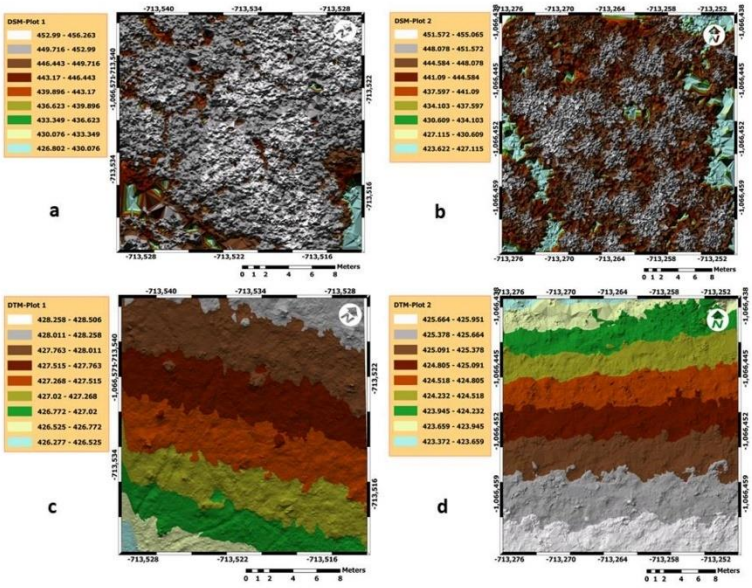

Figure 2. (a, b) Show the extracted digital terrain models DTMs and (c, d) digital surface models DSMs in both plots respectively using LAStools in ArcGIS.

2.6. Estimation of Diameter at Breast Height

The normalized points were used as input for the estimation of DBH. A buffer zone was applied to acquire the stem cross-sections between 1.25-1.35 m above ground level, using .Net framework in Visual Studio Enterprise 2015 V.14.0.24720.00 (Microsoft©, Redmond, Washington United States, 1975) (Figure 3). After the selection, points were extracted as .txt files to continue with the processing.

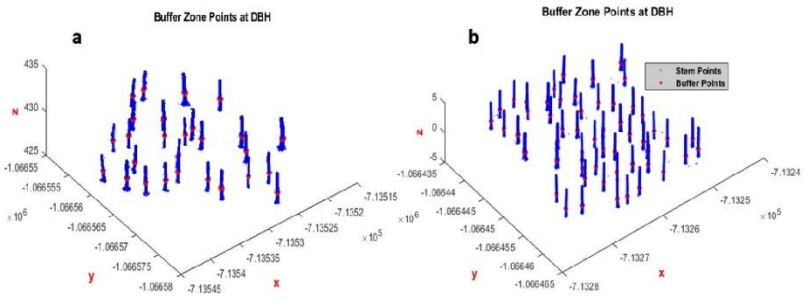

Figure 3. Shows the selection of stem cross-sections at diameter at breast height (DBH) in plot 1 (a) and plot 2 (b).

The next step comprises the estimation of stem radius in the produced stem cross-sections using the HCA method [42]. This method enables the creation of several clusters (one for each cross-section) based on the total number of trees presented in each plot. To do so, we initially had to calculate the euclidean distances between the x, y points Equation (2) using the pdist function.

$$d(x,y) = \sqrt{(x_1 - y_1)^2 + (x_2 - y_2)^2} \quad (2)$$

where (x, y) are two points with coordinates $x = (x_1, x_2)$ and $y = (y_1, y_2)$ in two-dimensional space.

Once the proximity between points has been computed, we were able to determine how the stem cross-section points should be grouped into agglomerative clusters using the linkage function. Ward's minimum variance method in linkage function was used to obtain the calculated distances and link pairs of x, y points into binary clusters Equation (3).

$$d(r,s) = \sqrt{\frac{2n_r n_s}{(n_r+n_s)}} \times \|\bar{x}_r - \bar{x}_s\|_2 \quad (3)$$

where $\|\|_2$ is the Euclidean distance, $\bar{x}_r$ and $\bar{x}_s$ are the centroids of clusters (r) and (s) and n_r and n_r refers to the number of elements in clusters (r) and (s).

The cluster function was then used to specify arbitrary clusters to partition data into the desired number of clusters, based on the total number of trees presented in each plot. In the following step, we used the algorithm proposed by Bucher [43]. This algorithm is a modified version of the [13] Circle Fit method (Equation 4), based on the least-squares fitting of 2D data to a circle. The circfit function was used to fit a circle to a set of measured points.

$$[xc, yc, R, a\sim] = \text{circfit}(x,y) \quad (4)$$

where xc, yc are the returned centers for each stem cross-section (cluster), R is the returned estimated radius and the fourth parameter a is an optional coefficient, describing the general circle form Equation (5).

$$x^2 + y^2 + a1 \times x + a2 \times y + a3 = 0 \quad (5)$$

As a final step, the constructed circfit function was iterated to ensure that simultaneously all stem cross-section points will be fitted, their respective radii will be estimated, and all the extracted information (number of trees in each plot) will be successfully stored in cell arrays. The entire processing phase was conducted in Matlab R2017b professional edition (MathWorks©, Inc., Massachusetts, United States) using the Statistics and Machine Learning Toolbox™.

2.7. Total Stem Volume Estimation

Equation (6) was used for calculating the total stem volume using DBH, total tree height, and form factor (F) as predictors, for both measured and estimated values. As an estimated height, the height from both methods (H_{TTD} and H_{TSP}) was considered for the estimation of total stem volume. For

stem diameter, the radius of each stem converted to diameter, and diameter was then converted to area using Equation (7).

$$V_{oak/spruce} = DBH \times H \times F \quad (6)$$

where $V_{oak/spruce}$ refers to the total stem volume, DBH is the diameter at breast height, H is the total tree height and F is the stem form factor.

$$g_{stem} = \pi \times \frac{(DBH)^2}{4} \quad (7)$$

where g_{stem} refers to the basal area, π is a mathematical constant, and DBH is the diameter at breast height. Based on the allometric equations by Petráš & Pajtík [44], F = 0.38 for European oak and F = 0.42 for Norway spruce.

2.8. Accuracy Assessment

Once tree heights and diameters were extracted, the accuracy of the proposed method was then evaluated. The estimated values were compared with the reference measurements by testing if there were any statistically significant differences between the estimated heights from H_{TTD} and H_{TSP}. Also, the same process was followed for the measured versus estimated diameters. In particular, a paired t-test was performed using box and whisker plots at a 0.05 significance level.

Finally, an analysis of variance (ANOVA) was used to test the degree of variability within the regression models (measured versus estimated total stem volumes). For evaluating the total stem volume model`s accuracy the following evaluation metrics were used:

$$R^2 = 1 - \frac{\sum(y_i - \hat{y})^2}{\sum(y_i - \bar{y})^2} \quad (8)$$

where $\hat{y}$ is the predicted value of y and $\bar{y}$ is the average value of y.

$$R^2_{adj} = 1 - \left[\frac{(1-R^2)(n-1)}{n-k-1}\right] \quad (9)$$

where R^2 refers to the sample R-square, k is the number of predictors, n is the total sample size.

$$SE = \frac{\sigma}{\sqrt{n}} \quad (10)$$

where σ is the standard deviation and $\sqrt{n}$ is the number of samples.

$$RMSE = \sqrt{\frac{\sum_{i=1}^{n}(Vol.Estimated_i - Vol.Measured_i)^2}{n}} \quad (11)$$

where $Vol.Estimated_i$ is the predicted volume, $Vol.Measured_i$ is the observed volume and n is the number of observations.

$$RMSE\% = \frac{RMSE}{\bar{x}} \times 100 \quad (12)$$

where $RMSE$ is the root mean square error and $\bar{x}$ is the average value.

$$Bias = \frac{1}{n} \sum x_i - \bar{x}_j \quad (13)$$

$$Bias\% = \frac{Bias}{x_j} \times 10 \quad (14)$$

where n is the number of samples, x_i the observed value and $\bar{x}_j$ is the average of estimated values.

$$MAE = \frac{\sum_{i=1}^{n}|p_i - x_i|}{n} \quad (15)$$

where p_i is the predicted value, x_i the observed value and n is the number of observations.

The entire statistical analysis was conducted in MatlabR2017b professional edition (MathWorks©, Inc., Massachusetts, United States). An overview of the workflow can be seen in Figure 4.

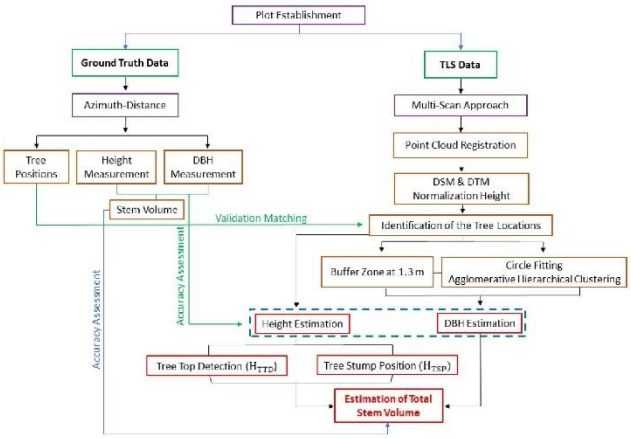

Figure 4. Shows the technical route followed for estimating total stem volume.

3. Results and Discussion

3.1. Modeling Tree Height

Total tree height from TLS was validated by comparing it to the reference measurements. After height was extracted from the two estimated methods, we tested if there were any significant differences between them. Moreover, in the case of H_{TTD} for plot 1 we also aimed to examine whether max or mean values will result in higher accuracy compared to the reference measurements. A paired t-test was used to determine whether the average difference between the two sets of observations and for both heights H_{TTD} and H_{TSP} was zero. In plot 1 and according to Figure 5, there were statistically significant differences only between the group of measured and estimated height from H_{TTD}MAX and no significant differences between the two other groups (measured versus estimated H_{TSP} and H_{TTD}MEAN) for tested p-value < 0.05. The average values for measured height were 24.86 m, for estimated H_{TSP} 24.14 m, for H_{TTD}MEAN 25.85 m and for H_{TTD}MAX 26.08 m. Also as shown in Figure 5 in plot 2, it was found that in both groups measured versus estimated (H_{TSP} and H_{TTD}MAX) there were significant differences. The average values were 24.19 m for the measured heights and 25.96 m for H_{TTD}MAX and 25.11 m for H_{TSP} respectively.

The findings from the cross-comparisons of total tree heights from both estimated methods (H_{TTD} and H_{TSP}) in both plots overestimated the height comparing to the reference measurements, except in the case of plot 1 from H_{TSP}, where the results revealed a slight underestimation of height (Figure 5). As shown in Figure 5 in plot 1, the height from H_{TTD}MEAN outperformed H_{TTD}MAX resulting in a height difference of 0.99 m compared to 1.22 m, whereas H_{TSP} showed better performance than H_{TTD}MEAN and H_{TTD}MAX with a height difference of 0.72 m in terms of average height. In plot 2,

height from H_{TSP} presented closer values to the measured, compared to the extracted height from $H_{TTD}MAX$ with a height difference of 0.92 m compared to 1.77 m.

Underestimation of tree height by H_{TSP} in plot 1 is due to the stem morphological characteristics of broadleaves. Overestimation of tree height from both methods in plot 2 is likely caused because coniferous trees are associated with cylindrical shapes, hence the locations of treetops were perfectly aligned with the centers of all stem cross-sections in stump height (Figure 6). However, H_{TSP} in plot 2 underestimated tree height compared to H_{TTD} as expected. Except for H_{TSP} in plot 1, our result is in disagreement with the result from [45].

Also, the medium crown closure in both plots allowed to catch higher stem portions in the majority of trees. In general, the vertical angular step-width of the TX8 laser scanning is relatively smaller compared to the inexpensive scanners, therefore the point density is higher in the vertical direction. Overall, except for H_{TSP} in plot 1, our findings are consistent with the results from [46,47].

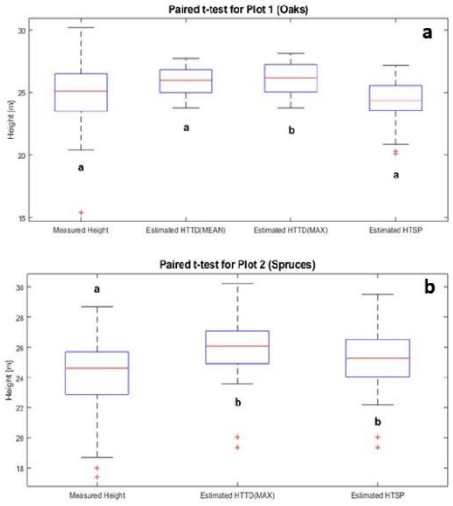

Figure 5. Shows the statistical analysis conducted between measured and estimated heights for plot 1 (a) and plot 2 (b). The letters (a, b) above and below box plots indicate if there were significant differences between the groups at a 0.05 significance level.

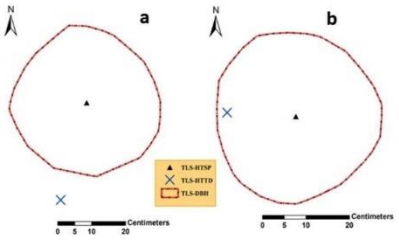

Figure 6. Illustrates the degree of stem deflection along height in two different spruce stems using nadir view in ArcGIS. The deflection is more visible in the case of H_{TTD} for the left stem cross-section compared to the right one, while for H_{TSP} that difference is negligible in both cases.

Figure 7, shows the produced nCHMs with the locations of tree positions from TLS overlayed with the positions from the local maxima. In the same figure, we can see the effect of multiple treetop detection by local maxima (H_{TTD}) in the case of plot 1 compared to plot 2 where a single treetop corresponded to one tree.

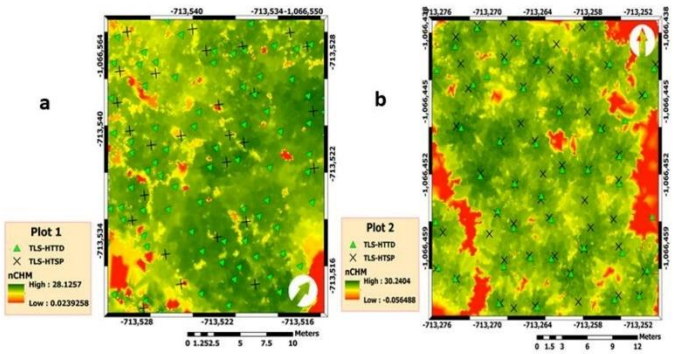

Figure 7. Shows the normalized canopy height models (nCHMs), and the locations of estimated tree heights from both methods (H_{TTD} and H_{TSP}) in plot 1 (a) and plot 2 (b). All trees were detected from TLS H_{TSP} in both plots.

3.2. Modeling Diameter at Breast Height

Using the circfit algorithm through the application of HCA, well-separated, and compact clusters were created for all the trees in both plots (Figure 8). The extracted diameters at ~1.3 m above ground were compared to the measured and a t-test was performed to investigate if there were any significant differences between the groups.

Also, single slices in Figure 8 show the well-rounded scanned stems, regardless of the tree size. The statistical evaluation displayed in Figure 9, clearly shows the enhanced detection capability and high accuracy of the method. Perhaps the reason for the high agreement between measured and estimated diameters was because point clouds were sampled to 1 cm, the application of multi-scan approach covered all the trees from several angles together with the small angular step-width in the horizontal direction of the device.

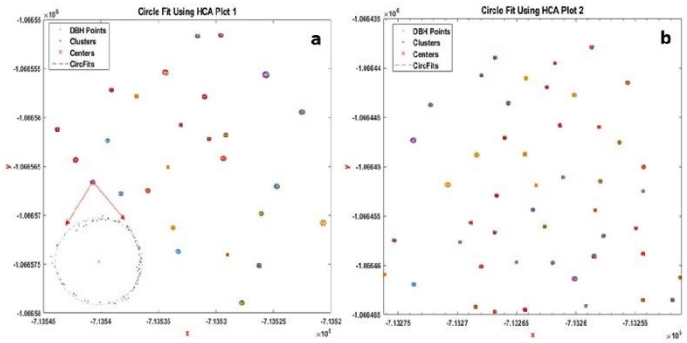

Figure 8. Shows the extracted stem cross-sections in plot 1 (a) and plot 2 (b) and the application of the circle fitting algorithm for the diameter estimation for all stem cross-sections between 1.25-1.35 m height above ground using hierarchical clustering analysis (HCA). Every cluster is depicted with a different color.

Alike with the height analysis, the statistical comparison between the two groups showed that there were significant differences (p-value < 0.05). Results revealed that the estimated DBH yielded estimates which are consistent with the reference measurements (Figure 9). TLS-based estimates of DBH slightly overestimated measured values [48] in both plots (Figure 9). In plot 1 the average value for the measured diameters was 329.46 mm whereas for estimated was 339.72 mm. Similarly, in plot 2 the average value for the measured diameters was 257.17 mm whereas for estimated was 262.64 mm respectively.

Furthermore, results showed that the difference between estimated and measured diameters in plot 1 was 10.26 mm, whereas in plot 2 the difference was 5.47 mm (Figure 9). The difference between the estimated diameters in both plots was 4.79 mm. Our findings are consistent with the results of [16,46,49,50,51].

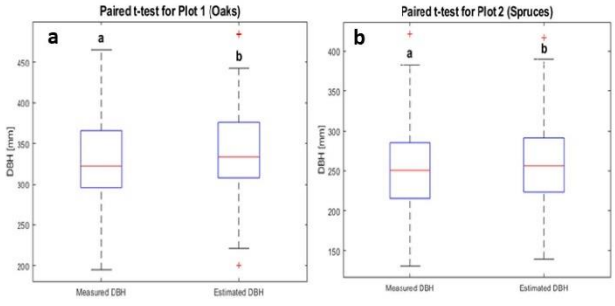

Figure 9. Statistical comparison between measured and estimated diameters at breast height (DBH) in plot 1 (a) and plot 2 (b). The letters (a, b) above and below box plots indicate if there were significant differences between the groups at a 0.05 significance level.

3.2. Modeling Total Stem Volume

As shown in Table 2 and Figure 10, an identical pattern can be distinguished for both plots between the estimated and measured total stem volumes ($Vol._{H_{TTD}} > Vol._{H_{TSP}} > Vol._{Measured}$). More specifically, in plot 1 the estimated volume from H_{TSP} outperformed the volume resulted from H_{TTD}, with a difference of 1.228 m^3. Estimated volume from H_{TTD} provided pooper yet comparable performance to the H_{TSP} with a difference of 2.732 m^3. Finally, the difference between the estimated volumes from H_{TTD} and H_{TSP} was 1.504 m^3.

Alike plot 1, plot 2 showed higher differences between measured and the two estimated volumes derived from H_{TTD} and H_{TSP} Although the differences between measured and estimated volumes were higher for plot 2, the difference between estimated volumes from H_{TTD} and H_{TSP} was 0.965 m^3. The difference between estimated (from H_{TTD}) and measured volume was 2.971 m^3 whereas, between estimated (from H_{TSP}) and measured volume the difference was lesser (2.006 m^3).

Overall, our results revealed an overestimation of volume compared to the measured values for both height estimation methods in both plots. Our findings are in line with the results of previous studies [52,53,54,55].

Table 2. Shows the extracted total stem volumes based on two different height methods as well as the measured volume.

Plot ID	Parameter	Estimated Volume (H_{TTD}) *	Estimated Volume (H_{TSP})	Measured Volume
1	Total Stem Volume in [m^3]	24.903	23.399	22.171
2		30.261	29.296	27.290

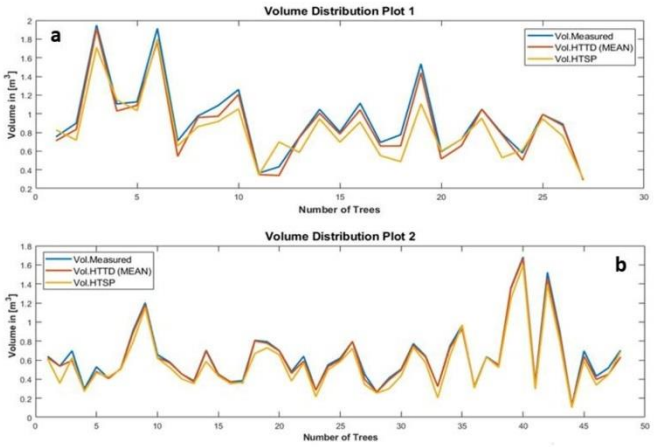

Figure 10. Graphical relationship between total stem volume from three different methods in plot 1 (a) and plot 2 (b).

Furthermore, the results from ANOVA revealed that there were statistically significant differences between estimated and measured total stem volumes in both plots for a tested p-value < 0.05. Hence, we conclude that the null hypothesis (H_0) can be rejected in favor of the alternative hypothesis (H_1) (Tables 3–4). Also, the coefficient of determination showed an identical relation between measured volume and estimated volume from H_{TTD} and H_{TSP} with $R^2 = 0.98$ in plot 2, whereas in plot 1 the relation was found poorer with $R^2 = 0.89$ for H_{TTD} and $R^2 = 0.87$ for H_{TSP}. As a measure of the standard deviation of the average within the datasets, the standard error was found lesser in plot 2 (0.043) in both height estimation methods. For plot 1 the standard error was higher yet insignificant

with 0.134 for H_{TTD} and 0.143 for H_{TSP}. Nevertheless, these numbers indicating the small spread of values in both cases and therefore higher dataset accuracy (Tables 3–4).

Table 3. Analysis of variance (ANOVA) and regression statistics, showing the relation between measured and estimated volume using as estimated height the height which derived from local maxima (H_{TTD}).

Plot ID		R Square	Adjusted R Square	Standard Error	df	SS*	MS*	F*	Prob>F*
1	Regression	0.89	0.89	0.134	1	3.67	3.67	203.226	0.00
	Residual	-	-	-	25	0.45	0.02	-	-
	Total	-	-	-	26	4.12	-	-	-
2	Regression	0.98	0.98	0.043	1	4.48	4.48	2417.746	0.00
	Residual	-	-	-	46	0.09	0.00	-	-
	Total	-	-	-	47	4.57	-	-	-

*SS: sum of squares; MS: the mean squares for each source; F: F-value Prob>F: the returned *p*-value.

Table 4. Analysis of variance (ANOVA) and regression statistics, showing the relation of measured and estimated volume, using as estimated height the height which derived from tree stump positions H_{TSP}.

Plot ID		R Square	Adjusted R Square	Standard Error	df	SS*	MS*	F*	Prob>F*
1	Regression	0.87	0.87	0.143	1	3.46	3.46	169.992	0.00
	Residual	-	-	-	25	0.51	0.02	-	-
	Total	-	-	-	26	3.97	-	-	-
2	Regression	0.98	0.98	0.046	1	4.32	4.32	2027.982	0.00
	Residual	-	-	-	46	0.10	0.00	-	-
	Total	-	-	-	47	4.42	-	-	-

*SS: sum of squares; MS: the mean squares for each source; F: F-value Prob>F: the returned *p*-value.

The validation metrics of total stem volume estimation for both plots are demonstrated in Table 5. Specifically, in plot 1 the volume estimation of H_{TSP} yielded better performance comparing to the H_{TTD} with RMSE = 0.14; RMSE% = 17.51; Bias = -0.338; Bias% = -38.63 and MAE = 0.119. The other method presented lesser, yet comparable performance with: RMSE = 0.17; RMSE% = 20.01; Bias = -0.307; Bias% = -32.98 and MAE = 0.132.

Similarly, in plot 2 the volume estimation of H_{TSP} yielded superior performance comparing to the H_{TTD} with RMSE = 0.06; RMSE% = 10.84; Bias = 0.042; Bias% = 6.85 and MAE = 0.048. The other method presented lesser, yet comparable performance with: RMSE = 0.08; RMSE% = 13.26; Bias = 0.062; Bias% = 9.82 and MAE = 0.063 (Table 5).

Table 5. Evaluation metrics for total stem volume accuracy.

Plot ID	Volume in [m³]	RMSE*	RMSE%*	Bias	Bias%	MAE*
1	H_{TTD}	0.17	20.01	-0.307	-32.98	0.132
	H_T	0.14	17.51	-0.338	-38.63	0.119
2	H_{TTD}	0.08	13.26	0.062	9.82	0.063

H_{TSP}	0.06	10.84	0.042	6.85	0.048

*RMSE: root mean square error; *RMSE%: root mean square error percentage; *MAE: mean absolute error.

4. Conclusions

The main merit of this study was to investigate the technical capabilities of Trimble TX8 laser scanning system to accurately estimate the total stem volume of single trees. Here, we demonstrated the use of two different height estimation methods (H_{TTD} and H_{TSP}) applied on detailed nCHMs for extracting total tree height from multi and single treetops using different descriptive statistics.

Since single treetop corresponded to one tree for plot 2, we assumed that for plot 1 mean tree height would be more meaningful due to the multi-treetop nature of the broadleaf trees. The comparison between estimated and measured heights revealed that the mean treetop performed better and as we assumed resulted in higher accuracy. Underestimation of tree height by H_{TSP} in plot 1 caused due to the stem morphological characteristics of broadleaves. On the other hand, overestimation of tree height in plot 2 is likely caused because coniferous trees are associated with cylindrical shapes, hence the locations of treetops were perfectly aligned with the centers of all stem cross-sections in stump height. Also, the presented method in combination with the TX8 TLS proved to be reliable for tree height estimation up to 30 m. To this contributed the small vertical angular step-width of the particular laser scanner, where the point density was higher in the vertical direction.

According to the results from circfit and HCA for the extraction of stem diameter at DBH, well-separated clusters (Figure 8) were created, revealing the robustness of the proposed method. Furthermore, the used algorithm for extracting tree DBH minimized the sum of squared radial deviations producing smaller errors and lower bias. The statistical analysis between extracted and reference values verifies the accuracy of the model in extracting tree DBH regardless of the tree size. The differences between measured and estimated diameters were 10.26 mm for plot 1and 5.47 mm for plot 2.

As determined by the coefficient of determination, a high agreement has found between measured and estimated total stem volumes from both height methods (H_{TTD} and H_{TSP}) in both plots. Even though better accuracy was found between measured and estimated total stem volume from H_{TSP} based on RMSE% (Table 5), the differences in volume from the two height estimation methods in both plots were rather low. Predominantly, for plot 2 the accuracy reached almost 90%. Conclusively, the proposed method is feasible for semi-automatic stem volumetric modeling of small-medium scale studies and can be used not only for practical (e.g. expeditious construction of single-entry volumetric tables) but for scientific purposes too.

Finally, it is worthwhile mentioning that a direct comparison between different studies is a challenging task since there is high uncertainty in the way field-measurements, as well as the forest conditions under each study, are carried out. Under these circumstances, how accurate and reliable are field measurements to be used as reference data?

Author Contributions: Dimitrios Panagiotidis conceived the idea for this manuscript; Dimitrios Panagiotidis and Azadeh Abdollhnejad designed and wrote the manuscript; Dimitrios Panagiotidis processed the data. Dimitrios Panagiotidis and Azadeh Abdollahnejad designed and performed the statistical analyses; Dimitrios Panagiotidis, Azadeh Abddollahnejad, and Martin Slavík collected the data. All authors have read and agreed to the published version of the manuscript.

Funding: This study was financially supported by EVA4.0 "Advanced Research Supporting the Forestry and Wood-processing Sector's Adaptation to Global Change and the 4th Industrial Evolution" (No. CZ.02.1.01/0.0/0.0/16_019/0000803) of the Faculty of Forestry and Wood Sciences (FFWS) from the Czech University of Life Sciences (CULS) in Prague.

Acknowledgments: We acknowledge that this study was supported by EVA4.0 "Advanced Research Supporting the Forestry and Wood-processing Sector's Adaptation to Global Change and the 4th Industrial Evolution"(No. CZ.02.1.01/0.0/0.0/16_019/0000803) of the Faculty of Forestry and Wood Sciences (FFWS) from the Czech University of Life Sciences (CULS) in Prague.

Conflicts of Interest: The authors declare no conflict of interest.

References

1. Repola, J. Biomass equations for Scots pine and Norway spruce in Finland. *Silva Fenn.* **2009**, *43*, 625–647.
2. Colgan, M.S.; Swemmer, T.; Asner, G.P. Structural relationships between form factor, wood density, and biomass in African Savanna woodlands. *Trees*, **2014**, *28*, 91–102.
3. Adekunle, V.A.J.; Nair, K.N.; Srivastava, A.K.; Singh, N.K. Models and form factors for stand volume estimation in natural forest ecosystems: a case study of Katarniaghat wildlife sanctuary (KGWS), Bahraich District, India. *J. For. Res.* **2013**, *24*, 217–226.
4. Socha, J.; Kulej, M. Variation of the tree form factor and taper in European larch of Polish provenances tested under conditions of the Beskid Sądecki mountain range (southern Poland). *J. For. Sci.* **2007**, *53*, 538–547.
5. Socha, J.; Kulej, M. Provenance-dependent variability of Abies grandis stem form under mountain conditions of Beskid Sadecki (southern Poland). *Can. J. For. Res.*, **2005**, *35*, 1–14.
6. Ikonen, V.P.; Kellomäki, S.; Väisänen, H.; Peltola, H. Modelling the distribution of diameter growth along the stem in Scots pine. *Trees,* **2006**, *20*, 391–402.
7. Pretzsch, H.; Bielak, K.; Block, J.; Bruchwald, A.; Dieler, J.; Ehrhart, H.P.; Kohnle, U.; Nagel, J.; Spellmann, H.; Zasada, M.; et al. Productivity of mixed versus pure stands of oak (*Quercus pretraea* (Matt.) Liebl. and *Quercus robur* L.) and European beech (*Fagus sylvatica* L.) along an ecological gradient. *Eur. J. For. Res.* **2013**, *132*, 263–280.
8. Vidal, C.; Alberdi, I.; Redmond, J.; Vestman, M.; Lanz, A.; Klemens, S. The role of National Forest Inventories for international forestry reporting. *Ann. For. Sci.* **2016**, *73*, 793–806.
9. Brolly, G.; Kiraly, G. Algorithms for stem mapping by means of terrestrial laser scanning. Acta *Silv. Lignaria Hung.* **2009**, *5*, 119–130.
10. Pál, I. Measurements of Forest Inventory Parameters on Terrestrial Laser Scanning Data Using Digital Geometry and Topology. *Int. Arch. Photogramm. Remote Sens. Spat. Inf. Sci.* **2008**, *37*, 373–380.
11. Wezyk, P.; Koziol, K.; Glista, M.; Pierzchalski, M. Terrestrial laser scanning versus traditional forest inventory first results from the polish forests. *Int. Arch. Photogramm. Remote Sens. Spat. Inf. Sci.* **2007**, *3*, 424–429.
12. Heinzel, J.; Huber, M.O. Detecting Tree Stems from Volumetric TLS Data in Forest Environments with Rich Understory. *Remote Sens.* **2017**, *9*, 9.

13. Kasa, I. A circle fitting procedure and it`s error analysis. *IEEE Trans. Instrum. Meas.* **1976**, IM-*25*(1), 8–14.
14. Pratt, V. Direct least-squares fitting of algebraic surfaces. *Comput. Graph.* **1987**, *21*, 145–152.
15. Taubin, G. Estimation of planar curves, surfaces, and nonplanar space curves defined by implicit equations with applications to edge and range image segmentation. *IEEE Trans. Pattern Anal. Mach. Intell.* **1991**, *13*, 1115–1138.
16. Pueschel, P.; Newnham, G.; Rock, G.; Udelhoven, T.; Werner, W.; Hill, J. The influence of scan mode and circle fitting on tree stem detection, stem diameter and volume extraction from terrestrial laser scans. *ISPRS J. Photogramm. Remote Sens.* **2013**, *77*, 44–56.
17. Koreň, M.; Mokroš, M.; Bucha, T. Accuracy of tree diameter estimation from terrestrial laser scanning by circle-fitting methods. *Int. J. Appl. Earth Obs. Geoinf.* **2017**, *63*, 122–128.
18. Dassot, M.; Colin, A; Santenoise, P.; Fournier, M.; Constant, T. Terrestrial laser scanning for measuring the solid wood volume, including branches, of adult standing trees in the forest environment. *Comput. Electron. Agric.*, **2012**, *89*, 86–93.
19. Wilkes, P.; Lau, A.; Disney, M.I.; Calders, K.; Burt, A.; Gonzalez de Tanago, J.; Bartholomeus, H.; Brede, B.; Herold, M. Data Acquisition Considerations for Terrestrial Laser Scanning of Forest Plots. *Remote Sens. Environ.* **2017**, *196*, 140–153.
20. Zhang, Z.; Murtagh, F.; Van Poucke, S.; Lin, S.; Lan, P. Hierarchical cluster analysis in clinical research with heterogeneous study population: Highlighting its visualization with R. *Ann. Transl. Med.* **2017**, *5*, 75.
21. Maas, H.; Bienert, A.; Scheller, S.; Keane, E. Automatic forest inventory parameter determination from terrestrial laser scanner data. *Int. J. Remote Sens.*, **2008**, *29*(5) 1579–1593.
22. Corte, A.P.D.; Rex, F.E.; Almeida, D.R.A.D.; Sanquetta, C.R.; Silva, C.A.; Moura, M.M.; Wilkinson, B.; Zambrano, A.M.A.; Neto, C.; Veras, H.F.; et al. Measuring individual tree diameter and height using GatorEye High-Density UAV-Lidar in an integrated crop-livestock-forest system. *Remote Sens.* **2020**, *12*, 863.
23. Yang, X.; Strahler, A.H.; Schaaf, C.B.; Jupp, D.L.B.; Yao, T.; Zhao, F.; Wang, Z.; Culvenor, D.S.; Newnham G.J.; Lovell, J.L.; et al. Three-dimensional forest reconstruction and structural parameter retrievals using a terrestrial full-waveform lidar instrument (Echidna). *Remote Sens. Environ.* **2013**, *7*, 36–51.
24. Iizuka, K.; Yonehara, T.; Itoh, M.; Kosugi, Y. Estimating Tree Height and Diameter at Breast Height (DBH) from Digital Surface Models and Orthophotos Obtained with an Unmanned Aerial System for a Japanese Cypress (*Chamaecyparis obtusa*) Forest. *Remote Sens.* **2017**, *10*, 13.
25. Panagiotidis, D.; Abdollahnejad, A.; Surový, P.; Chiteculo, V. Determining tree height and crown diameter from high-resolution UAV imagery. *Int. J. Remote Sens.* **2017**, *38*(8-10), 2392–2410.
26. Abdollahnejad, A.; Panagiotidis, D.; Surový, P.; Ulbrichová, I. UAV Capability to Detect and Interpret Solar Radiation as a Potential Replacement Method to Hemispherical Photography. *Remote Sens.* **2018**, *10*, 423.
27. Surový, P.; Almeida Ribeiro, N.; Panagiotidis, D. Estimation of positions and heights from UAV-sensed imagery in tree plantations in agrosilvopastoral systems *Int. J. Remote Sens.* **2018**, 1–15.
28. Srinivasan, S.; Popescu, C.S.; Eriksson, M.; Sheridan, D.R.; Ku, N. Terrestrial laser scanning as an effective tool to retrieve tree-level height, crown width, and stem diameter. *Remote Sens.* **2015**, *7*(2), 1877–1896.

29. Panagiotidis, D.; Surový, P.; Kuželka, K. Accuracy of Structure from Motion models in comparison with terrestrial laser scanner for the analysis of DBH and height influence on error behaviour. *J. For. Sci.* **2016**, *62*, 357–365.
30. Liang, X.; Hyyppä, J. Automatic stem mapping by merging several terrestrial laser scans at the feature and decision levels. *Sensors,* **2013**, *13*, 1614–1634.
31. Åkerblom, M.; Raumonen, P.; Mäkipää, R.; Kaasalainen, M. Automatic tree species recognition with quantitative structure models. *Remote Sens. Environ.* **2017**, *191*, 1–12.
32. Seidel, D.; Ammer, C. Efficient measurements of basal area in short rotation forests based on terrestrial laser scanning under special consideration of shadowing. *iFor.-Biogeosci. For.* **2014**, *7*, 227–232.
33. Fernández-Sarría, A.; Martínez, L.; Velázquez-Martí, B.; Sajdak, M.; Estornell, J.; Recio, J.A. Different methodologies for calculating crown volumes of Platanus hispanica trees using terrestrial laser scanner and a comparison with classical dendrometric measurements. *Comput. Electron. Agric.* **2013**, *90*, 176–185.
34. Bournez, E.; Landes, T.; Saudreau, M.; Kastendeuch, P.; Najjar, G. From TLS point clouds to 3D models of trees: A comparison of existing algorithms for 3D tree reconstruction. In *Proceedings of the International Archives of the Photogrammetry, Remote Sensing and Spatial Information Sciences-ISPRS Archives*; Nafplio, Grecce, 2017.
35. Culvenor, D.S.; Newnham, G.J.; Mellor, A.; Sims, N.C.; Haywood, A. Automated in-situ laser scanner for monitoring forest leaf area index. *Sensors,* **2014**, *14*, 14994–15008.
36. Kankare, V.; Vastaranta, M.; Holopainen, M.; Raty, M.; Yu, X.; Hyyppa, J.; Hyyppa, H.; Alho, P.; Viitala, R. Retrieval of forest aboveground biomass and stem volume with airborne scanning LiDAR. *Remote Sens.* **2013**, *5*, 2257–2274.
37. Astrup, R.; Ducey, M.J.; Granhus, A.; Ritter, T.; Lüpke, V.N. Approaches for estimating stand-level volume using terrestrial laser scanning in a single-scan mode. *Can. J. For. Res.* **2014**, *44*(6), 666–676.
38. Mayamanikandan, T.; Reddy, R.S.; Jha, C. Non-destructive tree volume estimation using terrestrial lidar data in teak dominated Central Indian forests. In Proceedings of the 2019 IEEE Recent Advances in Geoscience and Remote Sensing: Technologies, Standards and Applications (TENGARSS) 2019, Kochi, Kerala, India, 17–20 October 2019; pp. 100–103.
39. Zhang, W.; Qi, J.; Wan, P.; Wang, H.; Xie, D.; Wang, X.; Yan, G. An Easy-to-Use Airborne LiDAR Data Filtering Method Based on Cloth Simulation. *Remote Sens.* **2016**, *8*(6), 501.
40. Corral-Rivas, J.J.; Barrio-Anta, M.; Treviño-Garza, E.; Diéguez-Aranda, U. Use of stump diameter to estimate diameter at breast height and tree volume, for major pine species in El Salto, Durango (Mexico). *Forestry*, **2007**, *80*(1) 29–40.
41. Popescu, S.C.; Wynne, R.H.; Nelson, R.F. Estimating plot-level tree heights with lidar: Local filtering with a canopy-height based variable window size. *Comput. Electron. Agric.* **2002**, *37*, 71–95.
42. Rousseeuw, P.J.; Kaufman, L. Finding groups in data. *Ser. Probab. Math. Stat.* **2003**, *34*, 111–112.

43. Bucher, I. CircleFit. 2004. Available online: https://se.mathworks.com/matlabcentral/fileexchang /5557- circle-fit/content/circfit.m (accessed on 15 December 2016).
44. Petráš, R.; Pajtík, J. Sústava česko-slovenských objemových tabuliek drevín. *Lesnický Časopis,* **1991**, *1*, 49–56.
45. Wang, Y.; Lehtomäki, M.; Liang, X.; Pyörälä, J.; Kukko, A.; Jaakkola, A.; Liu, J.; Feng, Z.; Chen, R.; Hyyppä, J. Is field-measured tree height as reliable as believed—A comparison study of tree height estimates from field measurement, airborne laser scanning and terrestrial laser scanning in a boreal forest. *ISPRS J. Photogramm. Remote Sens*. **2019**, *147*, 132–145.
46. Olofsson, K.; Holmgren, J.; Olsson, H. Tree Stem and Height Measurements using Terrestrial Laser Scanning and the RANSAC Algorithm. *Remote Sens*. **2014**, *6*(5), 4323–4344.
47. Srinivasan, S.; Popescu, S.C.; Eriksson, M.; Sheridan, R.D.; Ku, N.W. Multi-temporal terrestrial laser scanning for modeling tree biomass change. *For. Ecol. Manag.* **2014**, *318*, 304–317.
48. Donager, J.J.; Sankey, T.T.; Sankey, J.B.; Sanchez Meador A.J.; Springer, A.E; Bailey, J.D. Examining forest structure with terrestrial lidar: Suggestions and novel techniques based on comparisons between scanners and forest treatments. *Earth Space Sci.* **2018**, *5*, 753–776.
49. Giannetti, F.; Puletti, N.; Quatrini, V.; Travaglini, D.; Bottalico, F.; Corona, P.; Chirici, G. Integrating terrestrial and airborne laser scanning for the assessment of single-tree attributes in Mediterranean forest stands. *Eur. J. Remote Sens.* **2018**, *51*(1), 795–807.
50. Pitkanen, T.P.; Raumonen, P.; Kangas, A. Measuring stem diameters with TLS in boreal forests by complementary fitting procedure. *ISPRS J. Photogramm. Remote Sens.* **2019**, *147*, 294–306.
51. Wang, P.; Li, R.; Bu, G.; Zhao, R. Automated low-cost terrestrial laser scanner for measuring diameters at breast height and heights of plantation trees. *PLoS ONE,* **2019**, *14*(1), e0209888.
52. Calders, K.; Newnham, G.; Burt, A.; Murphy, S.; Raumonen, P.; Herold, M.; Culvenor, D.; Avitabile, V.; Disney, M.; Armstong, J.; et al. Nondestructive estimates of above-ground biomass using terrestrial laser scanning. *Methods Ecol. Evol.* **2015**, *6*, 198–208.
53. Olschofsky, K.; Mues, V.; Kohl, M. Operational assessment of aboveground tree volume and biomass by terrestrial laser scanning. *Computers and Electronics in Agriculture,* **2016**, *127*, 699–707.
54. Saarinen, N.; Kankare, V.; Vastaranta, M.; Luoma, V.; Pyörälä, J.; Tanhuanpää, T.; Liang, X.; Kaartinen, H.; Kukko, A.; Jaakkola, A.; et al. Feasibility of terrestrial laser scanning for collecting stem volume information from single trees. *ISPRS J. Photogramm. Remote Sens.* **2017**, *123*, 140–158.
55. Lau, A.; Bentley, L.P.; Martius, C.; Shenkin, A.; Bartholomeus, H.; Raumonen, P.; Malhi, Y.; Jackson, T.; Herold, M. Quantifying branch architecture of tropical trees using terrestrial LiDAR and 3D modelling. *Trees Struct. Funct.* **2018**, *32*, 1219–1231.

Příloha č. 5 - Mokroš, M.; Výbošťok, J.; Tomaštík, J.; Grznárová, A.; Valent, P.; Slavík, M.; Merganič, J. High precision individual tree diameter and perimeter estimation from close-range photogrammetry. *Forests* 2018,

forests

MDPI

Article

High Precision Individual Tree Diameter and Perimeter Estimation from Close-Range Photogrammetry

Martin Mokroš [1,2,*], Jozef Výbošťok [3], Julián Tomaštík [2], Alžbeta Grznárová [2], Peter Valent [2], Martin Slavík [1] and Ján Merganič [4]

1 Faculty of Forestry and Wood Sciences, Czech University of Life Sciences Prague, 165 21 Praha 6–Suchdol, Czech Republic; mslavik@fld.czu.cz
2 Department of Forest Management and Geodesy, Faculty of Forestry, Technical University in Zvolen, 96053 Zvolen, Slovakia; tomastik@tuzvo.sk (J.T.); alzbeta.grznarova@tuzvo.sk (A.G.); peter.valent@tuzvo.sk (P.V.)
3 Department of Economics and Management of Forestry, Faculty of Forestry, Technical University in Zvolen, 96053 Zvolen, Slovakia; jozef.vybostok@tuzvo.sk
4 Department of Forest Harvesting, Logistics and Ameliorations, Faculty of Forestry, Technical University in Zvolen, 96053 Zvolen, Slovakia; merganic@tuzvo.sk
* Correspondence: mokros@fld.czu.cz; Tel.: +421-948-047-996

Received: 11 October 2018; Accepted: 8 November 2018; Published: 10 November 2018

check for updates

Abstract: Close-range photogrammetry (CRP) can be used to provide precise and detailed three-dimensional data of objects. For several years, CRP has been a subject of research in forestry. Several studies have focused on tree reconstruction at the forest stand, plot, and tree levels. In our study, we focused on the reconstruction of trees separately within the forest stand. We investigated the influence of camera lens, tree species, and height of diameter on the accuracy of the tree perimeter and diameter estimation. Furthermore, we investigated the variance of the perimeter and diameter reference measurements. We chose four tree species (*Fagus sylvatica* L., *Quercus petraea* (Matt.) Liebl., *Picea abies* (L.) H. Karst. and *Abies alba* Mill.). The perimeters and diameters were measured at three height levels (0.8 m, 1.3 m, and 1.8 m) and two types of lenses were used. The data acquisition followed a circle around the tree at a 3 m radius. The highest accuracy of the perimeter estimation was achieved when a fisheye lens was used at a height of 1.3 m for *Fagus sylvatica* (root mean square error of 0.25 cm). Alternatively, the worst accuracy was achieved when a non-fisheye lens was used at 1.3 m for *Quercus petraea* (root mean square error of 1.27 cm). The tree species affected the estimation accuracy for both diameters and perimeters.

Keywords: close-range photogrammetry; trunk perimeter; trunk diameter; point cloud; circle fitting; convex hull; fisheye lens

1. Introduction

Currently, demands for precise information about individual trees and forest stands are increasing in forestry [1]. The most important parameter for the estimation of forest information is the trunk diameter [2]. The diameter is related strongly to other descriptors of tree size such as total height [3] and crown dimensions [4]. Thus, it is a key predictor to estimate the stem and tree volume [5], biomass [6], and other information [7]. In addition to the forestry practice, the high demand for precise and complex three-dimensional (3D) data is evident in multiple research fields; for example, in functional-structural models [8] where it is crucial to obtain accurate temporal 3D data. Furthermore, the demand for a high-quality visualization of the forest environment is high.

Many types of measuring instruments exist that exhibit different properties (e.g., precision, accuracy, operational simplicity, and cost). The methods used can be divided into two categories: contact methods (tape, caliper, electronic tree measuring fork) and non-contact methods (optical calipers, rangefinder dendrometers, optical forks) [9]. The contact methods allow for the highest accuracy. Owing to time constraints and safety issues, they are limited to measurements of the lower bole. Meanwhile, non-contact methods are inaccurate or expensive in terms of time and instrument expense. Hence, alternative methods must be sought [1].

During the last two decades, development methods have rendered 3D point clouds as a useful data source for tree measurements [2]. The 3D data of trees from the ground may be characterized by three primary acquisition methods: (1) magnetic motion tracker, (2) terrestrial laser scanner (TLS), and (3) close-range photogrammetry (CRP) [10]. The magnetic motion tracker allows for the detailed 3D point clouds to be used as a basis for determining the tree diameter. However, this method is expensive and time-consuming [11]. Terrestrial laser scanning produces extremely high point densities and fills the gap between tree-scale manual measurements and large-scale airborne laser scanning measurements by providing a large amount of precise information on various forest structural parameters [12]. The TLS can provide an estimation accuracy of 1–2 cm when the diameter at breast height (DBH) and the diameter on stem curve are estimated [13]. The disadvantage of the TLS is its relatively high cost and lack of personnel training.

CRP is an approach allowing for the automatic reconstruction of 3D models using sets of overlapping two-dimensional digital images [14]. Terrestrial photogrammetry is a perspective method to create 3D point clouds, because hand-held cameras are appropriate for end-users owing to their low-cost, and low-weight sensors that are highly portable and easy to access [15]. Several authors used terrestrial photogrammetry to determine tree parameters [1,2,7,10,15–19]. For example, Liang et al. [15] described a method for terrestrial photogrammetry using a hand-held consumer camera. Forsman et al. [2] developed a method for terrestrial mapping of a tree structure using a multi-camera rig. Surový et al. [10] described the accuracy of point reconstruction on individual stems using a hand-held camera with stop-and-go. Miller et al. [18] designed and described a method for individual tree models. Bauwens et al. [7] used terrestrial photogrammetry as a tool for the non-destructive method of modelling irregularly shaped tropical tree trunks. However, in these studies, the authors did not focus on trunk perimeter estimation from CRP. The perimeter may be more accurate for deriving other parameters such as the diameter. Furthermore, the impact of different types of bark was not investigated. Most of the previous studies focused on trees within a research plot and created images for the whole research area. Capturing the trees individually within the forest stand can result in better estimation accuracies.

The aim of this study was to design an appropriate CRP method in order to create 3D point clouds of individual trees. Furthermore, we estimated the diameter and perimeter of individual trees with different types of bark, at different heights on the tree stem using a digital single-lens reflex (DSLR) camera with a non-fisheye lens and a fisheye lens, separately. The research itself is a first step towards the workflow development that starts from data acquisition to functional-structural forest modelling and visualization.

2. Materials and Methods

2.1. Study Site

The research area is located in the central part of Slovakia, which belongs to the Kremnica Mountains. The forest stands are unique according to the tree species composition, primarily European beech (*Fagus sylvatica* L.), sessile oak (*Quercus petraea* (Matt.) Liebl.), Norway spruce (*Picea abies* (L.) H. Karst.), and European silver fir (*Abies alba* Mill.). These four species differ significantly by bark type. Therefore, we chose 10 trees from each tree species. However, the light conditions and slope (0%–5%) were the same for all trees. The age varied from 55 to 80 years. Further, the age was equal, and the trees were located in the same forest stand within each tree species (Figure 1).

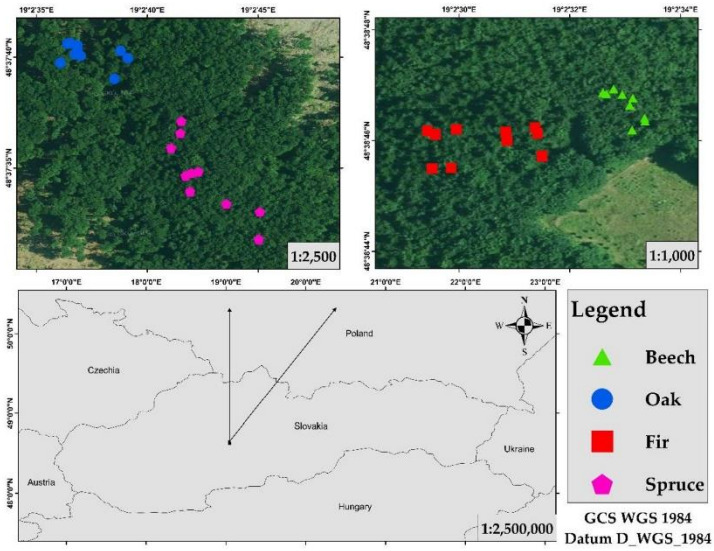

Figure 1. Overview of the trees' positions within the forest stands, and their positions within the Slovak republic are shown below.

2.2. Reference Data Acquisition

Tree diameter measurements were performed using a caliper and measuring tape. The diameter was measured at three heights: 0.8 m, 1.3 m, and 1.8 m. At each of those height levels, we marked the trunk on its perimeter with four markings. The diameter was measured with a caliper to be perpendicular to those markings, as shown in Figure 2. The caliper measurement was performed four times for every marking. After measuring with the caliper, we also measured the perimeter by measuring the tape four times starting from each of the markings, and then we calculated the diameter. Altogether, we measured the diameter 20 times at each of the three height levels on the trunk, thus 60 times per tree.

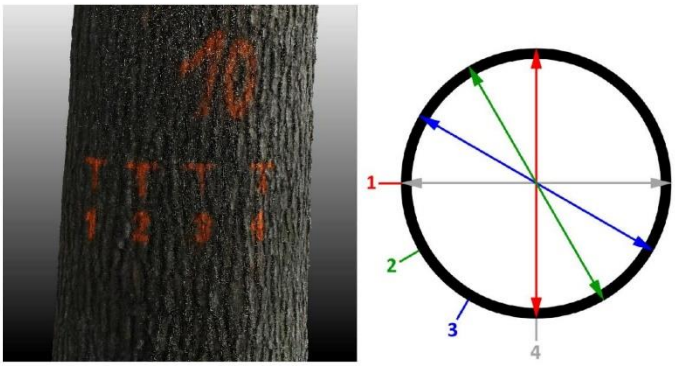

Figure 2. (**left**) Example of the signs for diameter measurement in the field and (**right**) diagram of diameter measurement based on the sign on the bark.

2.3. Image Acquisition

Images of trunks were captured using a DSLR camera, Canon 70D (Canon Inc., Tokyo, Japan), with a CMOS sensor and 20.2-megapixel resolution. Two different lenses were used. The first was the Canon EF 35 mm f/2 IS USM (Canon Inc., Tokyo, Japan) with fixed focal length (non-fisheye). The second lens was the Canon EF 8–15 mm f/4L Fisheye USM (fisheye) (Canon Inc., Tokyo, Japan). The fisheye lens was fixed to 15 mm.

Before the image acquisition, eight A4 papers formatted with 8-bit markers (two on each paper) were placed on the ground, and one was mounted on the reference stick. The reference stick was placed near the trunk (<1 m distance). These markers were used for the scaling and orientation of the point clouds. Altogether, we used nine such papers. For scaling purposes, only one was required. We used multiple papers for verifying the accuracy. The accuracy achieved was under 1 mm in almost all cases. Each tree was captured twice using the non-fisheye lens and subsequently by the fisheye lens. The distance from the tree was maintained at 3 m. The path was a circle around the tree for both lenses. The images were captured in the static position of the operator, and the distance between the positions was approximately 1 m. Two images per position were captured when the non-fisheye lens was used to include the ground and the highest section (1.8 m). When the fisheye lens was used, only one image was required to capture the ground and the highest section. The average number of positions was 35. The average time to collect the images was 4 min for the non-fisheye lens and 2 min for the fisheye lens.

2.4. Data Processing

Images were processed into scaled and oriented point clouds using Agisoft PhotoScan Professional 1.2.6 software (Agisoft LCC, St. Petersburg, Russia). The images were separated into non-fisheye and fisheye. The images were subsequently split into groups. Each grouping corresponded to one individual tree. Subsequently, the images were aligned with automatic camera calibration. When the non-fisheye lens was used, the "frame" camera type was chosen; for the fisheye lens, the "fisheye" camera type was chosen within the calibration options in Agisoft PhotoScan Professional. For all trees, reports were generated. In the reports is information about camera calibration, image overlap, scaling error, etc. Reports are available as Supplementary Materials. An example of the image overlap and camera locations is shown in Figure 3.

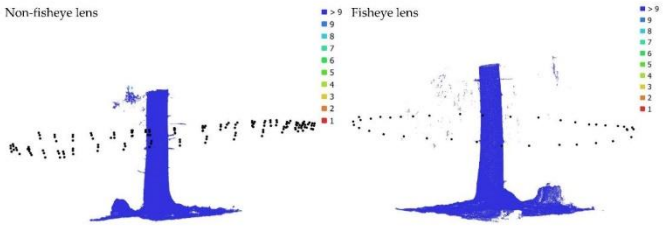

Figure 3. Camera locations and image overlap from the report generated by Agisoft PhotoScan Professional. The same tree is shown on both images (*Abies alba* Mill.).

Thereafter, we used an option where each image was compared to all other images within the grouping in full resolution with high accuracy, after the alignment markers were detected automatically. Each A4 paper contained two markers that were used for scaling. First, we paired the markers that shared the A4 paper and subsequently set a scale (Figure 4). The distance between the centers of the markers was 14.2 cm. The orientation of the Z axis was set by the markers placed on the reference stick. Subsequently, we generated the dense point cloud and exported the point cloud to the .txt format for further processing.

Figure 4. Scaling and orientation process using the coding markers.

First, the trunk cross-sections at 0.8 m, 1.3 m, and 1.8 m on the tree trunk were extracted from the point clouds. DendroCloud software was used for this task [20,21]. To cut the cross-sections at different height levels, a digital elevation model (DEM) was generated. We set 0.5 as the grid size where the minimum Z value was assigned from the point cloud. Based on the DEM cross-section at 1.3 m, it was sliced with a 2 cm thickness. The points within the cross-section were grouped spatially, and a circle fitting algorithm was used to calculate the initial diameter and position of the tree. We used the Monte Carlo method with the automatic initial method. More information about the algorithm is reported in [20]. The normalized DEM was calculated based on the position and diameter, and multiple cross-sections at the desired heights were generated. Subsequently, the points in each height were grouped spatially. Each tree contained three grouped cross-sections (0.8 m, 1.3 m, and 1.8 m) for the non-fisheye lens and fisheye lens. The results were exported to the .csv format and subsequently imported to ArcGIS for Desktop software 10.2 (Environmental Systems Research Institute (ESRI), Redlands, CA, USA). Within ArcGIS for Desktop, the convex hull algorithm was applied by the Minimum Bounding Geometry module. Altogether, 240 perimeters were calculated.

The calculated perimeter values were exported by the ArcGIS for Desktop software in a *.txt file, where the name consisted of the following identifiers: tree species with its number, lens type, and height of the tree referred by the calculated perimeter. The file itself contained the value of the calculated perimeter. We created a script in the Python programming language, version 2.7 (Python Software Foundation, Beaverton, OR, USA), to perform the automated acquisition of the above-mentioned parameters from the file name along with the calculated value of the perimeter as a record for each *.txt file. After processing all files, the script saved the array of records (dataset) into the database for further analysis.

To compare the diameters measured using the caliper, we used the position of the markers that were sprayed on the trunks. In Agisoft PhotoScan Professional, these markers were identified as control points. These markers indicated the position where the diameter was measured. Subsequently, the points were exported to ArcGIS for Desktop. Together with points from the cross-section, we measured the diameter in the same position and direction as in the field using the caliper for each tree and cross-section. The entire workflow is shown in Figure 5.

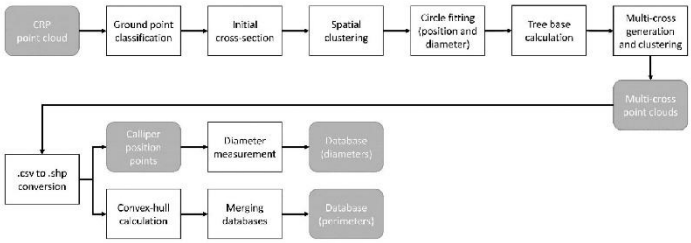

Figure 5. Workflow diagram of the point cloud data processing to the resulted perimeters and diameters of trees.

2.5. Data Evaluation

The estimation error was calculated as the difference between the reference measurement and the estimation from the point cloud. The root mean square error (RMSE) (1) of the diameter and perimeter estimation was also calculated. The error and RMSE were calculated for the estimations from the point clouds generated from both lenses that were used:

$$\text{RMSE\%} = \frac{\text{RMSE}}{\frac{\sum_{i=1}^{N} R_i}{N}} \times 100, \quad (1)$$

where R_i represents the reference diameter or perimeter.

Furthermore, the factorial analysis of variance (ANOVA) was performed to detect the effects of lens, tree species, and height of measurements (0.8, 1.3, 1.8) on the estimation error. The factorial ANOVA was used separately for the perimeters and diameters. Additionally, the datasets for the perimeters and diameters were separated based on the type of lens, and factorial ANOVA was used again on these datasets.

3. Results

3.1. Reference Data

The perimeters of the same position on the trunk were measured four times each. We calculated the variance of these measurements to determine the error originating from the operator. Figure 6 shows the graphs of the variance diameters and perimeters separated by the tree species and height on the trunk. *Fagus sylvatica* exhibited the lowest variance with no significant changes between the heights. *Quercus petraea* and *Picea abies* exhibited the highest variances. In most cases, we observed that the variance for a height of 1.3 m was the lowest within the same tree species and type of measurement (tape and caliper).

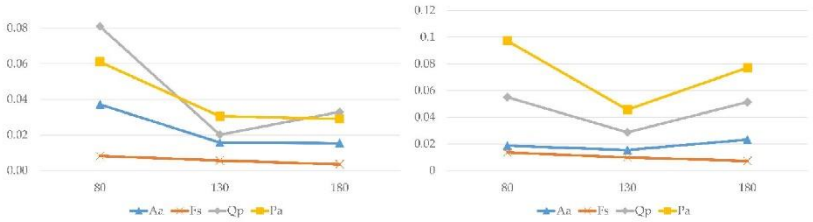

Figure 6. Variances of measured reference data separated by tree species. Perimeter is shown on the left and diameter on the right (cm) (Aa: *Abies alba* Mill.; Fs: *Fagus sylvatica* L.; Qp: *Quercus petraea* (Matt.) Liebl.; Pa: *Picea abies* (L.) H. Karst.).

3.2. Perimeter

The RMSE of the perimeter estimation for all tree species when the non-fisheye lens was used varied from 0.27 cm to 1.27 cm. When the fisheye lens was used, the RMSE varied from 0.25 cm to 1.21 cm (Table 1).

Table 1. RMSE (root mean square error) of perimeter estimation (cm) (Aa: *Abies alba* Mill.; Fs: *Fagus sylvatica* L.; Qp: *Quercus petraea* (Matt.) Liebl.; Pa: *Picea abies* (L.) H. Karst.).

	Non-Fisheye				**Fisheye**			
	80	130	180	All	80	130	180	All
Aa	0.57	0.27	0.48	0.46	0.56	0.31	0.42	0.44
Fs	0.86	0.75	0.76	0.79	0.39	0.25	0.57	0.42
Qp	0.91	1.27	0.77	1.00	0.98	1.21	1.06	1.08
Pa	1.03	1.17	1.10	1.10	0.55	0.75	0.76	0.69

The RMSE% varied from 0.21% to 0.99%. Thus, all RMSE% were under 1% (Table 2).

Table 2. RMSE% of perimeter estimation (Aa: *Abies alba*; Fs: *Fagus sylvatica*; Qp: *Quercus petraea*; Pa: *Picea abies*).

	Non-Fisheye				Fisheye			
	80	130	180	All	80	130	180	All
Aa	0.42	0.21	0.39	0.36	0.42	0.24	0.35	0.35
Fs	0.99	0.90	0.94	0.95	0.45	0.30	0.71	0.51
Qp	0.59	0.88	0.55	0.69	0.63	0.83	0.76	0.74
Pa	0.59	0.74	0.72	0.68	0.31	0.47	0.50	0.43

3.3. Diameter

The RMSE of the diameter estimation for all tree species when the non-fisheye lens was used varied from 0.423 cm to 0.71 cm. When the fisheye lens was used, the RMSE varied from 0.386 cm to 0.596 cm (Table 3).

Table 3. RMSE of diameter estimation (cm) (Aa: *Abies alba*; Fs: *Fagus sylvatica*; Qp: *Quercus petraea*; Pa: *Picea abies*).

	Non-Fisheye				Fisheye			
	80	130	180	All	80	130	180	All
Aa	0.49	0.43	0.43	0.45	0.50	0.49	0.51	0.50
Fs	0.51	0.48	0.43	0.47	0.38	0.39	0.43	0.40
Qp	0.45	0.40	0.41	0.42	0.52	0.53	0.38	0.48
Pa	0.67	0.49	0.46	0.55	0.50	0.45	0.54	0.50

The RMSE% varied from 0.90% to 1.85%. All RMSE% were under 2% (Table 4).

Table 4. RMSE% of diameter estimation (Aa: *Abies alba*; Fs: *Fagus sylvatica*; Qp: *Quercus petraea*; Pa: *Picea abies*).

	Non-Fisheye				Fisheye			
	80	130	180	All	80	130	180	All
Aa	1.17	1.10	1.13	1.14	1.19	1.24	1.33	1.25
Fs	1.85	1.83	1.70	1.80	1.39	1.51	1.67	1.52
Qp	0.92	0.90	0.94	0.92	1.08	1.18	0.88	1.06
Pa	1.21	0.98	0.96	1.07	0.92	0.90	1.13	0.98

3.4. Impact of Factors

The factorial ANOVA was used to identify if the tree species, height of measurement, and lens affected the errors of estimation significantly for both types of measurements (perimeter and diameter).

Within almost all cases, the tree species was the only factor that affected the estimated error significantly. The p-value ranged from 3.3×10^{-16} to 0.015. Furthermore, in terms of the diameter, the height of the measurement and the lens affected the estimated diameters significantly ($p = 0.037$ and $p = 0.021$). The influence of tree species on the errors is illustrated in Figure 7.

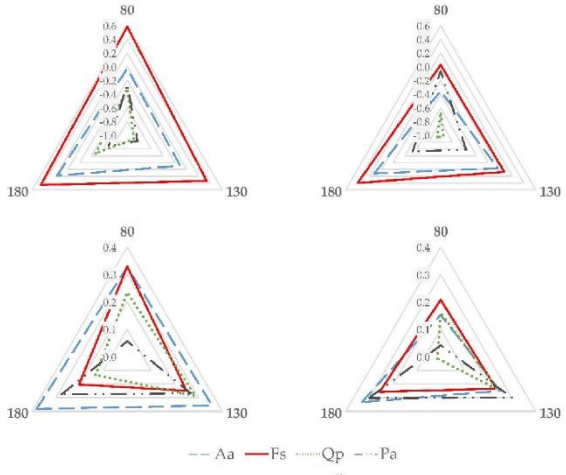

Figure 7. Tree species average error (cm) comparison of (first row) estimated perimeter and (second row) diameter using (first column) non-fisheye and (second column fisheye lens) (Aa: *Abies alba* Mill.; Fs: *Fagus sylvatica* L.; Qp: *Quercus petraea* (Matt.) Liebl.; Pa: *Picea abies* (L.) H. Karst.).

4. Discussion

Research on the application of photogrammetry (both terrestrial and airborne) in forestry has increased after the invention of the structure-from-motion (SfM) and multi-view stereo (MVS) techniques, which are closely related to computer vision and learning [14,18]. Forests are measured photogrammetrically at the stand [1], plot [15,17], and tree levels [10,18]. Our study provides the results of the 3D capture and reconstruction of individual trees that can potentially be applied towards quality and quantity estimations [22], the creation of high-precision tree models for growth models and simulations [23], etc. In addition to SfM and MVS, other photographic methods have been reported to be applicable in the evaluation of spatial relations in forests. For example, Dick et al. [24] used 360° panoramic images to measure forest stands using a relation between a known focal length and partially measured field data. Hapca et al. [25] used two converging digital images to reconstruct standing trees up to a height of 12 m.

The accuracy of the photogrammetric 3D reconstruction of trees has already been studied widely, where the DBH is the most frequently estimated parameter. For the DBH of 20 specimens of *Cryptomeria japonica*, Surový et al. [10] reported an RMSE of 0.59 cm with an SD of 0.72 cm, thus achieving sub-centimeter accuracy as reported in the current study. According to ANOVA, the tree species affected the accuracy significantly; however, these differences were only in the millimeter scale. Liang et al. [15] reported a DBH RMSE of 2.39 cm; however, the data acquisition was plotted based on a 30 m × 30 m rectangular plot. In another study [26], an average DBH error of 1.15 cm was reported for 500 m^2 circular plots.

For a fisheye camera, Berveglieri et al. [16] reported an average DBH error of 1.46 cm with a standard deviation of 1.09 cm for a small forest plot consisting of seven trees. They considered these results comparable with manual measurements and values generated from laser scanning. Rodríguez-García et al. [27] studied an application of stereoscopic hemispherical fisheye images and achieved a DBH RMSE of 1.51 cm. Fisheye lenses allow for the coverage of a large area, thereby requiring a lesser number of images. However, their imaging geometry causes large variations in scale, and must be addressed using proper calibration. Some authors [28–30] described this

calibration process. For example, Berveglieri et al. [16] calibrated a fisheye camera in a terrestrial calibration field composed of coded targets. Our results indicate that, currently, even the "on-the-job" calibration in specialized software can provide results comparable with non-wide-angle cameras. Furthermore, the reprojection errors (Supplementary Materials) ranged from 0.70 pix. to 0.95 pix. for non-fisheye lens and from 0.42 pix. to 0.57 pix. for fisheye lens (Table 5). "Reprojection error is the distance between the point on the image where a reconstructed 3D point can be projected and the original projection of that 3D point detected on the photo and used as a basis for the 3D point reconstruction procedure" [31]. Reprojection errors of fisheye lens are lower for each tree species. Reader should consider that the impact of the automatic camera calibration was not investigated.

Table 5. The average of reprojection error of both lenses that were used divided by tree species.

	Abies Alba		*Fagus Sylvatica*		*Quercus Petraea*		*Picea Abies*	
	Non-Fisheye	**Fisheye**	**Non-Fisheye**	**Fisheye**	**Non-Fisheye**	**Fisheye**	**Non-Fisheye**	**Fisheye**
Reprojection error (pixel)	0.90	0.57	0.75	0.52	0.70	0.42	0.76	0.44

In the present study, diameters and perimeters were tested at three heights up to 1.8 m. However, measurements of longer sections of the stem are often required. Bauwens et al. [7] conducted a research where tropical, irregularly shaped trees with massive buttresses were reconstructed up to 12 m in height with an RMSE under 5%. In terms of error variability with increasing height, Surový et al. [10] observed an increased variability in reconstruction errors only on the lowest part of the stem, 10 cm above ground. This likely demonstrates an advantage of the current CRP methods, as a higher error with increasing height was reported for older photogrammetric methods [25].

Laser scanning methods might still be more precise and less laborious, but the high price of the devices is restrictive with respect to a wider application [10]. In addition, if only basic parameters (e.g., tree position and DBH) are required, these can be measured quickly using simple equipment (compass, rangefinder, caliper). The applicability of "classical" methods is also confirmed in our study where references for both perimeters and diameters were measured with a variability of less than one centimeter. The advantage of point cloud applications is related to the estimation of advanced attributes such as the stem curve and stem quality [15].

As suggested by the afore-mentioned studies, the accuracy of the current CRP methods is high, and fully applicable for the most typical tasks related to the trees' dimensions. Although the computational power of the current computers is extremely high, photogrammetrical processing can be highly time-consuming, as it can potentially continue for days. A photogrammetric assessment of the inevitable data required could be crucial for the optimization of the whole process. Miller et al. [18] measured small trees using 150–180 photos per tree. Surový et al. [10] reported a crucial shift in accuracy for five to eight cameras simultaneously based on the same point. With more than eight cameras, the accuracy did not increase. To reconstruct the stem, 40 photos were captured. This corresponds with our study, where 40 images captured by the fisheye lens were used. The number of necessary images captured using the standard lens was approximately two times higher. The distance between the operator and the tree must also be considered. Bauwens et al. [7] processed the photographs of large tropical trees captured with the focal length of 25 mm; however, the processing of images captured with focal lengths of 35 mm and 50 mm failed. This was likely caused by the small distance between the operator and the tree that led to images with almost the same area and texture as those of the tree. The distance could also be crucial for accuracy. James and Robson [14] suggested a ratio of 1:1000 for the accuracy and distance; however, further testing is required. In our case, the DBH RMSEs ranged from ~4 to ~7 mm at a distance of 3 m. The accuracy could have been influenced by the artificial signs on and around the stems, which could facilitate photo alignment.

5. Conclusions

CRP is suitable for generating 3D point clouds of individual trees with a high accuracy of diameter and perimeter estimations of the tree trunk. We obtained the RMSE of perimeter estimation between 0.27 cm and 1.28 cm. Regarding the diameter, the RMSE varied from 0.39 cm to 0.71 cm. Surprisingly, the camera lens type (non-fisheye vs. fisheye) did not affect the estimation accuracy of the tree trunk perimeter significantly. Meanwhile, the tree species affected the accuracy significantly with regard to the perimeter and diameter estimations. The estimation accuracy of the perimeter and diameter of the trees was highly promising for the monitoring of annual tree trunk increment. Further research will focus on the tree trunk annual increment estimation by CRP, regardless of whether the technique is suitable. The increment in the stem curve should also be investigated.

Supplementary Materials: The following are available online at http://www.mdpi.com/1999-4907/9/11/696/s1, reports.

Author Contributions: Conceptualization, M.M., J.V. and J.M.; Data curation, M.M., J.V., A.G., P.V. and M.S.; Formal analysis, M.M.; Funding acquisition, M.M. and J.M.; Methodology, M.M. and J.V.; Supervision, J.M.; Validation, M.M.; Writing—original draft, M.M., J.V. and J.T.; Writing—review and editing, M.M., J.V., J.T., P.V. and J.M.

Funding: This work was supported by the Slovak Research and Development Agency through Grant No. APVV-15-0714 ("Mitigation of climate change risk by optimization of forest harvesting scheduling"), by the Scientific Grant Agency of the Ministry of Education, Science, Research, and Sport of the Slovak Republic under the grant VEGA 1/0881/17, and by Grant No. CZ.02.1.01/0.0/0.0/16_019/0000803 ("Advanced research supporting the forestry and wood-processing sector's adaptation to global change and the 4th industrial revolution") financed by OP RDE.

Conflicts of Interest: The authors declare no conflict of interest.

References

1. Mikita, T.; Janata, P.; Surovỳ, P. Forest stand inventory based on combined aerial and terrestrial close-range photogrammetry. *Forests* **2016**, *7*, 165. [CrossRef]
2. Forsman, M.; Börlin, N.; Holmgren, J. Estimation of Tree Stem Attributes Using Terrestrial Photogrammetry with a Camera Rig. *Forests* **2016**, *7*, 61. [CrossRef]
3. Zhang, L.; Bi, H.; Cheng, P.; Davis, C.J. Modeling spatial variation in tree diameter—Height relationships. *For. Ecol. Manag.* **2004**, *189*, 317–329. [CrossRef]
4. Hemery, G.E.; Savill, P.S.; Pryor, S.N. Applications of the crown diameter—Stem diameter relationship for different species of broadleaved trees. *For. Ecol. Manag.* **2005**, *215*, 285–294. [CrossRef]
5. Belyea, H.C. *Forest Measurement*; John Wiley & Sons, Inc.: New York, NY, USA, 1931.
6. Jenkins, C.; Chojnacky, D.; Heath, L.; Birdsey, R. *Comprehensive Database of Diameter-Based Biomass Regressions for North American Tree Species*; US Department of Agriculture, Forest Service, Northeastern Research Station: Newtown Square, PA, USA, 2004.
7. Bauwens, S.; Fayolle, A.; Gourlet-Fleury, S.; Ndjele, L.M.; Mengal, C.; Lejeune, P. Terrestrial photogrammetry: A non-destructive method for modelling irregularly shaped tropical tree trunks. *Methods Ecol. Evol.* **2017**, *8*, 460–471. [CrossRef]
8. Sievänen, R.; Godin, C.; de Jong, T.M.; Nikinmaa, E. Functional-structural plant models: A growing paradigm for plant studies. *Ann. Bot.* **2014**, *114*, 599–603. [CrossRef] [PubMed]
9. Clark, N.; Wynne, R.; Schmoldt, D. A review of past research on dendrometers. *For. Sci.* **2000**, *46*, 570–576.
10. Surový, P.; Yoshimoto, A.; Panagiotidis, D. Accuracy of reconstruction of the tree stem surface using terrestrial close-range photogrammetry. *Remote Sens.* **2016**, *8*, 123. [CrossRef]
11. Yoshimoto, A.; Surovy, P.; Konoshima, M.; Kurth, W. Constructing tree stem form from digitized surface measurements by a programming approach within discrete mathematics. *Trees* **2014**, 1577–1588. [CrossRef]
12. Liang, X.; Kankare, V.; Hyyppä, J.; Wang, Y.; Kukko, A.; Haggrén, H.; Yu, X.; Kaartinen, H.; Jaakkola, A.; Guan, F.; et al. Terrestrial laser scanning in forest inventories. *ISPRS J. Photogramm. Remote Sens.* **2016**, *115*, 63–77. [CrossRef]

13. Liang, X.; Hyyppä, J.; Kaartinen, H.; Lehtomäki, M.; Pyörälä, J.; Pfeifer, N.; Holopainen, M.; Brolly, G.; Francesco, P.; Hackenberg, J.; et al. International benchmarking of terrestrial laser scanning approaches for forest inventories. *ISPRS J. Photogramm. Remote Sens.* **2018**, *144*, 137–179. [CrossRef]
14. James, M.R.; Robson, S. Straightforward reconstruction of 3D surfaces and topography with a camera: Accuracy and geoscience application. *J. Geophys. Res. Earth Surf.* **2012**, *117*, 1–17. [CrossRef]
15. Liang, X.; Jaakkola, A.; Wang, Y.; Hyyppä, J.; Honkavaara, E.; Liu, J.; Kaartinen, H. The use of a hand-held camera for individual tree 3D mapping in forest sample plots. *Remote Sens.* **2014**, *6*, 6587–6603. [CrossRef]
16. Berveglieri, A.; Tommaselli, A.; Liang, X.; Honkavaara, E. Photogrammetric measurement of tree stems from vertical fisheye images. *Scand. J. For. Res.* **2017**, *32*, 737–747. [CrossRef]
17. Mokroš, M.; Liang, X.; Surový, P.; Valent, P.; Čerňava, J.; Chudý, F.; Tunák, D.; Saloň, Š.; Merganič, J. Evaluation of Close-Range Photogrammetry Image Collection Methods for Estimating Tree Diameters. *ISPRS Int. J. Geo-Inf.* **2018**, *7*, 93. [CrossRef]
18. Miller, J.; Morgenroth, J.; Gomez, C. 3D modelling of individual trees using a handheld camera: Accuracy of height, diameter and volume estimates. *Urban For. Urban Green.* **2015**, *14*, 932–940. [CrossRef]
19. Roberts, J.W.; Koeser, A.K.; Abd-Elrahman, A.H.; Hansen, G.; Landry, S.M.; Wilkinson, B.E. Terrestrial Photogrammetric Stem Mensuration for Street Trees. *Urban For. Urban Green.* **2018**, *35*, 66–71. [CrossRef]
20. Koreň, M.; Mokroš, M.; Bucha, T. Accuracy of tree diameter estimation from terrestrial laser scanning by circle-fitting methods. *Int. J. Appl. Earth Obs. Geoinf.* **2017**, *63*, 122–128. [CrossRef]
21. Koreň, M. DendroCloud: Point Cloud Processing Software for Forestry, Version 1.45. Available online: http://gis.tuzvo.sk/dendrocloud/download/dendrocloud_1_45.pdf (accessed on 21 August 2018).
22. Cieszewski, C.J.; Strub, M.; Antony, F.; Bettinger, P.; Dahlen, J.; Lowe, R.C. Wood quality assessment of tree trunk from the tree branch sample and auxiliary data based on NIR Spectroscopy and SilviScan. *Math. Comput. For. Nat. Sci.* **2013**, *5*, 86–111.
23. Fabrika, M.; Valent, P.; Scheer, Ľ. Thinning trainer based on forest-growth model, virtual reality and computer-aided virtual environment. *Environ. Model. Softw.* **2018**, *100*, 11–23. [CrossRef]
24. Dick, A.R.; Kershaw, J.A.; MacLean, D.A. Spatial Tree Mapping Using Photography. *North. J. Appl. For.* **2010**, *27*, 68–74. [CrossRef]
25. Hapca, A.I.; Mothe, F.; Leban, J.-M. A digital photographic method for 3D reconstruction of standing tree shape. *Ann. For. Sci.* **2007**, *64*, 631–637. [CrossRef]
26. Tomaštík, J.; Saloň, Š.; Tunák, D.; Chudý, F.; Kardoš, M. Tango in forests—An initial experience of the use of the new Google technology in connection with forest inventory tasks. *Comput. Electron. Agric.* **2017**, *141*, 109–117. [CrossRef]
27. Rodríguez-García, C.; Montes, F.; Ruiz, F.; Canellas, I.; Pita, P. Stem mapping and estimating standing volume from stereoscopic hemispherical images. *Eur. J. For. Res.* **2014**, *133*, 895–904. [CrossRef]
28. Marcato Junior, J.; de Moraes, M.V.A.; Tommaselli, A.M.G. Avaliação experimental de técnicas de calibração de câmaras com objetiva olho de peixe. *Bol. Ciencias Geod.* **2015**, *21*, 637–651. [CrossRef]
29. Schneider, D.; Schwalbe, E.; Maas, H.-G. Validation of geometric models for fisheye lenses. *ISPRS J. Photogramm. Remote Sens.* **2009**, *64*, 259–266. [CrossRef]
30. Garrido-Jurado, S.; Muñoz-Salinas, R.; Madrid-Cuevas, F.J.; Marín-Jiménez, M.J. Automatic generation and detection of highly reliable fiducial markers under occlusion. *Pattern Recognit.* **2014**, *47*, 2280–2292. [CrossRef]
31. Agisoft, L.L.C. *Agisoft PhotoScan User Manual: Professional Edition, Version 1.1*; Agisoft LLC: St. Petersburg, Russia, 2014.

Příloha č. 6 - Grznárová, A.; Mokroš, M.; Surový, P.; Slavík, M.; Pondelík, M.; Merganič, J. THE CROWN DIAMETER ESTIMATION FROM FIXED WING TYPE OF UAV. 2019, *XLII*, 10–14.

The International Archives of the Photogrammetry, Remote Sensing and Spatial Information Sciences, Volume XLII-2/W13, 2019
ISPRS Geospatial Week 2019, 10–14 June 2019, Enschede, The Netherlands

THE CROWN DIAMETER ESTIMATION FROM FIXED WING TYPE OF UAV IMAGERY

A. Grznárová [1]*, M. Mokroš[1,2], P. Surový [2], M. Slavík [2], M. Pondelík [1], J. Merganič [3]

[1]Department of Forest Management and Geodesy, Faculty of Forestry, Technical University in Zvolen, 96053 Zvolen, Slovakia, alzbeta.grznarova@tuzvo.sk; xpondelik@is.tuzvo.sk
[2] Faculty of Forestry and Wood Sciences, Czech University of Life Sciences Prague, 165 00 Praha 6–Suchdol, Czech Republic, mokros@fld.czu.cz; surovy@fld.czu.cz; mslavik@fld.czu.cz
[3] Department of Forest Harvesting, Logistics and Ameliorations, Faculty of Forestry, Technical University in Zvolen, 96053 Zvolen, Slovakia, merganic@tuzvo.sk

KEY WORDS: Unmanned aerial vehicle (UAV), crown diameter, Inverse Watershed Segmentation (IWS), forestry, tree species

ABSTRACT:

The forest inventory is an important instrument for sustainable forest management. Canopy Height Model (CHM) and Digital Surface Model (DSM) created from high-resolution UAV (unmanned aerial vehicle) imagery provide possibility to determine tree crown diameters for the whole stand at fast. The goal of this paper is to identify the influence of tree species on the accuracy of estimation of crown diameter from high-resolution UAV imagery. In Plot 1 with coniferous tree species we identified 21 trees from total of 22 trees that leads to a detection rate of 95%. In Plot 1 with deciduous trees species we identified 24 trees from total 34 trees that leads to a detection rate of 71%. The RMSE errors calculated between the reference crown diameters and estimated crown diameters by IWS on Plot 1and Plot 2 were calculated as 0.80 m (RMSE% = 21.85) and 1.89 m (RMSE% = 21.54), respectively. The results didn't show the significant influence of tree species on the accuracy of estimation of crown diameter from high-resolution UAV imagery. However, result showed the significant influence of tree species on the detection number trees on the plot. The detection of number trees on the plot by method Inverese Watersed Segmentation in software ArcGis is higher for coniferous tree species. It is mainly due to the overlapping crowns.

1. INTRODUCTION

The forest inventory is an important instrument for sustainable forest management. The purpose of forest inventories is to estimate means and totals for measures of forest characteristic over a defined area. Such characteristic include the volume of the growing stock, the area of certain type of forest and nowadays also measures concerned with forest biodiversity, e.g. the volume of dead wood or vegetation (Kangas and Maltamo, 2006). The data acquisition during forest inventory is time- and cost-demanding. Unmanned aerial vehicle (UAV) in combination with digital photogrammetry provides possibilities for effective data acquisition.

Several studies have focused on usage of UAVs and digital photogrammetry for forest inventory. Fritz et al., (2013) used UAV imagery to automatically detect and reconstruct individual trees. Study Lisein et al. (2013) aimed at determining how dominant height at stand level and individual tree height of an uneven-aged broad- leaved forest dominated. Puliti et al. (2015) used three-dimensional (3D) variables derived from UAV imagery in combination with ground reference data to fit linear models for Lorey's mean height, dominant height, stem number, basal area, and stem volume. Other studies have dealt with tree species classification. For example, study Michez et al. (2016) proposed a methodological framework to classification of riparian forest species and health condition using multi-temporal and hyperspatial imagery from UAV. Study Cao et al. (2018) investigated the capability of UAV hyperspectral images for distinguishing and mapping mangrove species using object-based approaches. Another study demonstrated how UAV images can be used for quantifying spatial gap patterns in forest related to the spatio-temporal dynamics of forests.

Crown diameter is one of tree characteristic that are collected during forest inventory. It is significantly important because it strongly correlates with other tree dimensions used to estimate the volume of the growing stock. Currently, crown diameter of each single individual tree in forest stand is measured separately by terrestrial methods. Canopy Height Model (CHM) and Digital Surface Model (DSM) created from high-resolution UAV imagery provide possibility to determine tree crown diameters for the whole stand at fast. Several studies used UAV photogrammetry to determine tree crown diameters. They used for example object-based image analysis technique (OBIA) (Guerra-Hernandez et al., 2016; Johansen et al., 2018; Torres-Sánchez et al., 2015) or algorithm Inverse Watershed Segmentation (IWS) (Panagiotidis et al., 2017). The technique OBIA is based on merging similar pixels to homogeneous segments. Individual pixels are merging with neighbouring ones based on by the following parameters: shape, scale, compactness and colour scale (González-Ferreiro et al., 2013). The algorithm IWS is based on inverting the CHM so the model is turned upside down the peaks become depressions. When the raster surface is configured as a depression model, watershed segmentation can then be performed to delineate basins (Edson and Wing, 2011). The technique OBIA were applicated in software eCognition, while the algorithm IWS were applicated in software ArcGIS.

For UAV imagery acquisition authors of studies used fixed-wing UAVs (Guerra-Hernandez et al., 2016; Shin et al., 2018) or rotary-wing UAVs (Patrick and Li, 2017; Yilmaz et al., 2017; Panagiotidis et al., 2017; Torres-Sánchez et al., 2015). UAV

* Corresponding author

This contribution has been peer-reviewed.
https://doi.org/10.5194/isprs-archives-XLII-2-W13-337-2019 | © Authors 2019. CC BY 4.0 License.

imagery were made by RGB camera (Díaz-Varela et al., 2015; Guerra-Hernandez et al., 2016; Panagiotidis et al., 2017; Patrick and Li, 2017) or multispectral camera (Johansen et al., 2018; Torres-Sánchez et al., 2015; Shin et al., 2018). UAV imagery were post-processed mainly in the Pix4D software (Díaz-Varela et al., 2015; Guerra-Hernandez et al., 2016; Johansen et al., 2018; Shin et al., 2018) or Agisoft Photoscan (Panagiotidis et al., 2017; Patrick and Li, 2017; Torres-Sánchez et al., 2015; Yilmaz et al., 2017).

They focused on various segmentation techniques or on discontinuous and continuous canopy cropping systems. However, to our best knowledge the studies did not focus on comparison of the diameter accuracy among various tree species and most of the studies used rotary-wing types of UAV. Which serve great detail and accuracy. On the other hand, rotary-wing UAVs need more time to cover larger areas with comparison to fixed wing UAV.

The goal of this paper is to assess the accuracy of crown diameter estimation and to identify the influence of tree species on the accuracy of estimation of crown diameter from high-resolution UAV imagery using fixed wing eBee Plus RTK/PPK.

2. MATERIAL AND METHODS

2.1 Study plots

For purposes of the study, two research plots were established (Figure 1). They were located near Zvolen, Slovakia (48°37'41" N, 19°02'19" E). The distance between the plots was approximately 600 m. Both plots were covered with forest stand with 0.9 stocking. Plot 1 had 22 trees with predominant Europeansilver fir (Abies alba Mill.) Plot 2 had 34 trees with mainly sessile oak (Quercus petraea (Matt.) Liebl.) and European beech (Fagus sylvatica L.). Both plots had circular shape with the area of 500 square meters.

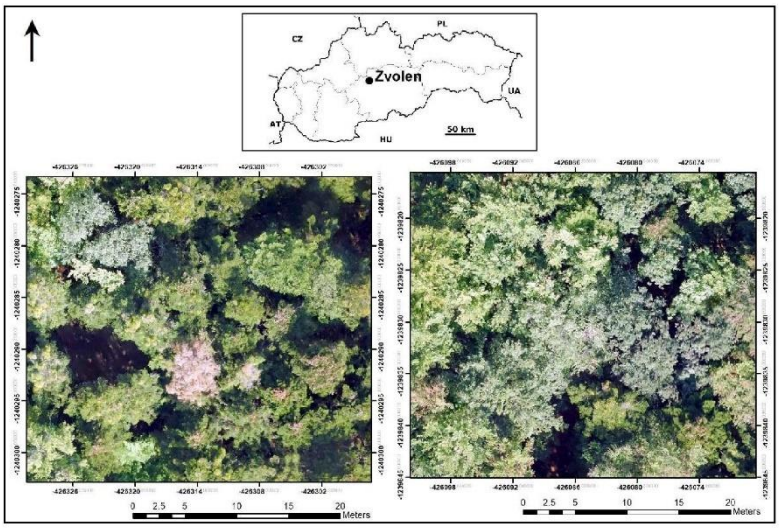

Figure 1. Location of research plots. The left is Plot1 and the right is Plot 2

2.2 Field measurements

The positions and crown projections of all trees on both plots were measured by FieldMap technology, consisting of digital compass, laser rangefinder and terrain computer. The positions were measured using the azimuth–distance approach from the plot centre. The crown projections were measured by 4 border points of the crown's outline in east–west and north–south directions. The field measurements for both plots were collected in the same month as the aerial images acquisition was performed.

2.3 Aerial images acquisition

For imagery acquisition was used the UAV eBee Plus RTK/PPK (Figure 2) during the leaf-on conditions on both plots. This fixed-wing UAV has wingspan of 110 cm, weights 1,1 kg, and can launch from hand. The camera, used for data acquisition, was SenseFly S.O.D.A. RGB, with an 18 MP resolution (5272 x 3648 pixels).

Figure 2. UAV eBee Plus RTK/PPK

This contribution has been peer-reviewed.
https://doi.org/10.5194/isprs-archives-XLII-2-W13-337-2019 | © Authors 2019. CC BY 4.0 License.

It was used a 1-inch RGB sensor and fixed focal length 10,6 mm. GNSS receiver used in the UAV configuration was the Septentrio AsteRx-m UAS. The flights were planned and processed in the eMotion 3 software. Planed image overlaps were 90x60%, GSD between one and two centimetres. This resulted into the flight height of approximately 70 m AGL. Each of the flight lasted approximately 13 minutes at a flight speed of 10m / s.

2.4 Processing of photogrammetric data

The UAV images were reconstructed by algorithm Structure from Motion and Multiview Stereopsis technique in the Agisoft Photoscan 1.4 software (Agisoft LCC, St. Petersburg, Russia). The standardly used workflow was applied. All images were geotagged using positions from postprocessed GNSS solution. Images were then aligned with Accuracy set to High and Pair Preselection set to Reference. Following steps included generation of dense clouds with Quality set to High and Depth filtering set to Mild. Finally, Digital surface model (DSM) and orthophotomosaic of both research plots were created from dense point cloud (Figure 3).

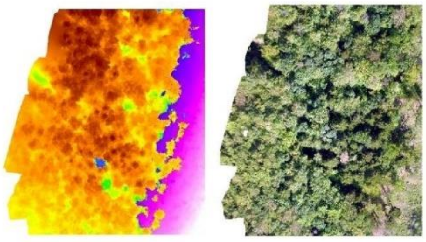

Figure 3. Inputs of software Agisoft Photoscan – DSM and ortophotomosaic from Plot 1

2.5 Estimation of Canopy Parameters

Individual tree crowns were delineated with using of Inverse Watershed Segmentation method in the environment of ArcGIS Desktop 1.4 software (ESRI). This methodology was proposed by Panagiotidis et al, (2017). As the input data were used DSM and orthophotomosaic. The tools Flow Direction and Basin was using on the inverse DSM. The original DSM were relocated to the Boolean raster and were multiplied by the result of the Basin tool by class 1 (including trees from the lowest to the highest tree) to remove large gaps between tree crowns. In other step, the raster displaying the edges of crowns was converted to polygons by the tool Raster to Polygon. However, a several small numbers of polygons belonged to one crown, so it was necessary to eliminate their number by several times using the Eliminate tool to correspond with the underlying orthophotomosaic (Figure 4). In the next step, crown polygons were converted to lines and lines were converted to points with using of tool Feature to Point. Finally, the distances points lying on the edge lines of tree crowns and centres of crowns were calculated with using of the tool Distance to points (Panagiotidis et al., 2017). The results of this workflow were average crown diameters of single individual trees on both research plots.

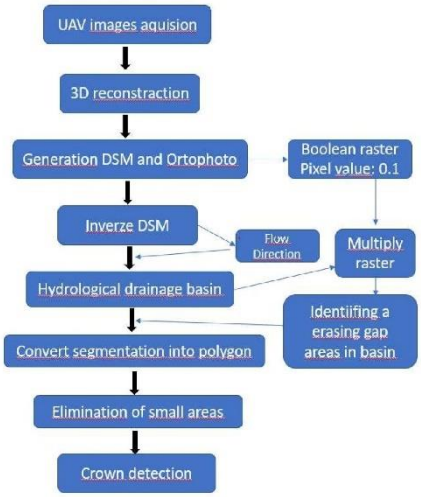

Figure 4. Scheme of crown detection (Panagiotidis et al., 2017) – edited

3. RESULTS

We compared estimated crown diameters with reference crowns diameter that were obtained by terrestrial measurements. We calculated differences and Root Mean Square Error (RMSE). In Plot 1 with coniferous tree species we identified 21 trees from total of 22 trees that leads to a detection rate of 95% (Figure 5). In Plot 1 with deciduous trees species we identified 24 trees from total 34 trees that leads to a detection rate of 71%. The RMSE errors calculated between the reference crown diameters and estimated crown diameters by IWS on Plot 1and Plot 2 were calculated as 0.80 m (RMSE% = 21.85) and 1.89 m (RMSE% = 21.54), respectively (Table 1).

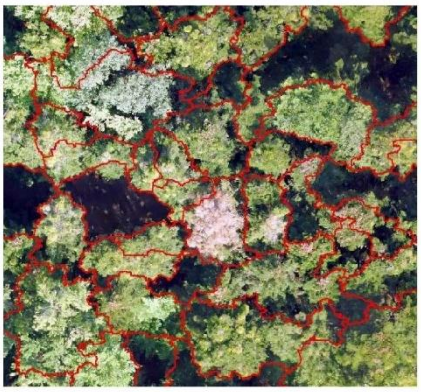

Figure 5. Polygon of tree crowns (Plot1)

This contribution has been peer-reviewed.
https://doi.org/10.5194/isprs-archives-XLII-2-W13-337-2019 | © Authors 2019. CC BY 4.0 License.

Plot (species)	Number of detected / total trees	Detection rate	RMSE (m)	RMSE%
Plot 1 (JD)	21/22	95%	0,80	21,85
Plot 2 (DB)	24/34	71%	1,89	21,54

Table 1. Statistics of the measured and estimated crown diameters

4. DISCUSSION

Our study focused on estimation of crown diameter by fixed-wing UAV in forest stands with dense canopy. There are some previous studies used the same type UAV on estimation of the crown. Study Shin et al. (2018) dealt with Ponderosa Pine Stand and achieved RMSE 0.88 m for crown diameter. We achieved similar accuracy (RMSE 0.80 m) on Plot 1 with conifer tree species and with only partially overlapped crowns. Other study Guerra-Hernandez et al. (2016) used fixed wing UAV eBee to estimate tree variables and achieved RMSE 0.66 m (rRMSE 6.14%). It is important to note that object of this study was Pinus pinea plantation on flat terrain with sparsely distributed trees.

Other studies were focused on estimation of crown diameter used rotary-wings UAV (Johansen et al., 2018; Patrick and Li, 2017; Panagiotidis et al., 2017; Yilmaz et al., 2017). Study Johansen et al., (2018) were focused on to establish the response of pruning in an orchard of lychee trees and used 3DR Solo cadrocopter and a Parrot Sequoia multi-spectral sensor. For crown diameter they achieved RMSE 0.26 m. Study Patrick and Li et al. (2017) researched the possibilities and accuracy of the low-cost unmanned aerial vehicle DJI Phantom 3 to determine the morphological characteristics of blueberries with discontinuous canopy. For crown diameter they achieved RMSE 5.57 cm. Study Panagiotidis et al. (2017) used DJI S800 UAV platform and achieved RMSE 0.82 m and 1.04 m rRMSE 14.29% and 18.56%. Study Yilmaz et al., (2017) used DJI Phantom 3 and were focused on comparation two various segmentation techniques Both the MR and RG segmentation algorithms detected 57 of them correctly, which leads to a detection accuracy of 90% for both algorithms. The RMS errors calculated between the reference crown diameters and MR and RG segmentation-derived crown diameters were calculated as 1.59m and 1.76m, respectively.

Advantage of fixed-wing type of UAV compared to the rotary-wing type is higher range. Disadvantage is impossibility to create enough quality DTM from the point cloud obtained from UAV images to estimate tree heights in forest stands with dense canopy. The solution is a combination UAV photogrammetry with airborne laser scanning (Jensen et al., 2016; Goldbergs et al., 2018). Aerial laser scanning provides data with high accuracy and quality. However, the data is poorly detailed and costly to collect. Therefore, aerial laser scanning is not suitable for detailed and regular monitoring in a short time period. On the other hand, UAS provides low cost, high spatial and temporal resolution data (Goodbody et al., 2017). Other alternative is usage of UAV-LiDAR (Sankey at al., 2017; Wallace et al., 2016).

5. CONCLUSION

The results did not show the significant influence of tree species on the accuracy of estimation of crown diameter from high-resolution UAV imagery. However, results showed the significant influence of tree species on the detection number trees on the plot. The detection of number trees on the plot by method Inverese Watersed Segmentation in software Arcgis is higher for coniferous tree species. It is mainly due to the overlapping crowns.

In further research we will validate our results on the other plots with various tree species. Further, we will focus to identify the influence of vegetation season and impact of flight altitude on the estimation accuracy of crown diameter from high-resolution UAV imagery.

ACKNOWLEDGEMENTS

This research was funded by the Slovak Research and Development Agency through grant No. APVV-15-0714 ("Mitigation of climate change risk by optimization of forest harvesting scheduling"), and by grants No. CZ.02.1.01/0.0/0.0/16_019/0000803 ("Advanced research supporting the forestry and wood-processing sector´s adaptation to global change and the 4th industrial revolution") financed by OP RDE.

We acknowledge the support of The ISPRS Foundation (TIF) in the form of TIF Travel Grants, which enabled us to attend the conference ISPRS Geospatial Week 2019.

REFERENCES

Cao, J., Leng, W., Liu, K., Liu, L., He, Z. and Zhu, Y., 2018. Object-based mangrove species classification using unmanned aerial vehicle hyperspectral images and digital surface models. *Remote Sens*, 10(1), 89. doi.org/10.3390/rs10010089

Díaz-Varela, R., Rosa, R., León, L., Zarco-Tejada, P., 2015. High-Resolution Airborne UAV Imagery to Assess Olive Tree Crown Parameters Using 3D Photo Reconstruction: Application in Breeding Trials. *Remote Sensing*, 7(4), 4213-4232. doi.org/10.3390/rs70404213

Edson, C. and Wing, M.G., 2011. Airborne light detection and ranging (LiDAR) for individual tree stem location, height, and biomass measurements. *Remote Sens*, 3(11), 2494-2528. doi:10.3390/rs3112494

Fritz, A., Kattenborn, T. and Koch, B., 2013. UAV-based photogrammetric point clouds –tree stem mapping in open stands in comparison to terrestrial laser scanner point clouds. *ISPRS Ann. Photogramm. Remote Sens. Spatial Inf. Sci.*, XL-1/W2 (UAV-g2013), 141-146. doi.org/10.5194/isprsarchives-XL-1-W2-141-2013

Getzin, S., Nuske, R. and Wiegand, K., 2014. Using unmanned aerial vehicles (UAV) to quantify spatial gap patterns in forests. *Remote Sens*, 6(8), 6988-7004. doi:10.3390/rs6086988

Goldbergs, G., Maier, S., Levick, S. and Edwards, A., 2018. Efficiency of individual tree detection approaches based on light-weight and low-cost UAS imagery in Australian Savannas. *Remote Sens.*, 10(2), 161. doi.org/10.3390/rs10020161.

González-Ferreiro, E., Diéguez-Aranda, U., Barreiro-Fernández, L., Buján, S., Barbosa, M., Suárez, JC., Miranda, D., 2013. A mixed pixel-and region-based approach for using airborne laser scanning data for individual tree crown delineation in Pinus radiata D. Don plantations. *International Journal of Remote Sensing*, 34(21), 671-7690. doi.org/10.1080/01431161.2013.823523

Goodbody, T.R., Coops, N.C., Marshall, P.L., Tompalski, P., Crawford, P., 2017. Unmanned aerial systems for precision forest inventory purposes: A review and case study. *The Forestry Chronicle,* 93(1), 71-81. doi.org/10.5558/tfc2017-012

Guerra-Hernandez, J., Gonzalez-Ferreiro, E., Sarmento, A., Silva, J., Nunes, A., Correia, A.C., Fontes, L., Tomé, M., Diaz-Varela, R., 2016. Short Communication. Using high resolution UAV imagery to estimate tree variables in Pinus pinea plantation in Portugal. *Forest Systems,* 25(2). doi.org/10.5424/fs/2016252-08895

Jensen, J., Mathews, A. 2016. Assessment of image-based point cloud products to generate a bare earth surface and estimate canopy heights in a woodland ecosystem. *Remote Sens.*, (1), 50. doi.org/10.3390/rs8010050

Johansen, K., Raharjo, T., McCabe, M.F., 2018. Using multi-spectral UAV imagery to extract tree crop structural properties and assess pruning effects. *Remote Sens.*, 8(1), 50. doi.org/10.3390/rs8010050

Kangas, A. and Maltamo, M. eds., 2006. *Forest inventory: methodology and applications (Vol. 10)*. Springer Science & Business Media. Dordrecht, 3-11.

Lisein, J., Pierrot-Deseilligny, M., Bonnet, S. and Lejeune, P., 2013. A photogrammetric workflow for the creation of a forest canopy height model from small unmanned aerial system imagery. *Forests*, 4(4), 922-944. doi.org/10.3390/f4040922

Michez, A., Piégay, H., Lisein, J., Claessens, H. and Lejeune, P., 2016. Classification of riparian forest species and health condition using multi-temporal and hyperspatial imagery from unmanned aerial system. *Environmental monitoring and assessment*, 188 (3): 1–19. doi.10.1007/s10661-015- 4996-2.

Panagiotidis, D., Abdollahnejad, A., Surový, P., Chiteculo, V., 2017. Determining tree height and crown diameter from high-resolution UAV imagery. *International Journal of Remote Sensing*, 38, 2392–2410. doi.org/10.1080/01431161.2016.1264028

Patrick, A. and Li, C., 2017. High throughput phenotyping of blueberry bush morphological traits using unmanned aerial systems. *Remote Sens.*, 9(12), 1250. doi.org/10.3390/rs9121250

Puliti, S.; Ørka, H.O.; Gobakken, T.; Næsset, E., 2015. Inventory of Small Forest Areas Using an Unmanned Aerial System. *Remote Sens.*, 7(8), 9632-9654. doi.org/10.3390/rs70809632

Sankey, T., Donager, J., McVay, J. and Sankey, J.B., 2017. UAV lidar and hyperspectral fusion for forest monitoring in the southwestern USA. *Remote Sensing of Environment*, 195, 30-43. doi.org/10.1016/j.rse.2017.04.007

Shin, P., Sankey, T., Moore, M., Thode, A., 2018. Evaluating Unmanned Aerial Vehicle Images for Estimating Forest Canopy Fuels in a Ponderosa Pine Stand. *Remote Sens.*, 10(8), 1266. doi.org/10.3390/rs10081266

Torres-Sánchez, J., López-Granados, F., Serrano, N., Arquero, O., Peña, J., 2015. High- Throughput 3-D Monitoring of Agricultural-Tree Plantations with Unmanned Aerial Vehicle (UAV) Technology. *PLoS ONE,* 10(6). doi.org/10.1371/journal.pone.0130479

Wallace, L., Lucieer, A., Malenovský, Z., Turner, D. and Vopěnka, P., 2016. Assessment of forest structure using two UAV techniques: A comparison of airborne laser scanning and structure from motion (SfM) point clouds. *Forests*, 7(3), 62. doi.org/10.3390/f7030062

Yilmaz, V., Yilmaz, C.S., Tasci, L. And Gungor, O., 2017. Determination of Tree Crown Diameters with Segmentation of a UAS-Based Canopy Height Model. *IPSI Bgd Transactions on Internet Research,* 13(2),63-7.